Development of a Novel Amphibious Locomotion System for use in Intra-Luminal Surgical Procedures

William Henry Mayfield

Submitted in accordance with the requirements for the degree of
Doctor of Philosophy

The University of Leeds
School of Mechanical Engineering

August 2015

The candidate confirms that the work submitted is his own, except where work which has formed part of jointly-authored publications has been included. The contribution of the candidate and the other authors to this work has been explicitly indicated in the acknowledgements and publications section. The candidate confirms that appropriate credit has been given within the thesis where reference has been made to the work of others.

Acknowledgements

This thesis covers the research carried out on the development of an amphibious locomotion system for use on intra-luminal robotic devices, as undertaken by the author. All work has been carried out by the author unless stated otherwise.

The work undertaken for this thesis forms part of a large research project titled: Colonic Disease Investigation through Robotic Hydro Colonoscopy (CoDIR). The CoDIR project is multidisciplinary collaboration between the University of Leeds and the University of Dundee, involving engineers and clinicians to deliver an innovative system to help investigate and prevent colonic disease. Funded by a research grant provided by the European Research Council, the project principal investigators are Professor Sir Alfred Cuschieri and Professor Anne Neville.

The University Of Leeds CoDIR team included *Miss Z. Ehteshami, Mr A. Hood, Dr J. Boyle, Dr A. Alazmani, Dr R. Hewson, Dr P. Culmer, Prof D. Jayne and Prof A. Neville*. My own contributions, fully and explicitly indicated in the thesis, have been the development and testing of the amphibious locomotion system, and the development of the testing platforms. The other members of the group and their contributions have been as follows: *experimental testing and quantification of mechanical properties of colon tissue, reconstruction of computer models of colons from CT images*.

I would like to thank my supervisors, Anne Neville, Pete Culmer and Rob Hewson for their support throughout the research; university faculty staff, particularly Andy Pickering, Dave Readman, and Graham Brown for assistance with electronics and rapid prototyping; my friends and fellow researchers for all the good times spent in the offices and labs; my parents for giving me the opportunity to study what I desired; and my girlfriend for understanding when I ignored her for my research.

Abstract

Colonoscopy is widely considered the gold standard for inspection of the colon. The procedure is however not without issue, current colonoscopes have seen little change or innovation throughout their 40 years of use with patient discomfort still limiting success. The aim of this PhD study was to develop a locomotion system for use on a robotic device that can traverse a liquid filled colon for atraumatic inspection and biopsy tasks. The PhD was undertaken as part of a larger two-centre EU project, which aimed to bring about a change in the way colonoscopy is done by moving to “robotic hydro-colonoscopy”.

In this thesis the initial development and testing of an amphibious locomotion concept for use in a procedure known as hydro-colonoscopy is described. The locomotion system is comprised of four Archimedes’ screws arranged in two counter-rotating pairs. These aim to provide propulsion through a fluid-filled colon as well as provide locomotive traction against colonic tissue in partially fluid-filled or collapsed sections of the colon, such as the splenic flexure.

Experimental studies were carried out on a single screw system in fluid and dual counter-rotating screws in contact conditions. These show the system’s ability to generate thrust in the two discrete modes of locomotion of the amphibious system.

A 2:1 scale prototype of the proposed device was produced and features compliant screw threads to provide atraumatic locomotion. The scale prototype device was tested in ex-vivo porcine colon. The developed system was able to traverse through lumen to limited success, which demonstrated that this concept has the potential for use on an intra-luminal robotic device

The key contributions of this research are: variable geometry locomotion system; amphibious locomotion using Archimedes’ screws; experimental assessment of the locomotion in fluid, contact and amphibious states; and analysis of the contact dynamics against tissue.

Table of Contents

List of Tables

List of Figures

List of Abbreviations

ALM	Additive Layer Manufacturing
CAD	Computer Aided Design
CD	Cohn's Disease
CoDIR	Colonic Disease Investigation through Robotic Hydro Colonoscopy
CPU	Central Processing Unit
cRIO	Compact Reconfigurable Input Output
CSV	Comma Separated Value
CT	Computerised Tomography
DoF	Degrees of Freedom
FDM	Fussed Deposition Modelling
FPGA	Field Programmable Gate Array
GI	Gastro-Intestinal
GUI	Graphical User Interface
HID	Human Interface Device
HMI	Human Machine Interface
IDB	Irritable Bowel Disease
IDE	Integrated Development Environment
LDPE	Low Density Polyethylene
MR	Motion Ratio
PID	Proportion Integral Derivative
PIG	Pipeline Inspection Gauge
PWM	Pulse Width Modulation
RT	Real Time
SLS	Selective Laser Sintering
SoC	System on Chip
UC	Ulcerative Colitis
UI	User Interface
VDU	Visual Display Unit

Publications

Preliminary Development of a Novel Amphibious Locomotion System for use in Intra-luminal Surgical Procedures; W. Mayfield, A. Alazmani, A. Hood; J. Boyle, P. Culmer; R. Hewson; A. Neville, D. Jayne; The Hamlyn Symposium on Medical Robotics, 2014.

This publication includes work covered in chapters 3-6 of the thesis. The design and testing of the robotic system along with the design of the testing platforms and software is directly attributable to the candidate. Work carried out on clinical trials of fluid medium tolerance and reconstruction of CT data has been carried out by authors of the publication and not attributable to the candidate

Chapter 1
Introduction

This thesis covers the development of an amphibious locomotion system for use in intra-luminal surgical procedures. The locomotion system must be able to allow a device to traverse the large intestine, or colon, of a human without causing damage while providing a stable platform for data collection (e.g. vision and biopsy) to allow clinicians to assess the state of the colon lining (mucosa).

1.1 Background

Colonoscopy is the gold standard for inspection of the colon (1-3). It is performed using a long flexible tube, which contains a fibre optic camera, passage for biopsy and a passage for fluid insertion or removal.

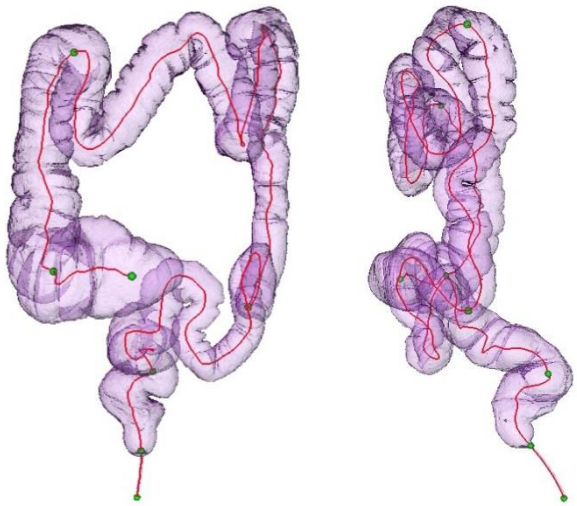

Figure 1.1 3D reconstruction of a human colon, built using CT images acquired from the National Cancer Image Archive (4).To the left is the colon as viewed from the coronal (front) plane and to the right is the colon as viewed from the sagittal (side) plane. The colonic walls are shown in transparent purple with the centre line shown in red. The green circles denote changes in anatomical landmark colonic section; caecum, ascending, traverse, descending, sigmoid and rectum colon, as discussed further in Chapter 2. 3D reconstruction carried out by Dr A. Alazmani and Dr P. Culmer for the CoDIR project.

The human colon is by no means straight, linear or regular (Figure 1.1) (1, 5): each colon although having the same general anatomy, features unique bends, lengths and folds. Some of these folds can be caused by obtuse bends, which pose particular difficulty in navigation. The current

colonoscope is inserted per rectum and pushed along the colon with a rear driven locomotion method. To pass these obtuse bends the clinician must manipulate the colonoscope and its curvature. This can cause damage where the tip perforates the colon or the colonoscope damages the mucosa through abrasion between the surfaces (1), although the rates of damage are low. Eight cases from a study of 20,085 colonoscopies by Gavin et al. (6) resulted in perforation, while 763 were aborted due to discomfort or looping.

Despite many years of development, the colonoscope still suffers from drawbacks, often resulting in patient discomfort and procedure difficulty as outlined above. The Colonic Disease Investigation through Robotic Hydro Colonoscopy (CoDIR) project[1] aims to explore and develop a novel system to replace the colonoscope. The project focuses on using a fluid filled colon, a process known as hydro-colonoscopy that will both open the colon lumen and provide a medium through which a device could navigate. Through using a warm fluid medium to insufflate, distend and relax the colon. Clinical trials show this is more comfortable than traditional colonoscopy (7). Studies carried out by the CoDIR team[2] using MRI scans show the bowel is successfully filled and opened up for assessment using this technique (Figure 1.2 and Figure 1.3). This new approach provides an opportunity for robotic systems that can traverse and inspect the colon, potentially improving assessment and ease of procedure for the clinician.

This thesis covers the development of a locomotion system for the CoDIR device, which could also be applied to other intra-luminal devices. While the colon is to be filled with a fluid, the method of locomotion was set only one requirement: it must be able to traverse the colon in a controlled state in a similar time span to a traditional colonoscopy procedure while minimising discomfort to the patient. Discomfort can often be linked to tissue damage: the body's natural defence against damaging actions is pain, such discomfort can be minimised through the use of atraumatic methods.

---

[1] The Colonic Disease Investigation through Robotic Hydro Colonoscopy (CoDIR) project is a joint venture between the University of Leeds and the University of Dundee, funded by a European Research Council grant.

[2] Clinical trial carried out by A. Hood as part of CoDIR. Trial consisted of 21 recruits split into two groups randomly. Group A received CO_2 then fluid insufflation, group B vice versa. Mean fluid volume: 1.6 litres, range: 1-2 litres, 6 received 2 litre delivery. Figure 1.2 and Figure 1.3 show CT images taken during trial. Work currently unpublished by CoDIR.

Due to the tortuous and challenging nature of colonic anatomy, and the fact that no two colons are the same, the device's locomotion system must be able to overcome fluid filled sections, partially fluid filled sections, fluid void sections and collapsed sections without causing trauma to the patient or becoming stuck and in need of surgical removal. The locomotion system must also be able to provide sufficient tractive force to traverse the colon carrying a payload such as surveillance equipment, e.g. a camera.

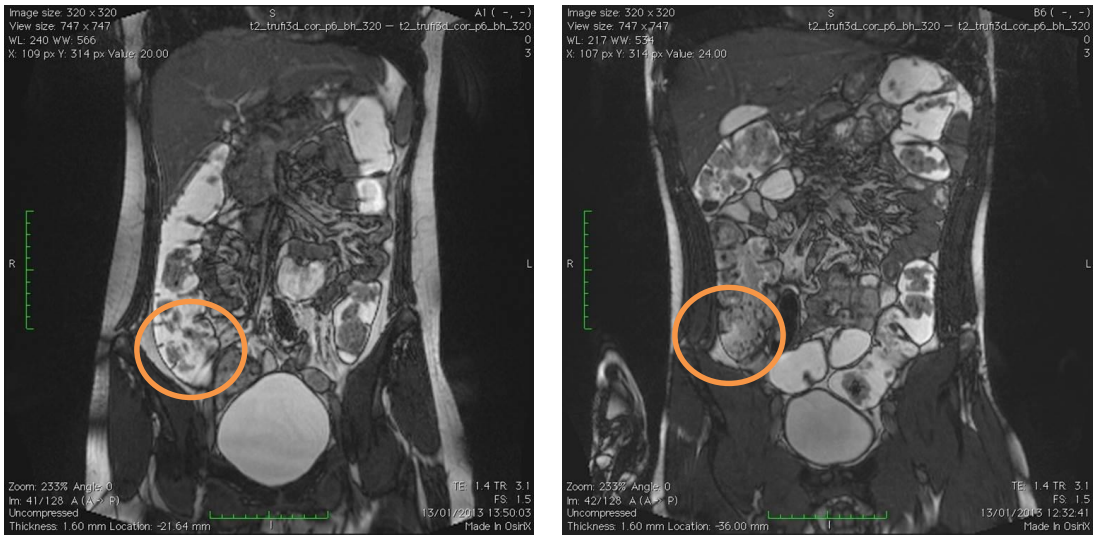

Figure 1.2 CT images taken of a fluid insufflated colon showing fluid (PEG solution, Klean-Prep®) reaching the caecum (circled). Each image is of a separate patient. Images taken as part of a clinical trial carried out by CoDIR, work undertaken by A. Hood, currently unpublished.

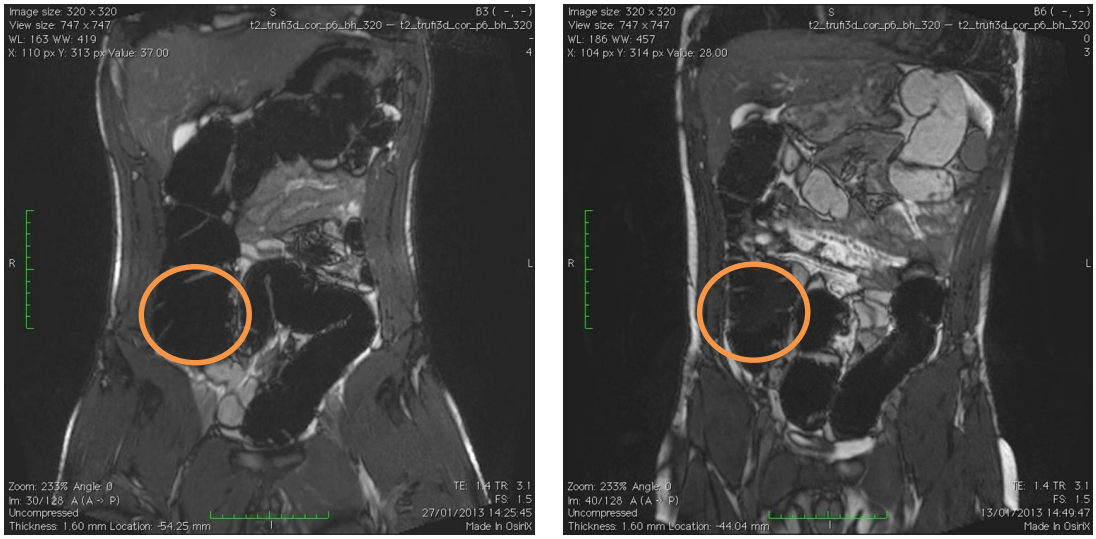

Figure 1.3 CT images taken of a CO_2 insufflated colon after insufflation with fluid, showing the caecum circled. The colon is very clean and free from debris after being purged of PEG solution post insufflation, as seen by the high contract between colon volume and colon wall. Each image is of a separate patient. Images taken as part of a clinical trial carried out by CoDIR, work undertaken by A. Hood, currently unpublished.

The clinical trials carried out by A. Hood as part of CoDIR show a significant proportion of the colon to be fluid filled. In using a fluid medium for insufflation, any device deployed for investigation purposes will require the ability to swim: however, this cannot be the sole form of locomotion as air pockets remain and some sections do not open sufficiently to pass without contact. An amphibious system is best suited for a fluid-filled colon environment.

1.2 Research Aim

To develop an amphibious locomotion system appropriate for traversing the human colon in hydro-colonoscopy procedure.

1.3 Research Objectives

- Design a locomotion system that:
  - Is able to generate propulsive force in fluid and air filled sections or combinations of such
  - Minimises trauma to colonic tissue
  - Can accommodate the varying geometry of the colon
- Evaluate the locomotion system in:
  - Fluid locomotion state (fluid filled colon sections)
  - Contact locomotion state (air filled colon sections)
- Construct and evaluate a scale prototype of the full system using ex-vivo porcine colon

1.4 Contribution of this thesis

The key contributions of this thesis are the development of a variable geometry locomotion system that utilises Archimedes' screws to provide amphibious locomotion; theoretical and experimental assessment of the locomotion system in fluid, contact and amphibious states; and analysis of the contact dynamics of rotating screws against tissue.

1.5 Scope of Thesis and Development Timeline

This thesis covers the development of the locomotion system split into chapters covering the design, implementation, fluid testing, contact testing and complete physical prototype evaluation. The chapters cover the research tasks chronologically, although the process was iterative. The flowchart in Figure 1.4 shows the key design and experimental tasks

arranged chronologically from top to bottom. The arrows show the flow of information throughout the research. The flowchart is included to aid the reader in how the work across chapters is linked, for example, the results from experimental testing in Chapters 5 and 6 inform design changes in Chapter 3.

Chapter 2 consists of an introduction, which sets the clinical context concerning the colon, ailments and current inspection means. The chapter also covers next generation colonic inspection devices alongside current inspection devices for medical and non-medical applications.

Chapter 3 covers the clinical and technical design requirements, which influenced the design process, and the development of the locomotion system throughout the research.

Chapter 4 discusses the tasks undertaken during the design and construction of the locomotion system, with the hardware choices made throughout the development process, which played a role in the final design.

Chapter 5 evaluates the locomotion system in fluid based environments. A single screw was modelled theoretically and experimentally assessed the for thrust production capabilities of screws in fluid.

Chapter 6 evaluates the locomotion system in contact-based scenarios, such as the device may experience when passing through air-filled sections of the colon. A dual counter-rotating screw system was assessed experimentally for the tractive capabilities of screws when in contact with colonic tissue.

Chapter 7 evaluates a 2:1 scale prototype in a range of experimental and environmental conditions ranging from single mode of locomotion through to in-vivo testing of the system in a porcine colon.

Chapter 8 discusses the developed locomotion system and contributions made by this work to exploratory robotic devices. Potential future modifications and improvements to the system are then considered.

Chapter 9 concludes the thesis and summarises the research undertaken.

Figure 1.4 shows the development of the prototype and associated testing apparatus. Green rectangles show development of the prototype device, including CAD design, fabrication and assembly (where applicable) and control software development (where applicable), as covered in Chapters 3 and 4. Blue rectangles show the development of the testing apparatus and the associated control software, as covered in Chapters 5 and 6. Purple

rhombi show experimental data gathering, development of analysis methods and data analysis, as covered in Chapters 5, 6 and 7. The orange rectangle shows the analysis study carried out on the fluid flow as covered in Chapter 3. Shape overlap vertically shows concurrent tasks.

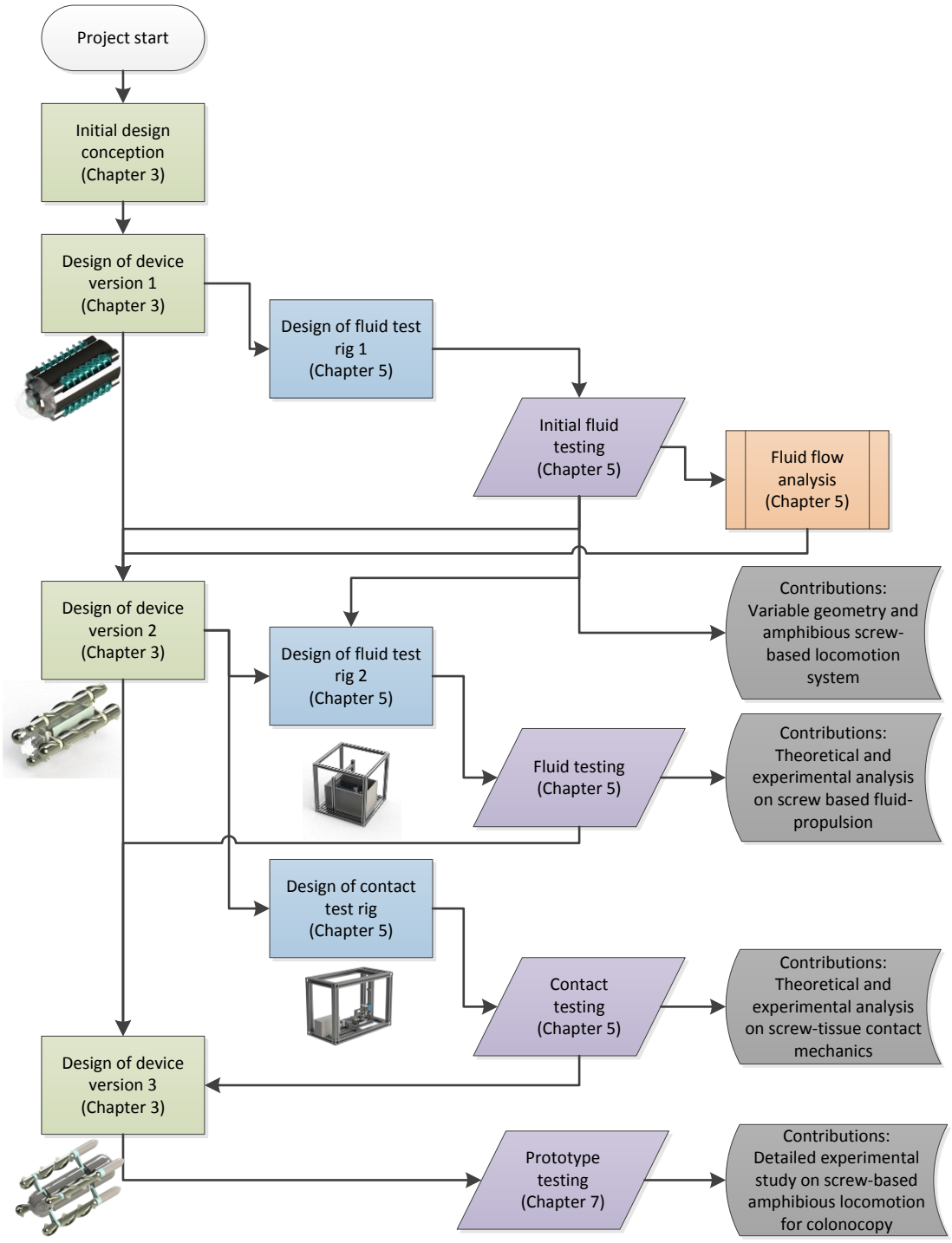

Figure 1.4 Development timeline of the research carried out as part of this thesis.

Chapter 2
Review of Literature on Colon Anatomy, Colonoscopy, Robotic Colonoscopy Devices and Robotic Locomotion Methods

A review of the current literature was conducted to understand the clinical context of this research, along with existing work undertaken to develop locomotion systems with similar goals. The review begins with the anatomy of the colon, to understand the environment in which the device will be deployed as well as the function of the colonic passage. Following this a brief overview of colonic ailments is covered, to aid understanding of why inspection of the colon is needed as well as the effects of these ailments on the passageway and the patient as a whole. Following this, a review of medical and non-medical inspection devices was carried out to establish the methods in which these robotic platforms traverse through their environment.

Before a replacement method for colonoscopy can be developed; the current methods, their benefits and their flaws must be understood. A review was conducted covering the current practice methods for inspection of the colon and variations of such methods. Hydro-colonoscopy is cited an improved method for inspecting the colon; current evidence, publications and clinical trial data covering this method was reviewed to ascertain why.

The review then considers methods of locomotion used in robotic applications, starting as a broad view then focusing on those applicable to and used on intra-luminal devices. Next-generation methods for performing colonoscopy and hydro-colonoscopy were reviewed with their locomotion methods compared across literature and against the methods discussed in the review of locomotion methods.

2.1 The Anatomy of the Colon

The colon, known also as the large intestine, is the last section of the passageway involved in the digestion of food, referred to as the gastrointestinal (GI) tract and typically 1.5m in length. A diagram of the upper and lower GI tract can be seen in Figure 2.1 with annotations to key organs. The main purpose of the colon is storage; such it has a poor blood supply. Throughout the colon are “haustrations”, inward foldings of the colonic wall. These never form a complete circumferential ring giving the

colon a triangular appearance when viewed from the inside, Figure 2.2. The surface is lined with a layer of mucosa, which protects the muscle wall.

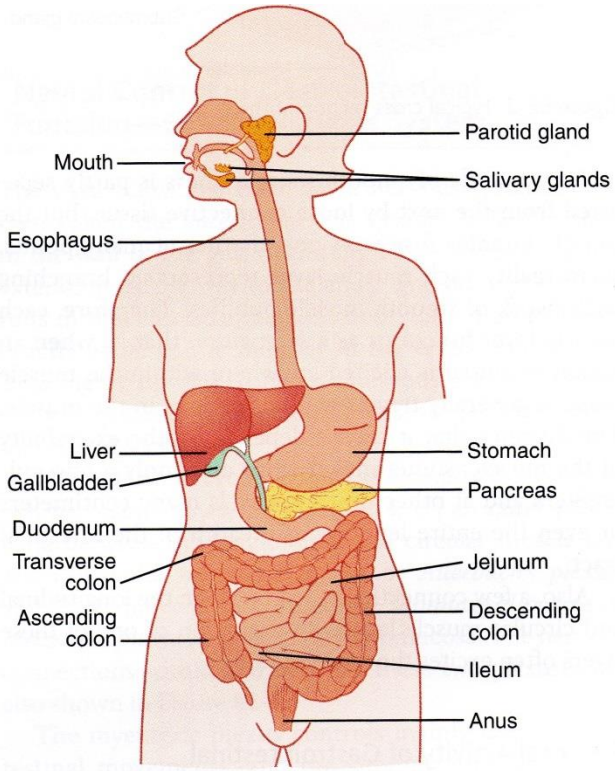

Figure 2.1 Upper and lower gastrointestinal tract diagram, Guyton and Hall P753 (8).

The colon is arranged circumferentially around the abdomen; it begins with the caecum to the patient's right, which is connected to the small intestine by the ileocaecal valve. The caecum is void of haustrations (Figure 2.2), has the thinnest wall of the colon and the most at risk from perforation. The caecum becomes the ascending colon as it passes vertically towards the upper body. Below the liver the colon turns left and traverses the abdomen, this section is known as the transverse colon with the bend known as the hepatic flexure. The transverse colon is typically mobile (able to move locally) and highly variable in length. As the colon approaches the far side of the abdomen, it turns downwards and becomes the descending colon. This bend is known as the splenic flexure as it is situated just below the spleen. As the descending colon enters the pelvic inlet it bends in an "S" shape, this is known as the sigmoid colon, which attaches to the rectum, (5). An illustration of the colon can be seen in Figure 2.3.

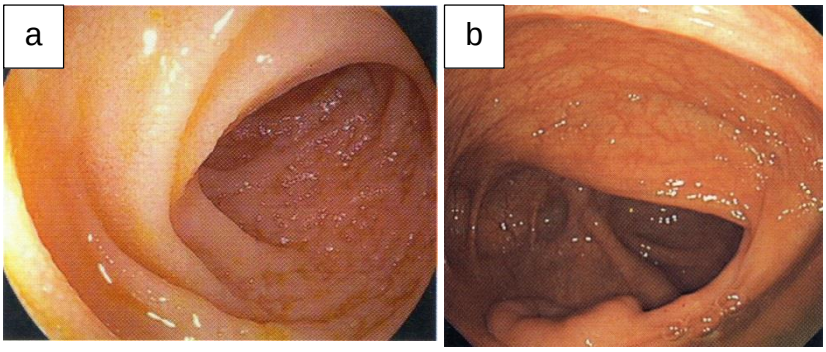

Figure 2.2 Haustrations seen in the colonic passage. a) haustrations along the colon wall b) caecum walls relatively void of haustrations. The photograph shows the triangular appearance to the colonic passage when viewed from inside. Meinhard P22, P147 (1).

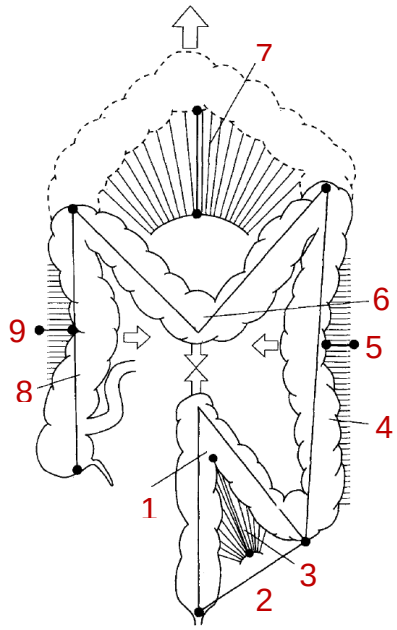

Figure 2.3 Schematic representation of the colon, Saunders et al. (9) The arrows represent the directions in which the bowel was displaced during the study on bowel length. 1) Maximum length of rectum and sigmoid colon. 2) Symphysis pubis-sigmoid/descending junction. 3) Maximum length of sigmoid mesocolon. 4) Length of descending colon. 4) Maximum length of descending mesocolon. 6) Maximum length of transverse colon. 7) maximum length of transverse mesocolon. 8) Length of ascending colon and caecum. 9) Maximum length of ascending mesocolon.

The colon becomes obstructed at the flexures with the soft tissue wall overlapping, blocking or partially blocking the passageway. In particular, the splenic flexure forms an acute angle as the end of the transverse colon overlaps the beginning of the descending colon, causing the flexure to “collapse” upon its self. These two colon sections may be attached making opening the flexure particularly challenging. The sigmoid colon may rise

above the pelvic inlet in some cases and typically remains folded with the start and end relatively fixed, (5).

A study by Saunders et al. (9) assessed the degree in which patient's colons were mobile through intraoperative measurements. A mobile colon is described at not being attached through tissue to the abdominal cavity wall, allowing the colon to move locally. 83% of patients had a mobile sigmoid colon, while 20% of patients had a mobile splenic flexure. The mean colonic length was 114.1cm with a range of 68 – 159cm. The length, position and size of the colon cannot be determined from outside the body without aids such as CT scans. Figure 2.4 shows the mean length and range of lengths for colon sections as measured by Saunders et al. (9), it can be seen that there is a large range in colonic geometry. Although larger (i.e. adult males vs females) people may have a larger colon, there is no evidence showing a strong correlation from which estimates could be built. The image in Figure 2.4 shows a schematic of the colon with annotations for anatomical landmarks. The variance in the geometry of the colon provides a challenging environment to navigate. Sections may be fixed in place preventing ease of opening or mobile such that they move with any progression attempt; both of which can make inspection difficult. Inspection methods are discussed later in this chapter.

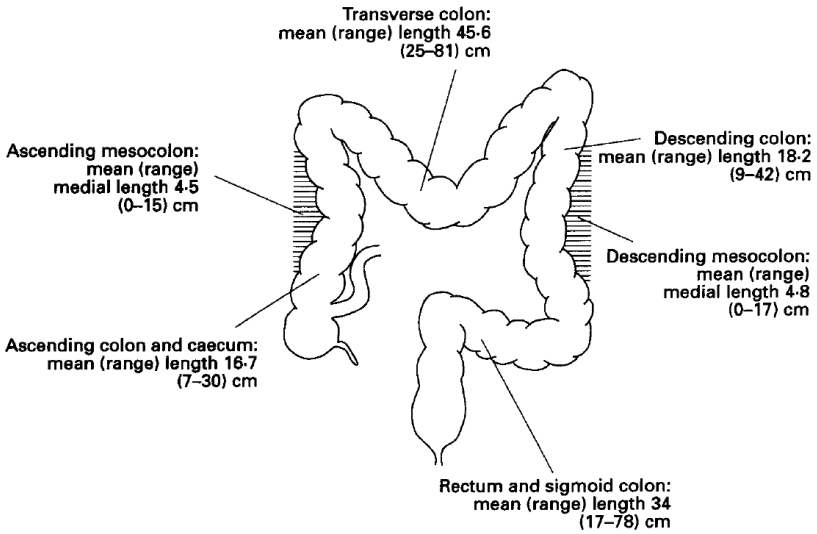

Figure 2.4 Schematic showing the mean length of colon sections and length range in parentheses, as measured by Saunders et al. (9)

Figure 2.5 shows the distribution and range of colonic radius as determined from CT images made available by the Cancer Image Archive (4). It can be seen that there is a normal distribution to the radius of the colon with 90% of measurements in the range of 10-25mm.

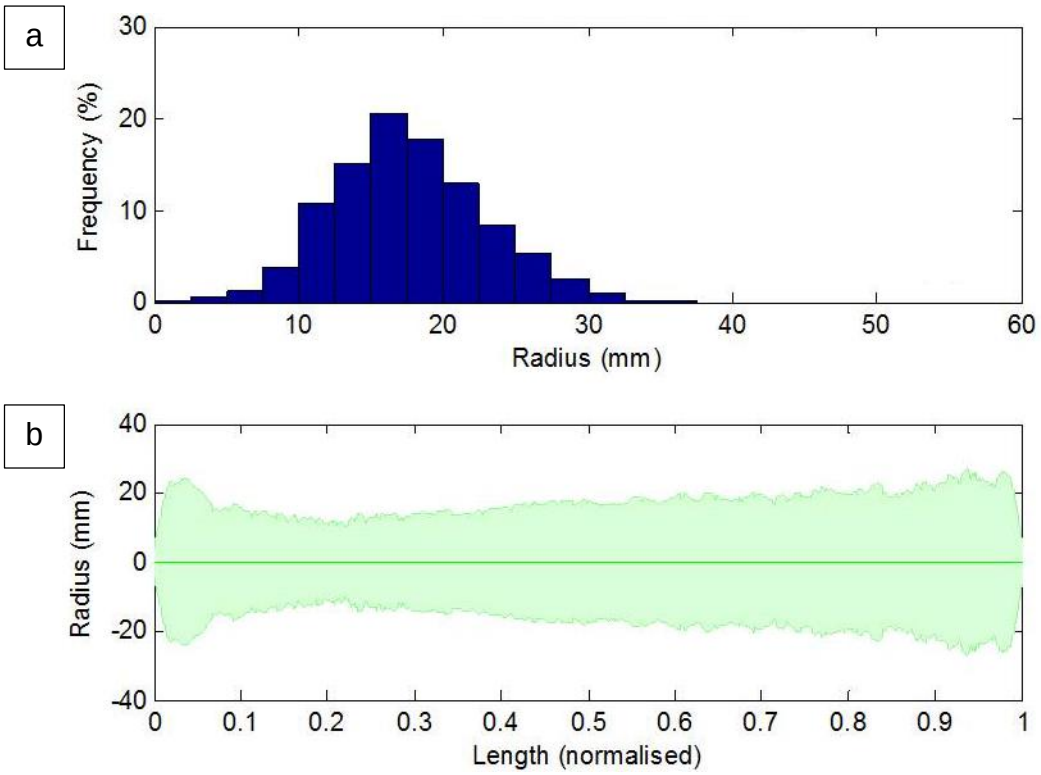

Figure 2.5 Spread of colonic radius a) and radius change along colon length b).Data extracted from CT scans made available from Cancer Image Archive (4), work carried out by Dr P Culmer and Dr A Alazmani as part of CoDIR. Work currently unpublished.

2.2 Colonic Ailments

The colon plays a vital role in the digestive process and ailments within it can have detrimental effects on the health and quality of life of the patient. While there are numerous issues which may arise with the colon, polyps are the most common, and often the precursor to cancers, (1). It is estimated that 31.9% of colonoscopies result in polyp removal (10).

Colorectal polyps (Figure 2.6) are raised intrusions into the colonic passage on the mucosa lining. While they are mostly singular and isolated, some may become malignant. Polyps can be found in the bowel of patients of any age and are most numerous in adults over 50 years of age. Pre-cancerous lesions can be found in up to a third of all adults. It is estimated it can take 10 years for a polyp of 10mm or larger to develop into an invasive cancer. The most common symptom of colorectal polyps is anaemia, caused by rectal bleeding (Figure 2.7) (1), which is easier to detect that visible bleeding. Screening looks for “occult” blood in the faeces to aid with diagnosis.

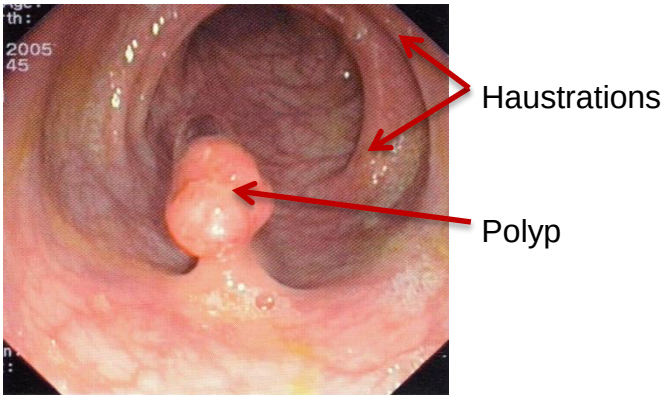

Figure 2.6 Polyp and haustrations of the colon Meinhard P602 (1).

Figure 2.7 Small asymptomatic cancer in the large intestine. The most frequent symptom of bowel cancer is bleeding, as seen in the photograph. Meinhard P605 (1)

While polyps may develop into cancers in any human, certain genetic traits may make specific patients more at risk to polyps and the development of such into malignant lesions. Colorectal cancer was the third biggest in terms of diagnosis of cancers in the US between 2006 and 2010, accounting for 8% of cancers (11). Globally in 2008, colorectal cancer accounted for 9.7% of newly diagnosed cancer (12). First and second place were lung (12.7%) and breast (10.9%) cancer respectively. Worldwide colorectal cancer is the 5th largest in terms of mortality, with an estimated 600,000 (8%) deaths in 2008 (12).

Diverticular disease is the presence of small hernias in the colon, which penetrate the mucosa (Figure 2.8, Figure 2.9). While it can be inherited, this is rare and most cases are acquired through low fibre diets. These hernias may cause pain and the feeling of being bloated and often result in thickening of the muscle wall around the affected area. In some cases, diverticulas may become infected with bacteria and become inflamed, known as diverticulitis. Diverticulitis can result in abscesses in the colon, fever, colonic bleeding and bowel perforation. Diverticulitis often starts as a single

site and spreads to the adjoining colonic tissue. Due to the increased risk of bleeding and perforation, colonoscopy procedures are often aborted when it is detected, (1).

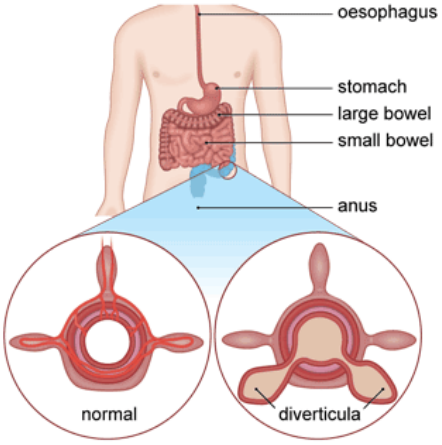

Figure 2.8 Schematic showing diverticula, image: BUPA (13)

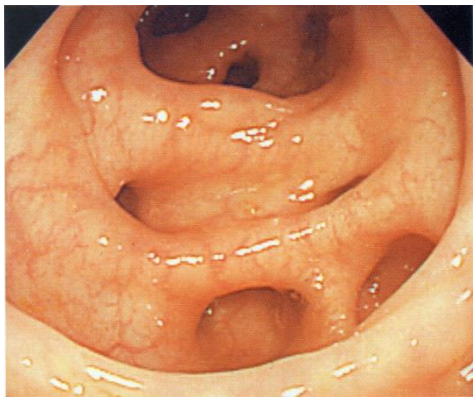

Figure 2.9 Severe diverticulum. These can pose a difficult challenge to navigate a colonoscope along the passage. Meinhard p143 (1)

Inflammatory bowel disease (IBD) is a term that covers two distinct disorders, ulcerative colitis and Crohn's disease. Either disease can be diagnosed through visual inspection and biopsy, (1)

Ulcerative colitis (UC) begins in the rectum and proceeds to spread along the colon. As the disease progresses the bowel mucosa becomes a single inflamed ulcer (Figure 2.10) which bleeds on contact with either stool or a colonoscope. The disease causes irritation to the bowel resulting in diarrhoea often containing blood and pus, and abdominal pain (1).

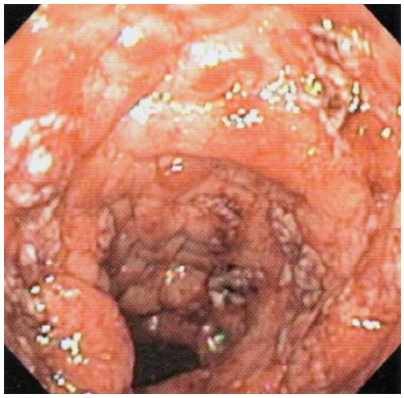

Figure 2.10 Inflamed mucosa of a colon with ulcerative colitis, Meinhard P622 (1).

Crohn's disease (CD) is most severe in the caecum and causes large lesions or ulcers to protrude from the mucosa, which resemble a "bear claw". Unlike the other ailments mentioned Crohn's disease may affect any part of the GI tract, (1). CD is most severe in the terminal ileum, caecum and ascending colon, where large ulcers form in bands separated by healthy tissue. These ulcers as they grow can adhere to form stellate ulcers, as seen in Figure 2.11. Advanced stages of the disease may result in sporadic haemorrhaging from ulcers and surrounding tissue, which can result in dark or black coloured stool.

Figure 2.11 Crohn's disease. Many ulcerations and sporadic haemorrhaging can be seen. Meinhard P624 (1)

While the aforementioned is not a complete list of the aliments that affect the colon, they are the more common and clinically relevant issues. Due to the location of the colon within the body, the clinician requires specialised instruments to assess and threat the colon.

2.3 Current Colonic Investigation Methods

Modern colonoscopy dates back to 1964 when the first colonoscope was produced by Olympus Optical as a tool to visually inspect the inside of the

colon. Although the design is approximately the same, advancements have improved the camera field of view, currently 140°, and flexibility, 160-180° (1).

The modern colonoscope, as seen in Figure 2.12, consists of a long flexible tube, approximately 1700mm long and 13-15mm diameter, with a fibre optic camera and light source mounted on a flexible tip (Figure 2.13). It has one or more accessory channels along the length for the insertion or removal of gas or fluids, and insertion of instruments for taking biopsies (tissue samples) for diagnosis.

Figure 2.12 Typical modern colonoscope. Device shown is an Olympus EVIS EXERA II, © Olympus America Inc. Annotations show: 1) Camera interface connection. 2) Handheld operating controls and accessory channel inlets. 3) Flexible tube. 4) Controllable tip with camera.

Figure 2.13 Maximum flexion in a modern gastroscope and endoscope (1)

The colonoscopy procedure is performed by inserting the colonoscope into the colonic lumen per rectum and advanced along the colon to reach the caecum (Figure 2.14). The primary inspection of the colon mucosa is carried out during the removal of the colonoscope by pulling it backward through the colonic lumen. The procedure is widely regarded as the gold standard for

screening, surveillance and diagnosis of colorectal ailments such as cancer, (1-3, 14). Procedure length ranges between 30 to 60 minutes depending on the patient and the clinician. The most complicated, and time-consuming step is caecal intubation with the retraction and removal of the colonoscope taking around 6 minutes (1).

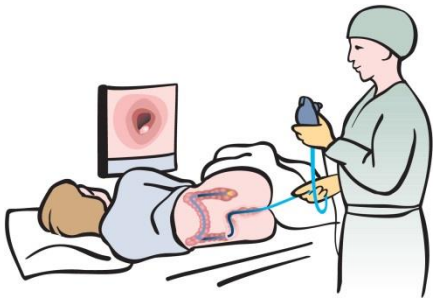

Figure 2.14 Illustration of the colonoscopy procedure, showing patient on their left side as the clinician inserts the colonoscope. Image: Cancer Care Manitoba, cancercare.ns.ca

Colonoscopy typically involves inflating the colon with carbon dioxide to allow clear imaging throughout. The colon does not have any structures to maintain a clear passage throughout, after removal of faeces the colon typically collapses. To allow the clinician to obtain clear images of the colon CO_2 is passed into the colon via one of the passages on the colonoscope. CO_2 is used over air as it is absorbed into the blood supply, whereas the N_2 in air (approximately 70%) is not absorbed. Gas remaining in the colon causes discomfort and is not easily passed, (1).

There is insufficient data to be able to establish how many colonoscopies are performed globally each year, however a study by Blotiere et al. (15) states over 1.2 million are undertaken each year in France alone. With colonoscopy being the major form of diagnosis of colorectal cancer, and an estimated 1.2 million cases of colorectal cancer diagnosed world-wide in 2008, (12), it can be safely assumed the number of colonoscopies performed globally each year far exceeds the millions mark.

The UK Colonoscopy study by Gavin et al. (6) shows 822 (4.1%) cases of cancer diagnosis, 1445 (7.2%) patients with IBD and 2741 (13.6%) with diverticulosis. Colonoscopy plays a huge part in the detection of bowel disorders and the removal of polyps has been shown to reduce the chance of bowel cancer developing (16). From this, it can be understood why colonoscopy is widely regarded as the gold standard for surveillance and inspection of the colon for disease.

2.4 Complications with the Traditional Colonoscopy Procedure

While the use of colonoscopy is well established in clinical practice, there are significant drawbacks. These include discomfort; the need to purge the bowel of its content prior to examination; the need for trained personnel; and the possibility of complications and failure to complete the procedure. A prospective study of colonoscopy provision in the UK reported the outcomes of 9223 procedures, Bowles et al. (17). It was revealed that in 23.1% of cases there was a failure to advance the colonoscope along the entire length of the colon. Where this occurred, the reasons given were: patient discomfort (35%); “looping” (30%); and poor bowel preparation (19%).

Of the patients in the study by Bowles et al. (17), 1.2% were admitted to hospital within 30 days for reasons relating to colonoscopy such as abdominal pain; and 13 patients suffered from bleeding due to the procedure. While these figures are small, the tales of discomfort, lasting pain and bleeding may be a factor that influences people to skip appointments and miss procedures. As previously stated, in terms of detecting colorectal cancer, screening is required to assess polyps and perform biopsies if needed.

A study was carried out on 20,085 colonoscopies performed in the UK (6), which reports the success rate to advance the colonoscope to the caecum (caecal intubation rate) at 92.3%. Of those which were not successful, 1553 procedures were not completed due to looping or discomfort (49%); obstructions (25.9%); poor bowel preparation (22.2%); the remaining unsuccessful procedures were due to severe disease or other complications. 52 of the procedures resulted in internal bleeding while a further 8 of the procedures resulted in perforation. A separate survey of 1351 colonoscopies (18) carried out looking at caecal intubation rate and reports 95% of all procedures resulted in reaching the caecum.

In patients with IBD, there is an increased risk of perforation (19, 20). For the patients who suffered from perforation there was not an increased rate of mortality however they did undergo surgery with an increased rate of suffering from post-procedure complications.

Looping is the term used when the colonoscope forms a loop or partial loop. It occurs when advancement of the colonoscope at the rectum results in no advancement at the tip, (1, 21, 22). Typically, this is because the tip is lodged in the colon, typically at an obstructive location such as the splenic

flexure. Simply pushing the colonoscope harder at the rectum may result in bowel perforation. Perforation may also occur due to rubbing of the colonoscope shaft against the mucosa, the friction between the two causing abrasive damage. In patients with a non-mobile sigmoid there is a much greater chance of perforation due to the complexities of navigating an S shaped bend through pushing at the anus alone, (1).

Cheng et al. (23) discusses means of preventing loop formation though adaptations to the colonoscope. Shape locking sections have been used to allow the colonoscope to pass through the sigmoid once successfully navigated while reducing force on the sigmoid (Figure 2.15). This approach does not aid loop reduction once the sigmoid has been passed and requires extra time to set up. Computer controlled colonoscopes have been tried too, with little success. The authors conclude that future systems should be capsule based over modifications to the existing colonoscope.

Figure 2.15 Shape locking guide (USGI Medical Inc.). Guide (seen in blue) can be used alongside a traditional colonoscope (shown in black) to allow easier passage through the sigmoid. Using a handle (shown bottom of photograph), the shape locking mechanism can be engaged once the guide is deployed in the desired position.

2.5 Hydro-colonoscopy

Hydro-colonoscopy is colonoscopy carried out using a fluid as an insufflation medium as opposed to a gas. A randomised trial carried out in the United States (24) shows that caecal intubation rates are higher in hydro-colonoscopy procedures than standard gas inflated procedures. Similarly a

separate study (7) reports ease of caecal intubation when using warm fluid or corn seed oil. The oil provides lubrication as well as relaxing the bowel.

Not only does relaxing the bowel aid caecal intubation (25), it was found that gas inflation extends the length of the bowel meaning a greater distance must be covered to reach the caecum (26). Fluid based insufflation methods do not have the same extension side effects, providing a shorter passageway to navigate.

Through clinical trials carried out by the CoDIR team, it was found a warm isotonic fluid relaxed the bowel more so than CO_2, while providing a high degree of colon distension. The colon is more used to being in contact with liquid mediums than gas and may decrease muscle spasms throughout the colonoscopy procedure.

2.6 Colonic Damage

The colon is a delicate organ and can be damaged easily, perforation of the colon can occur through colonoscopy procedures (1, 15, 19, 20, 27). A study carried out by Blotiere et al. (15) covering 947,061 colonoscopy procedures undertaken in France in 2010 reveals a perforation rate of 9.7 per 10,000. This is higher than the 8 cases out of 20,085 in the study carried out by Gavin et al. (6), however the occurrence is still rare at less than 0.01%.

As previously stated, diseased colons are at a higher risk of perforation (19, 20), Blotiere et al. states clinicians with limited practice at the procedure also increase the risk of a patient suffering a perforation during colonoscopy (15). This level of human error is something that a robotic system would aim to reduce.

The contact pressures that result in damage to a colon are widely unknown due to lack of knowledge of the mechanical properties of human colonic tissue. A study carried out by Shiels et al. (10) examined the pressures involved in causing perforations in porcine colons. The authors noted that a pressure of 120 mm Hg (16kPa) of fluid resulted in a perforation of a porcine colon, compared with air where perforation occurred at 108 to 145 mm Hg (14.4 to 19.3 kPa) depending on the inflation method. The authors note that air inflation is safer than fluid due to the higher pressures tolerated and perforations being smaller and reduced faecal spillage. This contrasts with the evidence that fluid insufflation in colonoscopy aids the procedure (24-26) and is better tolerated. With lower fluid pressures needed to insufflate the

colon, these operational fluid pressures are further from critical pressures than with gas insufflation.

The contact pressures required to puncture or perforate a colon will vary along the lumen as the wall thickness and muscle density changes. The caecum has the thinnest walls and is more susceptible to perforation (1). This would lead to expectation that the majority of perforations occur at this site; however this is not the case with perforations being most common at flexures (1).

The pressures required to perforate the colon are dependent on the surrounding tissue and the support it gives. A taut colon is likely to be at greater risk of perforation from point loading than a relaxed colon, due to the ability to stretch. Coupled with the method of steering the colonoscope, this adds explanation to why flexure sites are most prone to perforation. Similarly sharp points are of higher chance of causing perforation than blunt objects. Taking the pressures reported by Shiels et al. (10) and assuming an even colonic wall thickness throughout and a linear pressure distribution, a minimum pressure to cause perforation was taken to be $14kN \cdot m^{-2}$ (14kPa). Taking a colonoscope of 15mm diameter, this would calculate to be 2.5 N applied to the colonoscope in order for the tip, when rested flat against the colon, to perforate the colon.

2.7 Locomotion Methods

Before designing a locomotion system for a hydro-colonoscopy device it is important to understand the methods of locomotion established and used in vehicular and robotic applications.

2.7.1 Bio-Inspired Locomotion Methods

Nature provides a rich supply of developed and optimised locomotion systems. The most prevalent land type locomotion is crawling or walking, and for fluid based locomotion is swimming.

Although from initial inspection marine animals appear to move in very similar methods, the range of mechanics involved in swimming ranges greatly. Sfakiotakis et al. (28) carried out a review of the numerous modes in which fish swim. Muller et al. (29) assessed the hydrodynamics of the swimming methods used by fish and effects of the body size upon the locomotion method. Adult fish are able to coast longer distances and use less relative energy than infants; similarly, larger species exert less energy than small species for the same distance travelled. The authors note that

Reynolds number plays a large role in the ability to coast. There are of course other methods used by marine life, such as the jet type swimming of squid.

Typical fish-like swimming requires forward locomotion to turn; they are unable to turn on the spot, with few fish being able to reverse (28, 29). Fish inspired robots that have been used for inspection were typically designed as such for aesthetic purposes or the studying of fish themselves, Figure 2.16, (30-32).

Should a fish inspired locomotion system without reverse swimming abilities be deployed for colonic inspection there is a chance it may get stuck in a cavity formed at haustrations or diverticulas. Swimming strategies using fins or tails may also be unable to pass strictures, as these block the sideways motion required for generation of thrust; or pass non-fluid filled sections.

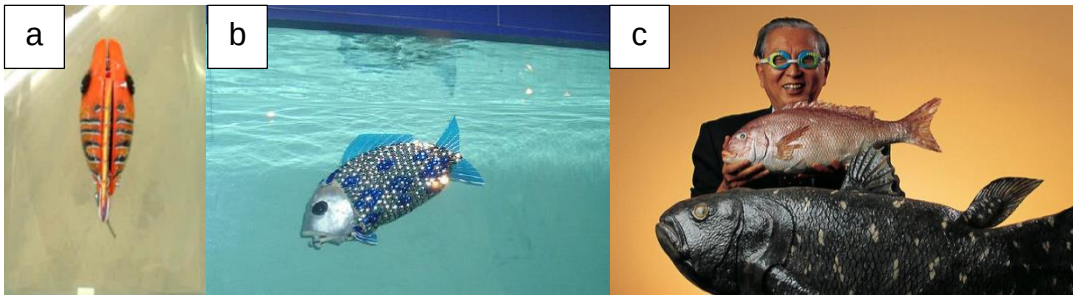

Figure 2.16 Fish inspired robots. a) Mobile fish robot, Xiaobo et al; (30). b) Autonomous fish robot, Huosheng et al. (31); c) Sea bream robot, Terada et al. (32).

Biologically inspired amphibious systems are numerous and many take the form of serpentine locomotion. Snake or serpentine-like locomotion systems are often used on robotic platforms for inspection purposes, as discussed by Hirose and Mori (33). While some are limited to a single medium for locomotion (34), other variations of the serpentine like locomotion system have been developed using wheeled body systems allowing full amphibious locomotion, such as those by Crespi et al. (35) and Shumei et al. (36) (Figure 2.17). These systems reduce the drag between the body sections and the surface along the length of the device using passive wheels. The coefficient of friction between the body sections perpendicular to the length of the device remains high, allowing the system to move. The passive wheels replicate the scales on a serpent's body while allowing for both forward and backward locomotion; a serpent's scales disallow backwards locomotion.

Serpentine locomotion also works in swimming situations, allowing for amphibious locomotion using a single method of articulation. A commercial example of this is the ACM-R5H (37) from HiBot Corp. The device is formed from several sections containing motors and batteries, each 80mm diameter and 170mm length, which are sealed to prevent moisture and dust penetration.

Figure 2.17 Serpentine robots. a) Lamprey based robot by Ayers (34); b) Passive wheeled system, Crespi et al. (35); c) Amphibious wheeled snake robot, Shumei et al. (36); d) ACM-R5H (37), HiBot Corp.

Placing aside the mechanical constraints and limitations of fitting the required actuators within a serpentine system for use in colonoscopy, the locomotion system requires a large sideways sweep of the body to progress longitudinally. This lateral movement is greater than the mean colonic diameter of approximately 40mm, rendering the locomotion system infeasible. This sweeping motion of the chassis will cause any camera view to move; limiting the ability to move closer to an object of interest without losing sight of it. The confined environment of the colon would also impose difficulties on a serpentine like locomotion system, hindering its ability to progress and traverse the colon.

2.7.2 Pipe Inspection Locomotion Systems

The colon is more similar to a pipe than a flat surface and therefore a review of pipeline inspection locomotion systems was undertaken. Pipe and pipeline inspection robots fall into 6 major categories: pig, wheeled, tracked, crawling, inchworm and screw type, as defined by Roh et al. (38). Pipeline inspection gauge (PIG) devices move along a passage by forming a seal against the pipe surface and through a difference in pressures between the sides move along a pipe, Figure 2.18a. Wheeled (Figure 2.18b) and tracked (Figure 2.18c) devices move by traction between the surface and their associated rotating components, with motion perpendicular to the rotation of the wheel or track. Crawling devices use legs or appendages which form a static contact point against the surface allowing some form of leverage to move the device along, Figure 2.18d. Inchworm devices use a set of two or more independently gripping sections separated by a variable length

actuator, in alternating which side grips and controlling the length of the attachment the device moves, Figure 2.18e. Screw based devices contain a helical outer body which when rotated against the pipe surface causes it to move along the pipe, Figure 2.18f.

The market is full of pipe inspection robots using wheels or tracks which operate within the pipe or grip to the pipe's outer surface, as reviewed by Roman and Pellergino (39). Pipeline inspection robots are primarily designed to allow continuous operation of the pipeline: i.e. not blocking the flow of gas or fluid through the pipe.

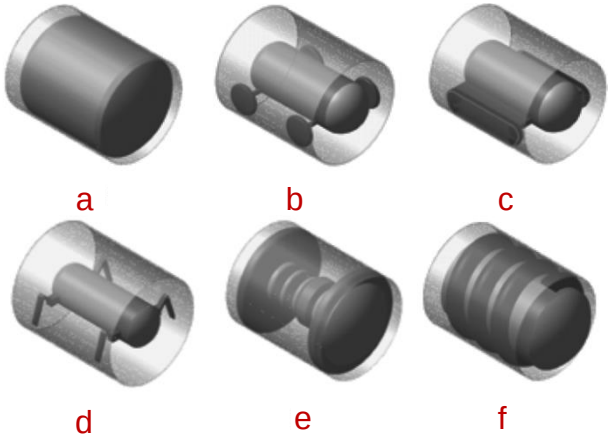

Figure 2.18 Pipe inspection robot locomotion types, adapted from Roh et al. (38) Showing: a) PIG; b) Wheeled; c) Tracked; d) Crawling; e) Inchworm; f) Screw.

The pig (pipeline inspection gauge) locomotion system, involves a smooth sided device of equal outer diameter to the inner diameter of the pipe being inspected. A pressure difference between the sides drives the device along the pipe.

Inchworm systems are typically used for pipe or shaft inspection and exploration, such as the device developed by Richardson et al. (40). The main advantage of an inchworm system is the point of contact between the device and the wall is static – leading to increased traction while reducing slippage. These systems typically have passive wheels which take the weight of the device, although not always. Choi et al. (41) developed an inchworm based system that traverses the outside of pipes, to allow surveying without disruption of the flow or pressure.

The inchworm wall pressing technique can be combined with wheels or tracks to maintain constant traction, such as on the commercially available inspection robot, MrInspect (Figure 2.19), Roh et al. (38). The advantage of

such is they can deal with changes in diameter of the pipeline. The wall push system also allows the device to maintain a central position within the pipe, this can be ideal for steady, vibration free video feed as well as for navigating past obstacles.

Figure 2.19 MrInspect IV, Intelligent Robotics & Mechanical System Laboratory School of Mechanical Engineering, Sungkyunkwan University, Korea.

2.7.3 Hybrid Locomotion Systems

A common requirement across all locomotion systems is the need to provide sufficient thrust or traction for controlled motion. Many specialised devices and locomotion systems are optimised for their designated environment and such become ineffective outside their designated environment. Amphibious devices are developed such that they can function in several environments. While adding wheels to a boat is a simple solution to producing an amphibious system, it is not elegant. One mode affects the other negatively: the wheels increase drag in fluid and the propeller provides limitations to the clearance on land. Jiancheng et al. (42) attempts to remove this limitation by combining the wheels on the developed device with propellers. Wheels with purpose shaped spokes can be rotated 90° such that they lay perpendicular to their original position allowing them to act as propellers moving the device in the same direction as on land when in fluid (Figure 2.20).

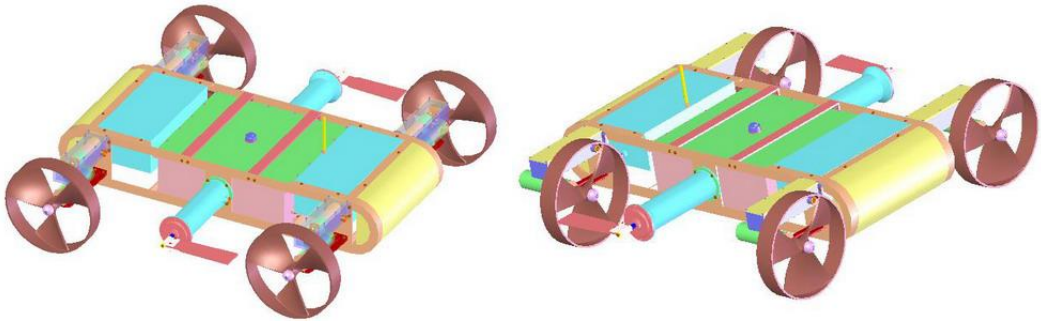

Figure 2.20 Wheel propeller hybrid device, Jiancheng et al. (42)

While the concept developed by Jiancheng et al. (42) is able to use the same drivetrain to power both modes of locomotion, it requires discrete switching between modes; there is no middle ground. The Ice Challenger team (43) developed an amphibious craft that is able to use the same locomotion drivetrain for both land based and fluid based locomotion. The developed craft “Snowbird” uses two Archimedes’ screws located at either side of the vehicle, which span the entire length to provide locomotion (Figure 2.21). Screw based locomotion is not suited for use on hard surfaces or over long distances as noted by the team (43), and so caterpillar tracks were added to the underside of the vehicle to allow the device greater manoeuvrability over distances.

Figure 2.21 Screw based locomotion: Snowbird 6, Ice Challenger team (43)

Using a similar locomotion strategy to that used in Snowbird, an amphibious device was developed by Liang et al. (44) (Figure 2.22). The device was developed for surveying of water and would need to traverse loose or unsteady ground, which would make wheels impractical. The authors note that their original device was too long for use on uneven ground, as the screws would not have enough contact to provide useful locomotion: the craft could become grounded over concave sections of terrain, or steep changes in terrain elevation.

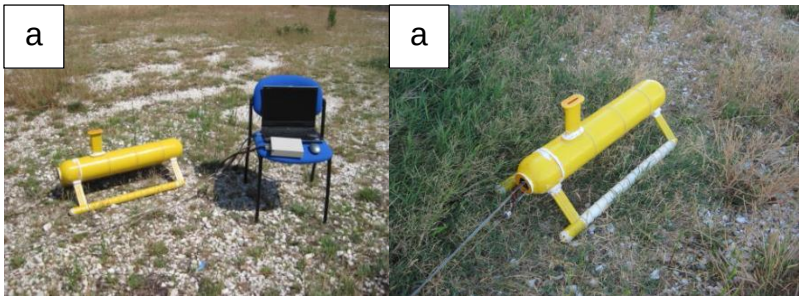

Figure 2.22 Screw based amphibious device, Liang et al. (44)

A means of avoiding becoming grounded can be as simple as shortening the length of the screws. To be able to provide greater controllability, articulated sections can be added each with their own set of screws. Liedke et al. (45), developed a device which uses multiple modules: the system is able to reconfigure itself through attaching or detaching modules, as shown in Figure 2.23. Multiple modules can compensate for the smaller and weaker drivetrain each unit possesses.

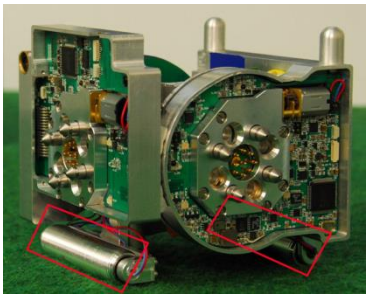

Figure 2.23 Modular screw drive device, Liedke et al. (45) showing screw based locomotion highlighted in red

The benefits of screw based locomotion over wheel based locomotion on soft ground are discussed by Nagaoka et al. (46) (Figure 2.24). While a wheel once sunk past 1/2 of its diameter into a ground medium becomes stuck, an Archimedean screw can continue to operate while completely submerged in a ground medium. This is particularly important when the vehicle or device is operating on soft soil or sand where the chance of submerged locomotion units is high and manually retrieval is difficult. An example would be the Mars Exploration Rover Spirit (MAR-A) which became stuck in quicksand in 2009 (47) when its wheels sunk too far into the Martian soil. A screw based locomotion system would have been able to escape this fate by being able to continue locomotion through the quicksand.

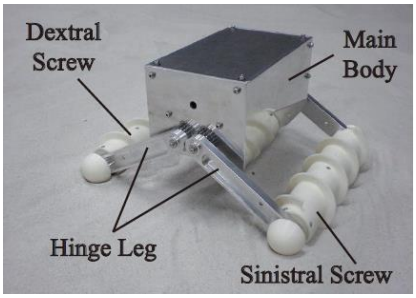

Figure 2.24 Screw Drive Rover, Nagaoka et al. (46)

Screw based locomotion for displaceable terrain can be traced back to the early 1900s though several patents on vehicular systems (United States patent numbers: US635501, US669210, US864106 and European patent number GB18674). These patents cover the use of Archimedes' screws providing locomotion on mud and snow, typically for agricultural and forestry purposes. The large surface area between the screw and the terrain aids the spreading of weight reducing the displacement into the terrain. Coupled with a screw's ability to provide locomotion even when entirely buried these vehicles were able to outperform wheel-based vehicles. However, their low efficiency on firm or solid ground has led to their overall demise with very few agricultural vehicles making use of Archimedean screws now. Large wheeled and tracked vehicles are now used in these situations and have a higher efficiency on solid ground.

Figure 2.25 shows original diagrams submitted alongside patents US635501 and US669210. It is interesting to note that the screw's poor performance on solid terrain was noted through the designs with the inclusion of wheels. These wheels allow for locomotion on roads while the screws allow the devices to traverse otherwise impassable terrain, resulting in amphibious locomotion.

During the 1960s and 1970s, several screw based amphibious vehicles were produced, such as The Marsh Screw Amphibian by Chrysler Corporation (Figure 2.26), for commercial and military purposes. The vehicles were able to traverse water expanses as well as marsh or bog land (48). Modern vehicles built for this terrain are often of the hovercraft nature; however, this mode of locomotion is not suitable for colonoscopy. Hovercraft vehicles are not able to operate while submerged and such are not suitable for use within hydro-colonoscopy.

a

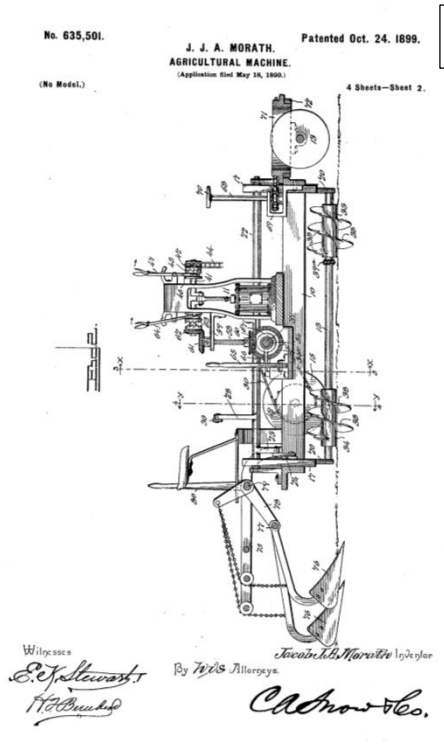

b

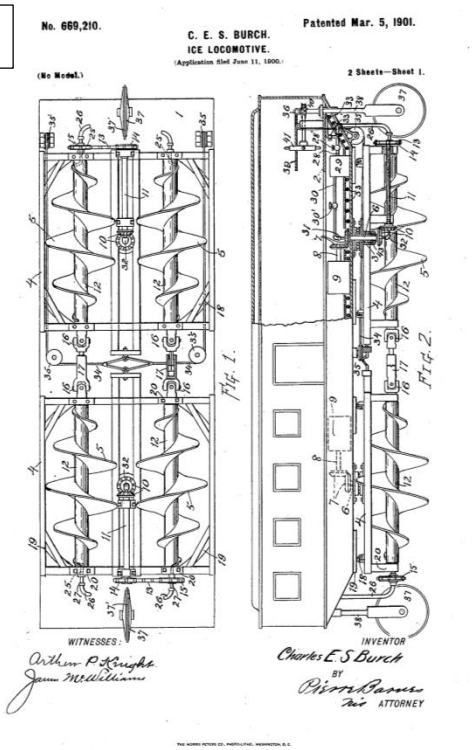

Figure 2.25 Screw locomotion patents. a) Patent US635501. Jacob J A Morath, Oct 24, 1899. b) Patent US669210, Charles E S Burch, Mar 5, 1901

Figure 2.26 The Marsh Screw Amphibian by Chrysler Corporation

2.8 Next Generation Colonoscopy Methods

While there are no commercially available colonoscopy robots, there is research into such system by several researchers. In this section, locomotion systems of surgical devices will be assessed for their practicalities and merits for use on a colonic investigation device. To understand the current level of acceptance of robotic apparatus in surgical procedures a short review of commercially available robotic surgical units

was carried out. This can aid the critical assessment of proposed systems and later aid the development of new systems.

2.8.1 Surgical Robots

Robotically assisted and robot performed surgical procedures are becoming more commonplace within today's healthcare systems. There are many tasks, which can be carried out by robots to a greater degree of accuracy than humans. The use of robotic devices can ease the procedure difficulty or reduce risks of complications. In understanding how robots have been accepted into surgery and the current view upon them can aid the development of future systems.

Ortiz-Oshiro et al. (49) discusses the advantages of robotics in regards to laparoscopic surgery. While the field of surgery is different to colonoscopy, there are more widely developed robotic systems for this area, which can show an improvement to traditional methods. It is interesting to note that the acceptance of robotic systems, such as the da Vinci® Surgical System by Intuitive Surgical (Figure 2.27), and their reduction in training times for procedures is promising to the field of robotic surgical devices as a whole. Initially the costs may be higher but as the usage increases such robotic systems will reduce in price per operation as well as overall effectiveness of those using them will increase.

Jayne et al. (50) discusses that while these robotic systems reduce trauma due to smaller access areas needed, the lack of haptic feedback to the clinician can be a strong disadvantage. Collisions between the robotic arms and those around them can cause other potential issues in the operating theatre. The operating clinician is not looking at the robot and does not know if their next movement will cause a collision between another member of staff in the room and the device. While collisions can be reduced through protocols and training for those working around the robotic device, the loss of depth perception and haptic feedback cannot be overcome so easily.

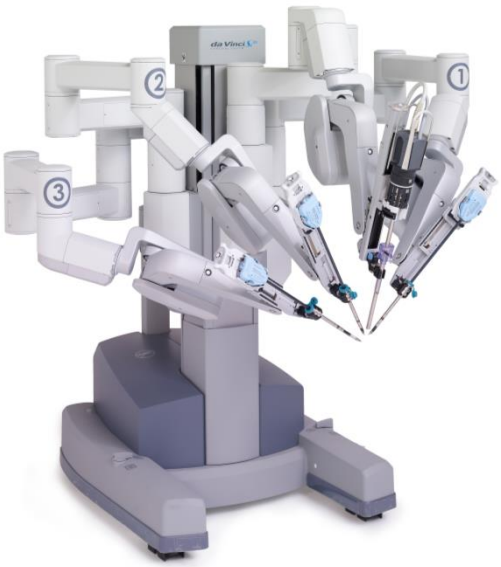

Figure 2.27 Da Vinci® surgical system, © 2015 Intuitive Surgical Inc.

2.8.2 Passive Capsule Systems

This section will cover devices aimed at replacing colonoscopy and provide rich data for clinicians in real-time. As a means of inspecting the lower GI tract there are several capsule devices that feature a single or dual cameras, such as PillCam® by Given Imaging (Figure 2.28), which stream back images at low rates: typically one image per 15 minutes. Capsule endoscopy carries a 1.5% risk of the capsule becoming stuck in the small intestine requiring removal either by surgery, colonoscopy or enteroscopy, Meinhard, P120 (1).

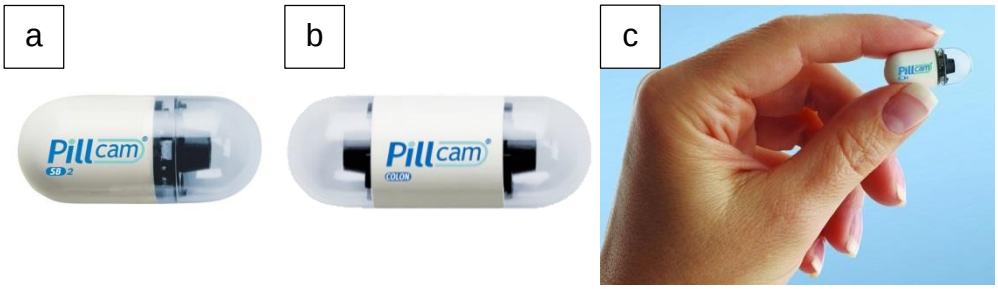

Figure 2.28 PillCam®, Given Imaging. Images show: a) PillCam SB®, a single camera capsule for small bowel inspection. b) PillCam Colon®, a two-camera capsule for large bowel inspection. c) Photograph of PillCam SB® held showing size of capsule.

A review of passive single capsule devices, such as PillCam® was carried out by Ciuti et al. (51). Non-drivable capsules are by design unable to control their view as they travel through the GI passage under natural peristalsis. Due to the high rate in which they pass certain parts of the GI passage, they require high frame rate video with a large depth of field to provide useful

images for a clinician. Although once the images have been obtained it can be difficult to accurately position each shot within the GI tract; leading to limited usage. The devices do have their uses though; they provide an easy way to assess the GI tract through a minimally invasive procedure. The patient does not even need to remain in the operating theatre or even the premises for the images to be collected.

2.8.3 Active Capsule Systems

While capsule systems are attractive due to their small size, their inability to control the direction of the camera and lack of tooling gives them only limited usability. Work has been carried out adding active systems to capsule based devices to allow for control over the camera direction and adding some tooling capability.

Menciassi and Dario (52) discuss the viability of two different active single capsule based colonoscopy robots developed by the authors alongside other researchers. The first system discussed, developed by Quirini et al. (53), uses shaped legs to allow the device to crawl along a lumen, Figure 2.29. The legs feature a passively compliant section midway allowing the leg to bed during the forward stroke. This section then locks in the backward stroke, forming a rigid length, allowing contact pressure between the leg and the colon to increase. The implementation of the legs raises concerns over possible perforation of the bowel if the muscle spasms or contracts. In making the device tether-less a secondary capsule was added to the rear to house the relatively large battery required for the system to operate. The authors calculated each leg needed 0.25N of thrust to allow the device to traverse the colon, 1.0N in total across the 4 legs. The system was designed to use shape memory alloy (SMA) actuators to power each of the legs, however through testing it was found that the actuators did not react fast enough to provide useful locomotion (2.7 cycles min^{-1}) and consumed a large amount of energy. The SMA approach was replaced with a conventional rotary motor and worm gear approach, however the power requirements were still too large to fit the power source within the main capsule and such a battery unit was added to the rear, as seen circled in Figure 2.29.

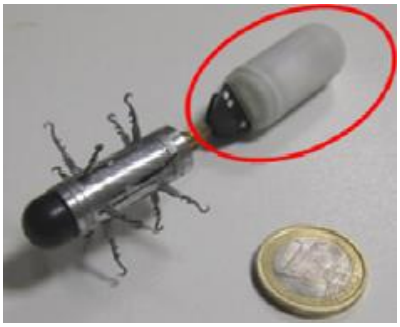

Figure 2.29 Legged based active capsule device developed by Quirini et al. (53) photographed next to €1 coin with battery unit circled in red.

A second system developed by Tortora et al. (54) was discussed by Menciassi and Dario (52) which uses four rear mounted propellers for locomotion through a fluid filled lumen, Figure 2.30. A swimming approach is stated to require less tissue manipulation than a crawling approach as it is presumed the colon will be inflated to an extent. A swimming device can operate with lower power output from its propulsion systems to move compared to a crawling system, allowing for a much more feasible approach than crawling for a small self-contained battery powered system. The lower thrust output does however limit the device in terms of its ability to pass strictures and collapsed sections of a lumen.

Tortora et al. (54) reported that the propeller device was able to propel through a PEG solution for 30 minutes averaging a velocity of 15mm·s^{-1}. The device was controlled wirelessly using a commercial joystick attached to a computer, and deployed using a modified gastroscope, Figure 2.30b. The authors however do not state the thrust output of the device.

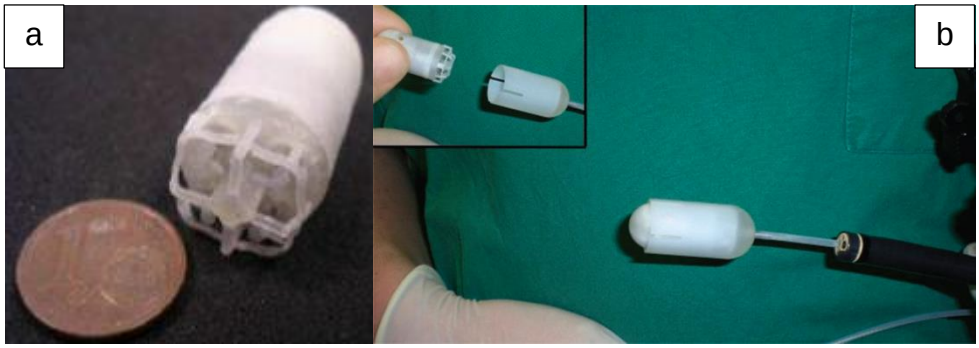

Figure 2.30 Propeller based active capsule, Tortora et al. (54). Showing a) (left) device shown next to one Euro cent coin, b) (right) device and deployment tool.

The feasibility of using multiple small capsule devices with one or two degrees of freedom which combine to form larger and more functionally complete robotic systems was discussed by Menciassi et al. (55). The previous two systems were covered alongside the means to attach modules

of different types together. While single module swallow-able devices can be used for diagnosis, the authors state that multi-module devices will be needed for more complex procedures if the overall platform should be small enough to swallow.

Menciassi and Dario (52) discuss a further single capsule approach which uses an external robotically controlled magnet to guide the capsule robot around the colon. This approach removes the need for actuators and locomotion systems within the capsule allowing either greater space for instrumentation or reducing the size of the device.

2.8.4 Robotically Controlled Colonoscope Systems

Capsule based systems have limited ability to carry out biopsies, especially if samples need to be stored on the device. The traditional colonoscope has a strong advantage here as an unlimited number of biopsies could be theoretically carried out. This is due to the specifically designed channel allowing the biopsy tool to be withdrawn and sample removed without removing the colonoscope. Several researchers have added robotic actuation to the traditional colonoscope to retain this functionality (23, 56-58), while increasing control over position and motion.

Externally controlled systems pose a means of producing a very compact capsule for internal investigation while maintaining a high degree of controllability. Combining this actuation method with a colonoscope could provide a much more ideal advancement method over the rear pushed method currently used. Valdastri et al. (56) discussed using a modified colonoscope with a soft tip and passive tether which may be robotically manipulated along the colon using an external magnet, Figure 2.31. The system uses existing means for biopsy already used in colonoscopy, with the colon being inflated with CO_2 as is typical with the current procedure. Arrezo et al. (58) carried out a study using this system and compared it to a traditional colonoscope. The authors set up ex-vivo porcine colons in a phantom model, with beads inserted to model polyps. Experts in colonoscopy and medical students with no previous skills in colonoscopy were given both the magnetic capsule and traditional colonoscope and instructed to explore the colon for polyps (coloured beads placed randomly for the trial). The operators was not given the position or number of polyps, which were randomised for each setup, and asked to locate as many as they could find.

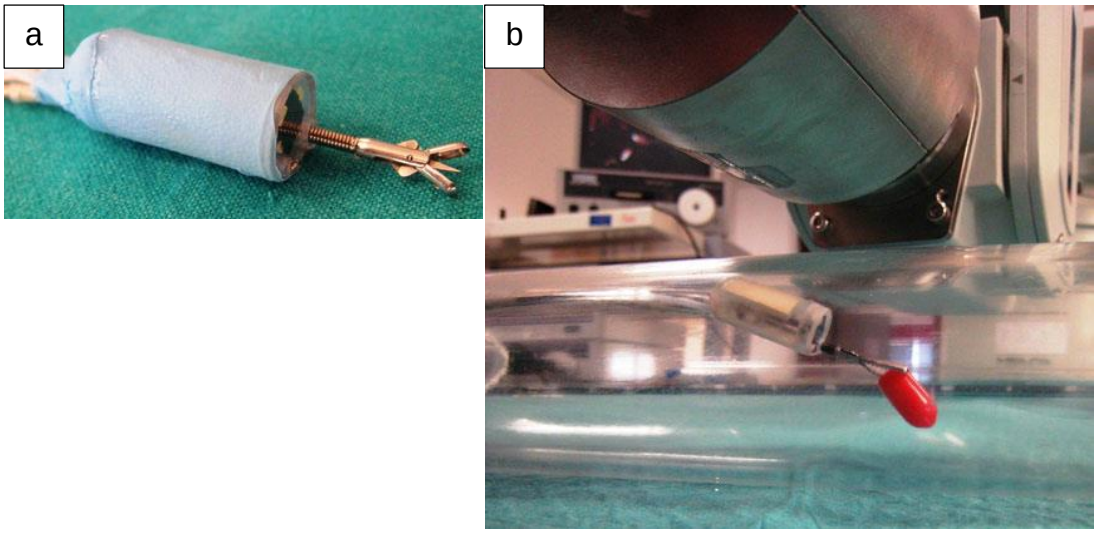

Figure 2.31 Magnetically guided colonoscope, Valdastri et al. (56) Showing (left) device on bench with tool deployed and (right) device suspended in a Perspex tube by the external magnetic manipulator.

For the colonoscopy experts the percentage of polyps found using the magnetic capsule was less than the traditional colonoscope, 74.2% compared to 83.9%. Interestingly the trainees attained the same detection rate for both the capsule and colonoscope, which is greater than the experts at 87.6%. The authors speculate that this may be because the experts performed the procedure quicker and may be prejudgmental of a robotic system. The artificially cleaned colon without peristalsis or patient comfort to consider may also attribute to why the trainees performed better.

Despite the reduced polyp detection by experts using the magnetically controlled system, it can be seen that robotic systems are viable, and as noted by Arrezo et al. (58) are more accurate in their movements when compared to the traditional colonoscope. Through greater use, it may be possible for experts to exceed polyp detection of traditional methods with robotically controlled systems.

2.8.5 Externally Actuated Robotic Systems

The use of external magnets for swimming is not a new idea and has been suggested for medical robotic devices for some time, such as the system developed by Honda et al. (59) in 1996. The developed system uses a permanent magnet attached to a coiled length of wire, such that rotating the external magnet causes the device to move in a spiral path through a fluid medium. This approach only works at low Reynolds numbers, where viscous forces dominate and inertial forces are negligible.

A bullet shaped device with a threaded nose was proposed by Ishiyama et al. (60) which is rotated by an external magnet to move. Although the device was tested, it had no ability to steer or carry on-board equipment such as cameras.

Sudo et al. (61) took the principle of using an external magnet and developed a system that oscillates as opposed to rotating (Figure 2.32). The developed system is formed by a small permanent magnet attached to a semi-flexible film, which acts as a tail. Through alternating the external magnetic field, the device swims with a basic fish-like motion. The original idea was to produce something to swim within blood vessels; however, the size of permanent magnets available restricts the system to sizes much greater than the majority of blood vessels within the human body.

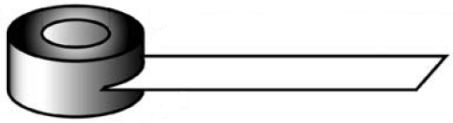

Figure 2.32 Oscillating magnetic device, Sudo et al. (61)

A similar device developed by Guo et al. (62) was used to assess the ability of permanent magnet swimming devices for surgical purposes (Figure 2.33). Although it is able to swim, it has limited ability to control in which direction it swims. The ability to corner is somewhat reliant on wall contact and as yet is far too large for the proposed intra-blood vessel task.

Figure 2.33 Oscillating magnetic device, Guo et al. (62)

The size requirements of the colon compared to blood vessels are not as restrictive and such a system may be a possibility for a colonic investigation device. The obvious reason not to use a system that oscillates or rotates is control. Both systems would provide very unsteady camera footage and pose complications in providing a stable platform for on-board tools.

A hybrid of the previously discussed external magnetic field controlled systems was developed by Qinxue et al. (63) (Figure 2.34). The system developed comprises of a helically rotating nose section with an oscillating tail section. Through positioning of several magnets, the system can rotate the nose section while oscillating the tail from the same alternating magnetic field. The screw-like nose is proposed to be able to overcome collapsed or blocked lumen while the tail can provide higher frequency fluid locomotion.

Figure 2.34 Hybrid magnetically powered device, Qinxue et al. (63)

The previous five systems mentioned rely upon the alteration of a magnetic field to move. Due to the way the two oscillating tail devices move, they are unable to reverse should they get stuck nose first into a recess. While the screw based devices could reverse by flipping the direction the screw rotates in, the tail on the device discussed by Qinxue et al. (63) will still drive the device forward. None of them have the fine degree of control that can be administered by the magnetically dragged device by Valdastri et al. (56). Simply magnetically dragging the device allows for greater dexterity over using magnets to power an on-board locomotion system, albeit through the use of expensive and large external manipulators.

Palagi et al. (64) took an oscillating tail fish-like concept and produced a paramagnetic soft-bodied micro system (Figure 2.35). Shaped like a teardrop, it moves in a similar method to small fish through shredding vortices at the tail. The soft-bodied nature allows the device to be more compliant and reduces the chances of tissue damage. By using a paramagnetic body, the device can be produced much smaller and with less mass than other approaches using permanent magnets. Whereas other swimming devices have to counter gravity to remain in the centre vertically, this system was produced using a buoyantly neutral material.

Figure 2.35 Paramagnetic soft-bodied micro system, Palagi et al. (64)

The control of soft bodied magnetic devices has been modelled by Abbott et al. (65). The authors present findings showing translation along x-axis, y-axis and z-axis to be not only possible but easy to perform however rotation about an axis is not possible on its own without some degree of translation. The speed of the translation can be altered by the relative strength of the magnetic field; however, without some feedback from the location of the

device closed loop control is not possible. In lab experiments, lasers were used on several of the magnetically controlled swimming devices to allow for closed loop control. This style of control would not be possible when the device was deployed within a human colonic lumen.

Many of these devices are not actually robots in themselves. They are systems guided by a magnetic field. The control of the magnet or magnetic field may be realised with robotic arms. The devices by Honda et al., Sudo et al., Guo et al., Qinxue et al. and Palagi et al. lack the ability to carry a payload in a stable fashion. The magnetically guided approach by Valdastri et al. and Arrezo et al. allows a greater degree of control of position and stability, while carrying a payload compared to magnetically driven robotic devices.

2.8.6 Helically Driven Swimming Systems

Non-magnetically driven swimming devices have also seen development. Bai et al. (66) discusses the development of a spermatozoa inspired swimming device (Figure 2.36). It features a series of helical tails which are rotated to provide thrust, similar to the helical rotating tail on the magnetically driven device by Honda et al. (59). The spermatozoa device can steer through variation of the angular velocity of each helical tail. The concept relies on low Reynolds number situations to move effectively.

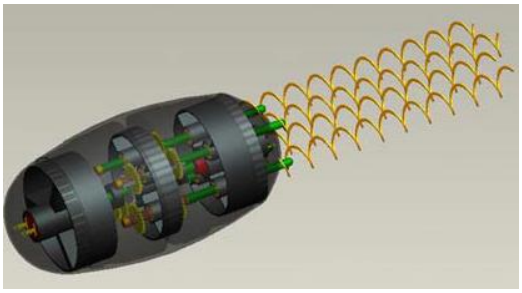

Figure 2.36 Spermatozoa inspired swimming device, Bai et al. (66)

Instead of trying to replicate bacterial style swimming locomotion in a robotic system, Andre et al. (67) produced a device which utilises bacteria for a propulsion. The aim was to produce a fleet of highly mobile devices to perform tasks; however, for use in hydro-colonoscopy the lack of ability to carry payloads such as a camera renders the method un-useful.

The methods in which devices, bacteria and other single cellular organisms, move at low Reynolds numbers is very different to larger Reynolds numbers, Purcell (68). A singular cellular organism swimming through water can be likened to a human swimming in molasses. At low Reynolds numbers, inertial forces net to zero, Lauga et al. (69), thus certain methods of

swimming net no gained displacement. Any method, which relies upon inertial forces to move, does not work at low Reynolds numbers due to reversibility of flow: a forward and backward motion result in equivalent forces netting to 0. The diagram in Figure 2.37 shows oar swimming (like a submerged rowing boat) at high Reynolds (left) and low Reynolds (right) displayed in four distinct steps as detailed below (68).

1. Ready for stroke.
2. Forward stroke; fins/flippers move backwards quickly to propel the body forwards.
3. Resting; for high Reynolds number the body glides (left) and for low Reynolds number the body remains stationary.
4. Return or reverse stroke; fins or flippers return to the start location slowly. For low Reynolds number this causes the body to move in reverse – netting a total distance moved as zero.

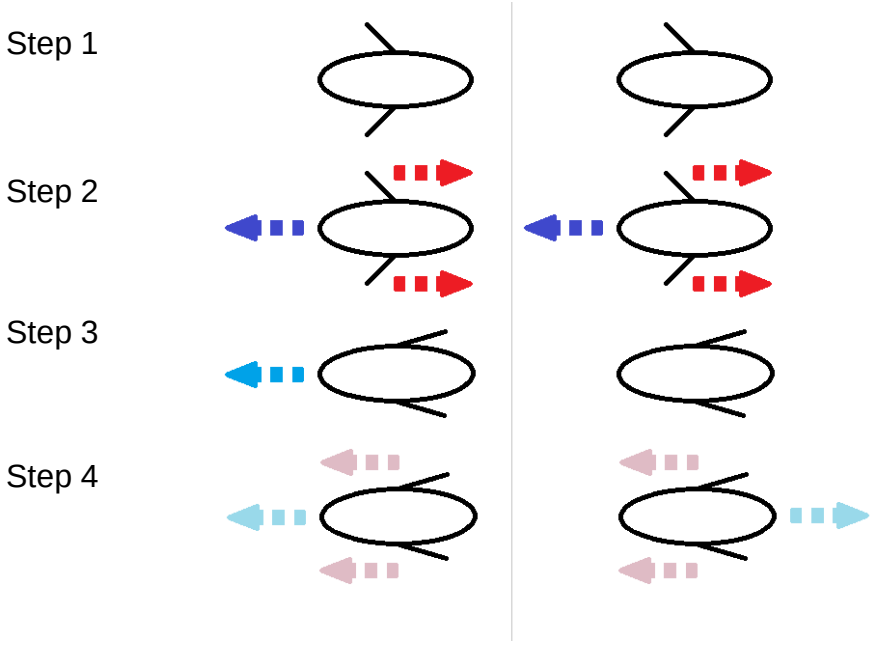

Figure 2.37 High Reynolds number versus low Reynolds number swimming, adapted from Purcell (68). Blue coloured arrows show direction of body with the colour intensity signifying velocity, deep blue relates to the highest velocity. Red coloured arrows show velocity of fins with colour intensity signifying velocity, deep red relates to the highest velocity.

While oar style swimming at low Reynolds does not yield any useful translation, flexible oar or corkscrew style locomotion do, Purcell (68). The locomotion systems of the aforementioned devices by Sudo et al. and Guo et al. utilise the flexible oar method while the devices by Honda et al. and Bai et al. use the corkscrew method. Purcell (70) later assesses the efficiency of such corkscrew locomotion methods and concludes that the efficiency of

such systems is low. As the screw rotates, a section of the screw will impart a motion on the fluid in the opposite direction to a separate section of the screw π radians of a rotation from it, i.e. opposite sides. As these motions counteract each other, they do not contribute to the motion of the device and reduce the efficiency. Further sheering interactions between the screw surface and fluid across the entire screw length decreases the overall efficiency of the locomotion system.

Zhang et al. (71) produced a swimming locomotion system at bacterial scales comprised of a magnet attached to a micro helical tail (Figure 2.38), similar to the device discussed by Honda et al. (59). The design is discussed by Abbott et al (72) and concluded that although simply pulling a micro robot using the magnetic field is more optimal in terms of speed, with decreasing field strength rotational devices are preferable in terms of movement and overall speed. A similar device using a magnetically driven system with flexible flagella was developed by Ye et al. (73) which at publication was not able to carry a payload.

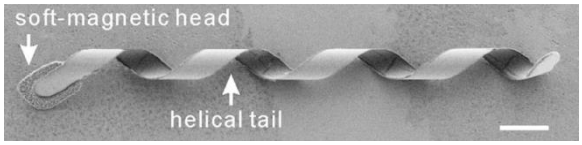

Figure 2.38 Artificial bacterial swimmer, Zhang et al. (71)

The space available for a locomotion system to operate within is crucial to the design of the locomotion system. Colonic investigation devices do not need to be in the micro region and such, will unlikely experience low Reynolds number flows – unless a very vicious fluid is used. An appropriate locomotion system could still however use helical appendages as a form of locomotion. Ikeuchi et al. (74) investigated using a rotating helical ribbed device to traverse along a lumen through sheering force interaction with a mucus film. The authors developed a test rig for collection of experimental data on the performance of a single screw, which did not progress into a standalone device. The single helically grooved cylinder achieved up to 1N in thrust generation at 15rads^{-1}, (the authors reported the cylinder rotated at 0.6ms^{-1} with a radius of 20mm). The trend between rotational velocity and thrust is near linear, with halving the velocity producing just over half the thrust. Should the rotational velocity be limited to restrict tissue damage the maximum thrust will be reduced.

Zhou et al. (75) developed the concept proposed by Ikeuchi et al. (74) into a two module device (Figure 2.39). It consists of two modules; each module is

5mm in diameter and 10mm long. The two modules each have a helically grooved outer face and house the required motors and electronics. The two sections are arranged longitudinally and counter rotate to remove the net torque on the system. The proposed system is designed to fit on the end of a traditional endoscope to provide some degree of forward driven control. However, the system cannot provide any steering capability and relies upon the lumen to steer the device though wall interaction.

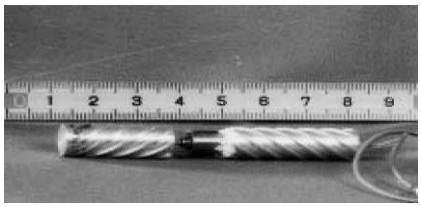

Figure 2.39 Counter rotating helical bodied device, Zhou et al. (75)

A similar idea of using concentric counter rotating sections was built by Shikanai et al. (76) (Figure 2.40). This approach uses several flexible sections with helical fins. Each section can be inflated such that it maintains contact with the lumen allowing for traction. Unlike the approach of Zhou et al. (75), the diameter of the device is much greater, 30mm, such that it presses against the mucosa to gain traction. The fins act against the haustrations to “screw” the device along the passage. A main limitation of this method would appear to be changes in the colon’s diameter, limiting traction, and the angle of flexion at the joints between the multiple sections, limiting passage through flexures of the colon. The developed device is able to inflate each body section independently to maintain traction overcoming local variations in the diameter of the lumen. However due to the overall length of the device, 190mm, it is considerably long and cumbersome at flexures due to the small degree of flexion at each join. The authors note while the device can move smoothly in straight sections at bends it struggles to progress, becoming stuck during testing in an ex-vivo porcine colon.

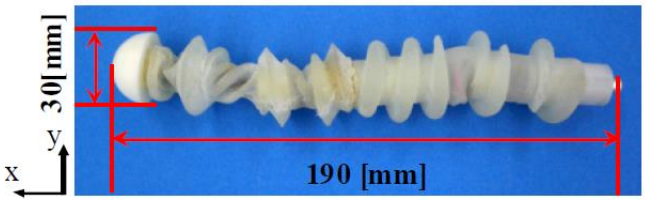

Figure 2.40 Concentric counter rotating section device, Shikanai et al. (76)

A single rotating threaded device was developed by Kim et al. (77), with the motor housing ideally remaining stationary (Figure 2.41). The authors found that the chassis and screw appendage rotated in opposite directions, reducing the propulsive output. The length of the shaft between the chassis

and screw affected the twisting effect on the colon when tested ex-vivo; in extreme cases the colon was twisted to a high degree around the system which would cause considerable discomfort if not damage to a patient. The authors noted that they could apply fins to the chassis to aid propulsion, which would result in a device not too dissimilar to that developed by Zhou et al. (75).

Figure 2.41 Threaded rotating device, Kim et al. (77)

Helically grooved rotating sections have also been used as more traditional wheels, such as on the device analysed by Rentschler et al. (78) (Figure 2.42). While not strictly an intra-luminal device, it is used for reduction in ports needed in laparoscopic surgery. The requirements of being atraumatic are still present in the design of the device, which was developed to provide biopsy capabilities from a single port surgical procedure. The device uses the elongated helically grooved wheels to traverse the abdominal cavity to reach the site required for the procedure. The abdominal cavity, when inflated, gives a large and reasonably flat surface making it easier for such a device to move. Inside the colon the environment is different, the varying diameter and tight flexures make a wheel driven system impractical, particularly systems with a flat chassis and wheels at the corners.

Figure 2.42 Mobile in-vivo camera biopsy robot, Rentschler et al. (78)

Combining the approach of using screw threads against the mucosa and an external magnet, Lee et al. (79) devised a system which is able to adapt the pitch of the screw to suit the environmental needs (Figure 2.43). The front end is able to rotate freely compared to the rear, with three flexible chains, at 120° separation around the circumference, connecting the two sections. As

the front is rotated with an external magnetic field, if the rear is restrained by the lumen the system will twist with the chains forming a screw thread allowing the device to move through constricted areas. This single module approach while novel in locomotion system does not have a static section in relation to the colon; any camera footage from the device would continuously rotate. This may be disorientating for the surgeon and difficult to stabilise in terms of control.

Figure 2.43 Chain drive device, Lee et al. (79)

2.8.7 Bio-Inspired Colonic Devices

More traditional modes of robotic locomotion in pipes are also present within colonic inspection robots. Naderi et al. (57) developed an inchworm type locomotion for a device used in colonoscopy (Figure 2.44). Using suction cups to dock against the colon the device can crawl along the lumen and is able to navigate bends due to the flexibility of the device. This locomotion system not only requires constant contact with the lumen, it also requires a firm connection to move. Geometric variations in the lumen, such as prominent haustrations, could pose impassable sections. If a suction cup cannot form an airtight seal with the lumen, the device will become stuck.

Figure 2.44 Suction driven colonoscopy robot, Naderi et al. (57)

A different approach using an inchworm locomotion system was proposed by Phee et al. (80), (Figure 2.45). The device comprises suction cups at each end to provide the gripping mechanism, connected by expandable bellows to allow translation. External pumps supplied the required pressure changes through a series of flexible pipes. The efficiency of the device was measured by the authors to be 76% when travelling along a straight unrestricted section of colon, which decreased to 0% when the device

attempted to navigate a flexion. The authors discuss the efficiency of the locomotion system, noting that due to the compliance of the colon the overall progress was hindered. When the device contracts or expands longitudinally, should the colon move with the device the net distance travelled may tend to zero. Due to the gripping mechanism requiring a negative pressure, should the pipes become kinked due to flexions in the colon there is also a chance that the pipes may collapse preventing the gripping mechanism from working; rendering the device immobile. Using stiffer pipes to reduce the chance of them collapsing or kinking would result in greater forces exerted on the colonic tissue and greater resistance to cornering.

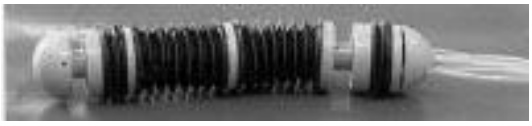

Figure 2.45 Bellow inchworm device, Phee et al. (80)

A different inchworm approach was developed by Kim et al. (77) (Figure 2.46) which does not rely upon active gripping for locomotion. The device uses angled wedge protrusions, which act like passive barbs to grip the mucosa. The midsection of the device can elongate allowing linear motion, with the entire body being covered in a compliant sheath, which protects the colon from becoming trapped and protects the components from contamination. The authors discuss that the elongation stroke when low limited the device's ability to transverse the lumen: due to the colonic tissue stretching the device made net no gain in distance for an entire stroke as similarly noted by Phee et al. (80). Lengthening the stroke of the system to allow for progression hampers the corning ability of the system; with it becoming too long to pass the flexures within the colon.

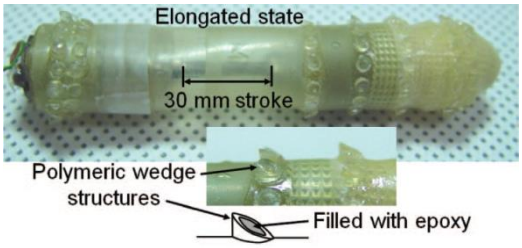

Figure 2.46 Passively gripping inchworm, Kim et al. (77)

2.8.8 Power and Communication

Many other projects have aimed to bring robotics into surgical procedures, in reviewing the methods used for communication better understanding of the technology available and its limitations can be gained. The ARAKNES

project aims to provide a platform of robots for natural orifice trans-luminal surgery. Poignet et al. (81) discusses control related issues with such a platform, some of which are relevant to a colonoscopy robot. Wireless devices pose an advantage in terms of less resistance due to tether fiction, fewer parts to spread infection and sterilise between usage, and no control issues due to tether manipulation. However, wireless systems require internal storage capacity for power for both locomotion and signal transmission. Radiation absorption of the human body degrades communication signals resulting in reduction of the signal bitrate and other issues. To overcome this greater signal broadcast power is required, putting greater strain on the limited power reserves. It has been shown that wireless systems expose the body to higher doses of radiation when the wireless signal strength between devices is poor (82, 83). It is imperative to maintain a strong active and continuous connection between any wireless device and the master computer when it is deployed within a patient and such the radiation exposure and battery drain will be high.

A wired or tethered approach would negate these power issues at the expense of needing to tow a tether through the lumen. Although the motor power output would need to be greater, the tether would be able to provide greater power to the device to compensate.

2.9 Critical Assessment of Locomotion Methods

The foremost requirement of any colonoscopy device is that it is atraumatic. Damage to the lumen is not acceptable and can be particularly easy to cause when combined with colorectal diseases. As such, a locomotion system should apply a minimal amount of force on the colonic walls. Wall press dependant systems cause the highest amount of contact and thus are non-ideal. Though filling the colon with a fluid, hydro-colonoscopy provides a suspension medium for any device to propel itself through. Although contact with the colonic tissue cannot be avoided due to the anatomy of the lumen and so any locomotion system should be able to deal with such. Amphibious locomotion methods show the most promise in being able to provide a minimally contacting locomotion system while being able to deal with strictures and collapsed sections of the colon.

Many systems used in medical situations and industrial situations use similar locomotion methods. There is a degree of cross over between the modes of operation, often with optimisations for their environment of operation. The

following summarises the major locomotion types and their suitability for a locomotion system for the CoDIR device.

2.9.1 Passive

The Pipeline Inspection Gauge, or PIG system shares its fundamental locomotion system with passive capsule devices, such as PillCam®. These systems do not have any means of locomotion and depend on the environment to move them. By using small and rounded devices the risk of patient damage is minimal. Trauma limitation is a large advantage to this locomotion system; however the inability to control the direction they face is a sever limitation. This disadvantage deems the system unsuitable for more advanced forms of observation and exploration of the colon.

2.9.2 Bio-Inspired Locomotion Methods

Crawling, inchworm, serpentine and fish locomotion systems are all bio-inspired. They mimic modes of locomotion found in nature.

Crawling systems can be very mechanically complex and difficult to miniaturise, coupled with the increased risk of perforation and increased power draw these systems have been shown to be incompatible with medical devices. These devices have been developed and tested however the drawbacks have halted further research.

Inchworm systems have been deployed with varying degrees of success in colonic passages. The systems are inherently well suited to traveling in straight lines and become stuck in corners. Inchworm locomotion requires constant contact with the walls of the environment, depending on how this contact is achieved and maintained the risk of patient damage increases. Anything that uses rigid arms for maintaining contact carries the same risk of perforation as crawling systems. While inchworm systems provide a strong method of locomotion and steady base for camera footage and tool use, the colon is never a straight passage. Any system deployed within the colon would need to be able to pass the many bends and twists with ease and such inchworm systems are not suitable for this environment.

Serpentine locomotion systems are well suited for amphibious operation, the same drivetrain can provide locomotion in land based and fluid based situations. These systems do however require a larger operational envelope due to the wave propagation along the body. The nature of the locomotion sweeps the head unit perpendicular to the intended direction of travel, which may cause disorientation. Industrial serpentine robots are often large in size and compensate for this motion through use of large field of view cameras

and slower articulation of the joins. A large field of view camera would have limited use within the colon, due to the confined space. This confined space would also limit the locomotion system's ability to produce usable thrust. Any aggressive sideways sweeps used to generate thrust would carry a high risk of patient damage. Serpentine systems are not ideal for use within the colon for these reasons.

Fish-like swimming can be very efficient on power usage, making use of gliding to minimise energy spend at high Reynolds number flows. While gliding is not feasible at low Reynolds number flows, the mode of operation is at higher Reynolds number flows allowing for coasting or gliding. Most fish have limited ability to reverse, more often than not flexing their body to allow for a forward stroke to move them away from an obstacle. This lack of reversing ability is due to their shape, a larger head tapering to the tail with a fin to provide a larger surface area for fluid movement. Should a fish-like swimming vessel become stuck nose first in a haustration, the inability to reverse would cause the device to become stuck requiring external help. Using a chassis, which is compliant and free of sharp appendages, would minimise risk of patient damage over other bio-inspired devices.

Mechanical complexities, manufacturing scales and limited degrees of freedom in terms of locomotion all form strong disadvantages for bio-inspired locomotion strategies. Possible future development in artificial muscles may alleviate these, however for the time being, conventional mods of locomotion are more desirable.

2.9.3 Magnetically Guided and Propelled

Using external magnetic manipulators for movement is an interesting method of motion and in many cases efficient. In removing the need for miniaturising the locomotion system the device can be made smaller and have greater room for on-board equipment. Through several different studies by researchers, magnetically dragged systems have shown promise in both their dexterity and ability to carry a payload. Providing the end effector of the system is compliant and the maximum magnetic force is limited, the risk of patient damage is minimal.

Systems which use rotating or oscillating magnetic fields to move permanent magnets attached to moving parts of the system to provide locomotion have the advantage over magnetically towed systems that expensive robotic arm manipulators may not be needed. Electro-magnetic coils are simply wrapped around the environment to provide the needed magnetic field. The ability to

carry a payload is reduced and the devices are often unable to remain stationary unless they are buoyantly neutral. Similarly to magnetically guided systems, maintaining a low magnetic force and using compliant materials can minimise patient damage.

Both systems do however have the side effect of exposing the body to large amounts of radiation, albeit magnetic. These systems would be inappropriate for infirm patients with pacemakers for example, but pose no more significant risk than routine CT scans.

Soft-bodied, paramagnetic devices may provide an atraumatic system, however magnetic devices may be unable to pass collapsed sections of colon and become trapped in recesses if magnetically towed. Magnetically driven devices may be more suited to operation in highly variable environment that is the human colon.

2.9.4 Helical Based

While some helical systems have also been driven through external magnets, those used in medical applications by researchers have used internal actuators to provide locomotion. Through rotating helically grooved sections, the locomotion system is able to provide locomotive properties in both contact and fluid filled situations. Should the rotating sections be separate from the main chassis, a relatively steady camera feed can be provided. Simply by reversing motor directions, the system is able to reverse. Through articulation between different sections or differentially driving the helical sections, steering of the device can be achieved.

A helical system may pose a trauma risk if rigid materials or sharp edges are deployed. Such systems do have the advantage of providing amphibious locomotion, which will allow passage through sections of mixed insufflation medium. Depending on the drivetrain the system may have reduced mechanical complexity compared to other amphibious systems, resulting in easier fabrication and smaller operation area needed.

2.9.5 Summary of Methods and Devices Assessed

Table 2.1 summarises the systems covered in this review in terms of locomotion method and size. The size required by a locomotion system is important, if the system is unable to be produced or operate at an appropriate size for colonoscopy then it does not meet the requirements.

Table 2.1 Summary of devices and systems reviewed

Device	Locomotion method	Size
Mobile fish robot, Xiabo et al. (30)	Bio-inspired swimming (fish)	43 x 43 x 120mm
Autonomous fish, Huosheng et al. (31)	Bio-inspired swimming (fish)	Length: 520mm
Sea bream robot, Terada et al. (32)	Bio-inspired swimming (fish)	Length: 600mm
Lamprey based robot, Ayers (34)	Bio-inspired swimming (serpentine)	Not stated, approx. 1000mm
Passive wheeled system, Crespi et al. (35)	Bio-inspired swimming (serpentine)	55 x 33 x 490mm
Amphibious wheeled snake robot, Shumei et al. (36)	Bio-inspired swimming (serpentine)	Diameter: 75mm, length: 1170mm
ACM-R5H (37), HiBot Corp.	Bio-inspired swimming (serpentine)	Diameter: 80mm, length: 1750mm
MrInspect, Roh et al. (38).	Wheeled wall press	Diameter: 109mm, length: 150mm length
Wheel propeller hybrid device, Jiancheng et al. (42)	Wheel-propeller hybrid	960x x 1000 x 200mm
Snowbird 6, Ice Challenger team (43)	Archimedean Screw	Not stated, larger than 1000mm

Table 2.1 cont…

Device	Locomotion method	Size
Screw based amphibious device, Liang et al. (44)	Archimedean Screw	1110 x 420 x 464mm
Modular device, Liedke et al. (45)	Archimedean Screw	Not stated: larger than 90mm
Screw Drive Rover, Nagaoka et al. (46)	Archimedean Screw	160 x 350 x 120mm
The Marsh Screw Amphibian by Chrysler Corporation	Archimedean Screw	Not stated, larger than 1000mm
PillCam ®, Given Imaging	Passive, peristaltic	Diameter: 11mm, length: 26mm
Crawling device, Quirini et al. (53)	Leg based crawling	Diameter: 12mm, length: 40mm
4 propeller device, Tortora et al. (54)	Swimming (propeller)	Diameter: 15mm, length: 30mm
Magnetically guided colonoscope, Valdastri et al. (56)	External robotic manipulator	Standard colonoscope driven by large external manipulator
Suction driven colonoscopy robot, Naderi et al. (57)	Suction driven articulation	Diameter: 19mm, length: 180mm
Oscillating magnetic device, Sudo et al. (61)	External magnetic field	4 x 5.5 x 19.25mm
Oscillating magnetic device, Guo et al. (62)	External magnetic field	15 x 40mm

Table 2.1 cont…

Device	Locomotion method	Size
Hybrid magnetically powered device, Qinxue et al. (63)	External magnetic field	Diameter: 10mm, length: 100mm
Paramagnetic soft-bodied micro system, Palagi et al. (64)	External magnetic field	Approx. 5mm
Spermatozoa inspired swimmer, Bai et al. (66)	External magnetic field	Not stated
Artificial bacterial swimmer, Zhang et al. (71)	External magnetic field	Approx. 25µm
2 module helical bodied device, Zhou et al. (75)	Archimedean Screw	Diameter: 10mm, length: 70mm
Multi module, soft bodied device, Shikanai et al. (76)	Archimedean Screw	Diameter: 30mm, length 190mm
Single screw, Kim and Kim (77)	Archimedean Screw	Diameter: 15.6mm, length: 78mm
Stretchable-Body Robot, Kim and Kim (77)	Barbed inchworm	Not stated. Approx. diameter: 30mm, length 100mm
Mobile in-vivo camera biopsy robot, Rentschler et al. (78)	Screw tread wheel	Diameter: 20mm, length: 100mm
Chain drive device, Lee et al. (79)	External magnetic field	Diameter: 18mm, length: 32mm
Bellow device, Phee et al. (80)	Inchworm	Diameter: 24mm, length: 115mm

2.10 Summary of Literature

The colon forms the last section of the GI tract (1, 5, 8), is located in the lower section of the abdomen (1, 5, 8), and is a highly deformable and variable organ (1, 5, 9). Although it has several “landmark” locations these vary greatly from patient to patient (1, 5, 8, 9). It plays a vital role in the digestion of food in humans and such is imperative to life compared to a limb.

The colon is susceptible to many ailments, which impact negatively upon quality of life in humans, such as cancer, diverticulitis, inflammatory bowel disease, ulcerative colitis, and Crohn’s disease (1). To diagnose these, visual inspection is required with more often than not biopsies taken, however some ailments such as diverticula disease and ulcerative colitis, make colonoscopy a very difficult procedure to perform.

The current means of inspection takes the form of a long flexible tube known as the colonoscope, a 1.5m long flexible tube of approximately 15mm diameter. The Colonoscope features a steerable tip with camera and light source, passageways for insertion and removal of air/fluid and a tool channel for taking biopsies. The procedure is often uncomfortable and the tortuous environment of the colon causes procedural difficulty to the performing clinician (1). The main difficulties as discussed are: risk of perforation or laceration due to steering of the colonoscope and looping; bowel blockages often due to poor preparation; severe disease preventing progression along the colon.

Hydro-colonoscopy involves filling the colon with a warm fluid medium to perform the procedure, and may reduce patient trauma and increase ease of procedure for the clinician (7, 24-26).

In replacing the colonoscope with a robotic system, it is hoped that many of the difficulties involved and associated discomfort, can be negated. The robotic system involved must be able to traverse through the colon while minimising trauma to the colonic tissue, as well as carrying the payload required for diagnosis of colonic ailments. Many researchers have carried out research in this area to mixed success.

The chapter reviewed the work of other researchers in producing locomotion systems and platform for improving colonoscopy, as well as locomotion systems as a wider approach. Using external magnetic fields to provide a

locomotion means overcomes the difficulties imposed by miniaturisation of actuators, however imposes further restraints on the usage of such devices. The large and bulky external manipulators can be difficult to work around and deploy in surgical environments.

Any locomotion system used on a colonoscopy device must be able to primarily traverse the colon. Locomotion systems, which require a large space envelope that available, are too mechanically complex to produce with current technology or are limited in their ability to provide a full range of motion are unsuitable. This reduces the methods available, which can be seen in the literature; intra-luminal devices use a small set of strategies compares to the wider field of exploration robots. While this does not directly mean new and un-used locomotion methods cannot be used, research must be carried out to show they are viable.

A chosen locomotion system must also be atraumatic, movement must not cause harm to the tissue. Through locomotion system development, material selection and control strategy an amphibious and atraumatic device may be developed. Several researchers have utilised screws in providing locomotion for prospective colonoscopy devices, however these have been developed for air insufflated colonoscopy not hydro-colonoscopy. For a future colonoscopy device to succeed in replacing the conventional colonoscope, combining the benefits of hydro-colonoscopy and an amphibious locomotion system may show to be the key to success.

Chapter 3
Design and Development of the Amphibious Locomotion System

In the literature review, locomotion systems were assessed for their merits and applicability to an intra-luminal medical device. The review focused on locomotion systems used on current and experimental robotic systems, including but not limited to other medical devices and industrial pipe inspection devices.

3.1 Requirements

In understanding the anatomy of the colon and the purpose of the overall device, a series of requirements was identified to inform the design process. These requirements fall into two categories: clinical and technical. Through these requirements, a novel locomotion system was designed and built allowing testing of the locomotion system; this is examined in detail in Chapters 5 and 6 with a completed prototype system tested in Chapter 7.

The clinical requirements cover the anatomy of the colon and the environmental conditions the device will be likely to be subjected to. The technical requirements cover the physical needs of the system such as payload and communications.

3.1.1 Clinical Requirements

- Atraumatic interaction with tissue
    - The device or locomotion system cannot damage the mucosa lining to a greater extent than current colonoscopy (1-3); preferably, no trauma will be sustained.
    - The mode of locomotion cannot cause risk of laceration or perforation of the colon wall, during normal operation nor should it fail to operate in the designated fashion.
        - Regions of colon with diverticular disease are of greater risk of perforation should part of the device become trapped in the recesses.
        - A minimum pressure to cause perforation is taken as 14kPa, derived from work published by Shiels et al. (10), as discussed in Chapter 2.
    - For degenerative conditions where the mucosa may be inflamed, contact with the mucosa must be minimised to reduce damage and bleeding (1).

- Amphibious locomotion
    - Air pockets along the colon will present a challenge for any fluid-based locomotion system to traverse.
    - The colon diameter varies greatly along its length and some sections may be narrow (5, 9). Fluid locomotion will be restricted in these sections, which may require contact based locomotion to progress, particularly if the colon is folded such that the passage is blocked.
- Appropriately scaled relative to a colonoscope
    - The colon can vary in diameter (5, 9); the device must be able to fit within the smaller colons.
    - The device is to be deployed via the anus and should be small enough to fit. Surgical opinion was consulted on what can be tolerated and 15-20mm diameter was suggested as an upper range.
    - The device must be short enough to turn the flexures without becoming wedged. In a 90° flexure, this can be approximated as the chord length formed across the lumen.

3.1.2 System Specifications

In order to develop a device that may operate within the colon, several requirements must be met.

- Communication and power supply
    - While the research does not cover the design of these directly, the locomotion system must be able to operate in the colon environment while powered externally via a tether.
- Generate appropriate propulsive thrust for movement
    - A preliminary experiment was carried out using an ex-vivo porcine colon to approximate the force needed to pull a tether through a colon[3]. The experiment yielded a force of 1N would be required to pull a multicore tether, similar to that which is expected to be used on the device, through a collapsed colon. Although a fluid filled, distended colon may require less force; this is a good measure of the device's ability to produce locomotive force.
- Payload capability

[3] Preliminary experiment to measure the force needed to pull a tether through a colon carried out by Dr Boyle and Dr Alazmani of the University of Leeds for the CoDIR project. Experiment involved a multi-core tether supplied by Karl Storz and fresh ex-vivo porcine colon.

- The locomotion system must be able to accommodate a payload such as a camera, inertial measuring unit (IMU) or other sensing hardware.
- The possibility for a biopsy tool to be added in future development .

3.2 Stages of Design

A systematic review of locomotion concepts was conducted from the literature review. A locomotion strategy was selected on its ability to meet the requirements detailed above. Through incremental testing and review of the concept was improved to provide a more robust and optimised locomotion system for a surgical device to be used within the colon. A summary of the locomotion strategies discussed is available in Table 3.1.

Table 3.1 Locomotion strategy comparison matrix

Locomotion strategy	Amphibious locomotion	Mechanical Complexity	Atraumatic nature	Comparison to colonoscopy procedure
Inchworm	No, contact only	Low	Constant contact needed	Speed: Slow Scale: Large
Fish-like swimming	No, fluid only	Low	Yes	Speed: Similar Scale: Large
Serpentine	Yes	High	Swimming may result in constant contact	Speed: Similar Scale: Large
Propeller	No, fluid only	Low	Unenclosed propellers pose laceration risk	Speed: Fast Scale: Similar
Wheel-propeller hybrid	Yes	High	Low	Speed: Similar Scale: Large

Table 3.1 cont…

Locomotion strategy	Amphibious locomotion	Mechanical Complexity	Atraumatic nature	Comparison to colonoscopy procedure
Archimedes' screw	Yes	Moderate	Low depending on screw material used	Speed: Similar Scale: similar-Large

3.3 Design Considerations and Selection

3.3.1 Inchworm

Starting with adaptions to the current colonoscopes, inchworm locomotion is an obvious solution. Using a device with a diameter matching the smaller sections of the colon, an inchworm system would easily fit within the space requirements. However, the inchworm system requires a means of gripping the mucosa to traverse the colon. The gripping mechanism involves either pressing against the mucosa or sticking to the mucosa. In pressing against the colonic wall, there is a risk of perforation. Sticking, through friction or chemical adhesion requires a firm contact with the mucosa. Suction will require some form of on-board generation of a vacuum or connection to a vacuum supply. Chemical adhesion is likely to wear out or become less effective through continuous use; there would also need to be a way to reduce this to move the contact point. Barbs would also provide a means of gripping; however, the notion of barbs would likely bring fears of perforation. A system with barbs would need to reverse the direction of grip, otherwise, the system would become stuck once it reached the caecum.

Through the literature review, the work of other researchers using an inchworm locomotion system was covered (77, 80). These were unable to pass tight flexures due to the device length; and the reliance upon gripping the colon to move became a disadvantage when the colon stretched with the device locomotion steps. Inchworm locomotion systems do not meet the requirement of minimising contact with the mucosa, which will be vital for acceptance and use in patients with degenerative bowel conditions. The inchworm locomotion system does not make use of the fluid in hydro-colonoscopy; in this case, the fluid may negatively affect the progress of an inchworm system.

3.3.2 Swimming

Fish-like swimming locomotion strategies have very limited use; they require continuous fluid and do not work as well in confined spaces that restrict the device-body motion. Should a fish-like swimming device come across a fluid void section it would become stuck. A fish-like locomotion system would provide propulsion through flicking of the tail from side to side (28). This produces a highly optimised locomotion system for forward travel and in many cases does not work in reverse: reversing the tail direction does not produce reverse thrust. To return along the colon lumen a device employing this style of locomotion system would need to turn around. A fish-like system would involve no gripping of the colon or rotating parts that may damage the lumen, producing an atraumatic approach. However, a locomotion system that is not able to traverse a fluid void section of the colon is unfavourable.

3.3.3 Serpentine

Devices, which employ a serpentine-like locomotion, are able to operate in both fluid and fluid void environments (36, 37). Reverse motion can be produced through altering the sinusoidal oscillation of the device body; this is dependent on the interaction between the device body and the medium it is in contact with. The mechanical complexities of serpentine-like systems have led to them being large in scale when produced and used within industry. The number of on-board actuators required for locomotion prevents them from being miniaturised with current technological limits. While small diameter systems are available, they require bulky external actuators to drive the wire tendons used for dexterity. A smaller diameter system that uses an external power system and wire tendons would be no different in principle to current computer guided colonoscopy techniques.

3.3.4 Propeller Based

For a mechanically simple system that utilises the fluid filled colon for locomotion, the propeller seems an obvious choice. Propellers operate through rotation at high speeds with sharp blade edges, these could potentially cause lacerations. Cowled or enclosed propellers would not pose the same risk as the contact between the rotating parts and the tissue is limited. However, sections without sufficient fluid depth could see the device grounded and unable to move: combining a propeller with land-based locomotion would be a means of solving this. A wheeled or tracked device could be coupled with propellers to allow for amphibious locomotion. The

wheels or tracks would be situated on the device such that at low fluid depth they rest upon the mucosa allowing locomotion to resume.

3.3.5 Drivetrain

To allow the device to operate both fluid and contact locomotion strategies, a single drivetrain could provide rotation to both the wheels or tracks and the propellers. However, these modes of locomotion are suited for different angular velocities, which would require multiple gearboxes to provide transmission at a suitable angular velocity. In sections of low diameter, it would be ideal to drive only the contact based locomotion: turning off the propellers would reduce risk of damage to the tissue. This would need a means of switching between locomotion modes. Combining wheels and propellers would compound the need to switch modes; both could not be operated at the same time resulting in situations where neither is optimal when used in separation. Any system used must be able to provide locomotion through both fluid filled areas and in contact without decisions being made by the clinician on which mode is appropriate.

Using the same drivetrain for both fluid and contact locomotion reduces the number of gearboxes needed, and thus the mechanical losses, device mass, the size required and in some cases the number of actuators required. Mechanical complexity will play a role in the feasibility of any device; multiple gearboxes and switching mechanisms will increase the minimum size of the device. With any mechanical system, the more components there are; the more modes of failure the system has. Micro gears suffer from wear to a much greater extent compared to macro gears, simply because the same wear causes a higher percentage loss. Each gear used will decrease the mechanical efficiency of the system, increasing the load on the actuators and the power draw. Smaller motors in turn produce less torque and so larger more complex gearing systems have a detrimental effect. To keep the system small the mechanical design must be simple.

3.3.6 Archimedes' Screw

The use of Archimedes' screws has been seen in applications where the device is in need of amphibious locomotion from the same drivetrain and locomotive effectors (43, 44). Using a locomotion system based on Archimedes' screws could simplify the control for the piloting clinician while simplifying the design of the mechanical system. The use of screws would provide an amphibious locomotion system, with a simplified drivetrain fitting it in the small workspace envelope needed, providing a novel locomotion

system. The method in which an Archimedes' screw produces thrust in fluid and contact is covered in detail in Chapters 5 and 6.

At a section of collapsed colon, possible due to a flexure, where the luminal walls of opposite sides are in contact, the device cannot avoid contact with the lumen. Luminal contact will be required to open the lumen as well as pass through the section. In these cases, the contact between the device and the lumen must be atraumatic; as the device passes through the collapsed section it must not damage the colon wall. When in contact with a surface a screw is required to slip in the direction of its rotation to produce thrust: this interaction could be atraumatic through material selection. This is examined in detail in Chapter 6.

3.4 Amphibious Screw Concept

Archimedes' screws provide a locomotion strategy that is able to operate in an amphibious state without needing to swap between discrete states: the same drivetrain and locomotion effectors provide locomotion in all modes. This locomotion strategy has been utilised in both non-surgical (43-46) and surgical devices (75-77, 79). With evidence that Archimedes' screws are able to provide a viable means of locomotion; this strategy was chosen for its mechanical simplicity and amphibious potential over the other strategies reviewed. The utilisation of such on an atraumatic intra-luminal device was explored.

In rotating a shaft, the system experiences a torque opposing the rotation (Newton's 3rd law). While in larger systems the mass difference between the shaft and the system can negate any adverse effects, net torque on the system for use in hydro-colonoscopy is likely to cause adverse effects: such as undesirable rotation of the device during locomotion in fluid. To combat this, counter rotating pairs can be utilised to reduce the net torque to zero: unless it is desired for control.

Using counter rotating pairs the number of screws must be equal; thus, 4 screws is the minimum needed for accurate control. As seen in Figure 3.1, a 4-screw device will have 4 degrees of freedom (DoF). It will be able to translate along the X-axis and control rotation about all 3 axes. Any increase in screws will not increase the DoF of the system however reducing the system to 2 screws will reduce the DoF to 3: vertical arrangement would lose rotation about Y and horizontal would lose rotation about Z. The device must be able to drive in a forward and reverse direction while allowing for steering

in any direction about the axis of travel, the minimum number of screws required for this is 4.

By arranging the counter rotating pairs such that no screw is next to a screw of the same rotation handedness, in contact conditions on a flat surface there will always be a pair of counter rotating screws in contact. In this condition, the system will have 3 DoF: translation along X and Z while being able to control rotation about Y, assuming the surface the device rests against is the X-Z plane.

When providing locomotion to a system and steering it, the point of effect of these can affect the control. Rear driven systems are mechanically unstable, with the rear tending to move out of line from the front and desired direction of travel. This instability increases with the distance between the front and the point of effect and is notable on the conventional colonoscope: the driving force comes from the rear, which makes the direction of tip advancement difficult to control. The advantage of using a robotic system is that the distance between the point of locomotion and steering, and the front is shortened; this makes the system easier to control.

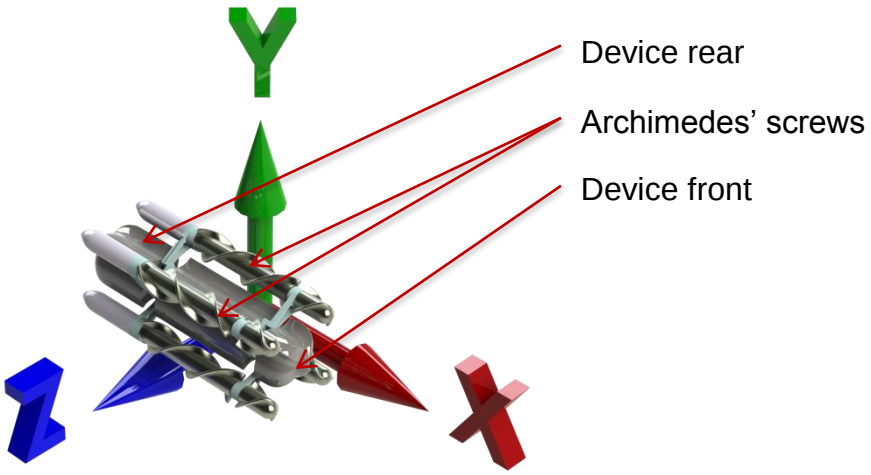

Figure 3.1 Axis orientation. X-axis (red) designates forwards, Y-axis (green) designates up, Z-axis (blue) designates right. Final 4-screw device as developed in this thesis shown alongside axis system to aid orientation.

To house 4 screws such that when resting on a flat surface two screws are in contact the chassis needs to take the form of a square based prism, with the screws located at the long edges, Figure 3.2. To remove the sharp edges, a rounded cuboid chassis was used as the basis for the design. Figure 3.3 shows a sketch of the initial idea for Quad Screw Device version

1. It features a rounded tip for safely passing through collapsed sections of the lumen; four edge mounted screws to provide locomotion; and a tapered tail section for attachment of a tether. The cut through section shows a single motor and gear arrangement, which powers all 4 screws at the same time. Although this reduced the degrees of freedom the system has, the initial design was kept simple to allow exploration of the concept without overcomplicating the design.

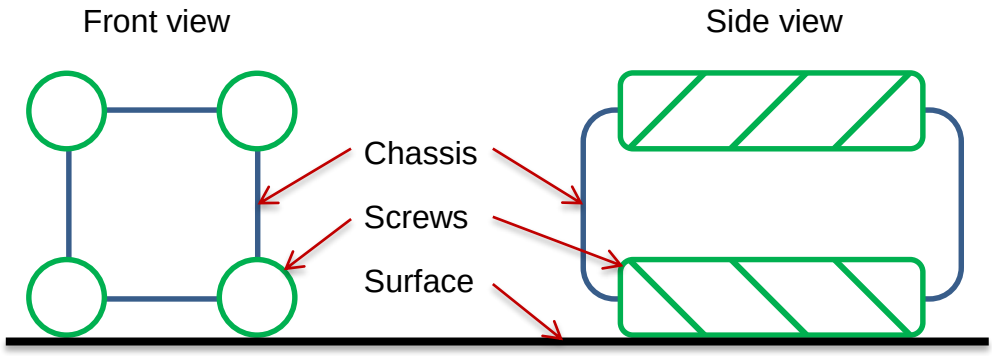

Figure 3.2 Screw location about chassis

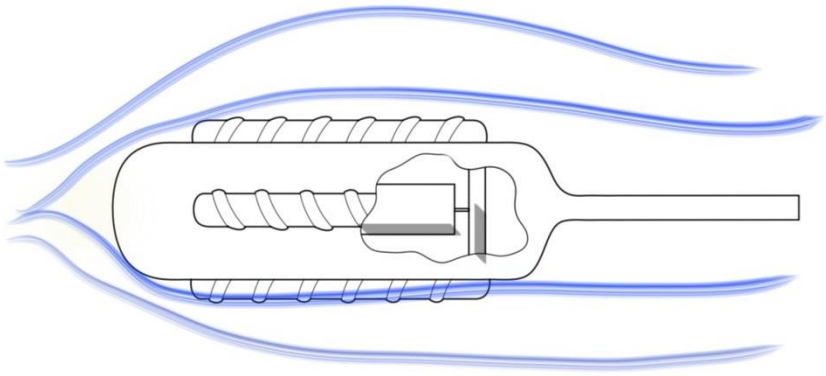

Figure 3.3 Initial design sketch for Quad Screw Device, incorporating Archimedes' screws

3.5 Design Prototype Version 1

To develop and prototype the design a 3D computer aided design (CAD) package was used (SolidWorks, Dassault Systèmes SolidWorks Corp). The first iteration of the locomotion system design can be seen in Figure 3.4. The initial design sketches featured a single motor powering the 4 surrounding screws, as shown in Figure 3.3. This arrangement allows for only 1 DoF, translation along the X-axis. To increase the ability to control the system's orientation, the system was designed such that each of the 4 screws was powered by a different motor, increasing the system's degrees of freedom.

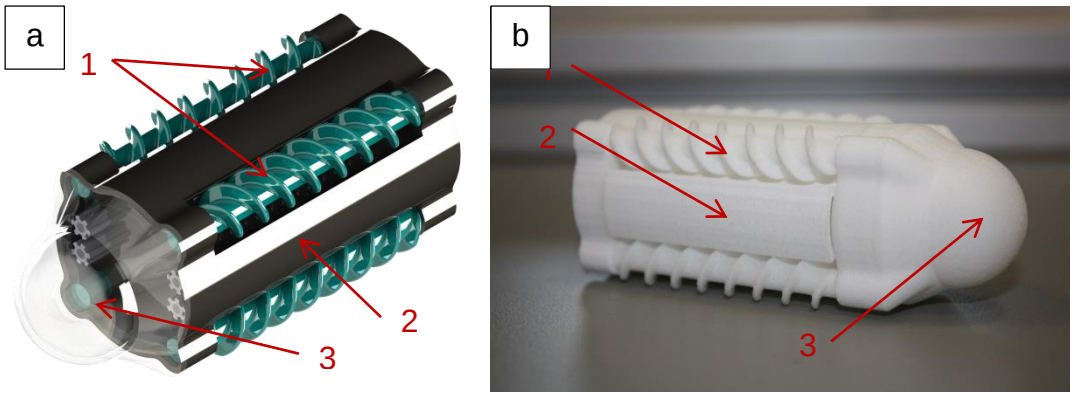

Figure 3.4 Quad Screw Device Version 1 locomotion system. Shown a) is a computer render of the device; b) is a rapid prototyped (SLS) solid, non-functioning scale model. Annotations show: 1) Archimedes' Screws; 2) Chassis; 3) Front section in which a camera module would be housed.

The central section of the chassis features mounting space for a camera and motor controllers. The front of the device is covered by a transparent rounded nosepiece to allow the camera to view the colon while providing a rounded face to push through collapsed sections of the colon.

The screws are mounted at equidistant intervals around a cylinder with bearing mounts at either end supporting them. The screws are mounted such that they form the point of contact against a flat surface with the chassis clear of the surface.

A solid non-functional 3D prototype was produced using a selective laser sintering (SLS) rapid prototyping unit, as shown in Figure 3.4. This model was used for discussions with clinicians on the device and their thoughts on the design; the major feedback element was concern over potential trauma caused by tissue becoming stuck in the screws. A single screw model was also produced to allow initial testing to the device in fluid, as discussed further in Chapter 5.

A testing rig was designed such that a single screw, resembling a quarter of the overall system, was developed, as detailed in Chapter 5. Using this testing apparatus initial testing was carried out to ascertain the thrust potential of a single screw rotating in fluid. This revealed insignificant thrust generation from a single screw model; the data was barely distinguishable from signal noise and showed forces of less than 0.01N. Investigation into this revealed that the bearing housing at either side of the screw was blocking the fluid flow into the screw (Figure 3.5). As the screw rotated, the fluid at the end of the screw would not be able to continue in a direction parallel to the screws' rotational axis and would be ejected in a direction

perpendicular to the screws' rotational axis, as designated by the blue arrows in Figure 3.5. This introduces large losses to the system as the flow becomes turbulent. Similarly at the head of the screw, fluid could not enter the screw without a change in flow direction; resulting in greater losses in the system.

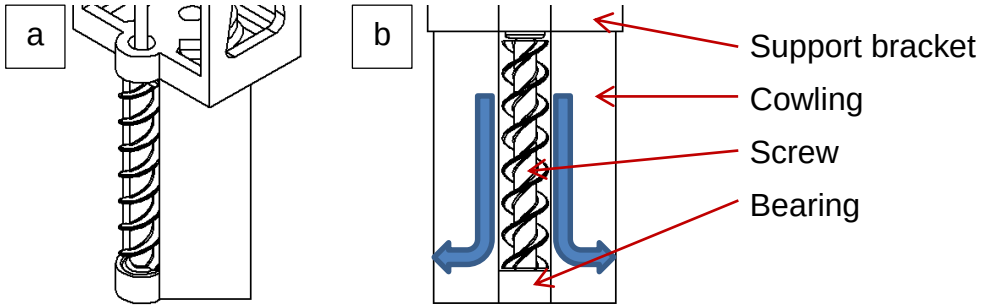

Figure 3.5 Single screw system used during initial testing a) isometric view; b) front view,. All shown components are submerged during experimentation The blue arrows show the fluid flow path, as it is forced perpendicular to the screw due to the closed end.

3.6 Computational Fluid Model

To understand the fluid flow between the screw blades as the screw rotates, and allow the design of a system with greater thrust potential a computational model was built (Comsol Multiphysics).

A cross sectional area of the fluid between two blades was created in the X-Y plane, using the inner and outer screw diameters. This was extruded along the Z-axis with a rotation about the Z-axis such it formed a single rotation of the dual sweep screw. The volume was duplicated and rotated by π radians about the Z-axis. The open top and bottom faces in the X-Y plane had boundary conditions applied such that fluid would flow between them creating a theoretically infinitely long screw channel. The inner faces of the fluid (the fluid touching the screw) had boundary conditions applied such that the fluid layer was stationary (boundary layer theory (84) P266). The outer faces were displaced along the Z-axis and rotated about the Z-axis to resemble the screw rotating.

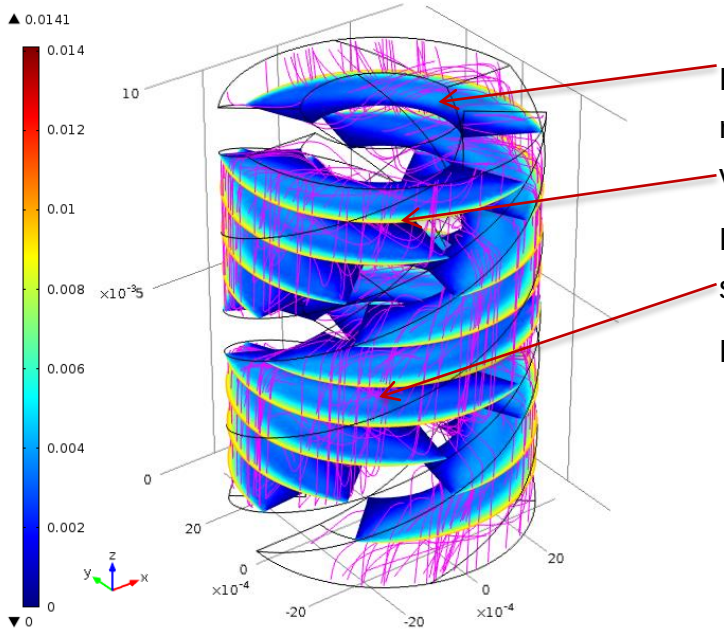

Figure 3.6 Fluid velocity (gradient) and streamlines (pink) of fluid flow within a screw during rotation of the system, generated in Comsol Multiphysics computational package. Units show ms^{-1}. Discrete slices taken through the flow at 1mm increments.

The simulation showed that the fluid swirls within the screw veins and does not travel along the threads as anticipated, as shown by the pink lines in Figure 3.6. This concludes that the fluid does not leave the screws at the ends and thrust that was being generated was simply shearing forces from the blade tips (shown by the bright coloured edges in Figure 3.6) and not from the volume of fluid being pushed.

3.7 Design Prototype Version 2

To overcome the fluid flow issue caused by the screw location a new approach was taken. The first approach at solving this involved using larger outer diameter screws. While leaving the mounting and axles the same, increasing the blade diameter would allow more fluid to escape, however due to the positioning of the screws only ¼ of the flow was exposed. Increasing the blade diameter also had the side effect of reducing the space within the chassis for other components.

Instead of the screws being directly mounted on the chassis the design was adapted such that the screws could be located away from the body. This adaptation would allow greater than ¾ of the flow to be exposed, allowing for greater thrust potential.

While mounting the screws away from the chassis would allow for greater fluid propulsion, the maximum diameter of the system was increased. This could be used to an advantage: by controlling the diameter of the system, collapsed sections could be opened up allowing better visibility and access.

The system was redesigned with 4 controllable arms, each with a screw mounted, as shown in Figure 3.7. Each of the arms are mounted on a chassis length axle, connecting the front and rear sections of the arms. Each of the axles are connected to an internal gearing system, which allows them to move together in unison from a single chassis mounted motor. As the arms interlock, moving each on their own would not be possible without high precision timing. Using a single motor reduces the complexity of control as well as allowing the use of a single motor to control the expansion.

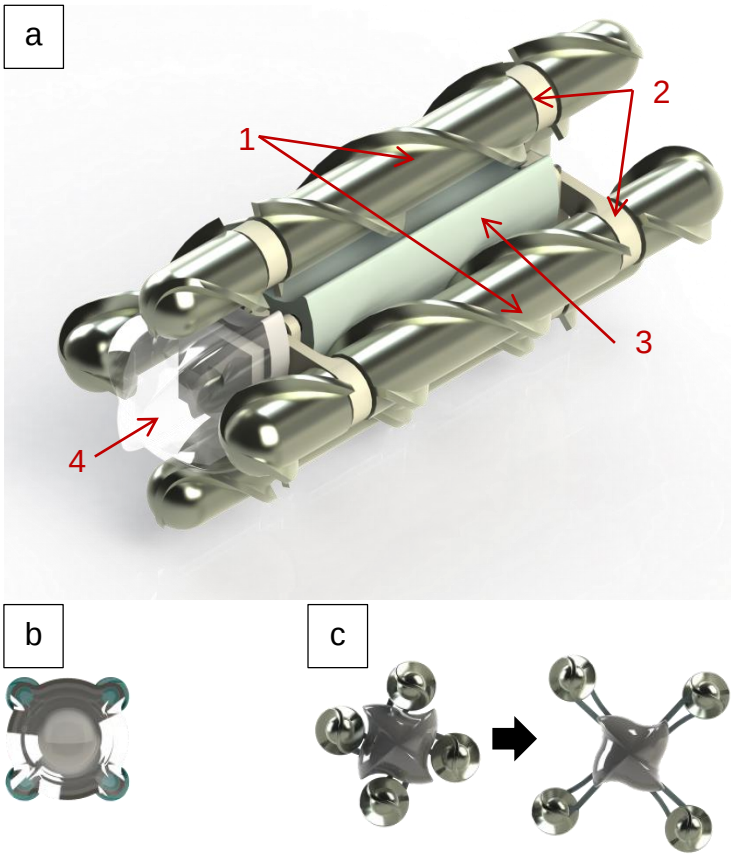

Figure 3.7 Computer model showing the locomotion system version 2, Quad screw device version 2. a) Isometric view of version 2; b) front view of version 1 (for comparison); c) front view of version 2 showing expansion. Annotations show: 1) Archimedes' Screws; 2) Controllable arms; 3) Chassis; 4) Front section with location for camera module.

In re-designing the chassis to incorporate the screws rather than adding screws to the chassis, the ends of the screws are exposed allowing fluid flow. The chassis has been designed such that while the screw arms are

retracted the screws nestle in designed channels along the chassis side, decreasing the minimum diameter of the system. This design allows a high proportion of the screw to be open to the fluid allowing for greater thrust as well as allowing greater contact on a surface increasing tractive capability. In Figure 3.7 the increase in exposed screw can be seen from the 1st (shown left) to 2nd (shown right) generation of the concept.

A functional rapid prototyped scale model of quad screw device version 2 was produced using SLS with each screw driven by 6mm diameter motors (Precision Microdrives model 206-101), as seen in Figure 3.8. The motors were selected based on their size and inclusion of a gearbox; although the torque output was not ideal, the low lead times and availability when compared to other motors meant they could be implemented for initial builds. The prototype was produced at 2:1 scale allowing use of commercially-available gears and motors while allowing ease of assembly.

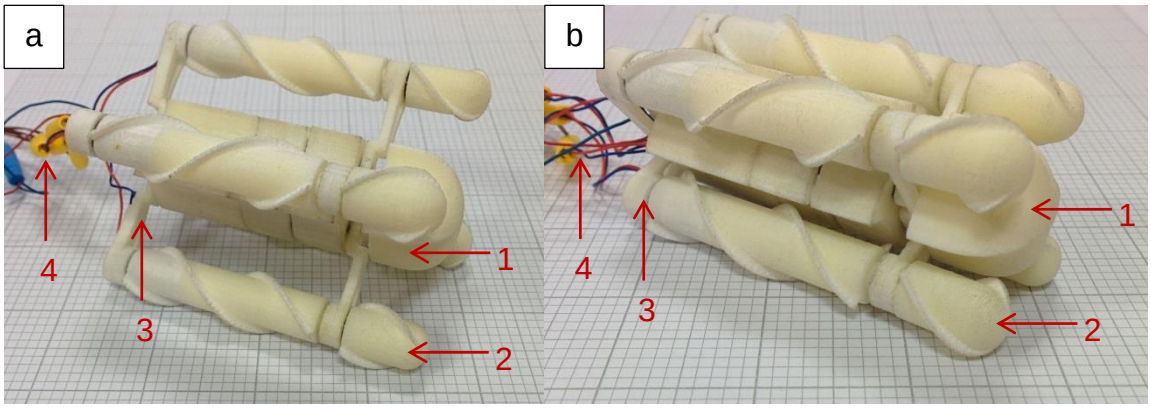

Figure 3.8 Rapid prototyped functional scale model of Quad Screw Device Version 2 a) shown in open state; b) closed state. Annotations show: 1) Nose; 2) Screws; 3) Arms; 4) Tether.

3.8 Design Limitations with Design Prototype Version 2

While mounting the motors in the screws for direct drive allows a simple way to drive them, it does pose several issues with the design. With front mounted gearboxes on the motors, there is no way to access the transmission from the rear of the motor. This means that while the screw rear-sections would ideally be powered, with no transmission they will remain stationary.

The transmission between the mid-section of the screw and the front-section of the screws is solved using a short axle that passes through a bearing in the front arm. The rear of the screw is directly connected to the motor gearbox shaft with the motor being secured from the rear.

The mounting of a geared motor should be by the designated mounting point located on the front of the gearbox. This prevents torque being transmitted through the gearbox and motor shaft, which can damage the unit.

The front mounting section typically has a thread or tapped holes specifically for mounting which manufactures strongly advise should be used. The motors in quad screw device version 2 are secured using an adhesive at the rear of the motor chassis. The motor mounting is shown in Figure 3.9.

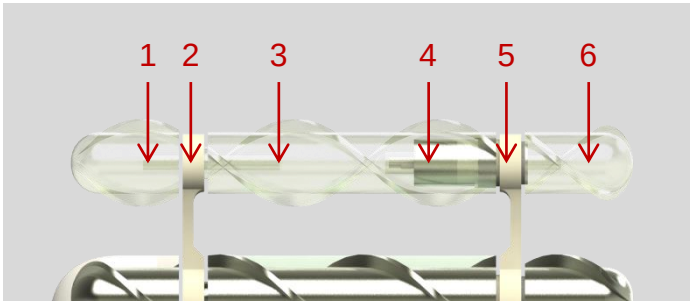

Figure 3.9 Motor arrangement for the screw actuation motor in Quad Screw Device Version 2. Annotations show: 1) Front-section screw; 2) Front controllable arm section; 3) Mid-section screw; 4) Screw motor; 5) Rear controllable arm section; 6) Rear-section screw.

Not only does the positioning of the motors risk adverse torque on the motor chassis, it also applies normal loading to the motor shaft when resting on a surface. Motor shafts are very sensitive to normal loading, which can misalign the inner gears, and wiring. As the screw mid-section rests against the motor chassis, this creates a wear surface and a means for which contaminates may enter the system.

3.9 Exploration of Design Solutions

To resolve these issues different motor types and mounting locations were explored.

Outrunner motors, typically used in model aircraft and quadcopters, feature a stationary central axle with the chassis and electrical coils rotating about the axle. Through attaching the central axle to the arms either side of the screw, the screw sections could be attached to the motor chassis to provide rotation. While this method would be ideal for transferring locomotion from

the motor to the screw, there would be no simple way to transfer drive to the front-section and rear-section screws without multiple shafts and gearing.

A second possible solution would be mounting the motors on the arms with a 90° gear system allowing the transmission to the screw sections. This would allow all three sections to be actuated, at the cost of greater complexity of design. The length required for the motors and the length of the arms prohibits this solution.

An adaptation to the arm mounted motors would be to mount the motors in the chassis and have a transmission system to power the screws. This could be done through the use of belts, chains or 90° gearing systems. However due to the sizes involved, this is an impracticality with current manufacturing methods available.

A third possible solution would be to mount the motors on the rear arm. While this would remove the rear-section screw, this is an acceptable compromise as it allows direct drive of the other screw sections while allowing ease of assembly.

3.10 Design Prototype Version 3

The third mounting solution explored in the previous section was adopted for the next generation of the locomotion system. In mounting the motors on the rear of the arms, direct drive is possible from the motor's inbuilt gearbox simplifying the mechanical design. The motors selected for this design are discussed further in Chapter 4. A computer model of the system can be seen in Figure 3.10.

With the motors moved in their location, the rear-section screws were removed. In their place are streamlined pods, which house the motors, protecting them from the environment. Using a sealed unit for the motors protects from intrusion of substances aiding with prevention of cross-contamination. Some motor manufacturers produce motors for medical applications, which may be sterilised in an autoclave, these may be utilised to aid with cross-contamination. A computer model of the new arrangement can be seen in Figure 3.11.

The expansion of the system is key to its ability to provide stable contact with the lumen, open collapsed sections and reduce wall contact or pass through narrow regions. This is provided through inter-linking the four arms to a 5^{th} internal motor – allowing synchronous movement of the arms, Figure 3.12. Where contact locomotion is needed, the arms allow the system to

maintain constant contact with the lumen increasing the ability to provide thrust. In collapsed sections of the lumen, the device may fold into the closed state, enter the passage using contact-based locomotion and then unfold the arms opening the lumen. This allows for greater visibility increasing the inspectional outcomes.

The series of computer models shown in Figure 3.12 illustrates how the mechanism for expanding the device works. Each of the arms is attached to the chassis by a separate axle, which runs parallel to the centre of the chassis. Viewing the device front on, as the arms rotate anti-clockwise, the screws travel away from the central chassis reaching their maximum displacement when the arm becomes parallel to an imaginary line connecting the screw centre and chassis centre. The orange marker denotes the same screw throughout the rotation, starting at the left of the figure. The rotation covers 150° and the distance between the screw centre and chassis centre increased by 10mm (14mm to 24mm).

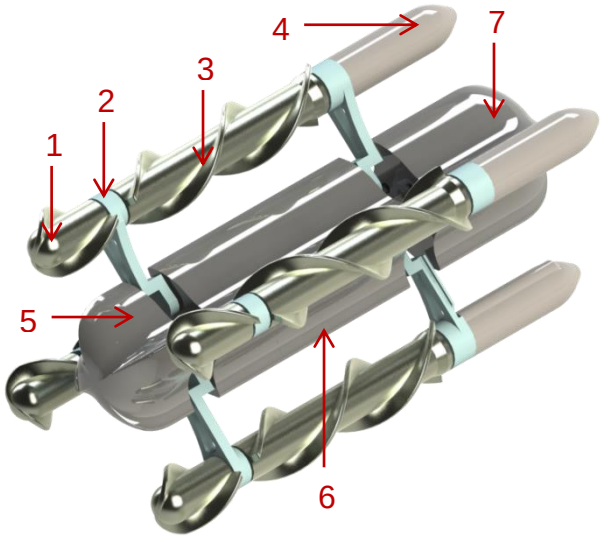

Figure 3.10 Computer model showing the locomotion system version 3, Quad Screw Device Version 3. Annotations show: 1) Front-section screw; 2) Controllable arm section; 3) Mid-section screw; 4) Screw motor housing; 5) Front chassis section with space for camera module; 6) Central chassis section housing arm motor and gears; 7) Rear chassis section with space for motor controllers, communication electronics and tether mount.

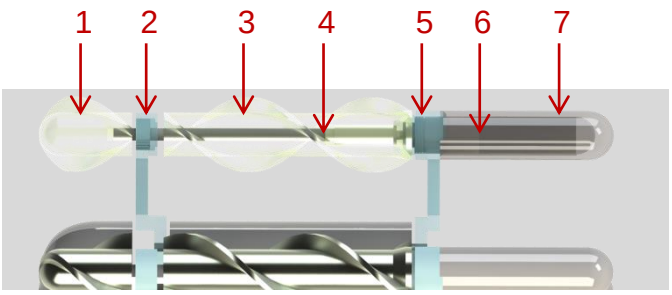

Figure 3.11 Motor arrangement for the screw actuation motor in Quad Screw Device Version 3. Annotations show: 1) Front-section screw; 2) Front controllable arm section; 3) Mid-section screw; 4) Transmission shaft; 5) rear controllable arm section; 6) Screw motor; 7) Screw motor housing pod.

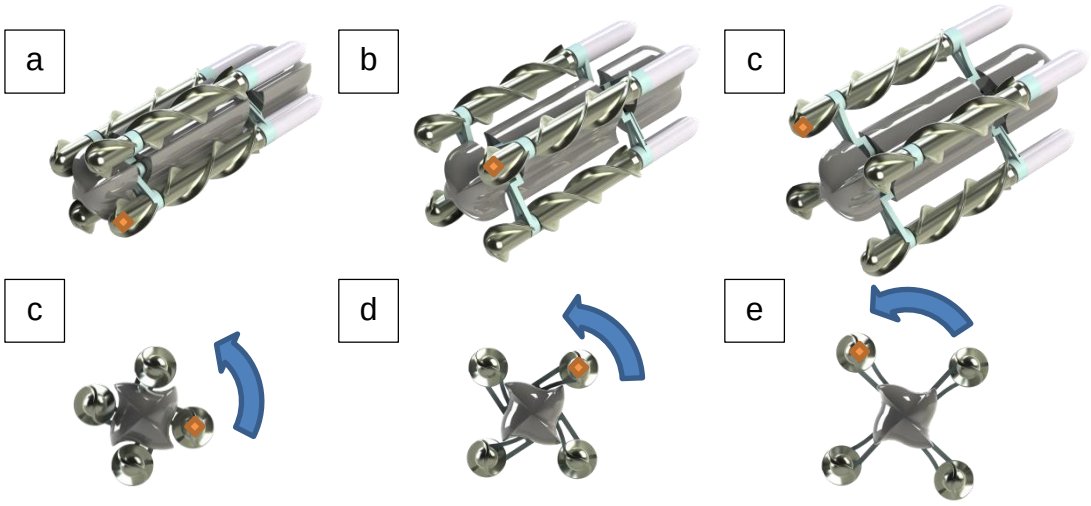

Figure 3.12 Arm expansion of the locomotion system. The orange dot donates the same arm throughout the expansion to aid visualisation of the motion. In the collapsed state, (a: isometric view, c: front view), each of the 4 screws are nestled against the chassis. As the expansion occurs, the arms rotate about the body, reaching full expansion as shown right (c: isometric view, e: front view).

3.11 Summary of Design Process

The final iteration of the design comprised 4 independently driven Archimedes' screws, each mounted at the end of a controllable arm. The 4 arms are controlled by a single motor such that they move in unison. Throughout this chapter, several changes were made to the design to compensate for issues raised. This section addresses the requirements laid out for the design in section 3.1, and how the requirements are met.

3.11.1 Clinical Requirements

The design meets the clinical requirements as set out at the start of this chapter. Further evidence for meeting the requirements can be found in Chapters 4-6.

- Atraumatic tissue interaction
    - Through material selection and screw design, the system may be atraumatic, meeting the clinical requirement. This is discussed further in Chapter 4.
- Amphibious locomotion
    - As discussed through the literature review in Chapter 2, Archimedes' screws are able of providing amphibious locomotion using the same drive effectors, the screws themselves, in a wide range of environments. Further analysis of the developed locomotion system and experimental assessment is discussed in detail in Chapters 5 - 7.
- Appropriately scaled relative to a colonoscope
    - Current technology in additive layer manufacturing and market available actuators can be used to produce the system at an appropriate scale for hydro-colonoscopy. This is assessed further in Chapter 4.

3.11.2 Technical Requirements

The technical requirements of the system have been met by the design process and further analysis and discussion can be found in Chapter 4.

- Communication and power supply
    - The locomotion system can be used in either a tethered or tether-less approach. A tethered approach has been initially chosen based on recommendations in literature on power supply and data communication, as discussed in Chapters 2 and 4. Should battery technology improve then the system is able to be adapted to make use of such improvements.
- Generate appropriate propulsive thrust for movement
    - The 4 screws allow a high degree of freedom of the system giving it the possibility to traverse the colon. Further assessment is carried out in Chapters 4-7.
- Payload capability
    - Through conscious design decisions, the locomotion system has a dedicated location for camera mounting with the possibility that other payload equipment may be attached. This is further assessed in addition to this chapter in Chapter 4.

Chapter 4
Detailed Design and Implementation of the Concept Locomotion System

To assess the prototype locomotion design for its ability to provide locomotive force and thus deem it fit for purpose, it must be realised into a functioning system. Throughout the process of analysis, several challenges were overcome involving the locomotion system and sub-systems. This chapter covers the processes involved in realising a functioning locomotion system. Theoretical study and experimental assessment of the locomotion system design in isolated fluid (Chapter 4) and contact (Chapter 5) states were carried out, the results of which have fed into the design stages, forming an iterative design process. This chapter focuses on the findings of the studies in following chapters and the implementation of the design changes, which results in the production of a 2:1 scale prototype, which is assessed later in this thesis in Chapter 7.

4.1 Driving the screws

As with any mechanical system, control plays a vital role in both its design and operation. Closed loop control allows the regulation of velocity through different regimes, and is preferable in any system. This requires feedback from the output to correct the input. One method of closed loop control is through the use of proportional-integral-derivative (PID) control: the locomotion system's screws were controlled using this approach in conjunction with signal conditioning to reduce signal noise. PID control is widely used in industry due to the only input to the control system being the process variable; the controller does not need any knowledge of the underlying processes affecting the control variable.

4.1.1 Motor Control

The purpose of motor control is to maintain the output of a motor while the operating conditions change. Motor control should also be able to adapt to changes in the demand velocity, applying the appropriate change in motor output to change to and maintain the new output.

For the designed system, the velocity of each motor relative to the other motors is more important than the accuracy of the individual motor. As the system is propelled by four independent motors, their combined output

affects the motion of the device. The control system should be able to compensate for a lower thrust than desired from a single or multiple motors and maintain desired end location over velocity. For the development of the overall control system, control of the individual motors will be focused on initially. This will allow more complex control systems to be built throughout the project. A responsive controller for each motor is more desirable than a highly accurate one, such that minor errors or overshoot can be dealt with providing the system responds quickly to inputs.

Proportional-integral-derivative, PID, control is widely used in industry for closed loop systems (85, 86). The controller calculates the error between the desired set point and the current set point, adjusting the control signal accordingly (Figure 4.1). Three separate functions make up the controller, each of which are applied to an internal variable; the summation of these with the previous signal forms the control signal. The three functions apply a constant to a specific error type: Proportional, the current error; Integral, the sum of past errors; and Derivative, the rate of change of error, (85, 86).

Each of the three separate functions effect the rise time, overshoot, settle-time and steady state error of the control signal. Proportional and integral gain decrease rise time however both increase overshoot while the integral signal increases settle-time. The derivative signal decreases overshoot and settle-time however, it is sensitive to signal noise.

In the terms of controlling the motor velocity, the derivative component of the PID controller is important as overshoot and settle-time can have an undesired effect on motor control. Signal noise in the process variable (position or velocity measurement) is amplified by differentiation, which can result in greater noise in the derivative component. A custom-built PID control algorithm was designed such that the derivative gain could be filtered.

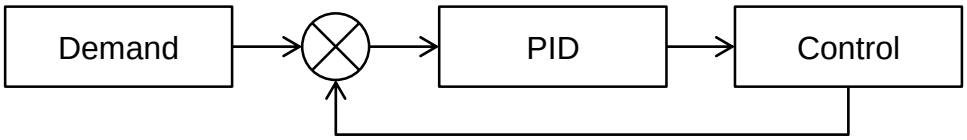

Figure 4.1 PID control diagram (85, 86)

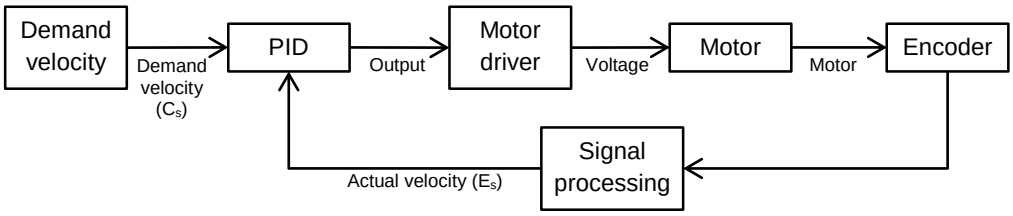

Figure 4.2 Motor control using a PID controller

A PID controller takes the demand and actual velocities as input and generates an output signal. This output, typically a voltage, is sent to a motor driver, which amplifies the signal or generates a pulse width modulated (PWM) signal to drive the motor. The motor velocity, read through the encoder feedback can be then fed back to the PID controller (Figure 4.2).

The PID system can be represented by the following equation.

$$\frac{C_s}{E_s} = [k_P] + \left[\frac{k_i}{S}\right] + [kdS] \qquad \textbf{4.1}$$

Where C_s and E_s are the control and error signals, and k_P, k_i and kd are constants for P, I and D. An analogue filter, also known as a continuous filter is in the S domain, where S is the Laplace operator; while a digital filter, or discrete filter, is in the z domain. An analogue filter can be approximated in discrete time systems using the z operator, given by the following equation. T is the time period and z^{-1} is the delay.

$$S = \frac{1 - z^{-1}}{T} \qquad \textbf{4.2}$$

To discretise the equation into a form that can be run continuously within computer code, equation 4.2 is substituted in equation 4.1 to give:

$$C_z[1 - z^{-1}] = E_z\left[k_P(1 - z^{-1}) + k_i T + \frac{kd}{T}(1 - z^{-1})^2\right] \qquad \textbf{4.3}$$

Finally giving the discretised form:

$$C_t = k_p(e_t - e_{t-1}) + k_i T e_t + \frac{kd}{T}(e_{t-2} - 2e_{t-1} + e_t) + C_{t-1} \qquad \textbf{4.4}$$

This can be separated into three sub functions for use within a control system, with the values for the constants and the filtering options exposed as the input arguments.

The PID control scheme in equation 4.4 can be realised into structured computer code. The following section of pseudo code shows a realisation specific to this implementation. Each time the loop runs, the errors e_t and e_{t-1} must be passed along with the demand and actual set points. The code shifts the errors such that error e_{t-1} of the last loop is error e_{t-2} in the current

loop etc. The demand and actual set point values are used to calculate the new error, e_t. T is the loop time in seconds. The values for P, I and D may be returned at the end of the code execution to process the signals, i.e. apply filtering.

```
e2=e1;            // error for t-2 is error t-1 from last loop
e1=e0;            // error for t-1 is error t from last loop
e0=demand-actual;// current error is difference between
                  //demand and actual
P=kp*(e0-e1);     // calculation for P component
I=ki*T*e0;        // calculation for I component
D=(kd/T)*(e2-2*e1+e0) // calculation for D component
```

4.1.2 Signal Filtering

Signal conditioning allows for undesired frequencies to be attenuated from a signal while maintaining the desired frequencies (85). This can take the form of removing background noise from analogue channels while preserving the data contained within the signal. A common usage is removing mains noise (50Hz sine in the UK) which is imprinted on signals acquired from non-battery powered equipment.

Within a PID controller, the derivative component is very sensitive to signal noise from the current set point. Through use of a PWM signal to drive the motors, the set point signal can be noisy resulting in less than desired stability in the control signal. To overcome this, the derivative signal can be filtered to reduce the effect of noise without greatly decreasing the functionality of the controller.

Low pass filters are used to attenuate high frequency noise from a signal (85). Each order of magnitude for a filter decreases the roll-off rate. For a Butterworth filter, this is 20dB/decade. Such that a 1st order filter has a roll-off of -20dB/decade, 2nd order of -40dB/decade and 3rd order of -60dB/decade and so forth. Each order increases the phase lag, due to more information being required for the process. In this respect, it is important to select an appropriate attenuation level while minimising the order or magnitude to decrease the response lag.

In this specific case, the measured signal is of low frequency while the noise is high frequency. A second order low-pass Butterworth filter was used as it applies a high attenuation on frequencies greater than a cut off value while maintaining lower frequencies in the signal and can operate within the timescale required for the control (>10ms). This allows the higher frequency noise to be removed while preserving the lower frequency control signal.

The analogue prototype for a second order low pass Butterworth is as follows.

$$H_a(s) = \frac{1}{(S+a)\cdot(S+\bar{a})} \quad \textbf{4.5}$$

Where $H_a(s)$ is the transfer function in the s-domain.

Using Euler's identity, $a = e^{\frac{j\pi}{4}}$, the following is obtained from equation 4.5

$$H_a(s) = \frac{1}{\left(S+e^{\frac{j\pi}{4}}\right)\cdot\left(S+e^{\frac{-j\pi}{4}}\right)} = \frac{1}{S^2+\sqrt{2}S+1} \quad \textbf{4.6}$$

To use the filter within a computer system the filter must be digitalised. An analogue filter, also known as a continuous filter is in the S domain; while a digital filter, or discrete filter, is in the Z domain. To convert from S to Z, a bilinear transform is used,

$$S = c\cdot\left(\frac{1-Z^{-1}}{1+Z^{-1}}\right) \quad \textbf{4.7}$$

This allows the difference equations to be obtained allowing operation within computer code. Where c is a constant calculated from the cut off frequency, ω_c,

$$c = \omega_c cot\left(\frac{\omega_c T}{s}\right) \quad \textbf{4.8}$$

Applying the bilinear transform to equation 4.6,

$$H_d(Z) = \frac{1}{\left[c\cdot\left(\frac{1-Z^{-1}}{1+Z^{-1}}\right)\right]^2+\sqrt{2}\left[c\cdot\left(\frac{1-Z^{-1}}{1+Z^{-1}}\right)\right]+1} \quad \textbf{4.9}$$

$$H_d(Z) = \frac{1}{\left[c\cdot\left(\frac{1-Z^{-1}}{1+Z^{-1}}\right)\right]^2+\sqrt{2}\left[c\cdot\left(\frac{1-Z^{-1}}{1+Z^{-1}}\right)\right]+1}$$

$$H_d(Z) = \frac{1}{\frac{[c\cdot(1-Z^{-1})^2]}{(1+Z^{-1})^2}+\frac{\sqrt{2}\cdot c\cdot(1-Z^{-1})}{(1+Z^{-1})}+1}$$

$$H_d(Z) = \frac{(1+Z^{-1})^2}{[c\cdot(1-Z^{-1})^2]+\left[\sqrt{2}\cdot c\cdot(1-Z^{-1})\cdot(1+Z^{-1})\right]+[(1+Z^{-1})^2]}$$

$$H_d(Z) = \frac{(1+Z^{-1})^2}{\left(c^2+c\sqrt{2}+1\right)\cdot Z^{-2}+(2-2c)\cdot Z^{-1}+\left(c^2+c\sqrt{2}+1\right)} \quad \textbf{4.10}$$

The digitalised filter (equation 4.10) can be used in an algorithm for signal processing.

4.1.3 Control System Hardware and Software

A digital control system was selected over an analogue due to the ability to reconfigure the system without rebuilding circuits. A digital control system can be run alongside data acquisition (DAQ) hardware, performing operations on the signals and providing output signals. A digital system is also able to log readings to file of input and output values to allow analysis on the data. In being able to adjust the code that runs on the digital system, modifications can be applied and features added. This re-configurability outweighs the cost increase over an analogue system. An analogue system is most suited for deployment but it cannot be easily altered and such a digital system was selected.

The digital system selected must be able to handle analogue and digital input and output signals, as well as perform analysis on the signals such as PID control and signal filtering. Expandability is key to being able to adapt for unforeseen requirements and such any digital system selected must have the ability to alter the input and output system and code executed on-board.

The DAQ system must have the ability to read 4 digital inputs (encoder channels) and a minimum of two analogue inputs for reading load cell values. Analogue outputs are required to send commands to motor drivers and other hardware.

Initially a MyDAQ system was selected from National Instruments. The USB powered system has an array of analogue and digital input and output channels. The LabVIEW programming environment by National Instruments, which accompanies the hardware, is able to connect to, and utilise any ports on the hardware in a reconfigurable approach. The hardware features on-board digital counter for encoder TTL signals. However, the MyDAQ was found to be unable to simultaneously read from multiple analogue input channels. Opening a second channel would leave the first open and such the reading would become a combination of the two inputs. For this reason, a second system was researched.

National Instruments provide a compact reconfigurable input output system (cRIO) which features an embedded controller and a reconfigurable chassis with a Field Programmable Gate Array (FPGA) system on a chip (SoC) module. The chassis can be expanded through modules that can be plugged

in. These modules provide input or output capabilities for both analogue and digital signals.

National Instruments' LabVIEW integrated development environment (IDE) allows the design of skeuomorphic graphical user interfaces (GUIs) and development applications for a wide range of hardware targets. Using the same IDE to develop and deploy code for the embedded controller, FPGA SoC and host machine simultaneously allows for faster development of larger applications. The IDE also takes care of discovering the attached hardware and handing connections between the host machine and the cRIO. The extensive IDE decreases the time spent on development and debugging enabling greater time to be spent on the outcomes.

The solution provided by National Instruments allows a reconfigurable digital system to be developed with scope to adapt and expand when needed. For this reason and the aforementioned, it was selected for use with the project.

To build a control system for the motors and attach any measurement devices needed such as load cells and encoders, a cRIO was selected along with appropriate input and output modules. Simultaneous analogue reads are important for sequencing input data from several load cells, with other analogue channels available for less time-sensitive measurements etc. Analogue output is needed for motor control signals and communication with motor driver boards. Digital input is needed for reading encoder TTL signals to ascertain the velocity of a motor etc. The specification of the hardware set up is listed in Table 4.1.

Table 4.1 National Instruments hardware

Hardware item	ID	Features
Real-time controller	NI 9024	Embedded real-time controller, 800MHz CPU, 512 MB DDR2 memory, 4GB non-volatile storage.
Chassis	NI 9114	8 slot chassis, Xilinx Virtex-5 FPGA SoC.
Analogue input module	NI 9205	16 differential analogue channels, 16b resolution, 250kS/s.
Analogue output module	NI 9264	16 analogue channels, 16b resolution, 25kS/s.

Table 4.1 cont…

Hardware item	ID	Features
Digital input and output module	NI 9401	8 bidirectional channels, 100ns I/O.
Analogue input module	NI 9223	4 differential channels, 16b resolution, 1MS/s, simultaneous reads.

The custom PID controller and Butterworth filter were implemented using LabVIEW and deployed onto the embedded system FPGA for use in motor control. Hardware implementations of algorithms run with increased stability in loop timing. FPGA operations are inherently parallel; *n*-tasks can be run at the same time where *n* is defined by the programming structure. Running the control of several motors in parallel allowed for a higher stable control clock while allowing for reliable time steps between readings. Hardware run tasks run at higher cycle rates than their software cousins reducing load and resource usage on the host computer improving stability of the control system.

Using the digital module in input mode, the FPGA SoC was used to read the motor encoder TTL signals and determine the motor velocity. This was used within embedded code as an input to the PID control algorithm to calculate the control signal, which is sent to the motor controller board from the analogue output module.

The FPGA SoC was used to collect load cell data from the analogue channels with timestamp data and feed this to the embedded controller on the cRIO along with the motor velocities. This assured all readings were taken in parallel allowing direct comparisons to be made.

The schematic in Figure 4.3 shows the arrangements of hardware and the connection types between them over which data is sent. The NI hardware is assembled and then connected to the host machine using an Ethernet connection. Data between the host machine and the NI hardware is packaged and sent every 10ms, this allows for transfer latency. The data read by the NI hardware is at the hardware's clock speed of 40MHz although this volume of data is not required for analysis and such it is sampled at a lower rate which can be set by the user (typically 100Hz).

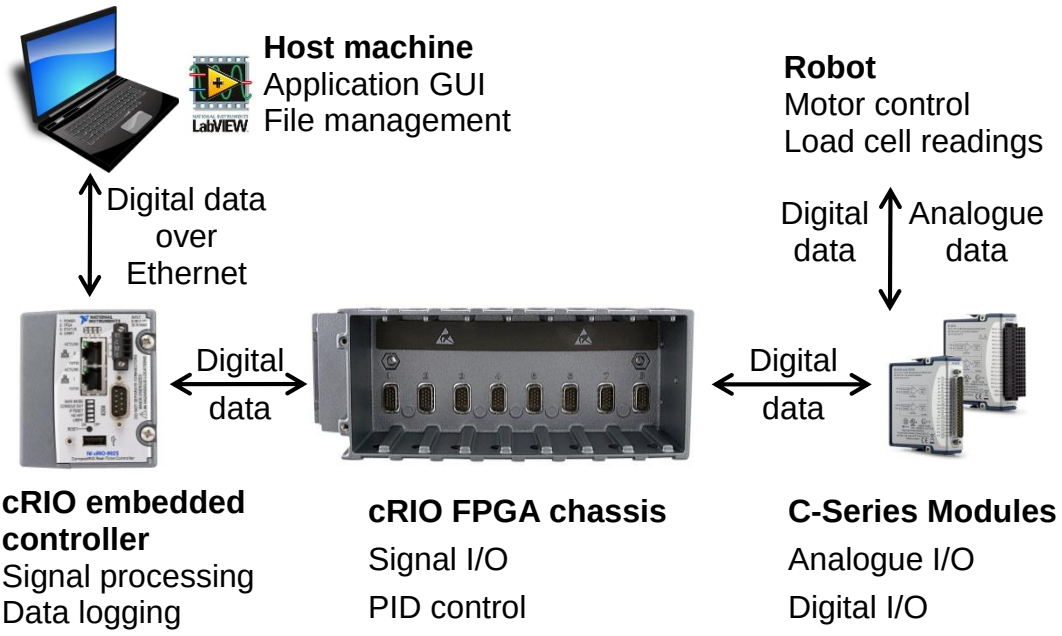

Figure 4.3 Hardware utilised and data flow between components

4.2 Components

While many of the components used within the locomotion system are specifically designed and custom produced, other components were sourced from commercially available sources: these include motors and bearings.

4.2.1 Motor Criteria

In selecting motors, several criteria had to be met as listed below.

Motor criteria

- The overall device must fit within the colon (diameter: 20-60mm), the motors therefore must be smaller.
- Provide sufficient output rotational velocity to provide fluid locomotion (velocity required discussed as part of Chapter 5)
- Provide sufficient torque to move the device when in contact (discussed in Chapter 6)
- Sterile or possibility of sterile manufacture (important for medical applications)

4.2.2 Motor Selection

From the design of the locomotion system as per Chapter 3, a 6mm diameter motor is of ideal size. To fit within a colon of 20mm diameter, the motors must smaller than this. The concept design features five motors as discussed in Chapter 3 and illustrated in Figure 4.4. To fit within a diameter of 20mm, the maximum diameter a motor can be is 6.6mm. Motors of 6mm

diameter are readily available on the market, which makes them an ideal selection for the initial concept.

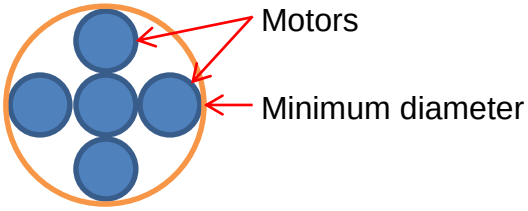

Figure 4.4 Motor arrangement for minimum diameter

Several manufacturers produce motors in this scale, Precision Microdrives, Maxon Motors and Faulhaber (Table 4.2). Each have a range of 6mm motors with integrated gearboxes with customisable gearing ratios. The motors supplied by Maxon have the highest stall torque and operational torque, which is ideal for high demand situations such as contact based location. While the Faulhaber motors have a higher maximum angular velocity, the larger gearing ratios needed for torque increases the size requirements.

Table 4.2 Comparison of 6mm diameter motors

	Precision microdrives	Maxon	Faulhaber
Diameter	6mm	6mm	6mm
Length	12.2 mm	15.6 mm	15 mm
Stall torque	Not stated	0.485 mN·m	0.22 mN·m
Nominal torque	0.05 mN·m	0.324 mN·m	Not stated
Maximum velocity	14000 rpm	18600 rpm	20200 rpm

To rotate a screw in contact with a surface, the coefficient of friction in the parallel direction (C_P) must be overcome. This is explored in greater depth in Chapter 6. As this coefficient of friction increases, the torque required to rotate the screw increases proportionally. The value of C_P is dependent upon the materials in question and the contact mechanics; it will vary between fluid and contact states of locomotion. Fluid based locomotion requires a higher angular velocity and lower torque to generate thrust (87), as discussed further in Chapter 5. Thus in selecting a motor and gearbox

combination to suit both situations requires several trade-offs: ideally an adjustable or variable gearbox would be used.

For the final locomotion system, Maxon motors were selected. Maxon are able to offer sterilisable systems for use in medical applications, which is of importance to any inter-luminal device. These motors are available on special order and were not used for the work detailed in this thesis.

The motor selected for the locomotion system is a Maxon RE6 motor, (part number 349190). The motor is compatible with several planetary gearboxes and can be purchased as part of a motor-gearbox combination.

The RE6 349190 motor has a peak torque of 0.324mN·m at 5670 rpm, running with a supply of 3v and 0.242A. The stalling torque for the motor is 0.485mN·m (Table 4.2, Figure 4.5). Through mathematical analysis of the gearboxes available, the predicted max angular velocities and torque can be calculated.

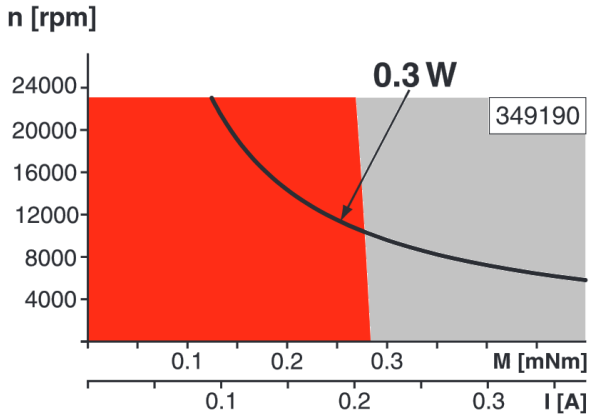

Figure 4.5 Operating range of selected Maxon motor. Red denotes continuous operation; grey denotes short-term operation in which the motor may be briefly overloaded (recurring). Graph taken from Maxon catalogue (EN) 2013/14.

The information in Table 4.3 indicates the output shaft velocity and torque of three gearboxes at the motors maximum torque output.

Table 4.3 Motor gearbox combination output angular velocity and torque at motor peak torque velocity

Motor (RPM)	5670	5670	5670
Gearbox ratio	15:1	57:1	221:1
Output (RPM)	378	99.47	25.67
Output (rad s^{-1})	39.58	10.42	2.69
Maximum output torque (Nm)	0.01	0.02	0.06

The information in Table 4.4 indicates the performance of the same three gearboxes at the motor's maximum velocity.

Table 4.4 Motor gearbox combination output angular velocity and torque at motor peak velocity.

Motor (RPM)	18600	18600	18600
Gearbox ratio	15:1	57:1	221:1
Output (RPM)	1240	326.32	84.16
Output (rad s^{-1})	129.85	34.17	8.81
Output torque (Nm)	0.005	0.01	0.03

As it can be seen from Table 4.3 and Table 4.4 while the 221:1 gearbox produces the highest torque, as expected, the output velocity is relatively low at 84RPM. The 54:1 gearbox produces a third of the torque but is able to operate at a higher angular velocity, 3.8x that of the 221:1 gearbox. As expected the 15:1 gearbox runs the fastest but produces the least torque.

The 15:1 gearbox provides a high angular velocity output, which is suited towards fluid based locomotion: however, the torque produced may not be great enough to overcome contact-based obstacles. The 57:1 gearbox can provide double the output torque at a quarter of the angular velocity, which may greater hinder the fluid based locomotion.

For providing expansion of the arms, the process of selecting a motor and gearbox combination is much simpler: high output torque is needed. The 221:1 is ideally suited at being able to provide toque to distend the bowel. Mathematical analysis was carried out to calculate the forces experienced by the system and the bowel during expansion of the arms.

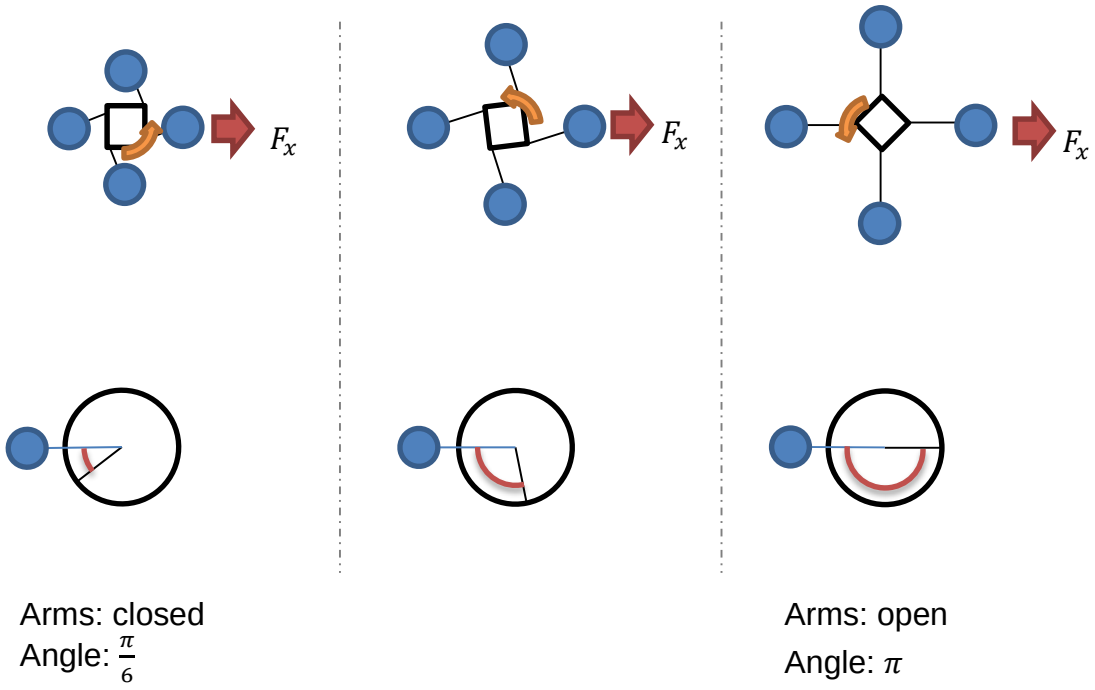

Figure 4.6 Expansion of arms with angle subtended between chassis and arm

Throughout the expansion of the arm mechanism, the normal force exerted upon the colon wall will vary. As the device moves from the closed state to the open state, it is predicted that the greatest force will occur at an arm angle of $\pi/2$ radians. Equation 4.11 links the arm-tip force to the arm angle, and Figure 4.7 shows the derivation of the arm angle. When the arms reach the open state, where no further increase in device diameter is possible, the force exerted by the device will tend to zero, as no further displacement is possible.

$$F_x = \frac{motor\ torque}{arm\ length} \cdot \sin(arm\ angle) \qquad \textbf{4.11}$$

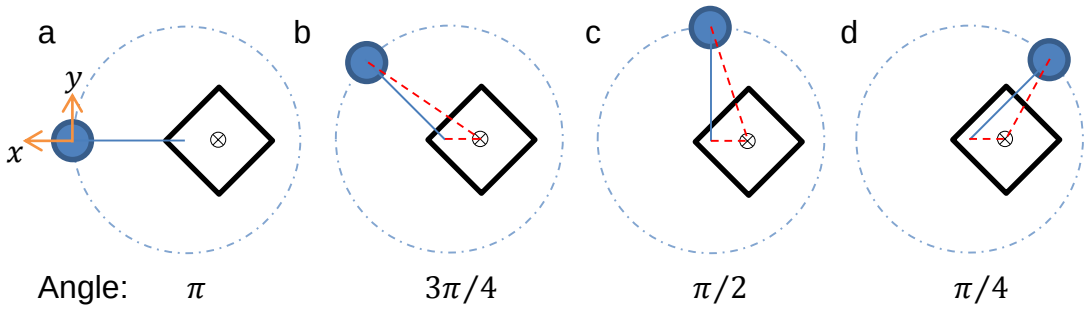

Figure 4.7 Angle formed as an arm moves from open to closed position. The black square denotes the chassis; the blue solid circle denotes the screw with the connecting blue line the arm. The dotted red lines shows the construction of the angle, the dotted blue line shows the path the screw may take about the chassis.

For each of the gearboxes the force was calculated through the arm expansion motion, the results can be seen in the graph in Figure 4.8.

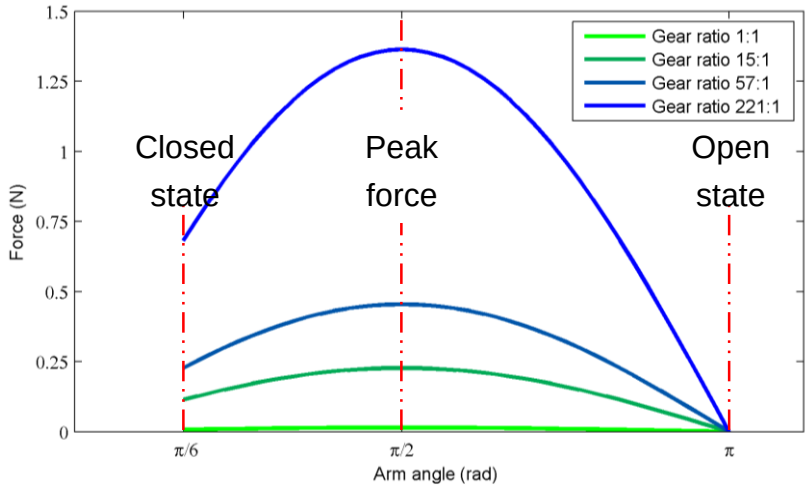

Figure 4.8 Force exerted at arm tip in the x-axis during arm expansion for varying motor gearbox combinations

As expected the outwards force tends to zero as the arms reach their full expansion, with the greatest force being exerted part way through the operation. The highest ratio gearbox produces up to 1.36N per arm. Taking the contact surface area of an arm against tissue to be half the surface area of a screw, 301.6 mm^{-2}, the pressure on the colonic wall imposed by each arm is calculated to be 4.5 kPa. This is less than the minimum force required to perforate colonic tissue of 14 kPa as established in Chapter 2, leading to safe operation of the system.

4.3 Screw design

The screw geometry defines the system's ability to generate thrust. The thread depth, pitch and number of threads have effects on the thrust generation, as discussed further in Chapters 5 and 6.

In locating the motors within the screws as initially designed, the thread depth is reduced due to a larger shaft diameter. Housing the motors on the rear of the device allows for a smaller shaft diameter, as discussed in Chapter 3.

The screws were designed around the position of the motor and the sizes feasible using rapid prototyping, to have the largest outer diameter feasible in line with the chassis and arm configuration. The screw dimensions were selected to be 12mm outer diameter (blade tip to blade tip), 4.8mm inner diameter (base of threads), and a 3mm shaft diameter along the centre to allow attachment to an axle (Figure 4.9). The threads are 1.2mm thick at the

tip with a 1% chamfer towards the base. Two pitches were selected, 20mm (40° blade angle) and 40mm (60° blade angle), for use within the experiments. Each screw is 40mm in length. The surface area of a screw shaft, without threads, is 603.2 mm^{-2}. The total contact area against tissue will be dependent on the compliance of the threads and tissue, and the loading applied. An increased loading will result in an increased surface area as the threads collapse and the tissue envelops the screw.

An increased pitch will result in a larger displacement per rotation of a screw along the screw length. The increased displacement in turn requires a higher torque to rotate the screw. In contact, the ability to provide thrust comes from the difference in friction coefficients between the normal and parallel direction, this is explained in greater detail in Chapter 6. Pitches past a certain magnitude are unable to generate thrust due to the breakdown in the relationship of the coefficients: i.e. they contradict each other in terms of locomotion along the screw length. Maximum efficiency of helical paths in gears can be obtained between 40° and 45° (88) in terms of the ability to transmit locomotion. A screw pitch was chosen such that it provides maximum theoretical efficiency and the length of the screw chosen such that it contained an integer number of thread helices: 20mm pitch and 40mm length. A second pitched screw was chosen such that it contained half the number of helices to provide a comparison.

To increase the blade contact without increasing the blade thickness a dual sweep screw was used. This allowed greater contact with the fluid and tissue for locomotion generation without increasing the dimensions of the individual blades. The dual sweep screws are also balanced in terms of rotating mass. For a single sweep screw, incomplete turns would result in an unbalanced rotating mass which would cause control and stability issues.

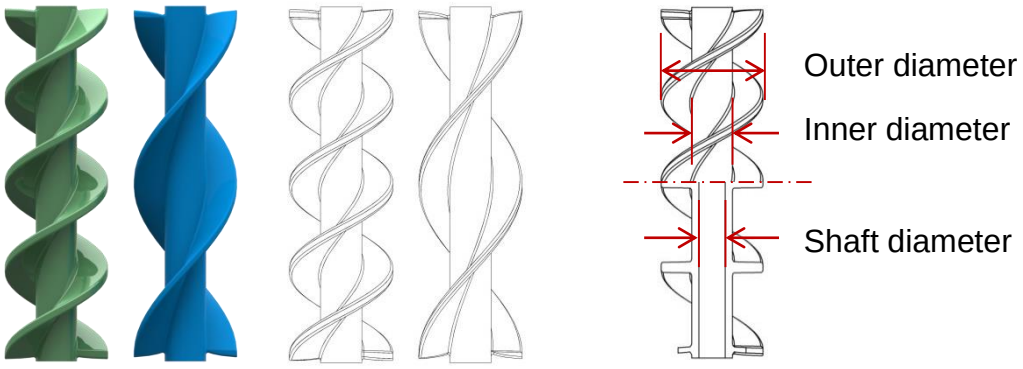

Figure 4.9 Computer image and line drawing of the screws used in fluid and contact testing. From left to right: a) computer image of the 20mm pitch screw; b) computer image of the 40mm pitch screw; c) line drawing of the 20mm pitch screw; d) line drawing of the 40mm pitch screw, e) annotated line drawing of 20mm pitch screw showing definitions of measurements given.

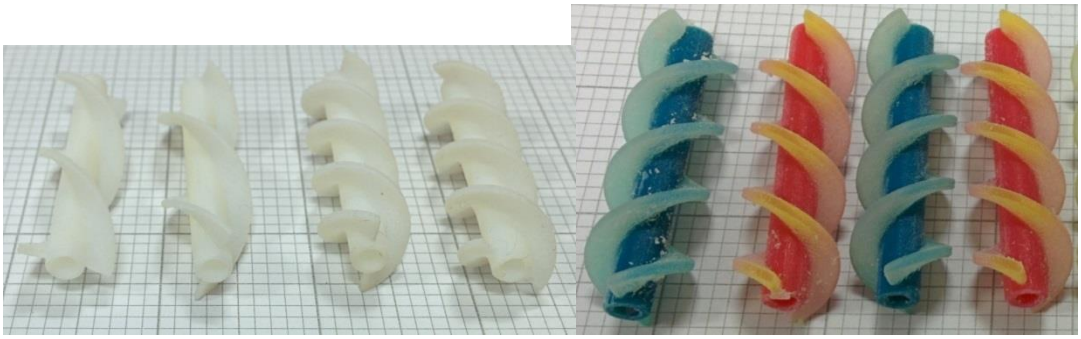

Figure 4.10 Rapid prototyped screw sections. a) Shown left to right: two rigid single material 40mm pitch screws; two rigid single material 20mm pitch screws. b) Shown left to right: four compliant multi material 20mm pitch screws arranged in two pairs of opposite handed threads. Colours are for identification purposes only.

Originally, the screws were produced using a single material, using rapid prototyping (Figure 4.10). In changing the build to include the use of a compliant material for the screw blades, the risk of trauma could be reduced. A digital material ‘DM9860’ was selected for use as the screw blades; the manufacturer states a digital material as a mixture of resins selected for rapid prototyping purposes. The material has a shore hardness of 60 and a tear resistance of 8N/mm. The material was experimentally assessed using a mechanical strain device and found to have a Young’s modulus of 250kNm^{-2}, which is comparable to that of colonic tissue, 212kNm^{-2}. Although the compliant screw blades are stiffer than tissue, due to their thickness relative to tissue, it is hypothesised that they will yield before tissue damage.

Further testing of rigid and compliant threaded screws is discussed in Chapter 6. The effects of compliant screw threads on propulsion through a fluid medium is assessed during Chapter 7. Mechanical properties of tissue were measured by Miss Z Ehteshami, as part of the CoDIR project, work currently unpublished.

4.4 System Concept Modelling

A complete 3D computer model was built using a 3D CAD package (Solidworks, Solidworks Corp. Dassault Systèmes). This model was used to explore the mechanism in which the arms would fold allowing changes in diameter as well as fit the components. A complete breakdown of the final model is shown in Figure 4.11 through Figure 4.15.

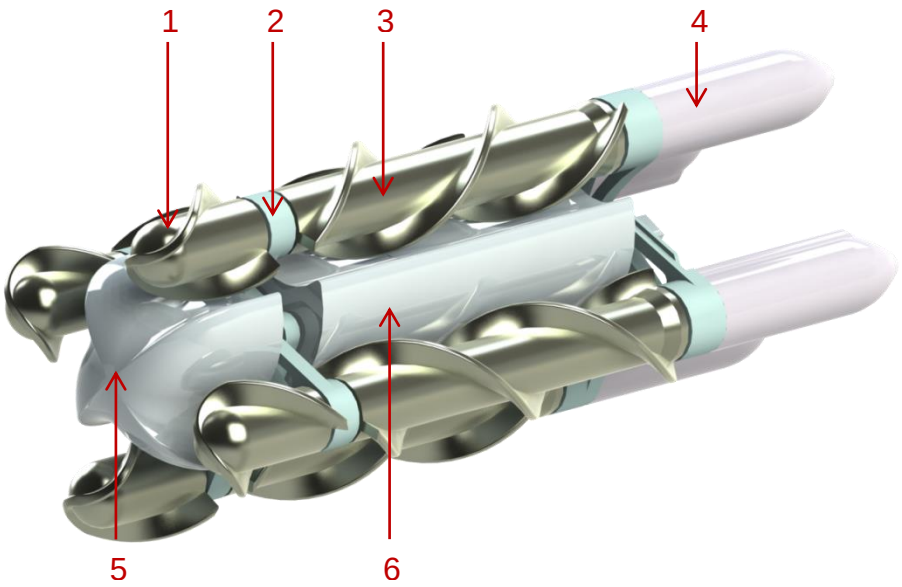

Figure 4.11 Computer model showing the final design of the locomotion system. Annotations show: 1) Front-section screw; 2) Controllable arm section; 3) Mid-section screw; 4) Screw motor housing; 5) Front chassis section with space for camera module; 6) Central chassis section housing arm motor and gears.

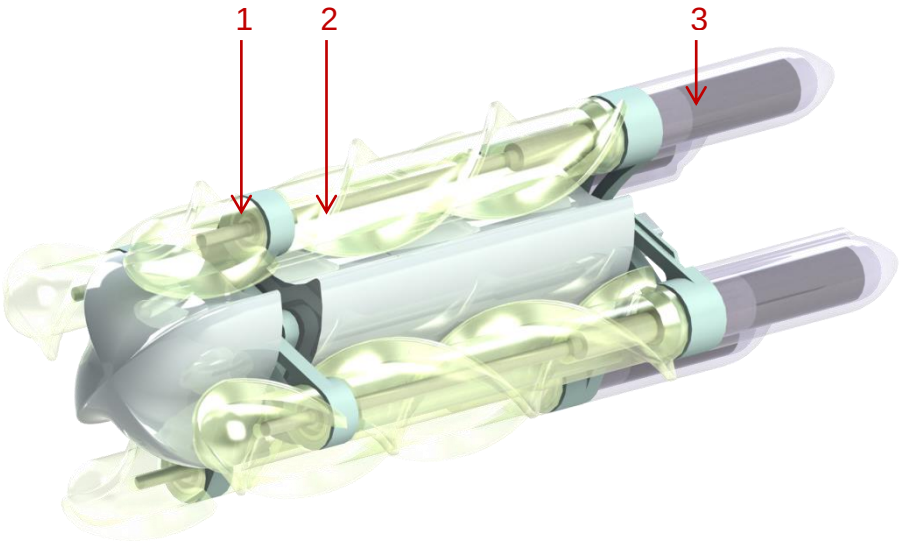

Figure 4.12 Computer model showing the shafts running along the screws connecting the motors at the back to the front screw sections. Annotations show: 1) Bearing housed within arm; 2) Shaft connecting motor output and screw sections; 3) Screw motor.

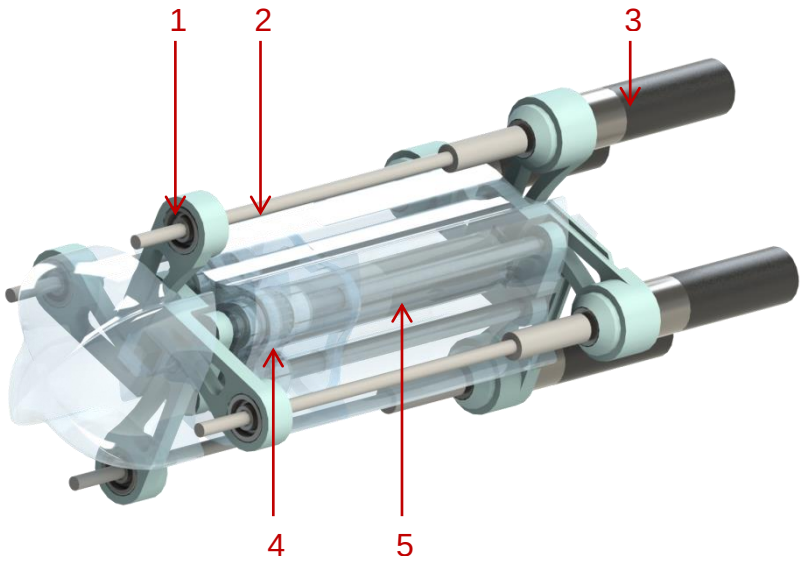

Figure 4.13 A computer model showing the screw motors exposed at the rear and the screw shafts transmission powering the screws. In the centre of the system, the internal motors and gears can be seen. Annotations show: 1) Bearing housed within arm; 2) Shaft connecting motor output and screw sections; 3) Screw motor; 4) Arm expansion mechanism; 5) Central motor used for arm expansion.

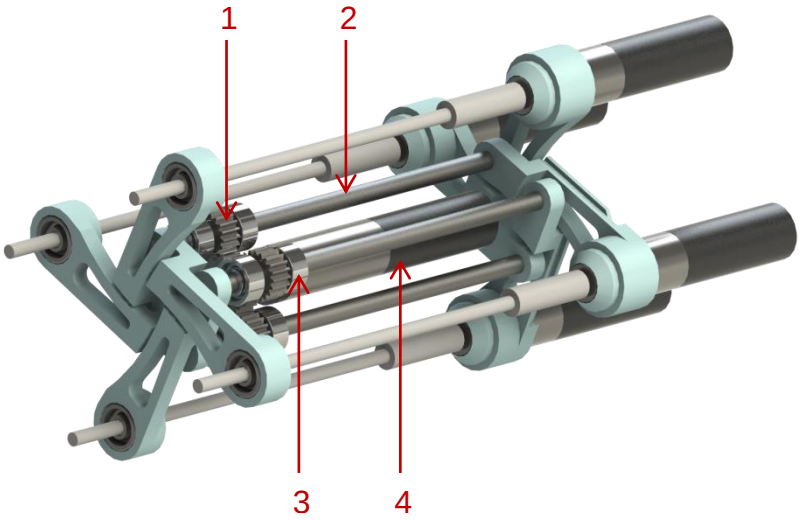

Figure 4.14 A computer model showing the screw motors and transmission exposed. The motor and gears that operate the expansion of the arms are also exposed in the centre. The central motor is connected to a gear, which turns the four surrounding gears, which in turn rotate the arm axles. The arms can be seen in their overlapping state. Annotations show: 1) Arm expansion gears; 2) Arm shaft connecting front and rear arms attached to gearing allowing for synchronous movement between arms; 3) Bearings to maintain alignment of arm shafts; 4) Central motor which drives movement of the arms.

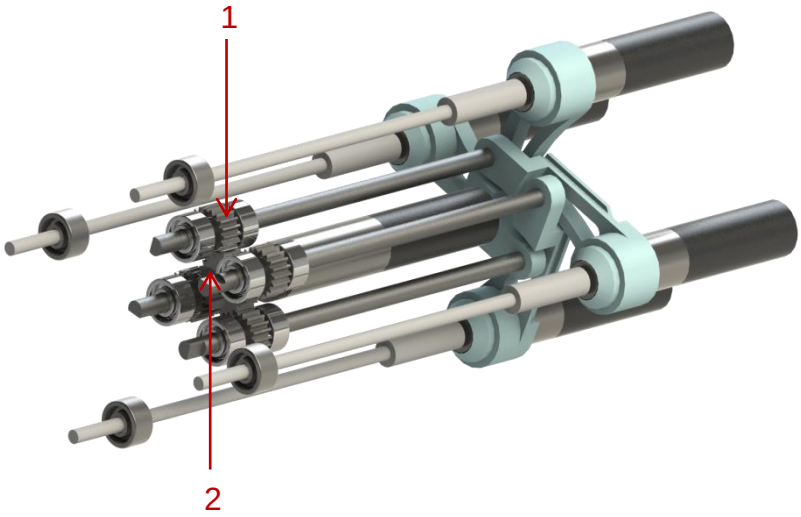

Figure 4.15 A computer model showing the shafts, gears and motors exposed. The central arm shafts have an edge keyway to locate the arms in their correct position and allow synchronous expansion. To the right the method in which the arm overlap to allow for the large percentage change in diameter can be seen. Each arm overlaps the one after it and is overlapped by the one before it. Annotations show: 1) Arm shaft gear; 2) Central motor gear.

4.5 Manufacture

Throughout the construction of the locomotion system, several new fabrication processes were utilised. 3D printing methods allows for complex geometry to be produced, which would be otherwise impossible with destructive methods.

4.5.1 Technologies Used

The process of additive layer manufacturing (ALM), also known as rapid prototyping and 3D printing, builds parts from fusing or setting a powder or liquid medium to form a solid component. The first machines which were able to produce parts using ALM techniques were developed in the 1980's (89), however the use of such machines have only recently hit common knowledge through media coverage through their availability and sometimes controversial usage (90).

The following four methods have been used throughout:

- Selective layer sintering (SLS) uses a laser to melt and bind a powered material to form solid components.
- Stereo lithography uses a light source to set a fluid medium to form solid components.
- Fused deposition modelling (FDM) builds solid components by melting and extruding a thermoplastic filament.
- Polyjet sprays tiny amounts of curable liquids onto the build tray and model to build the component. This process can build in multiple materials simultaneously including compliant materials such as rubber.

Table 4.5 Comparison of strengths and weaknesses for ALM processes listing the components produced using each process.

Process	Strengths	Weaknesses	Used for
SLS	• High accuracy	• Single material • Porous	• Initial fluid testing rig. • Concept prototype versions 1 and 2
Stereo Lithography	• Very high accuracy • Non-porous	• Single material	• Concept prototype 3 chassis

Table 4.5 cont…

Process	Strengths	Weaknesses	Used for
FDM	• Quick to produce • Relatively cheap	• Brittle • Low accuracy • Porous	• Testing apparatus components
Polyjet	• High accuracy • Multi-material • Non-porous	• Becomes weak with long exposure to water	• Multi-material screw sections

4.5.2 Limitations

While ALM enables many designs that would be impossible using traditional tooled manufacturing, ALM is not without its own limitations. With destructive manufacturing, the material is always uniformly dense; ALM can produce non-liner densities throughout the material. This can be to do with the material supplied, the resolution of the production process and the design of the part. While this can be sometimes useful, it can inadvertently cause weak points within a structure leading to an unexpected failure. FDM is particularly susceptible to this, as the finished component can have weakly attached layers leading to planes of weakness.

Support material is used in some processes to allow the main material to cure or set, the support material is removed after production and acts as a scaffold during fabrication. While functioning actuating parts can be produced, such as a wheel produced on axle, the support material used in ALM can be difficult to remove if the design does not allow for this. This can result in parts being produced in a jammed or fused configuration. During the design, if the gap between the fixed and moving parts is too small then they can be produced in a fused state. This is because the machine's resolution does not allow it to distinguish between the separate parts and simply "prints" an approximation of each slice through the design. Should the gap be designed too large then the parts will not fit well resulting in unwanted local movement. For parts that have hollow sections, the machines fill these cavities with a support material to prevent the main section from collapsing[4]. This means it is not possible to produce a completely hollow and continuous

[4] Support material utilisation depends on technology used, machine vendor and print optimisation software. Water soluble support material is entering the market, however this still requires passageways for fluid ingress and waste extraction.

part: holes for removal of the support medium must be built into the design. To overcome these, the designs must be produced with the limitations in mind.

The resolution of the machine and technique being used is critical to utilising the technology. For each technique and machine, there are two specific resolutions for effective use of the technology: layer thickness and printing resolution. The layer thickness is the distance between horizontal layers (in the upwards, or Z, axis). The “HP DesignJet Color 3D” printer (FDM), a consumer level machine, has a layer thickness of 0.33mm while the “Stratasys Object 1000” (Polyjet), an industry leading machine, has a layer thickness of 16µm. The former produces parts that the layers are clearly visible to the eye and can be felt; these pose a significant weakness in these planes, from experience often lead to sheering and failure of the part. Figure 4.16 shows a side-by-side comparison of two different resolution techniques. The latter is able to produce a part with constant density throughout and no layer-based weaknesses, as claimed by the manufacturer. This layer-based weakness can be an issue with for example, wheels. When printed in the Z direction, the wheels can have a stepped edge leading to less than desired smoothness and plane based weaknesses in the spokes and across the wheel edge. The printing resolution defines the smallest change in a direction within the XY plane the device can produce. The aforementioned HP Designjet machine has a resolution of 0.91mm (28dpi), with this being the thinnest part it can produce. The Objet 1000 has a resolution of 0.085mm (300dpi). The management software will round features to the nearest amount the machine can handle and such the designed part may not entirely resemble the produced part.

While ALM may seem like a wonder-technology and a solve-all for designing, it requires knowledge of the techniques used to make the best of its features much like traditional manufacturing.

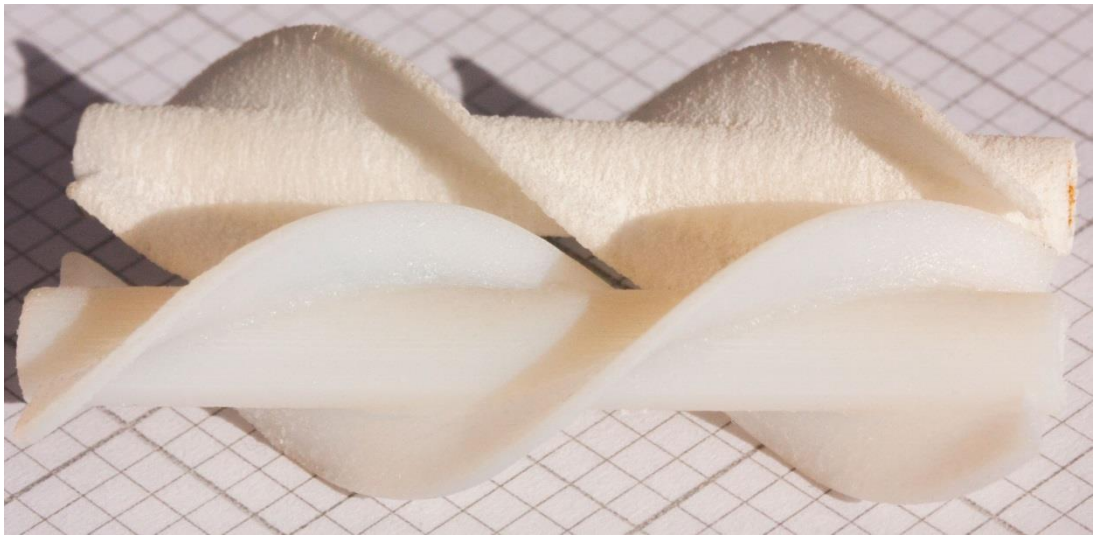

Figure 4.16 Two rapid prototyped dual sweep helical screws, photographed on a 2mm grid. Foreground screw produced using Polyjet manufacturing process; rear screw, produced using SLS, shows clear layer based stepping in the geometry along the screw length.

4.6 Summary of Design and Implementation process

The design of the final concept has been built around the expansion mechanism for the arms. Each of the arms overlaps the arm following it when in the closed state increasing the length of each arm while maintaining a small minimum diameter. To allow for use of off-the-shelf components and ease of assembly, the designed prototype has been produced at a scale of 2:1. The ALM produced parts can readily be produced at a scale of 1:1 in future development to incorporate smaller gears and motors. Although the prototype does not feature on-board motor control or a camera, these have been taken into consideration with dedicated space for the additional hardware available.

ALM has seen a large change in the way in which components can be produced, opening up new design possibilities, which would not have been possible with traditional destructive manufacturing. The combination of different materials in a single component has allowed the design of the prototype to include compliant screw blades with a rigid central structure. The prototype has been designed to take advantage of these new possibilities, allowing the production of small, high accuracy components featuring complex geometry. Components that house motors have built-in attachment threads allowing the motors to be screwed in and held securely without the need for adhesives. ALM allows these threaded sections to be

designed without the need to tap the hole after manufacture, removing the space and access requirements for tapping tools.

Chapter 5
Fluid Locomotion – Theoretical and Experimental Analysis of the Locomotion System

The prototype locomotion system, featuring 4 Archimedean screws, has been designed to produce amphibious locomotion through a flooded colon. In allowing for amphibious locomotion, the screws must function in both pure fluid and pure contact scenarios. This chapter covers the analysis of the performance and characteristics of the screws in a pure fluid state both theoretically and experimentally. A theoretical model of a single screw rotating in fluid was built in order to establish the effects of angular velocity and pitch upon thrust. This was used to aid development of a testing rig and allow characterisation of the effects upon thrust of the variable geometry and compliant screw blades that would be increasingly difficult to model.

5.1 Screw Propulsion Background

Although nature has produced many effective fluid based locomotion methods, the propeller remains the main form of locomotion for macro scale man-made aquatic based craft. The conventional propeller has been a wonder of the modern world in terms of transport and shipping; increasing the speed, efficiency and reliability of vessels over sail and oar based locomotion. In developing a model for fluid based locomotion, it is important to understand the origins of the much taken for granted propeller.

The use of screw propellers is not a new concept, the first accounts date circa 250 BC when Archimedes devised the first recorded screw propeller, which to this day takes his name. The screw propeller consists of one or more veins or blades of constant cross-section, extruded helically along the rotational axis of the shaft. Figure 5.1 shows a two bladed screw propeller. The alternative to the screw propeller, the fan propeller, can be traced back to circa 1500 AD when it was depicted by Leonardo da Vinci in his sketches (87). The fan propeller, as designed by Leonardo da Vinci, consists of paddles or blades located at the end of radial arms with the blades being inclined with the plane of rotation (87), as seen in Figure 5.1.

While propellers were known of for at least 2000 years, the paddle wheel remained the main form of powered locomotion for marine craft until the 19th century. In 1845 the famous tug of war trial lead by Isambard Kingdom

Brunel showed that the screw propeller was more efficient than the paddle wheel (91, 92). The higher efficiency allowed vessels to travel greater distances and at higher speeds than before, revolutionising the industry. This new technology saw a rapid increase in research into fluid based locomotion and through what could be attributed as a serendipitous moment, the paddle propeller was rediscovered after a screw propeller sheered partway along the shaft and the vessel's speed increased (91). The screw propeller originally featured a single swept thread with one complete rotation; increasing the number of blades and decreasing the length was found to increase efficiency and decrease vibrations produced during locomotion.

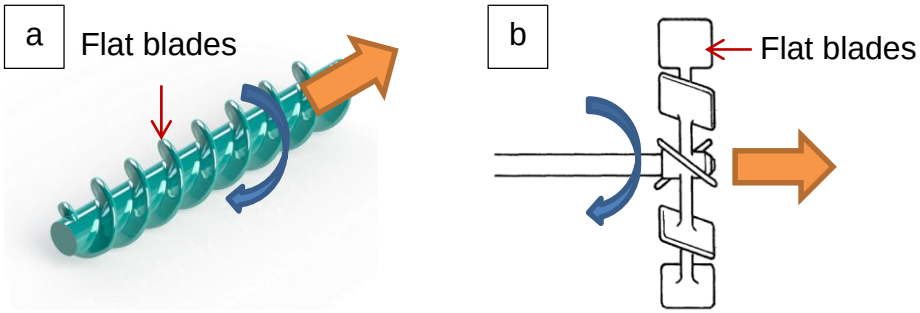

Figure 5.1 Screw propeller (a) and fan propeller (b), (J. Carlton, 2007). Blue arrow shows rotation of the propeller and orange arrow shows direction of thrust.

The aerofoil propeller is an adaption of the fan propeller in which the flat propeller paddles are replaced with a curved blade with an aerofoil cross-section (87). A typical marine propeller is shown in Figure 5.2, propellers feature between 3 and 5 blades depending on the size and output required. The aerofoil blade propeller uses differences in geometry to accelerate the fluid towards the back of the blade. The geometry causes a difference in flow speed between flows over the top and bottom of the blade, which results in a pressure difference (Figure 5.2). This pressure difference, accompanied by Bernoulli's principle, result in lift generation (93). The blades of a propeller are aligned such that this lift force is parallel to the direction of travel, such that this lift force aids motion. To maintain a constant angle at which the tip approaches the flow, known as the attack angle, the blade twists, as can be seen in Figure 5.2. With decreasing scale of operation the thrust produced does not scale proportionally, to maintain thrust production the propeller would need to be driven at higher speeds. (93-95).

In contrast with the conventional aerofoil propeller, the screw propeller produces thrust through a more simplistic mechanism. With each rotation, a

body of fluid is displaced along the length by the veins or blades. These blades are of constant cross section throughout the length of the screw and may form several rotations about the screw shaft. The blades do not accelerate the flow like the aerofoil propeller blades. Due to these differences in operation, there is a notably higher efficiency in thrust production from the aerofoil blade propeller. This is most noticeable in high Reynolds[5] number flows, in the range of 10^6 and higher (87, 94), such as those associated with large ships (87).

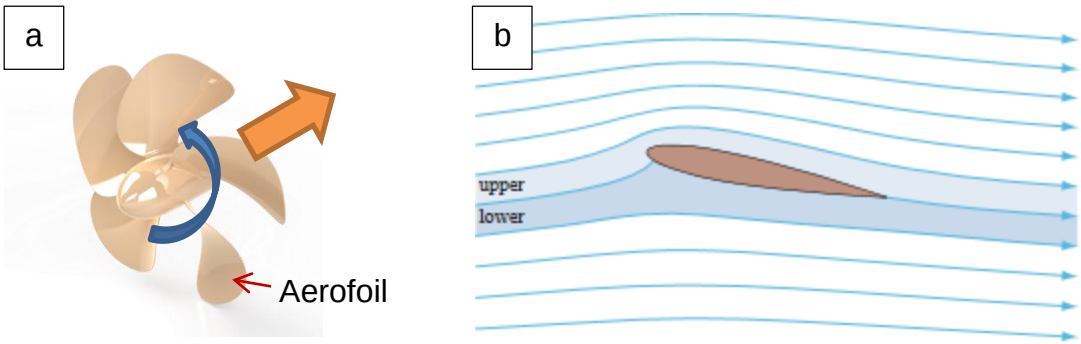

Figure 5.2 The aerofoil marine propeller, a) typical 5 blade propeller; b) aerofoil cross section showing streamlines, M. Belisle 2008.

As screw propellers do not generate thrust in the same process as aerofoil propellers, the aerofoil theory cannot be applied. Archimedes' screws are still in use within industry in extruder pumps. In this application, the screw is operated within a closed environment, running at low angular velocity and high toque to extrude very viscous media such as clay. This is significantly different to the approach taken by this research and such theory regarding these is not useful without major alterations.

5.2 Development of a Theoretical Model

Taking a simplified view, when a screw rotates within a fluid, the body of water constrained within the threads is pushed along the length of the shaft; thus the thrust would be directly proportional to the volume of fluid moved per time step. This is however, a simplistic model of thrust production, to expand upon this the interaction between the fluid and the screw must be understood. During operation, the fluid in the veins formed by the screw

---

[5] Reynolds number is a dimensionless quantity that describes the disorder or turbulence in a flow. Developed by Stokes in 1851 it is defined as the ratio of inertial forces to viscous forces (96. STOKES, G.G. *On the Effect of the Internal Friction of Fluids on the Motion of Pendulums.* Pitt Press, 1851.)

threads and central shaft will have an interaction similar to fluid in a pipe. The vein effectively forms an open top quadrilateral pipe. Consequently boundary layer theory (84, 97) provides a useful method of developing an appropriate thrust generation model.

When a flow passes a body, the surface friction causes a thin layer of fluid to adhere to the body on the surface such that the fluid is stationary relative to the body. As the distance increases from the body, the fluid velocity increases until it matches the velocity of the unaffected fluid. As this graduation in fluid velocity increases towards the velocity of the unaffected fluid it reaches a point known as the boundary layer (97), as seen in Figure 5.3.

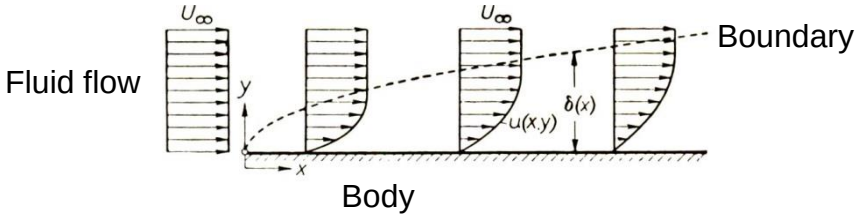

Figure 5.3 Boundary layer of an ideal fluid as it passes a body, Schlichting (97). Arrows represent fluid velocity, dashed line represents where the flow reaches maximum velocity of the flow known as the boundary layer.

In the case of screw based fluid locomotion, the fluid is stationary and the screw body is moving. The fluid at the screw surface will be dragged along with the screw with decreasing fluid velocity with increasing distance from the screw body until the fluid becomes stationary at a distance from the screw. Thus, the fluid in the veins will move with the screw, this movement of fluid will form part of the thrust the system produces.

The definition of thrust is the product of the mass flow rate of the exhaust and the velocity of this exhaust relative to the emitting body. The equation for this can be seen in equation **5.1**.

$$T = \frac{dm}{dt} \cdot v \qquad \textbf{5.1}$$

The mass flow rate of the exhaust, in this case the fluid, can be calculated from knowing the speed of the fluid as it exits the system, the density of the fluid and the cross sectional area, A, equation **5.2**.

$$\frac{dm}{dt} = \rho \cdot A \cdot v \qquad \textbf{5.2}$$

Substituting equation **5.2** into the equation of thrust (equation **5.1**), an equation for thrust from a screw in terms of the fluid properties and screw geometry is obtained, shown in equation **5.3**

$$T = \rho \cdot A \cdot v^2 \qquad \textbf{5.3}$$

To calculate the exit velocity of the fluid from the screw, a model of the fluid flow relative to the screw was established. Theoretically unfolding the screw produces a long channel with a static surface along the base and sides, the top of the channel is open to the fluid body. As the channel moves, the fluid in contact with the screw surface will move with the surface and an assumption is made that the fluid velocity will tend to zero as it approaches the open body. This is shown in Figure 5.4.

The diagram shown in Figure 5.4 shows a 2D representation of the screw, which rotates about the central axis at an angular velocity of U. The angle between the blades and horizontal, α, is set by the pitch of the screw, where $\alpha = tan^{-1}\left(\frac{P}{2 \cdot d_1}\right)$. Figure 5.4 shows the dimensions of the fluid channel and the velocity of the fluid along the channel correcting for the blade angle. A table detailing the symbols and units used within Figure 5.4 can be found in Table 5.1.

The diagram shown in Figure 5.4 shows a 2D representation of the screw, which rotates about the central axis at an angular velocity of U. The angle between the blades and horizontal, α, is set by the pitch of the screw, where $\alpha = tan^{-1}\left(\frac{P}{2 \cdot d_1}\right)$. Figure 5.4 shows the dimensions of the fluid channel and the velocity of the fluid along the channel correcting for the blade angle. A table detailing the symbols and units used within Figure 5.4 can be found in Table 5.1.

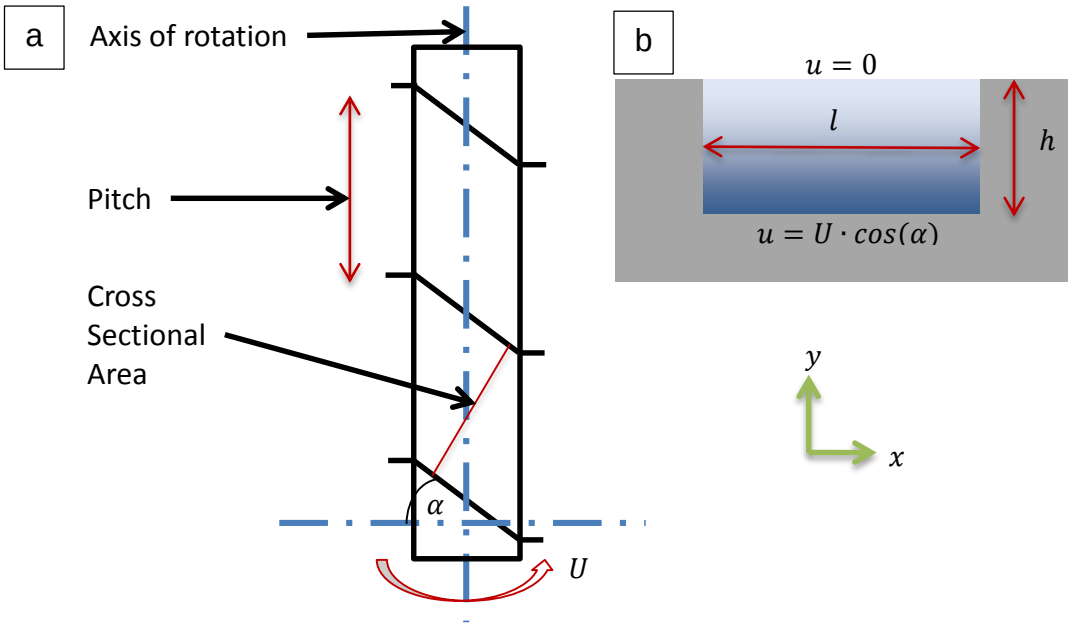

Figure 5.4 Modelling of fluid flow within the screw as the screw rotates Shown left a schematic of the screw propeller; Shown right a cross section of the vein formed between two screw threads. A screw of pitch P forms an angle $\boldsymbol{\alpha}$ between the screw blade and the x-axis and rotates at angular velocity of $\boldsymbol{U}$ about the y-axis. $\boldsymbol{l}$ and $\boldsymbol{h}$ are the length and height of the screw vein respectively, in which the fluid has a velocity of $\boldsymbol{u}$ which varies with distance from the screw. Shading in the vein cut-out (right) denotes relative fluid velocity.

Table 5.1 Symbols and units used within calculation of the fluid flow and diagrams in Figure 5.4

A	Cross sectional area of channel, $h \cdot y$
α	Angle formed between blade and x axis (horizontal)
d_1	Diameter of screw shaft
d_2	Diameter of screw blades
h	Height of channel formed by screw threads
l	Width of channel formed by screw threads
P	Screw pitch
ρ	Density of fluid (taken as $1000 kgm^{-2}$)
T	Thrust
U	Angular velocity of screw about y-axis
u	Fluid velocity along the screw vein
v	Exit velocity of fluid from screw in y direction

Using the boundary layer theory model for fluid flow within the screw veins and substituting into the equation for thrust (equation **5.3**), an equation for thrust generated from the screw is obtained,

$$T = \frac{5\rho U^2 hl}{6} \cdot v \qquad \textbf{5.4}$$

Equation **5.4** calculates the theoretical thrust generated from a single screw when rotated in a fluid. By varying the pitch of the screw, the effect upon the thrust can be calculated. Varying the screw pitch will result in the vein length (l) and fluid exit velocity (v) also varying while the remaining screw geometry is constant. It can be seen from equation **5.4** that an increase in pitch will result in an increase in thrust. This is illustrated by considering two screws of 20mm and 40mm pitch (screw pitch selection discussed in Chapter 4.3), and calculating the thrust generated by each, as shown in Figure 5.5.

It can be seen from Figure 5.5 a 2x increase in screw velocity results in a greater than 2x increase in thrust. This relationship is to be expected due to the squared term on the angular velocity of the screw. An increase in pitch also results in an increase in thrust. This is also to be expected due to the fluid exit velocity increasing with an increase in pitch. The 40mm pitch screw produces a greater thrust than the 20mm pitch because of this.

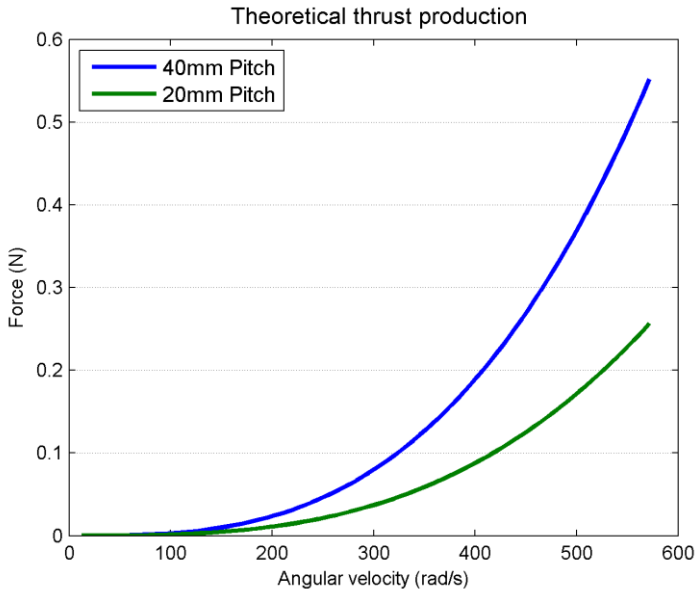

Figure 5.5 Theoretical thrust produced from a single screw

5.3 Development of the Testing Platform

Development of a mathematical model allows for effects of parameters to be ascertained without large volumes of experimental testing: through this

simulation, time and resource usage can be reduced. However, it is important to validate any model against experimental data to ensure it is producing meaningful data and capture modelled aspects of the physical system.

A rig was designed to allow the thrust developed by a single screw rotating in fluid to be measured. Through changing physical parameters such as the screw pitch and angular velocity, the mathematical model can be validated. The rig was also developed to allow exploration into the effects upon the thrust the variable geometry of the 4-screw prototype system would have, such as the arms being located in the open or closed position.

To carry out the above requirements, the rig must include the following:

- Motor velocity control
- Adjustable components to model:
    - Changes in screw pitch
    - Changes in cowling coverage.

Motor velocity control allows for the angular velocity of the screw to be adjusted, as well as recorded. The unloaded motor velocity can be modelled as proportional to input voltage, but with unknown loading feedback control was required to actively achieve and maintain a desired velocity. Screws of differing parameters were manufactured using rapid prototyping techniques. The rig must allow for the part mounted to be changed. Depending on the arm position, the screw may have part of the rotation covered; the rig must be able to simulate this through changeable or adjustable pieces.

5.3.1 Rig Hardware Design

The Fluid Propulsion Testing Rig was designed to provide experimental data on thrust production from a device submerged in a body of fluid. To provide a means of collecting this data, this rig may be suspended in a water tank from a beam load cell (Part No. 1004-00.3-JW00-RS, Tedea Huntleigh, as detailed in Table 5.2). In this case, a single screw assembly was attached to the load cell such that the screw was suspended in the fluid in a vertical position (Figure 5.6). Any reaction forces in the vertical direction generated by the screw would act against the load cell allowing the data on thrust to be acquired.

Table 5.2 Load cell specifications

Load cell	Excitation	Range	Error	Safety overload	Output
Tedea beam cell	10v DC	0-300g	±0.0067%	150%	0.9±0.1mV/V

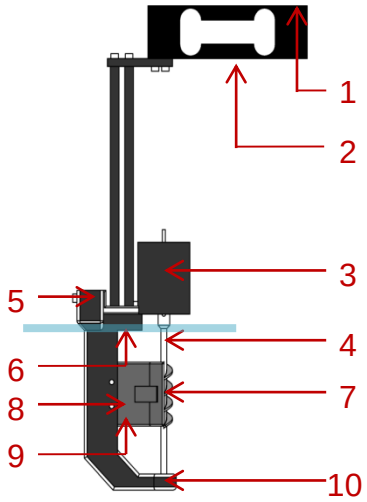

1. Mounting point to frame
2. Beam load cell
3. Motor and motor housing
4. Shaft for mounting screws
5. Attachment arm
6. Fluid level
7. Screw section
8. Cowling mounting location
9. Inter-changeable cowling piece
10. Shaft bearing and bearing mount

Figure 5.6 Fluid Propulsion Testing Rig schematic showing key components.

The screw sub assembly consists of a motor (24mm, 12v, Part No. 222049, Maxon Motors) with encoder (512 pulses/rotation, 2 channels, Part No. 201937, Maxon Motors), connected to a shaft on which the screw pieces may be attached. The tail end of the shaft is housed in a radial bearing mounted in the mounting arm. The motor and shaft are arranged such that the axis of rotation passes through the load cells calibration point and the shaft is vertical.

The load cell was connected to an amplification unit (DR7DC, RDP Electronics) which outputs a signal of ±10v. The unit was tuned such that at zero load it would output 0v and full load (beam cell limit: 300g) would output 10v. The output from the amplification unit was connected to analogue input channels on data acquisition hardware (MyDAQ, National Instruments) allowing the data to be collected using a computer. Custom software (developed using LabVIEW) read the signals from the hardware, calibrated to voltage to SI force and saved this data to file alongside motor velocity and time stamp for sample point.

The motor was controlled using a commercially available motor controller (TReX Jr, Pololu) which generated a PWD signal (10kHz) based on an analogue control signal. The analogue control signal was generated using signal generation hardware (MyDAQ, National Instruments), which was calculated by the host computer using PID control. The encoder was connected to the digital inputs on data acquisition hardware (MyDAQ, National Instruments) and using the in-built hardware counter the motor velocity was determined. This was used in the PID control of the motor.

An outline of the electronic hardware arrangement for the Fluid Propulsion Testing rig can be seen in Figure 5.7, with the data flow direction shown by the arrows.

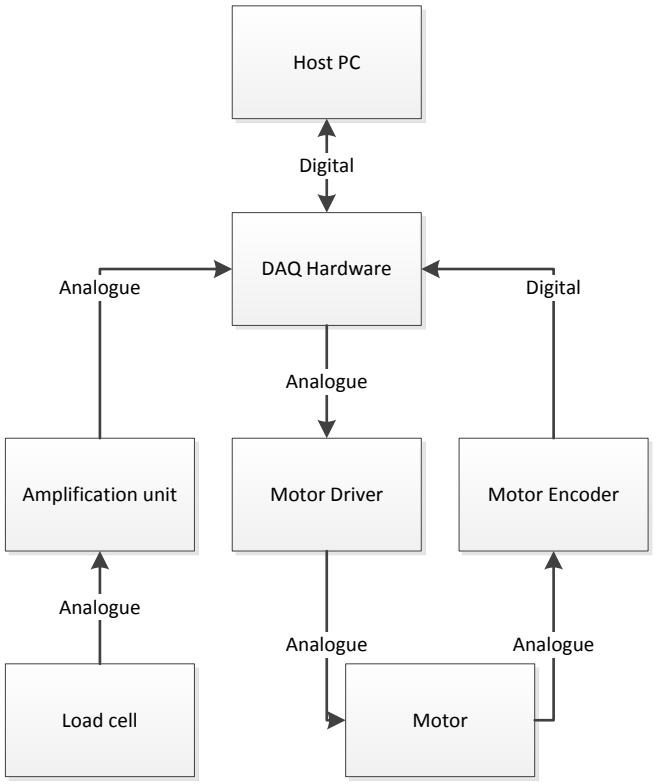

Figure 5.7 Arrangement of hardware and data types in the Fluid Propulsion Testing Rig.

5.3.2 Screw configuration

Screw sections were produced using rapid prototyping in two different pitch lengths, 20mm and 40mm (pitch discussion can be found in Chapter 4.3). The inner shaft diameter of these was equal to that of the shaft connected to the motor such that they could be mounted. The screws were secured to the shaft with an adhesive (Superglue, Loctite) to prevent local movement along the shaft during operation. The adhesive was broken and residue removed from the shaft using acetone after testing.

A schematic of the rig hardware can be seen in Figure 5.6; a computer image of the complete rig can be seen in Figure 5.8.

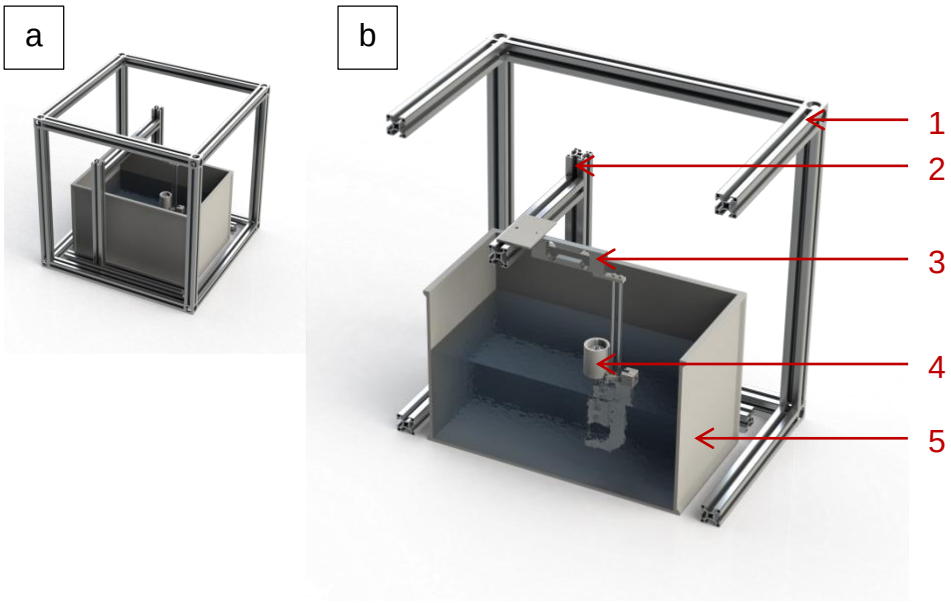

Figure 5.8 Computer images of the complete Fluid Propulsion Testing Rig. a) full rig assembly; b) Section view of the rig assembly, showing the screw and cowling section suspended in the fluid. Annotations show: 1) Outer framing; 2) Adjustable accessory support structure; 3) Load cell attached to accessory support; 4) Motor and screw sub assembly; 5) Fluid tank.

When the screws are next to the chassis, 90° (25%) of the screw is against a surface, referred to as cowled. This surface is curved to match the radius of the screw such throughout the curve it is equidistant from the screw, 1mm. When the arms expand, the screw is then situated in open fluid such that 0° (0%) of the screw is cowled. Two further cowling types were produced and experimented with to allow a trend to be established, 180° and 360° cowling. A computer image of the cowling pieces used can be seen in Figure 5.9. For the three pieces of cowling (360°, 180° and 90°), the holes shown to the left are used in mounting to the attachment arm using M3 bolts. When the screw is open fluid it does not have any surface close, there is no 0° cowling piece; for this, no piece is attached to the attachment arm.

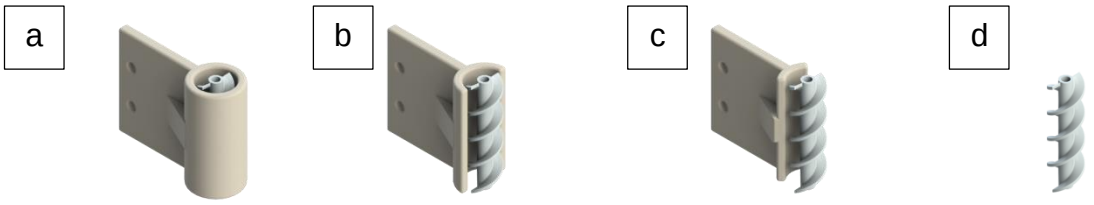

Figure 5.9 Computer model of the cowling pieces used, shown with a screw to show their relative location. a) 360° cowling; b) 180° cowling; c) 90° cowling; d) 0° cowling. Cowling of 90° resembles the device with the arms in the closed position, 0° resembles the arms in the open position.

5.3.3 Motor Speed Control

To control the angular velocity of the screw, speed control of the motor was utilised. Using NI DAQ hardware (MyDAQ) and NI LabVIEW the encoder TTL signals from the motor encoder were captured and compared to the desired number of pulses (based on the number of pulses per rotation and the desired angular velocity). The MyDAQ device features a built-in encoder counter (3 channel, 100MHz, 32-bit) which can be configured through user adjustable counts per rotation setting (configured to 512 pulses per rotation). This was used to provide the process variable for the PID control. A PID controller was used to generate an analogue signal, which was sent to a motor controller board to generate the PWD signal to drive the motor. The PID was experimentally tuned (85) through adjusting the parameters to achieve the desired velocity (proportional: 0.053, integral: 0.005, derivative 0), effectively running as a PI controller. Software was used to measure the motor velocity during tuning and the parameters selected such that the measured velocity was within 5% of the desired.

5.4 Experimental Method

An experimental protocol was designed to investigate the thrust generated by a screw rotated in a fluid medium. To investigate the effects of angular velocity, the device's screw would be rotated at a series of controlled velocities starting from the motor's idle velocity up to the motor's maximum stable velocity. Varying cowling pieces were produced to investigate the effects of cowling upon thrust. Although the screw would not experience complete enclosure during normal operation, these were included in the protocol to allow any trend to be established. Two different screw pitches were used, as discussed previously. Each of the combinations were assembled in turn and fixed into the test rig. The depth of the screw within the fluid was kept constant throughout the procedure, with the fluid level

when stationary reaching the bottom of the top mounting on the attachment arm, as seen in Figure 5.6. Each of the individual setups was repeated 6 times using an automated system. The experimental variables can be seen in Table 5.3.

For each of the screws the surface finish was left unaltered from the production process. The screws were produced using the same ALM process (polyjet, Chapter 4) to minimise the effects of differing surface finishes. Surface finish has an effect on the fluid thrust capabilities of conventional propellers however the effects on fluid thrust produced by screws was not investigated. Once the system has been developed for amphibious locomotion, further optimisation on the discrete modes can take place as future work.

Table 5.3 Experimental variables for fluid based testing

Screw material	Rigid centre and blades Rigid centre and compliant blades (Shore: 60)
Screw pitch	20mm, 40mm
Screw cowling	360°, 180°, 90°, 0° (none)
Angular velocity	20-90 RPS in 10 RPS steps
Repeats	6 for each unique configuration

For each of the experiments, data was collected at 100Hz for 50s and saved to data file for analysis. Data was collected over a period of 50s to allow averaging out of transient effects and identification of signal noise from useful data. The software logged the physical set up parameters in the file names with the angular velocity, load cell reading and time stamp saved in the data file.

The control software was developed to enable the velocity to be adjusted for each combination of screws and cowling with repeats handled automatically. The velocity was set to the minimum value and the experiment run with data collected. The screw was halted and the internal value for velocity incremented by 10. A wait of 60s was built in to allow the water to settle. This was repeated until the velocity variable exceeded the maximum, when this occurred the repeat variable is incremented and the velocity set back to the minimum. Once the repeats had reached 6, the loop would end. At this point, the physical parameters such as screw and cowling piece were

changed before running the experiment again. A flow chart of the application loop can be seen in Figure 5.10.

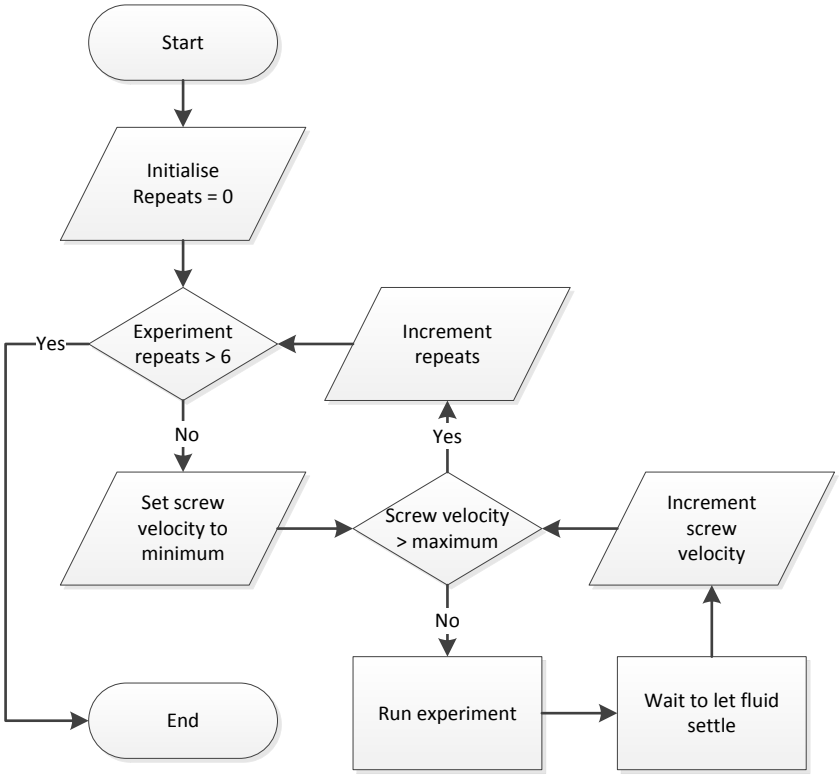

Figure 5.10 Program logic for the automatic velocity and repeat loop process. A control system was used to programmatically sweep through a range of velocities, conducting repeats of each based on setup parameters.

5.4.1 Data Analysis

Custom software was written to process and plot the data (Matlab, MathWorks). The software scanned a given directory for all data files and the file names loaded into memory. The file names were split based on the metadata parameters in the file name, such as screw type and cowling coverage. For each file, the data was loaded into a 3 dimensional matrix and the metadata stored in a separate 2 dimensional matrix. A flowchart of this process can be seen in Figure 5.11. The data matrix contains each of the values in the file, filling 2 dimensions and each separate file forming the third dimension. The metadata matrix contains the pitch, cowling and velocity for each of the entries in the data matrix.

A second algorithm (developed in Matlab, MathWorks) scans the metadata matrix for unique combinations of pitch, cowling and velocity and collects each repeat of such. A mean of the load cell readings for all data points in the collected results is taken and saved in a third matrix, the results matrix. This matrix contains the unique parameters as internal metadata, which is

used for plotting. Once all the unique combinations have been scanned, a plot of the data is produced. A flow chart of this process can be seen in Figure 5.12. In selecting a directory to be scanned, different results sets, such as for rigid and compliant screws, can be analysed with the same algorithm with minimal adjustments. The algorithm was built such that any number of pitches, cowling coverage, angular velocities or repeats could be used without any hard coded changes needed.

Signal noise was removed from the data using a 2nd order low pass Butterworth filter with cut off frequency of 10Hz. This was chosen as the response was expected to be low frequency (constant thrust) and any high frequency change would be primarily due to motor oscillation (velocity dependant), mains noise (50Hz) and other sources such as resonance within the rig.

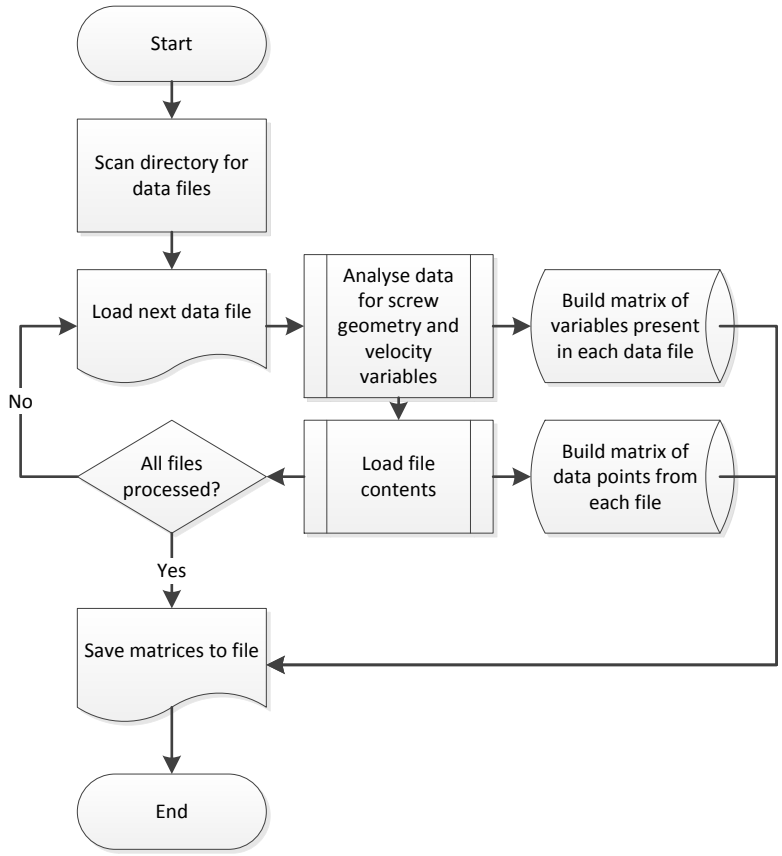

Figure 5.11 Process of loading data from files produced by the Fluid Propulsion Testing rig. Each file contains meta data stored in the file name such as screw geometry, and data stored in the file contents such as screw velocity. This is collected and stored in a matrix for processing.

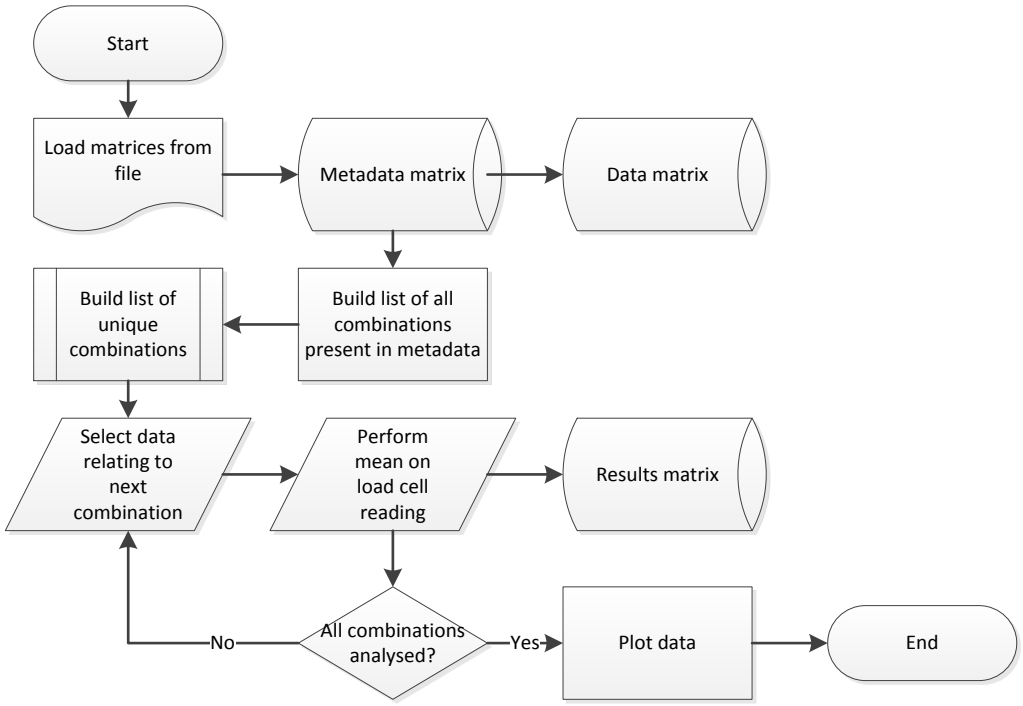

Figure 5.12 Data processing and plotting. A list of unique configurations is built, allowing repeats to be collected together for processing, once these have been joined, the results are processed and plotted.

5.5 Results

The data collected using the Fluid Propulsion Testing rig was analysed and the mean thrust value from the screw plotted against the angular velocity of the screw, with error bars showing standard deviation. This can be seen plotted in Figure 5.13 and Figure 5.14 for the rigid and compliant screws respectively.

The angular velocity of the screw is proportional to the thrust produced with higher angular velocities producing greater thrusts. This is the case for both data sets (rigid and compliant), with a non-linear increase in thrust compared to screw velocity visible for the rigid screws. This non-linear increase resembles the trend seen in the theoretical model.

For both data sets, the 40mm pitch screws produce greater thrust than the 20mm pitch screws. This is a clear trend in both data sets, which corresponds to the theoretical model.

With increased coverage (cowling angle), there is a decrease in thrust produced for rigid screws. The greatest thrust comes from screws which did not have any cowling (0° cowling) while the least thrust was generated from the screws with complete coverage (360° cowling). Cowling conditions between these states produce thrust that follows the same trend, increased

cowling results in less thrust. There is no clear trend between cowling and thrust for the compliant screws.

The rigid screw data produces a series of smooth curves following the same exponential trend between angular velocity and thrust. The compliant screw data shows greater variance in results. The standard deviation for each sub-set of data is greater which has an evident effect on the overall trends seen in the data. There is no clear trend between cowling coverage and thrust.

The peak force generated by a 40mm pitch screw is 0.28N for a rigid screw and 0.25N for a compliant screw; for the 20mm pitch screws the peak force is 0.1N for rigid and 0.12N for a compliant screw.

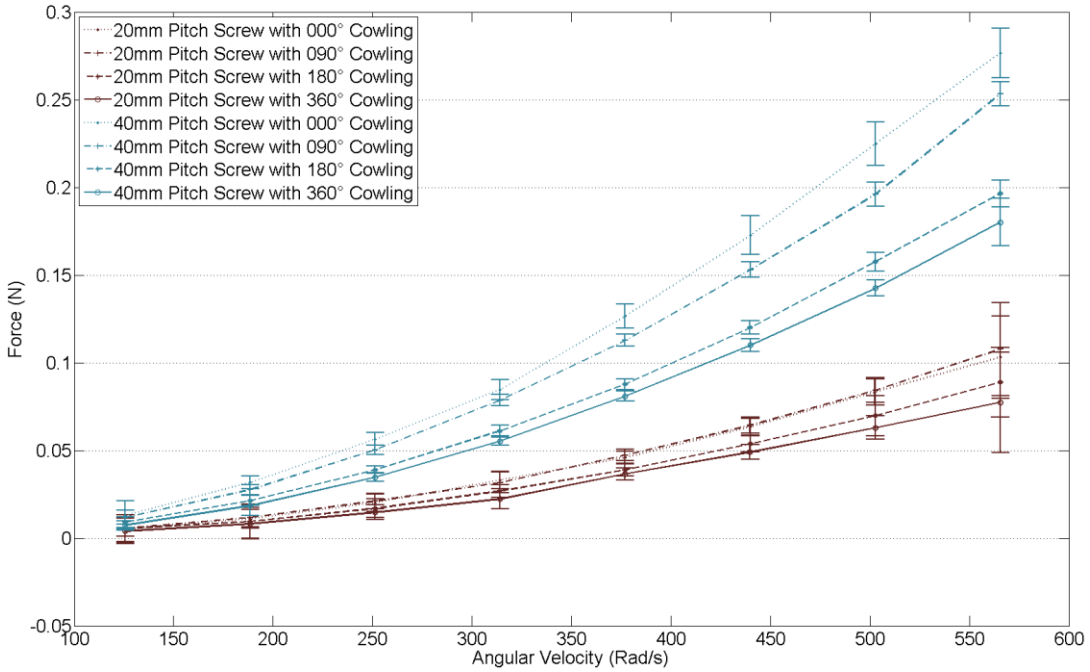

Figure 5.13 Thrust generated from a single rigid screw. Blue lines represent a 40mm pitch screw while red lines represent a 20mm pitch screw. Error bars show standard deviation. The degree of cowling can be identified by the line type, a solid line is shown for 360° cowling and dashed lines with decreasing width dashes for 180°, 90° and 0° cowling, as shown in the legend. A legend for each graph is present to aid identification.

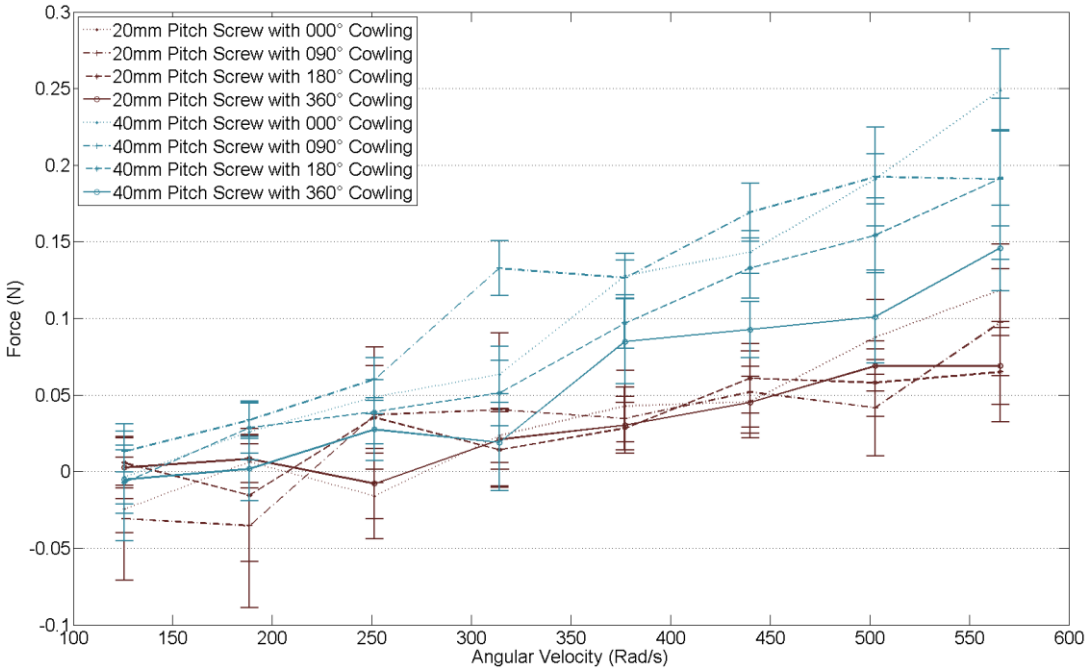

Figure 5.14 Thrust generated from a single compliant blade screw. Blue lines represent a 40mm pitch screw while red lines represent a 20mm pitch screw. Error bars show standard deviation. The degree of cowling can be identified by the line type, a solid line is shown for 360° cowling and dashed lines with decreasing width dashes for 180°, 90° and 0° cowling, as shown in the legend. A legend for each graph is present to aid identification.

5.6 Discussion

The experimental data was analysed for the effects of pitch, cowling and compliance on the thrust produced.

5.6.1 Effect Of Pitch

From the datasets collected, it can be seen that the pitch of a screw has a clear effect upon the force produced. A 40mm pitch screw produces greater thrust than a 20mm pitch screw. The theoretical model predicted that a 40mm pitch screw would produce approximately twice the force a 20mm pitch screw would produce. For both the rigid and compliant screws, this can be seen to hold true. The theoretical model predicts that increasing the pitch past 40mm will result in further increases in thrust, however this may not hold true for experimental data. As the threads tend to parallel to the axis of rotation the thrust will diminish as the fluid displaces around the system and not along the screw length.

5.6.2 Effect Of Cowling

Within the datasets, the screws perform best in an open fluid, with decreasing thrust as a result of increasing cowling around the screw. It is predicted that some of the thrust generation of the screws comes from sheering of the fluid around the screw, the introduction of cowling around the screw would inhibit this; resulting in loss of thrust. The 360° cowling creates a full-enclosed screw; the developed locomotion system does not make use of a fully enclosed screw and so this does not resemble an applicable state for the prototype locomotion system. Using boundary layer theory, the cowling poses a static body that will retard the flow. While the screw imparts motion upon the fluid, the cowling will decrease the fluid velocity about the screw, diminishing the force produced.

When the locomotion system is folded into its smallest state, the screws will effectively have 90° cowling. The data shows that when the device is in the closed position it will produce less thrust than in the open position. The fluid thrust potential of the device is not severely compromised by the adjustable geometry of the system; however, greater thrust will be produced in the open state. The arms do not need to be completely open, they only need to move sufficiently to move the screws away from the central chassis. Depending on the final scale of the device, it may be able to operate in a less than completely folded state allowing for the greater fluid thrust to be utilised.

The effects of cowling were not modelled by the theoretical model, however it was predicted that greater thrust will be produced in a cowled state. This is true for propeller design with cowling designed with an aerofoil cross-section to increase the efficiency. Through experimental examination of the system, it was shown that enclosing the screws in cowling had an adverse effect on thrust, and so the screws should be operated with minimal cowling to aid thrust production.

5.6.3 Effect Of Compliance

Comparing the rigid and compliant screw thrust data; where the rigid data forms a clear correlation between angular velocity and thrust, the compliant screw data is of a variable response. The rigid screw data sets form smooth curves with a trend of $T \propto u^2$. The compliant screws show a similar trend however there is much higher variation at each sample point. Due to the compliant nature of the material, it will behave differently in response to driving frequencies and will distort to a greater degree. This will introduce another noise source to the signal, increasing the signal noise as seen by

the larger error bars in Figure 5.14 compared to the rigid screws (Figure 5.13). The response to driving frequencies for the screws has not been simulated or explored further. The scope of this work is to explore amphibious locomotion and optimisation of individual modes of locomotion will be carried out after the complete system has been analysed for overall performance.

The screw blades, which are produced from a compliant material, may vary in geometry throughout the rotation, resulting in the higher noise seen in the data. This expected deflection of the material will be caused by both the centripetal forces acting on the screws and the response to the driving frequencies generated by the system noise. Further investigation into this has not taken place however it is expected that an increased distance between blade tip and cowling face would decrease some of the interaction and thus noise. From comparing the result between the rigid and compliant screw it can be seen that the peak thrust difference is in the order of 10%.

A working hypothesis for the discrepancy between the thrust produced by the rigid and compliant screws is while rotating the compliant material screw threads have a frequency response in the range of driving frequencies that induces noise into the system. As the material is able to deflect to a greater extent than the rigid material, a combination of centripetal forces induced by the rotation and the frequency response from the material may be the source of the increased signal noise. If the threads do expand radially with rotation, this would explain the higher deviation seen in the data at higher frequencies.

The overall thrust production for both rigid and compliant screws are similar, however there is greater variance in the thrust produced point to point for the compliant screws. While this may not have a large effect on the ability of the system to produce propulsive thrust, it may affect the control of the system. The data shows in some cases a decrease in angular velocity of the screw may result in an increase of thrust and vice versa. This will cause control complications in terms of producing a stable device. The device may experience greater system vibrations through the use of compliant screws, which may reduce the clarity of the proposed video feed, increasing procedure complexity for the piloting clinician.

5.6.4 Theoretical Model

The experimental data shows the same trend as the theoretical model, although the experimental data does not produce the same magnitude,

different by a factor of 2. This may be due to the theoretical model not taking into account other factors that influence the flow. The model assumes a constant gradient in fluid velocity through the height of the vein and does not take into account the sides of the vein. These will also have the same boundary layer effect upon the fluid flow and will alter the thrust produced.

The model assumes all fluid leaves the screw parallel to the axis of rotation; however it is more likely that the exhaust forms a cone shaped dispersion with some of the thrust lost as flow perpendicular to the axis of rotation (Figure 5.15). This is not something that could be changed easily with the geometry, it can be seen that using cowling to channel the flow does not result in an increased force produced.

A: Thrust leaving screw parallel to rotational axis (blue arrow)

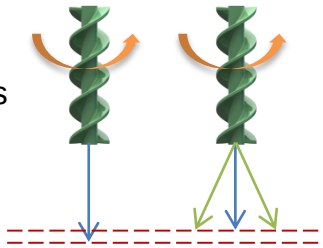

B: Thrust leaving screw in cone shaped dispersion (green arrows). Resolved thrust (blue arrow) is of less magnitude due to resolved parallel thrust component.

Figure 5.15 Thrust dispersion of a screw rotated in fluid. Orange arrow shows rotation, blue arrow shows thrust component parallel to rotational axis, green arrows show actual dispersion of thrust, red lines illustrate difference in parallel thrust component (illustrative only).

A third assumption that the model makes is the fluid surrounding the screw is stationary. The thrust generated is proportional to the difference between the exhaust velocity and the velocity of the surrounding fluid, as the surrounding fluid moves this will reduce the step change between the exhaust flow and the environment. While the fluid was left to settle between repeats, the instant the screw begins to impart motion on the fluid the velocity of the exhaust relative to the surrounding fluid will decrease.

The theoretical model aided the predictions that increased screw angular velocity and screw pitch would result in increased thrust, however the model was not used in the prediction of the effects of cowling and compliance. The experimental work complimented the model in the respect, allowing basic characterisation of the thrust potential and exploration of the un-modelled cowling and compliance.

5.6.5 Thrust Predictions Of Four-Screw Locomotion System

The peak thrust generated by a single rigid screw was recorded as 0.28N. The peak thrust generated by a compliant screw was recorded as 0.25N.

Both these thrusts was measured with a 40mm pitch screw, 0° cowling, and rotated at an angular velocity of 565 rad·s^{-1} (90Hz). Assuming there are no diminishing returns for addition of screws to a system, a four-screw system will be capable of producing 1.12N and 1.0N of thrust for rigid and compliant screws respectively.

For 20mm pitch screws, the predicted maximum thrust generated by a four-screw system is 0.4N for both rigid and compliant screws.

It is expected that there will be some factor of diminishing returns for increasing number of screws added to the system, however the 40mm pitch screws are able to provide the predicted 1N of thrust in their current state: further optimisations may increase the total thrust output.

5.7 Summary of Fluid Locomotion Analysis

Both rigid and compliant screws have been shown to generate an appropriate level of thrust when rotated in a fluid. Both an increased pitch and decreased angle of cowling result in greater thrust, with the 40mm pitch screw producing the greater thrust when in an open state. Compliance does not show a great effect upon the thrust although it may have an effect on the control due to the increased chassis wide vibrations. Through adaption of the application of the materials, this may be reduced, allowing for a smoother performance.

Overall, experimental data shows the screws are a viable means of providing locomotion through a fluid. As predicted in Chapter 3, the system would need to be able of providing a combined thrust of 1N to traverse the colon; scaling the experimental data for a single screw to a 4-screw system, this 1N of thrust is achievable. Although propellers are more efficient and replaced screw based systems in aquatic locomotion, the reason for using screws lays upon their ability to provide locomotion when in contact with the tissue. This is examined in the next chapter. Should screws provide sufficient tractive forces in contact then their amphibious properties should be utilised within the aim of providing a locomotion system for an intra-luminal device.

Chapter 6
Contact Locomotion – Theoretical and Experimental Analysis of the Locomotion System

The amphibious prototype locomotion system, featuring 4 Archimedean screws, has been designed to produce amphibious locomotion through a flooded colon. To allow for amphibious locomotion the screws must function in both pure fluid and pure contact scenarios. This chapter covers the theoretical and experimental analysis of the performance and characteristics of the screws in a pure contact state. A theoretical model of how screws would generate thrust was built to understand their strengths and weaknesses in a contact state, allowing the experimental testing parameters to be established (6.1). A counter-rotating pair of oppositely handed screws was experimentally assessed against ex-vivo porcine colon for their ability to produce traction in non-rotating (static) and rotating (dynamic) configurations (6.3). Following on from the traction experiments, a parametric sweep was conducted to establish the effects of screw blade material compliance, normal loading and screw velocity on thrust (6.4).

6.1 Development of a Theoretical Model

A theoretical model provides a useful tool to understand a system. The model may inform further experimental testing and allow the design of procedures to capture the characteristics of a system. The theoretical model will also assist with understanding the results produced from the experimental testing.

6.1.1 Theoretical Model Development

The work by Nagaoka et al. (46) on screws moving against soft ground was analysed for its application against a deformable yet non-displaceable surface such as colonic tissue. While soil and sand can be permanently displaced, tissue cannot be permanently displaced without major consequences to the patient such as bowel perforation. A model developed for screws acting on soft ground has limited use in this situation. The motion that a serpentine-like system creates is similar to the motion of the Archimedean screw: contact points remain stationary relative to the ground and move relative to the body (98), Figure 6.1.

During the rotation of a screw against a plane, the points relative to the plane where contact is formed do not move, as shown in Figure 6.1 by the orange arrow.

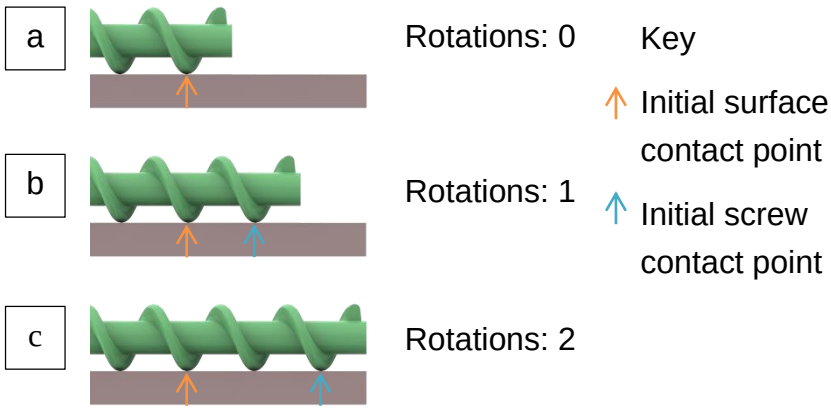

Figure 6.1 Contact point change relative to the surface and screw during rotation of the screw. At the start, the contact between the screw and surface is identified by the orange arrow. After one rotation, the contact point relative to the surface (orange arrow) has not moved although the initial contact point on the screw has (blue arrow). After two rotations, the original contact point on the screw has progressed further with the original surface contact point remaining stationary.

For Archimedean screws, the contact point must move relative to the screw body for locomotion to occur in the desired direction. If the contact point remains stationary relative to both the screw and the surface, the screw will roll perpendicular to the desired direction. Thus when a screw rotates against a surface to generate thrust there must be a difference in the coefficients of friction in the normal (C_N), and parallel (C_P), directions relative to the surface of the screw thread (Figure 6.2). The ratio of these coefficients (C_K), as shown in equation 6.1, can be used to describe the performance of the screw on a surface. Performance can be defined as the distance travelled along the axis of rotation, per rotation, compared to the pitch length. From this, it is apparent that the surface needs to deform to allow useful locomotion to be generated from a rotating screw.

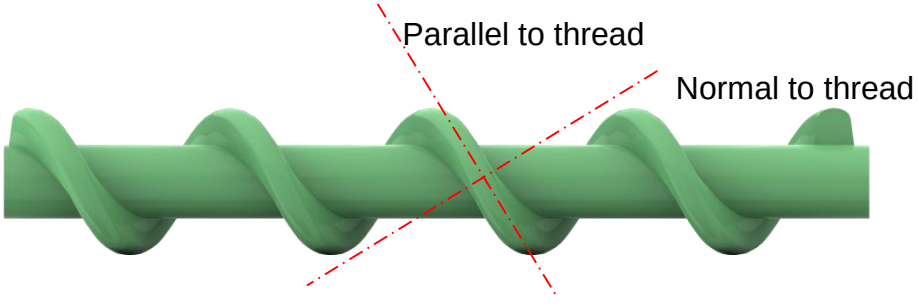

Figure 6.2 Normal and parallel directions to a screw thread

$$C_K = \frac{C_N}{C_P} \tag{6.1}$$

The traction between a screw and a surface is dependent on the coefficient C_K. Perfect traction will result in the screw progressing by one pitch length in the axial direction per rotation, giving a performance of 1; this will occur when $C_N \gg C_P$. Zero traction will result in no movement in the axial direction per rotation and will occur when $C_N \ll C_P$. Traction can be summarised as a function of the inverse tangent of C_K,

$$Traction = f\left(\frac{\tan^{-1} C_K}{\frac{\pi}{2}}\right) \tag{6.2}$$

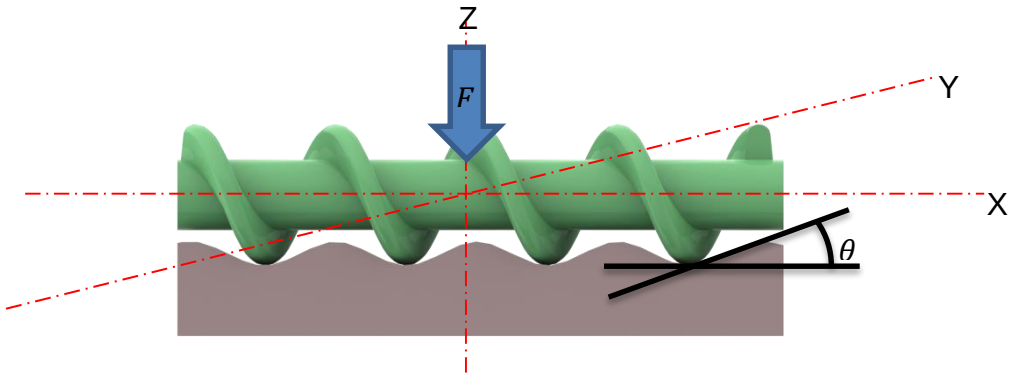

Figure 6.3 Interaction between a screw and a deformable surface. Screw axes, deformation angle and loading shown in annotations.

When a screw section is loaded in the normal direction to a deformable surface, the z-axis as seen in Figure 6.3, the tips of the screw blades deform the surface. The angle of this deformation, θ, is a function of the force, F and the stiffness of the surface, K,

$$\theta = f(F, K) \tag{6.3}$$

The contact angle, in radians, has the natural limits: $0 \leq \theta \leq \pi/2$. At either end of the limits are two distinct cases, non-deformable surface ($\theta = 0$) and perfectly-deforming ($\theta = \pi/2$) with in-between values of θ producing a mixture of these cases. This analysis was developed as part of this thesis to further understand how screws act upon a surface that does not displace, and takes into account the surface deformation due to contact.

6.1.2 Rotation Of A Screw On A Non-Deformable Surface

On a non-deformable surface, the screw blades do not produce any deformation; the screw simply rests upon the surface thus $\theta = 0$ (Figure 6.4).

Any friction between the blade tips and the material surface will be equal, and so the coefficients C_N and C_P are equal thus $C_K = 1$.

On a frictionless surface, as the screw rotates there will be no dominant direction of locomotion, $C_N = C_P = 0$, thus $C_K = 0$ and so traction is 0. If all coefficients of friction between the screw and the surface are zero, there will be no traction in any direction. This can be likened to a screw resting on a polished glass surface.

If there is friction between the blade tips and the surface, for example if the blades are made from rubber or there is some adhesion between the materials of the screw and surface; the screw will roll across the surface in a direction perpendicular to the rotational axis; along the Y-axis.

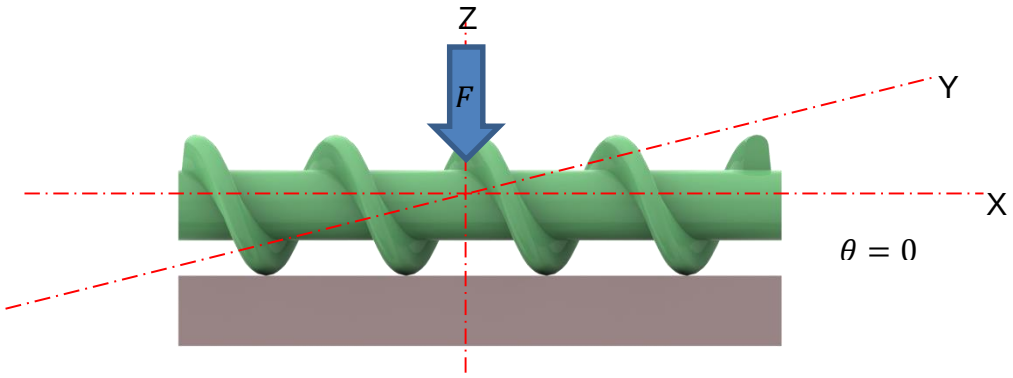

Figure 6.4 Screw resting on a non-deforming surface, $\boldsymbol{\theta = 0}$**.** In this configuration, a screw is not effective at generating thrust in the axial direction.

6.1.3 Rotation Of A Screw On A Binary-Deforming Surface

When the screw rests upon a binary-deformable surface, the blades will deform the surface giving a contact angle of $\frac{\pi}{2}$ (Figure 6.5). The deformation occurs in discrete blocks at point of contact, note this is a theoretical case and will not occur in continuous materials such as biological tissue. At this case, $C_N \gg C_P$, thus $C_K \to \infty$ giving a value of traction as 1. The system will move one pitch length per rotation; this case is not too dissimilar to a bolt in a tapped hole.

For cases where the friction between the screw and surface is 0, the screw will rotate unhindered. In the presence of friction, this will affect the speed of rotation without causing translation along the Y-axis.

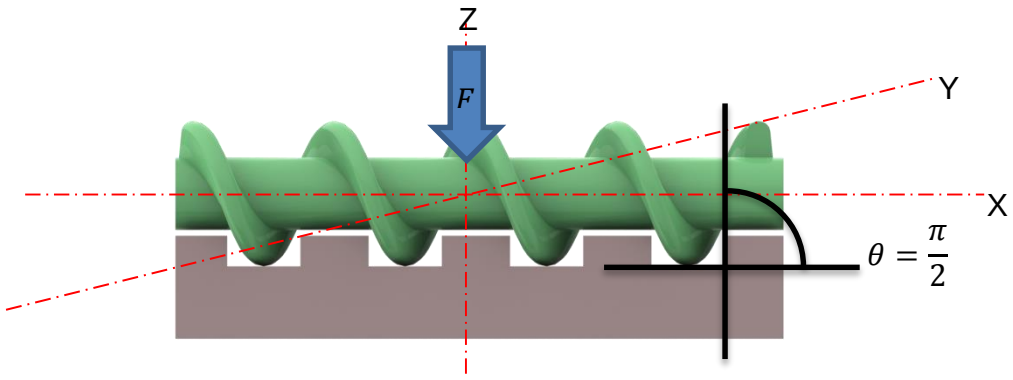

Figure 6.5 Diagram showing a screw resting on a binary-deforming surface, $\boldsymbol{\theta} = \pi/2$

6.1.4 Rotation Of A Screw On An Idealistically-Deforming Surface

The previous section described that in order for a screw to translate along its axis of rotation there must be some deformation of the surface upon which it is actuating. Greater deformability of a surface when in contact with the screw leads to an increase in traction. Reducing the friction between the screw and the material surface will reduce the energy needed to rotate the screw: increasing the efficiency.

A contact angle of $\frac{\pi}{2}$ is highly unlikely to occur between a screw thread and tissue due to the mechanical properties of biological tissue. It is assumed, informed by laboratory experimentation with ex-vivo porcine colon tissue samples, that the tissue will locally deform to a lesser extent, enveloping the screws as shown in Figure 6.6. This however is exaggeration for display purposes and the depth of recession will likely be $d \ll \frac{\emptyset}{2}$, where d is the recess depth and $\emptyset$ is the screw diameter. It is also estimated that relationship between recess depth and screw diameter will be inversely proportional; larger diameter screws will result in a lower percentage of screw recession into the tissue.

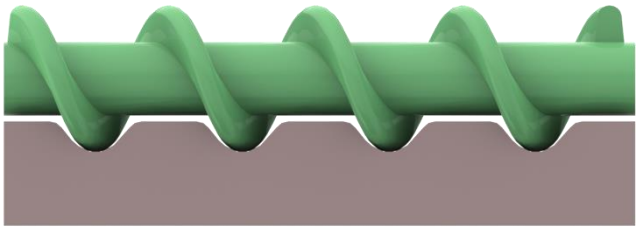

Figure 6.6 Idealised contact between screw and tissue

A photograph taken during testing is shown in Figure 6.7, showing the tissue deforming about the screw threads. It is evident that this is close to the situation presented in Figure 6.6. The compliant screw blades deform slightly with the screw central shaft resting against the tissue.

Figure 6.7 Biological tissue deforming about screw threads during testing

6.1.5 Screw Locomotion Against Tissue

A screw can be sunk past its entire height into a surface and still be able to provide useful locomotion. Although it is unexpected that this will occur during ordinary operation, should the screw sink its entire height into the mucosa during operation it will not prevent locomotion. The greatest recession of the screw into the tissue is predicted to be no greater than the radius of the screw. At this point, the visco-elastic nature of the tissue would suggest it would stretch about the full system and not form local recesses around the screws.

To provide locomotion in contact, the locomotion system must overcome two key obstacles: insufficient traction due to a flooded environment and becoming encapsulated in a local recess. The screw system will overcome the first obstacle through means of fluid propulsion, and as screws can operate when fully enveloped in a local recess, the second obstacle will not prevent progress.

During deployment in a fluid filled colon, the mucosa may provide a near frictionless surface. This will provide a challenging surface on which to provide locomotion. A screw can provide locomotion in a friction-free environment, providing the surface is deformable.

6.2 Development of the Testing Platform

From theoretical analysis, the tissue deformation against the screw would appear to be key to the success in providing motion. While some deformation is needed, complete covering the screw may have adverse effects due to the increased resistance to rotation of the screws. The variable geometry of the 4-screw locomotion system allows control over the force applied to the screws pushing them into the tissue and such the deformation caused by the screw. A testing rig therefore must be able to alter the normal loading to simulate the effects of this and explore the results of changing tissue deformation caused by increased normal loading.

If the tissue perfectly deforms around the screw, the screw moves by one pitch length per rotation. Thus increasing the angular velocity of the screw would increase the overall linear velocity of the system. While increasing the angular velocity of the screw in fluid has a direct link to increased thrust output, as discussed in Chapter 5; this may not be true for contact states. It is known that increased speed results in less torque and so the effects of angular velocity on tractive force will not be as pronounced: a minimum torque will be required in order to rotate the screws against tissue. It is estimated that an increased angular velocity will result in an increased thrust and such the testing apparatus must be able to vary this and measure the resultant thrust. The ability to generate tractive forces (referred to as dynamic traction) while the screws are rotating is crucial to the device's ability to move; if no dynamic traction can be produced then the device will simply not move.

The screws also need to provide traction when stationary, allowing the system to "dock" if required for medical procedures such as biopsy. For this, the test rig should be able to test the screws ability to provide traction as they are dragged or slip across the tissue surface without being rotated (referred to as static traction). While the screws are rotating against the tissue, there is a slipping contact point, as described in the previous section. In allowing the screws to be moved along the tissue without rotation, the tractive capabilities can be established in a simplified situation through removal of the rotational component. Thus, the rig should have the ability to test the screws in both terms of:

- static contact (screws stationary and dragged)
- dynamic contact (screws rotated)

Avoidance of tissue damage is a key requirement of the locomotion system. Although detailed clinical trials and tissue histology will need to be carried out before any system is released for public use, this testing will focus on visible damage as an indicator of trauma. Tissue trauma is evident at a cellular level through a number of indications such as inflammatory response and necrosis in living tissue. However, in these experiments, ex-vivo tissue samples will be used and therefore different indications of trauma are necessary. In this preliminary work, the tissue surfaces will be inspected for signs of wear to mucosa as an indication of trauma.

Examining the testing platforms used by other researchers in the field can help ascertain limitations to be avoided and strengths to be incorporated while designing a testing platform. Kim and Kim (77) built a testing platform for measuring the thrust from a single rotating screw against tissue, Figure 6.8. This rig features a tissue platform situated on a linear slide with the screw resting against the surface of the tissue. Dead weights are used to alter the normal loading and load cells used to measure the thrust output. While the testing platform has a large scope for adjustability, the single screw causes a net force perpendicular to the desired direction of thrust. A different screw based propulsion system as devised by Ikeuchi et al. (74) was tested on a custom built testing apparatus which consists of a screw mounted such that it is in contact with a sample bed attached to a linear slide, Figure 6.9. A load cell is connected to the linear slide to allow measurements of the forces generated by the screw to be measured. Similarly, here a single screw will produce a net thrust perpendicular to the desired direction of motion.

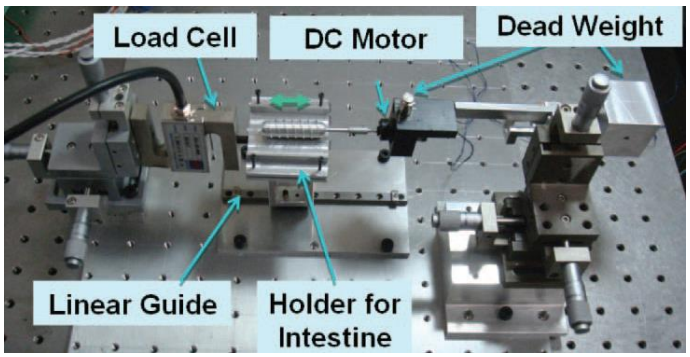

Figure 6.8 Testing platforms used by Kim and Kim (77). Image of testing apparatus taken from referenced journal paper.

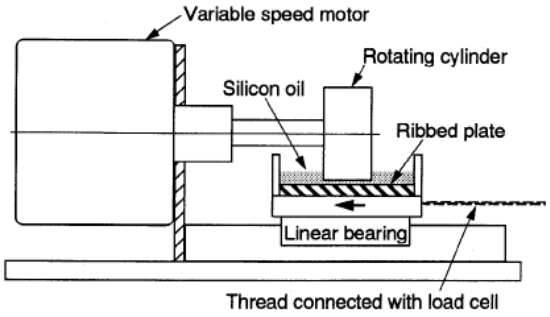

Figure 6.9 Testing platforms used by Ikeuchi et al. (74). Image of testing apparatus taken from referenced journal paper.

Based upon these considerations, a testing rig to allow the experimental testing of the designed screw based locomotion system, a set of requirements was developed.

- Utilise counter-rotating screw pair
    - Alter angular velocity of screws
    - Alter screw compliance of screws
- Apply varying normal loading
- Measure thrust produced in the axis of screw rotation

6.2.1 Rig Hardware Design

The Traction and Contact Testing rig consists of a tissue bed mounted on a horizontal linear slide at the centre of the rig (Figure 6.10, Figure 6.11). Above the tissue bed a beam load cell is attached to a vertical linear slide from which the screw sub assembly is attached. This allows a normal force to be applied and measured to the screw sub-assembly, which is in contact with the tissue sample. To allow measurement of the normal or reaction force, the sub-assembly unit is held static while the tissue is allowed to move from under the sub-assembly.

The screw sub-assembly consists of two independently driven shafts which screw pieces can be attached. The shafts are held at a fixed 20mm centre-to-centre distance and restrained by bearings at either end of the shafts. A motor (Maxon Motor, DCX22S GB KL 12v) is connected via a flexible coupling to each of the shafts, allowing individual control over the shaft velocity. The motors are fitted with two channel encoders (Maxon ENX16) which produce 1024 pulses per rotation allowing for fine control of velocity. The max velocity of the motor is 12400 RPM and produces 14.6 mNm of torque (stall torque of 108 mNm). These motors were chosen as they would allow many different drive motors and gearbox combinations to be simulated through the same hardware set up by limiting the supply current and voltage.

The encoder was selected to allow accurate control over the velocity at low rotational speed (5Rad/s) compared to the default 128 count unit.

The tissue bed has two different connection options for measuring forces applied to the bed in the horizontal direction. The first option (static traction testing) has the load cell connected in series with a linear actuator and the tissue bed. The position and force applied to the tissue bed can be directly controlled while the resultant force between the tissue bed and the actuator being measured, this allows experimental data on static friction. The second option (dynamic traction testing) involves connecting the bed to a statically mounted load cell. Using this set up the forces imparted on the tissue bed in the horizontal direction can be measured, allowing experimental data to be gathered on dynamic friction.

To allow the tissue bed to be moved in a controlled fashion, a linear actuator was selected (SMAC Moving Coil Actuator, LAL95-050-7), which is capable of producing 26N of force over a 50mm stroke while powered. The actuator was chosen to provide a stroke length greater than a single screw length to allow any trends caused by screw threads collapsing to be explored. When the device is unpowered it is fully back-drivable and passive, this allows positioning by hand of the system while it is completely powered down and safe to place hands inside the enclosure. The fully back-drivable nature also allows the system to be powered down should damage to the rig be imminent without need to drive the actuator into a safe position. The actuator can provide a constant force output throughout the range of the stroke, allowing for local adjustments of the tissue bed without compensating the actuator’s performance. The actuator has a built in encoder (200 counts per mm), integrated PID controller and configurable maximum acceleration and shaft velocity.

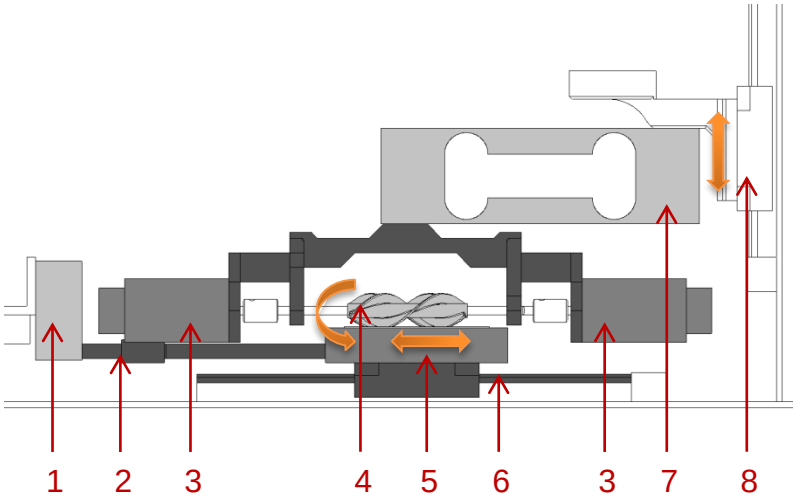

1. Bed load cell with attachment bracket for static mounting or attachment to linear actuator
2. Bed load cell and tissue bed connection rod
3. Screw motor
4. Counter rotating screw pair, rotation shown as orange curved arrow.
5. Tissue bed, translation permissible along direction shown by orange arrow.
6. Tissue bed linear slide
7. Beam load cell
8. Vertical linear slide, translation permissible along orange arrow. Counter weights may be attached via a pulley to the linear slide carriage allowing adjustable normal loading.

Figure 6.10 Traction and Contact Testing Rig schematic showing key components, screw sub assembly consists of parts 3, 4 and the connection chassis pieces shown in dark grey.

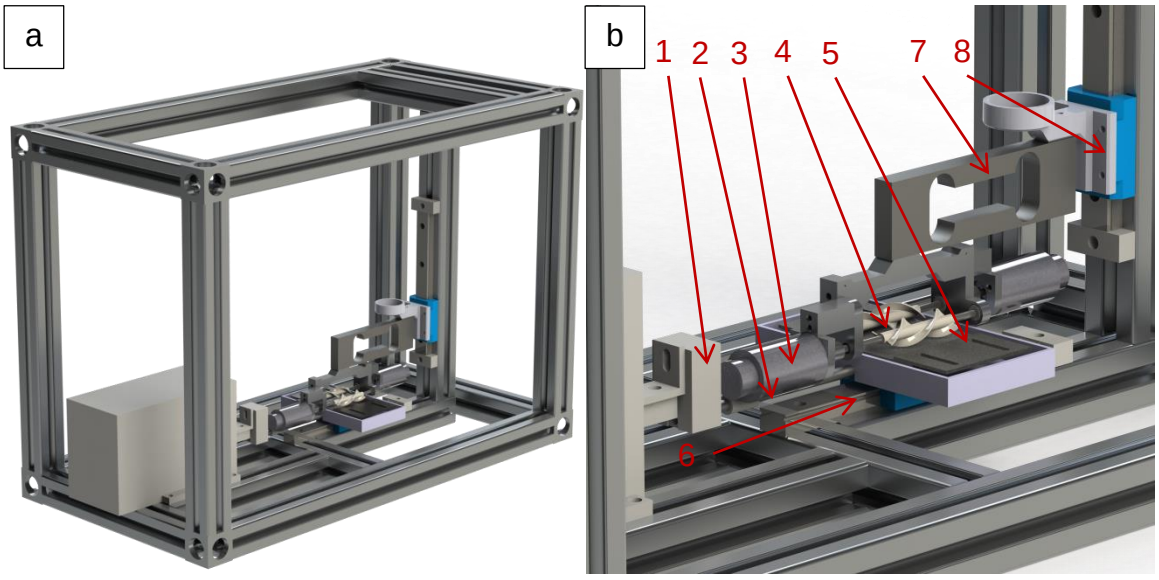

Figure 6.11 Computer images of the complete Traction and Contact Testing rig. a) full rig assembly; b) zoomed in view of the screw sub assembly, tissue bed and load cells. Annotations same as Figure 6.10.

To provide force measurements, loading cells were utilised in the testing rig. The beam load cell (300g cell, 1004-00.3-JW00-RS, Tedea Huntleigh), which is connected to an amplifier (RD7DC, RDPE) allows normal loading measurements to be taken. The bed load cell (GSO 50g cell, GSO-50, Transducer Techniques) is connected to an amplifier (Transducer Techniques) allowing horizontal loading measurements to be taken. Specifications for the load cells are detailed in Table 6.1.

Table 6.1 Load cell specifications

Load cell	Excitation	Range	Error	Safety overload	Output
Tedea beam cell	10v DC	0-300g	±0.0067%	150%	0.9±0.1mV/V
Transducer Techniques GSO	10v DC	0-50g	±0.05%	150%	1mV/V

The mass of the dual screw sub-assembly with motors and screws is 230g, to allow safe use with the system, a 300g load cell was chosen such that the dual screw sub-assembly could be safely attached. To reduce the normal loading applied to the tissue bed, a mass counter balance system was attached. A pulley was mounted above the vertical rail with a low mass strong (nylon) wire connecting the vertical slide (shown in blue in Figure 6.11, label 8) and a weight basket (HDPE bag, >1g) hung over the pulley. This allows masses to be attached countering the mass on the carriage from the attached equipment. A series of precision masses could be placed in the basket. The additional mass alters the resultant normal loading experienced by the screws when in rest against the tissue bed.

The normal loading predicted on the tissue by the screws is in the range of 0.5-1.5N, Chapter 4. For a 4-screw system to pull the tether, 1N of thrust would be required as previously discussed. The 0.5N bed load cell was chosen for the increased accuracy across the lower loading conditions. The safety factor of 150% allows for unexpected impulse loading to be measured should the dual screw system fair better than predicted. Should the screws produce greater than the expected thrust the load cell may be changed to provide a greater measurement range.

6.2.2 Rig Electronic Hardware And Data Flow

The Traction and Contact Testing rig features several different pieces of electronic hardware, which includes programmable and non-programmable hardware.

An embedded real-time (RT) system was selected to form the main component for the control and operation of the rig, as detailed in the following section. The embedded RT system manages the control of the system, data acquisition and communication between the systems. A laptop computer (Latitude E6430 ATG, Dell), referred to as the host system, provides a graphical user interface (GUI) to allow settings to be adjusted and data to be viewed on screen; and data saving capabilities. The embedded RT and host system are connected via an Ethernet connection. Data from the host is transferred to the embedded RT system over Ethernet, which includes parameters for the motors such as a demand velocity or linear actuator demand position. Data acquired from the sensors is transferred via the same Ethernet connection to the host allowing the readings for motor velocity, linear actuator position and load cell readings to be displayed onscreen. The linear actuator is controlled via a dedicated hardware controller that interfaces over RS-323. A diagram showing the arrangement and connections can be seen in Figure 6.12. A detailed discussion of each of the electronic hardware items can be found in the next sections.

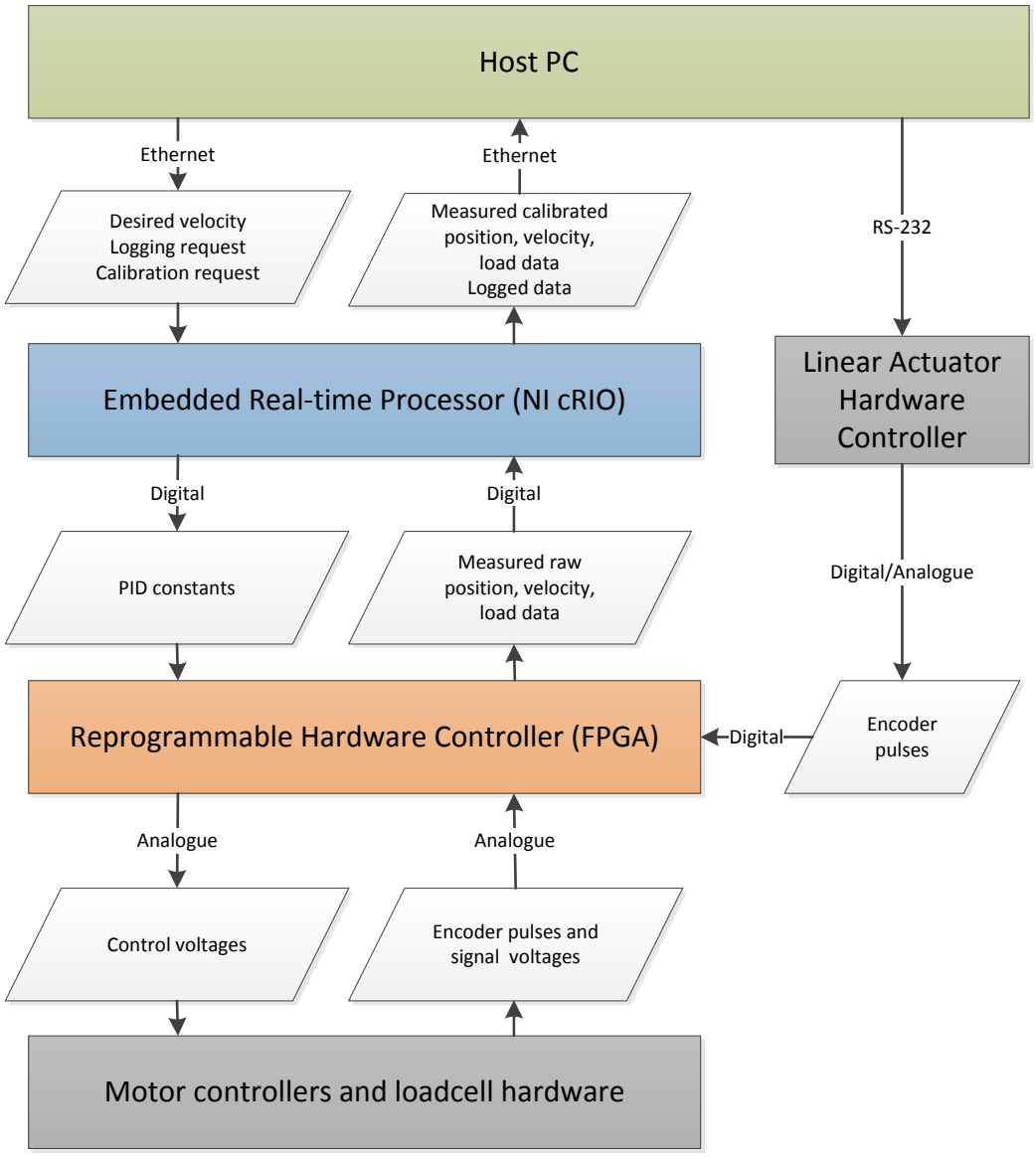

Figure 6.12 Traction and Contact Testing rig control system

6.2.3 Rig Computational Hardware

An embedded real-time system (Compact RIO, NI-9024, NI-9114, National Instruments, detailed in Chapter 4) was programmed to control and provide measuring capabilities to the Traction and Contact Testing rig.

A laptop computer (referred to as host machine) was used to display a graphical user interface (GUI) allowing configuration of running and logging settings. The real-time system was used for time-critical operations such as running control of the rig and collecting data from the rig. Data is transferred between the RT system and the host via an Ethernet cable, in data packets that contained several samples. Transferring larger data packets between the systems at less regular intervals leads to a more sustainable system.

The graphs showing the data on the GUI do not need to be updated at high frequency and are less sensitive to minor lag compared to the control tasks.

The embedded real-time system consists of two discrete subsystems, a real-time (RT) processor and a field-programmable-gate-array (FPGA) system-on-a-chip (SoC), as detailed in Chapter 4. The RT system is used for communication with the host and saving of data. The FPGA SoC is used for time critical control and data acquisition.

Data logging is performed by the real-time system, allowing for high accuracy of sampling rate. Once the data has been collected, it is transferred to the host in a single large data transfer to be saved to disk. This minimises any disruption to the sampling period caused by file systems delays on the host. Data is continuously transferred at a reduced rate to the host to allow the GUI to be updated, in a separate task further reducing disruptions to the data logging process from network latency.

The FPGA SoC can be loaded with different tasks at start-up depending on the mode of operation of the rig. For controlling the linear actuator, the FPGA provides a means of sampling the encoder pulses to acquire the real-time displacement and log the load cell readings at a high frequency. This allows the exact force at a displacement value to be logged. In a second mode, the FPGA provides PID control for the motors and sampling of the encoder pulses to determine the instantaneous velocity of the motor and log the load cell readings. These link to the static and dynamic traction testing states respectively, as previously discussed in this chapter.

6.2.4 Linear Actuator Control

The linear actuator is controlled via a manufacturer supplied, dedicated hardware controller (LAC-10, SMAC). This interfaces over a serial data communication protocol (RS-232) which is connected to the host laptop via a USB to RS-232 bridge. The controller sends and receives commands in ASCII, which can be sent from a terminal or composed within LabVIEW. Due to the communication path between the host PC and the linear actuator controller, the latency for commands being received by the hardware and the response being read was between 800ms and 1000ms. Latency was timed using a simple timing application built in LabVIEW, which measured the time from sending a command and the reply from the hardware being read. The high latency and variability of the latency means this is not ideal for recording the real-time position of the tissue bed. To provide real-time position of the linear actuator, the lines feeding the encoder pulses between

the actuator and the controller were duplicated. This allowed the cRIO to read the pulses to establish the position while allowing the linear actuator controller to read the signals for its own control process.

6.2.5 Control Systems Overview

An overview of this control system can be seen in Figure 6.12. Each of the discrete computational sections are coloured separately and match the colour of their respective subsystem overview in Figure 6.13, Figure 6.14 and Figure 6.15.

Figure 6.13 shows the dataflow within the host program. The architecture features an event driven GUI that queues commands to different loops for processing. This architecture allows for a responsive UI that captures all user interactions and splits off longer tasks to separate threads within the CPU for background processing making use of the multi-core CPU within the host system. This architecture further allows for delays in hard drive read/writes without affecting other tasks carried out within the host system. The linear actuator is operated from the host control system with an event queue allowing many commands to be queued up and each processed in order with the appropriate delays for the SMAC control hardware to respond.

The host control application is able to issue commands to the embedded systems for various control states as well as issue the shutdown sequence command. This ensures all the connected hardware items are powered down safely and channels are closed ready for power off.

Figure 6.14 shows the dataflow within the “Compact-RIO” RT control system. The control program collects the settings from the host over Ethernet and pushes the data collected from the FPGA SoC back to the host over Ethernet. The RT performs processing on the data to convert to standard units, offloading processing from the host. This is performed on the RT to allow data logging to take place on RT due to the temporal precision of hardware-timed events.

Figure 6.15 shows the dataflow within the FPGA SoC. Depending on the configuration (static or dynamic traction tests) one of two programs may be deployed in the FPGA. Both situations feature data acquisition from the load cells, with the static testing variation gathering data from the linear actuator encoder; and the dynamic testing variation acquiring encoder pulses from two motors to calculate velocity and providing PID control for the motors.

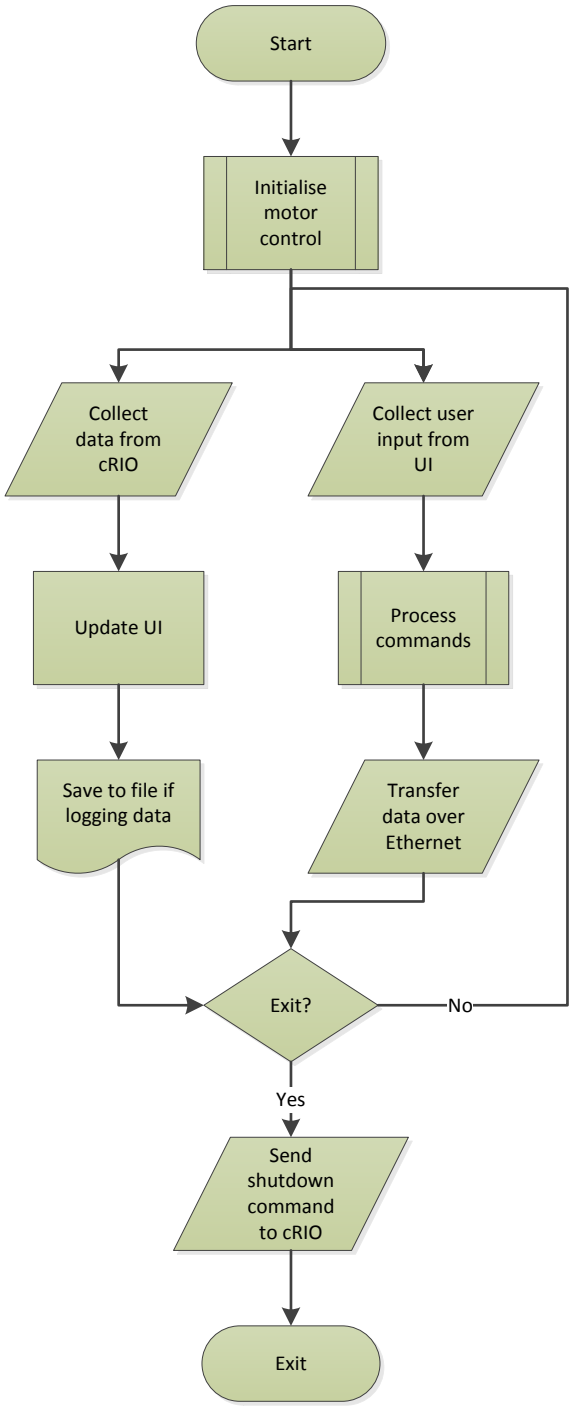

Figure 6.13 Traction and Contact Testing rig host machine control program.

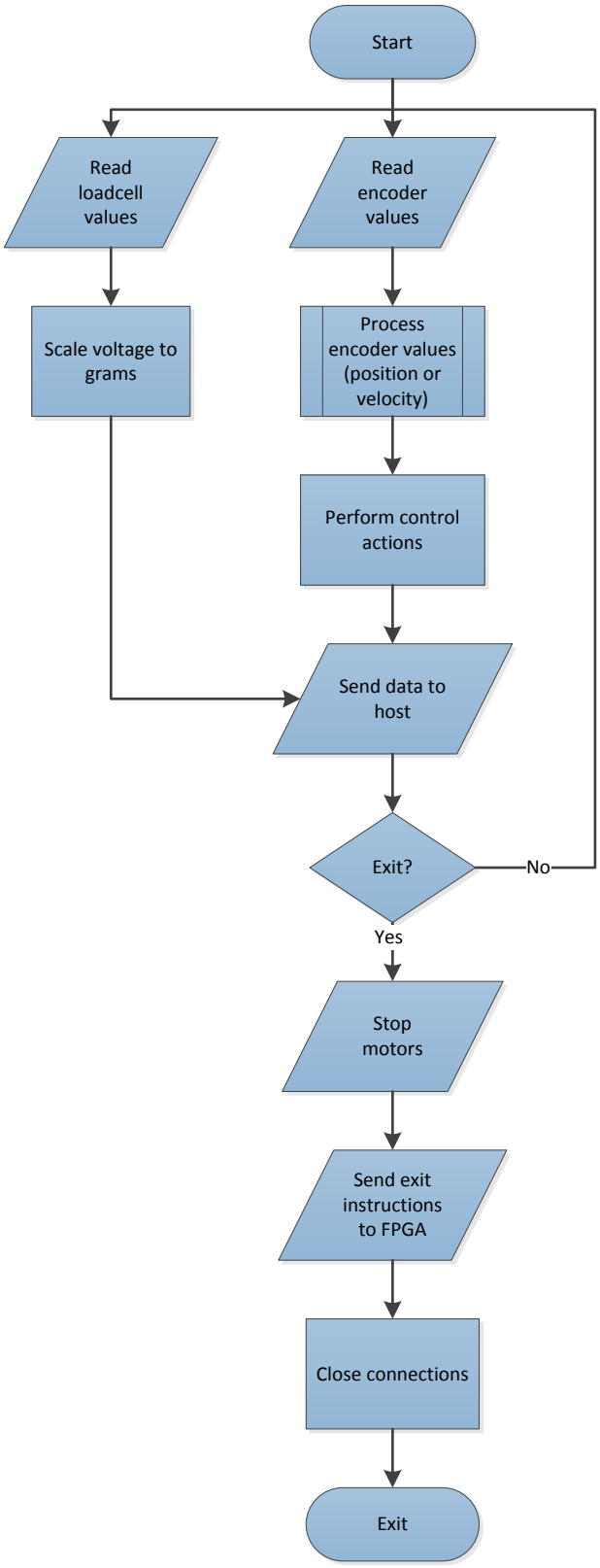

Figure 6.14 Traction and Contact Testing rig cRIO real-time control program.

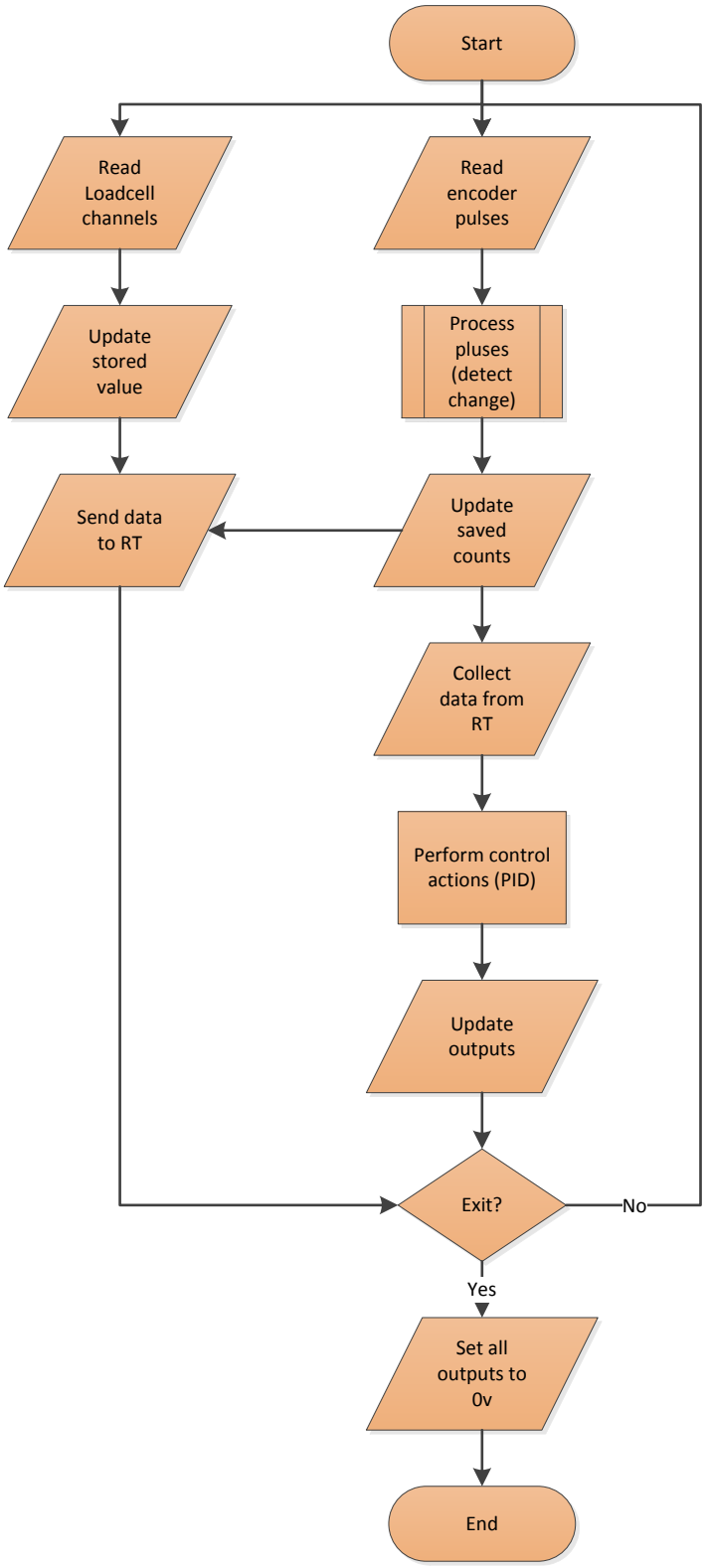

Figure 6.15 Traction and Contact Testing rig FPGA SoC control program.

6.3 Experimentally Assessing the Traction of Screws on Tissue

To ascertain the ability of screws to generate traction against tissue two experimental procedures were devised to test the two traction cases; referred to as static and dynamic traction. While both use the same testing apparatus, Traction and Contact Testing rig, the utilisation is slightly different and yields different resulting data. This section covers the methods and results for both static and dynamic traction experimental procedures.

6.3.1 Ex-vivo Porcine Colon Tissue Sample Preparation

For each of the contact tests, a separate sample of ex-vivo porcine tissue was prepared.

A section approximately 80mm in length was taken from an ex-vivo colon and cut along its length to form a rectangle; the size of which fits on the tissue bed allowing the screws to be in contact along their length. The faeces were removed using deionised water and the tissue mounted on the sample holder on the tissue bed. While porcine and human colons are not of the same geometry, their mucosa structure is similar and a widely accepted substitute (99).

To ascertain the traction against a clean colon, the faeces were removed. However, during the removal the mucosa had to be left intact. For this reason, the sample was carefully cleansed of faeces by rinsing the surface with deionised water. The samples were left in a saline solution to prevent them drying out and prevent electrolyte loss which would occur if stored in a non-isotonic solution. This also helped preserve the tissue to produce reliable tests. The electrolyte and water content of the tissue will have an effect on the mechanical properties; this is not within the scope of this research and has not been researched. This method of preparation ensures the conditions inside a colon are as accurately resembled as feasible within the testing parameters.

6.3.2 Experimental Method For Static Traction

Two screws of opposite handed, equal length pitches were mounted on the shafts of the screw sub-assembly. This was then attached to the beam load cell, with the tissue bed attached to the linear actuator via the bed load cell. A tissue sample was placed on the tissue bed and the screws rested against the tissue, as shown in the schematic in Figure 6.16.

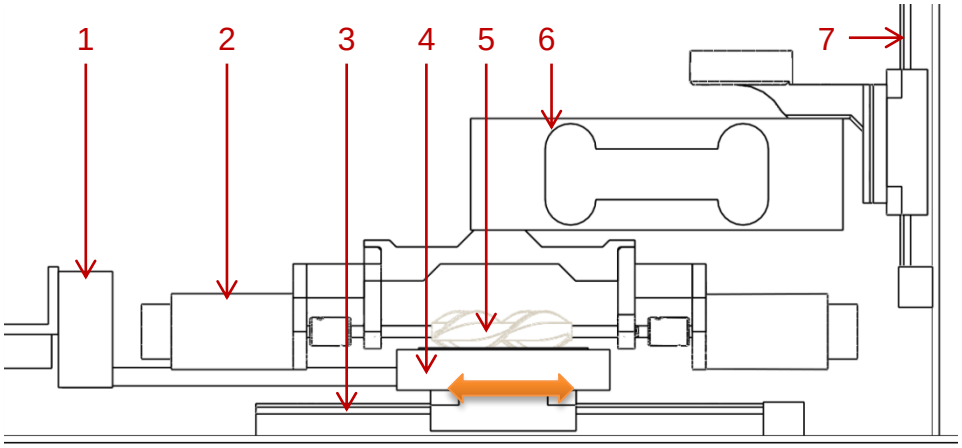

1. Horizontal load cell attached to linear actuator
2. Motor, unpowered throughout static testing
3. Horizontal linear rail
4. Tissue bed with tissue sample
5. Dual counter rotating screws
6. Vertical load cell
7. Vertical linear slide

Figure 6.16 Static testing setup, orange shows direction of motion during testing

The linear actuator was moved by a displacement of 5mm at a rate of $0.25mms^{-1}$, this was selected through initial experimentation to allow detection of thread deformation with displacement. The displacement was selected such that the threads of the screws remained in constant contact with the tissue throughout the displacement and the contact area of each thread vein did not overlap. The displacement demand velocity was set to allow any point of slippage to be detected, i.e. not instant through shock loading which would result in ambiguous and unrealistic data and without generating excessively large data files through long sampling periods. The displacement of the bed was recorded along with the force exerted upon the tissue bed. Two different normal loads were applied through the screw sub-assembly: 1N and 2N (to simulate expected contact pressures as detailed in Chapter 4); and two different screw types were used: stiff (material: vero-white) and compliant blades (material: DM9860, shore hardness 60); produced using rapid prototyping (Objet 1000, Stratasys). Each set up was repeated 6 times on separate samples of tissue. A table showing the experimental variables is shown in Table 6.2.

Table 6.2 Experimental variables for static contact testing

Screw material	Rigid, rigid + compliant
Screw pitch	20mm
Screw normal loading	1N, 2N
Repeats	6 for each unique configuration

Data were recorded at 100Hz for the course of the displacement and saved to CSV file for analysis. The file name included metadata on the screw type, normal loading and experimental method.

The shore hardness for the compliant screws was selected based on a material of similar mechanical properties to colonic tissue (100). For initial comparison between compliant and rigid materials, a single compliant material was used. A parametric sweep of compliance is carried out later in this chapter.

6.3.3 Experimental Method For Dynamic Traction

For the dynamic testing, the Traction and Contact Testing rig was set up similar to method 1; this time the tissue bed was held in a static position via the bed load cell (Figure 6.17). Any horizontal forces imposed on the tissue bed along the direction of horizontal displacement would be measured but would result in no displacement.

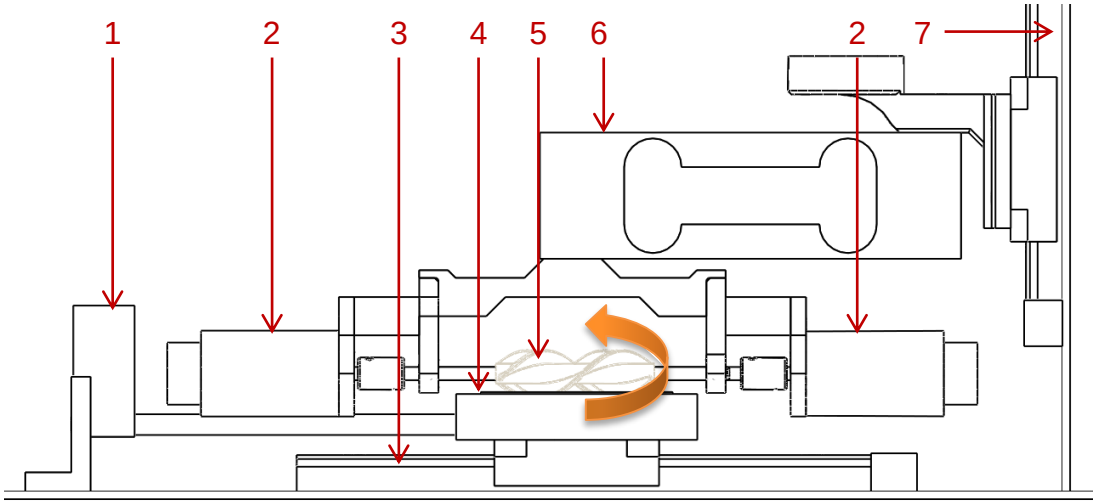

1. Horizontal load cell connected to fixing bracket
2. Screw motors, energised throughout testing
3. Horizontal linear slide
4. Tissue bed with tissue sample
5. Dual counter rotating screws
6. Vertical load cell
7. Vertical linear slide

Figure 6.17 Dynamic testing setup, orange shows screw rotation during testing

The screws were rotated at a controlled velocity of 5 or 10 $rads^{-1}$ with either 1N or 2N normal loading applied, these values were selected from the calculations in Chapter 4 to model the likely forces applied to the colonic tissue. The forces imposed on the tissue bed by the screws were recorded along with the motor velocities. Each separate set up was repeated 6 times.

Table 6.3 Experimental variables for dynamic contact testing

Screw material	Rigid, rigid + compliant
Screw pitch	20mm
Screw normal loading	1N, 2N
Angular velocity	5 $rads^{-1}$, 10 $rads^{-1}$
Repeats	6 for each unique configuration

Data was logged at 100Hz for 60s and saved to CSV file for analysis. Meta data for the method, screw type and normal loading was saved in the file name.

6.3.4 Data Analysis

For both of the experimental methods (static and dynamic), the data was analysed using a custom written Matlab program. An overview of the program dataflow can be seen below in Figure 6.18. The program loads all data files within a set directory and builds a database of the testing parameters involved from the filename metadata. This allows repeats to be grouped together and data files from other tests to be ignored for each specific testing type.

The data was filtered to remove noise using a 2nd order Low Pass Butterworth filter. A cut off frequency of 10Hz was selected as it was expected that the desired data would have low frequency change. Sources of noise such as screw rotation (motor velocity dependant) and mains power (50Hz) would have a frequency much greater than the cut off and would receive a high attenuation removing their effect from the results. A second order filter was selected due to the high attenuation applied to undesired frequencies with minimal phase lag to the desired signals.

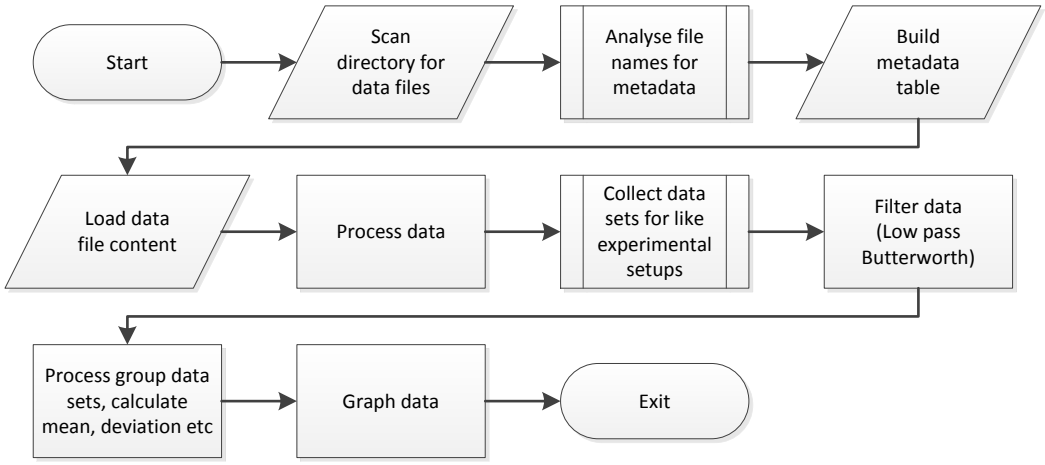

Figure 6.18 Matlab program for analysing screw contact data files

6.3.5 Static Traction Results and Discussion

For the static traction results, the results show a period of rising force in the horizontal direction against displacement as seen in Figure 6.19. This can be attributed to the screws sticking against the tissue causing an increase in load with increasing displacement. When this loading becomes greater than the traction force between the screw and the tissue the sample moves beneath the screws, resulting in a near constant force for increased displacement, as seen in region B in Figure 6.19. At this point, the maximum traction force can be extrapolated. To find this point, software was used to calculate the moving average across *n* points and compare the difference in

each sample range. Once the difference in the values for the moving point mean were within a pre-defined range of 5% (allowing for signal noise) this was taken as the point of slip. A combined mean of all the data points after this was used in calculating the maximum traction force achievable. These parameters are displayed in Figure 6.20.

Figure 6.19 shows a sample trace of recorded data through static traction testing. As seen by a typical example of static friction test result, the load upon the tissue sharply rises with initial displacements. The loading on the tissue reaches a maximum when the tissue begins to slip against the screws (region B), at this point the loading is greater than or equal to the traction force between the tissue and screws.

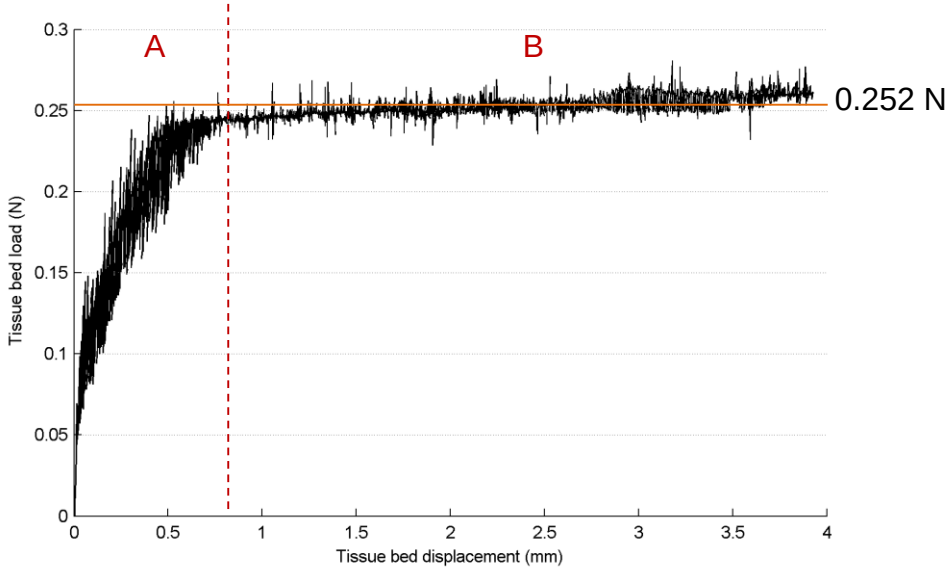

Figure 6.19 Sample trace from a single experiment showing the output from static contact testing for compliant screws. Section marked ‘A’ shows the stick interaction with increasing force for increasing displacement. Section marked ‘B’ shows the slip interaction. Sections were determined computationally using software that detects a change in moving average of less than 5%. Orange line shows mean (0.252N) of region B.

The bar chart seen in Figure 6.20 shows the mean maximum static traction between tissue and screws once slip has occurred, for all repeats for each particular unique hardware configuration. Slip was computationally determined using a moving average with a change less than 5% denoting slippage. The error bars show the standard deviation across all data points for all repeats with the same physical setup. It can be clearly seen that rigid screws produce higher traction than compliant screws against tissue in static

testing. Table 6.4 shows the mean static tractive force and standard deviation for each result as shown in Figure 6.20. Results show normal loading does not have a significant effect on the tractive force compared to screw compliance.

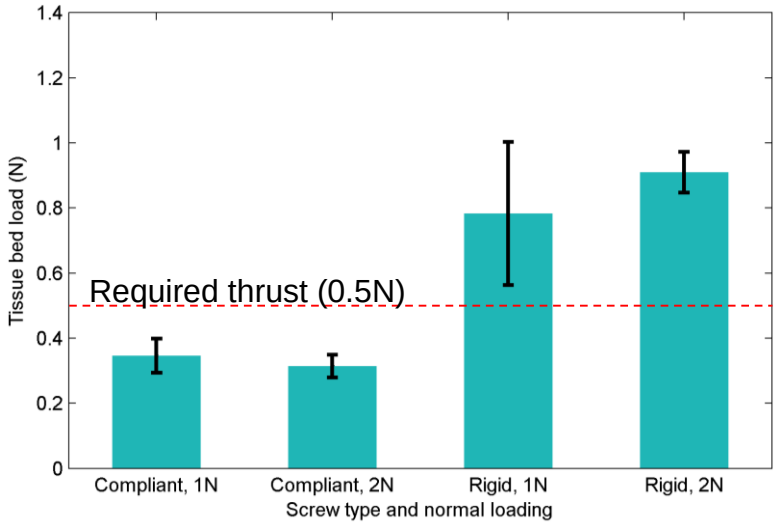

Figure 6.20 Mean static traction force between screws and tissue. Screw threads are compliant or rigid, loading applied normal to tissue surface. Tissue bed loading refers to the force required to remain stationary. Error bars show standard deviation. Discrete data sets were appended for like testing parameters, statistical techniques were applied to this total data set for each unique hardware parameter.

Table 6.4 Mean static tractive forces measured for screws against tissue

	1N loading	**2N loading**
Rigid screws	0.78N (SD: 0.21)	0.92N (SD: 0.05)
Compliant screws	0.32N (SD: 0.04)	0.36N (SD: 0.03)

The traction seen here will be due to the tissue between the threads of the screw. As the screw is displaced, this tissue will be displaced to a limit with the threads. The compliant threads will not grip the tissue as aggressively as the rigid threads, resulting in less traction. This is the ideal scenario as displacing the tissue may result in damage such as tears in the mucosa.

For each of the experiments carried out for static traction, there is a region of increased loading as the displacement of the bed increases, as show in Figure 6.19 region A. After a certain point, the loading flattens out into a continuous load for increased displacement, Figure 6.19 region B. This increase in loading can be attributed to the tissue properties. As the tissue is loaded, there is a degree of stretch in the tissue. After a maximum

displacement (approximately 0.75mm), the tissue does not stretch and slipping will occur between the tissue and the stretching implement. Should no slip occur then tissue damage will occur; such as tears in the mucosa. As slip occurs the force stretching the tissue is sustained which can be seen by the relatively flat line between 1 and 4mm displacement as highlighted region in Figure 6.19 marked B and annotated horizontal line showing the mean force during section B.

As tissue is not linear or constant in its properties, each sample will give variations in results not only across the repeats but also locally within the same sample, which can be seen by the micro stick-slip peaks in the trace seen in Figure 6.19.

The traction seen here will be due to the tissue between the threads of the screw. As the screw is displaced, this tissue will be displaced to a limit with the threads. For the compliant threads, they will not grip the tissue as strongly as the rigid threads, resulting in less traction. This is the ideal scenario as displacing the tissue may result in damage such as tears in the mucosa.

It can be seen that the rigid threaded screws produced the greatest traction; approximately twice that of the compliant threaded screws. The compliant threaded screws indented the tissue less; due to their compliant nature, they would deform. It was observed that the screw threads would buckle and collapse at 2N normal loading after some displacement. This resulted in the decrease in traction at 2N normal loading compared to 1N normal loading.

Across both screw types, during slip the motion was not constant or linear. It is hypothesised that the minor variations in force are due to micro stick-slip interactions between the screw threads and the tissue. For the compliant screws, the standard deviation is smaller when compared to the rigid screw threads, Figure 6.20. This may be due to the higher peak forces building between the rigid screws and the tissue, whereas the compliant screws will dissipate some of the force due to bucking of the compliant threads.

6.3.6 Dynamic Traction Results and Discussion

The dynamic experimental testing does not produce a slip point as with the static testing and thus was analysed using a separate approach. Using the metadata database, repeats for each of the unique hardware configurations (screw type, motor demand velocity etc.) were collected. A mean across all samples within the repeats was calculated, with the standard deviation, and plotted on a single graph showing the different experimental configuration,

Figure 6.21. The bar chart (Figure 6.21) shows the mean traction force between two counter-rotating screws and a tissue sample, taken across all repeats.

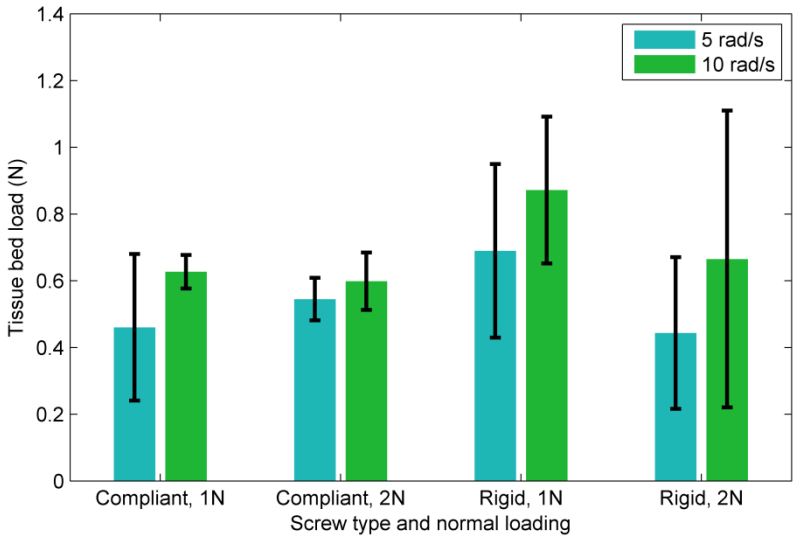

Figure 6.21 Mean dynamic traction force between screws and tissue. Error bars show standard deviation. The left most two pairs shows the results for the compliant screws while the right two pairs show the results for the rigid screws. Loading applied normal to tissue surface. Tissue bed loading refers to the force required to remain stationary. The blue bars show the results for a demand velocity of 5 rad s^{-1} while the green show the results for 10 rad s^{-1}. The error bars show the standard deviation across all repeats.

The high standard deviation seen in some of the data sets above can be attributed to “stick-slip” phenomena, which is explained later in this chapter.

From the results seen in Figure 6.21 for dynamic traction, a higher angular velocity results in a higher tractive force. This increase tractive force could be attributed to the increased rate of thread displacement along the sample.

For the compliant threaded screws, a greater tractive force was produced while the screws were rotating (dynamic) than when static. While this is true for the 1N normal loading case for the rigid threaded screw, the 2N loading case resulted in less tractive force being produced. It is proposed that this is due to the increased stick-slip interaction resulting in less traction.

6.3.7 Tissue Trauma

Throughout the experiments using ex-vivo tissue, samples were inspected for signs of wear to mucosa as an indication of trauma. The static traction experimentation resulted in no visible wear to the tissue sample, however the dynamic traction experimentation using rigid screws left visible indication of wear. To best demonstrate this, sample piece of tissue was prepared and

screws actuated against it under 2N normal loading at a demand velocity of 10 rad s^{-1} for 60s with a rigid and compliant (shore 60) screw, replicating the worst-case scenario for tissue trauma from the dynamic traction experiments. This can be seen in Figure 6.22, with the areas of compliant and stiff screw articulation highlighted. The stiff screw section, highlighted in red, shows clearly a patch of thinned mucosa due to damage from the screw. The compliant screw section (blue box) when compared to the control section (green box) shows no visible tissue damage. It is worth noting that serious and major tissue trauma would have a visible aspect to it (for example perforation and laceration), it is encouraging to note that the screw system does not induce this level of damage onto the tissue. More detailed testing would be required in the future, for example using histological techniques to look at microscopic damage to the tissues. This is beyond the scope of this work.

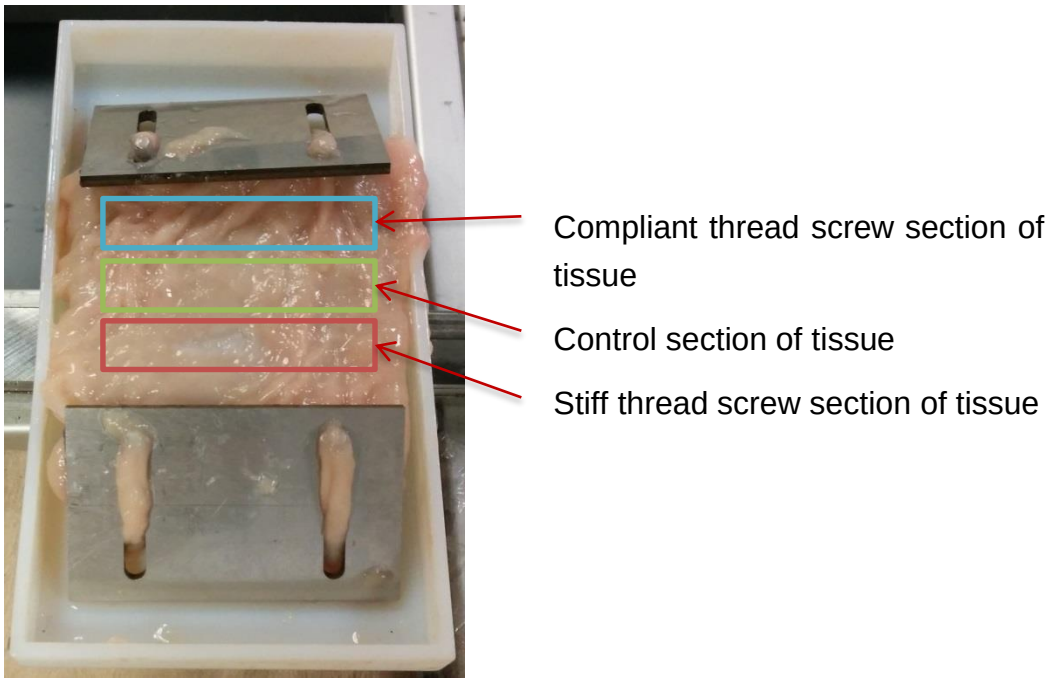

Figure 6.22 Demonstration of screw thread type against tissue

6.4 Investigating the Effect of Screw Compliance on Traction

The effect of compliance on traction cannot be summarised by a single compliant screw set, as the thrust produced showed high variability and no clear trend.

Therefore, a further experiment was conducted to investigate the effect of compliance in detail. Due to the high degree of variation in the thrust produced, a further experiment was carried out.

6.4.1 Experimental Method

A larger study was conducted using the same testing apparatus (Traction and Contact Testing rig) as the dynamic traction experiment, with an increased range of normal loading conditions and screw compliances. Normal loading was applied to the screws in 4 discrete categories using weights attached to the dual screw assembly such that the normal load was either of 0.5N, 1.0N, 1.5N or 2.0N. Seven different pairs of opposite handed screws were used, each produced from the same material with varying compliance. The range of compliant screws were produced using a rapid prototyping machine (Object1000, Stratasys) in shore values of 30, 35, 40, 50, 60, 70 and 85, shown in Figure 6.23.

Fresh samples of ex-vivo porcine colonic tissue were prepared using the method as described in the previous section. These were stored in a saline solution to prevent dehydration until they were used. For each screw pair, the screws were actuated at a demand angular velocity of 5 and 10 rad s^{-1} for all four normal loading conditions. Each unique setup was repeated 3 times on the same tissue sample; the sample was removed from the tissue bed and allowed to relax before being replaced in a different position. This reduced the overall samples needed allowing the experiment to be carried out using a single porcine colon, while still allowing the high number of configurations to be tested. Each time the tissue was replaced it would be positioned such that the screws would actuate against a fresh section of tissue. Visual examination would take place at this point for signs of wear to the mucosa, any damage would be noted and a fresh section of tissue used.

Table 6.5 Experimental variables for experimental parametric sweep of screw compliance

Screw material shore values	30, 35, 40, 50, 60, 70, 85
Screw pitch	20mm
Screw normal loading	0.5N, 1.0N, 1.5N, 2.0N
Screw demand angular velocity	5 rad s^{-1}, 10 rad s^{-1}
Repeats	3 for each unique configuration

A total of 168 individual experiments were carried out, each for 60s with data recorded at 100Hz using the same system as detailed previously in this chapter. For each of the samples, the data file filename for the recorded data included the screw shore value, normal loading and unique test number. The other parameters can be obtained through analysing the file contents.

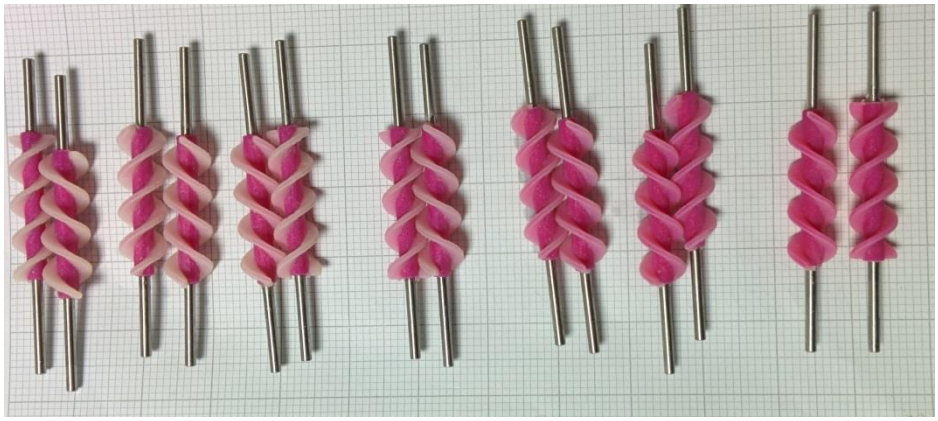

Figure 6.23 Prepared counter rotating screw pairs, photographed on a 2mm grid for scale. Shown left to right in pairs with shore values of: 30, 35, 40, 50, 60, 70 and 85. The screw body is rigid and has a darker colour, the more compliant the screw blade the lighter the colour.

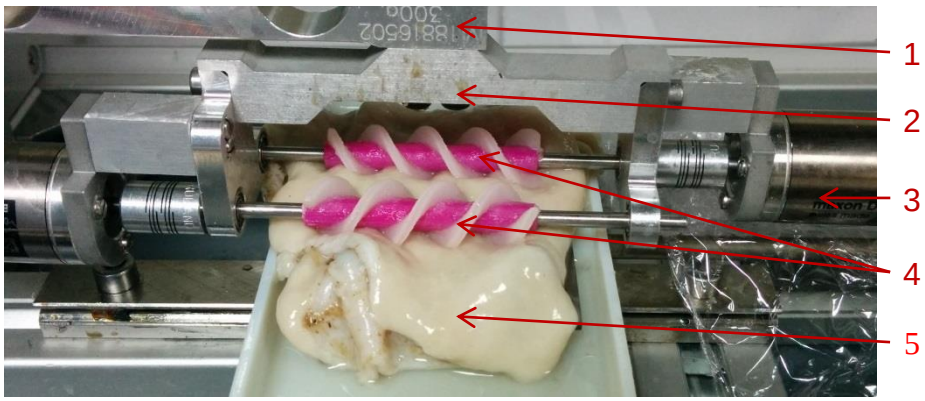

Figure 6.24 Tissue sample in the Traction and Contact Testing rig ready for testing. Annotations show; 1: beam load cell; 2: dual motor sub assembly; 3: motor; 4: screw pair; 5: tissue sample.

Figure 6.24 shows a sample of tissue in the tissue bed of the Traction and Contact Testing rig with a pair of screws resting against the tissue. The screws shown are shore value 30 with 2N normal loading. From the photograph, it can be seen that both the tissue and screws are deformed by the normal loading. The tissue is visibly recessed at the threads with it protruding between the threads, as described in section 6.1.4.

Figure 6.25 shows the same set up as above, screw pair of shore value 30 with 2.0N normal loading, against the tissue sample holding plate. From this

photograph, the deforming of the screw blades is evident, with the tips of the screw blades deflected to the left of the photograph.

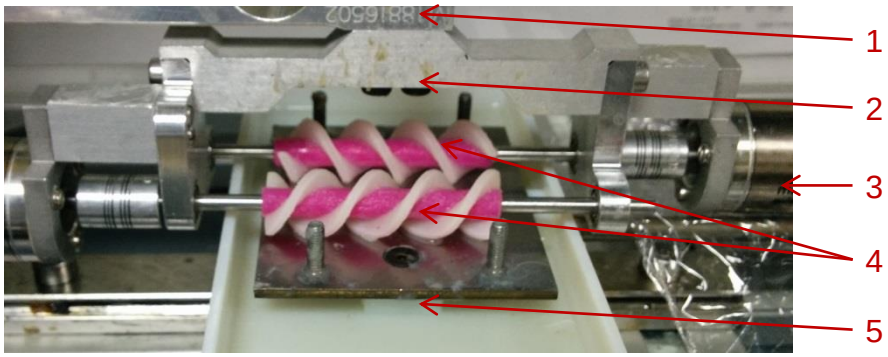

Figure 6.25 Screw pair resting against tissue sample holding plate of the tissue bed in the Traction and Contact Testing rig ready for testing. Annotations show; 1: beam load cell; 2: dual motor sub assembly; 3: motor; 4: screw pair; 5: tissue bed.

6.4.2 Data Analysis

Data files were analysed based on metadata in the file name. Using this, the shore value and loading condition for each data set was ascertained. The actual angular velocity of the screws differs from the demand due to loading conditions. This effect was used to quantify the stick-slip behaviour by defining the motion ratio, equation 6.4.

The motion ratio (MR) is a fraction composed of the total number of rotations performed by a screw divided by the expected number of rotations. Rotations may be replaced with encoder counts, which results in the same value being produced.

$$Motion\ ratio = \frac{total\ number\ of\ rotations}{expected\ number\ of\ rotations} \qquad \textbf{6.4}$$

For example, if the screw performed 2 rotations with the expected as 5, the ratio is 0.4.

To understand the grouping within the motion ratio of the screws, three groups were devised into which a dataset would fall. These groups are, Slip (<25% stall) (Figure 6.26), stick (>75% stall) (Figure 6.27) and stick-slip (~50% stall) (Figure 6.28). These bands were selected from analysing the data: the data sets band into the groups with few varying from the clusters. The percentage stall is arbitrary and selected as they provide a numerical description that bisects the distinct groups of data. The following three plots show datasets that show the characteristic velocity spread of the three motion ratio groups.

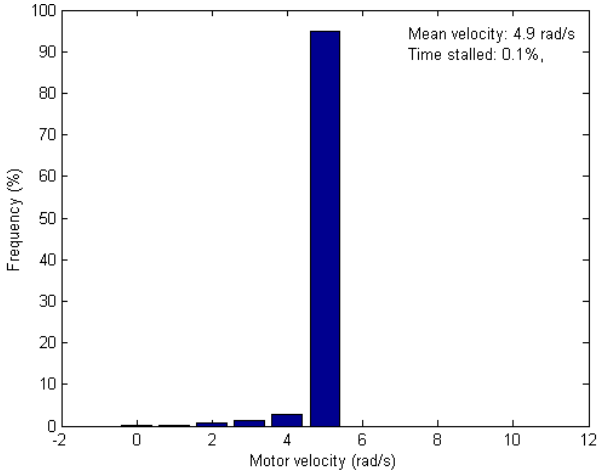

Figure 6.26 Slip case: histogram showing distribution of angular velocity, displayed in integer form. Data taken from results for Shore 60, 0.5N normal loading

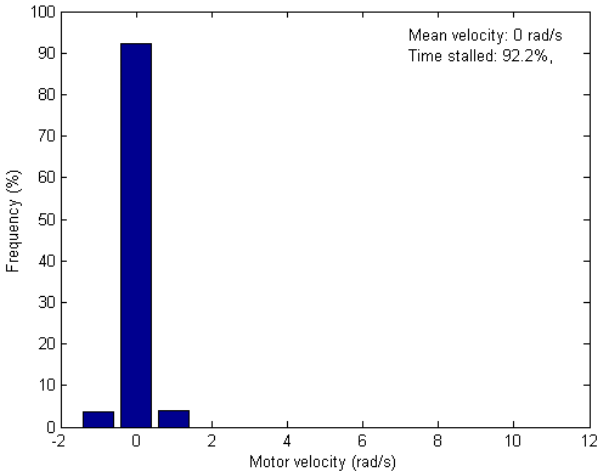

Figure 6.27 Stick case: histogram showing distribution of angular velocity, displayed in integer form. Data taken from results for Shore 85, 2.0N normal loading

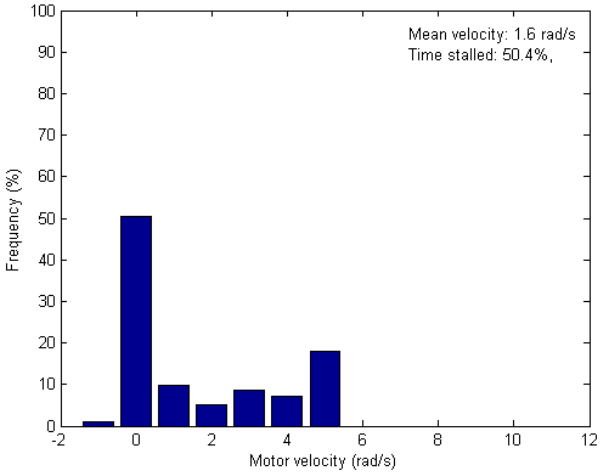

Figure 6.28 Stick-slip case: histogram showing distribution of angular velocity, displayed in integer form. Data taken from results for Shore 30, 0.5N normal loading

6.4.3 Results

To allow the data to be analysed for trends several plots have been produced with their significance discussed further in the discussion section to follow.

The plot in Figure 6.29 shows all data sets within the parametric sweep. Two clusters of data points can be seen which form vertical clusters. The marker shape denotes the shore value of the screws used, as detailed in the legend alongside the figure. The colour of the marker denotes the loading condition upon the screw set, as detailed in the legend alongside the figure.

For a screw to have a motion ratio of one, it must have rotated the same number of rotations as expected based on the desired velocity. This will occur when the screw has not experienced any retarding forces that have hindered the rotation. A screw, which does not encounter resistance against a surface during rotation, will result in a motion ratio of one. A line showing MR=1 can be seen in Figure 6.29. A high MR is defined as being between 10^{-1} and 10^{0}. It can be seen that the majority of results, which fall into this region, are made up from normal loading cases of 0.5N and 1.0N.

Low motion ratio occurs when a screw experiences a high resistance to motion. This may be caused by adhesion of the screw blades to the tissue or high resistance opposing rotation of the screw against the tissue. Defining a low MR as below 10^{-2}, it can be seen in Figure 6.29 that all cases of 2.0N loading are in this region. With high loading, the screws recess further into the tissue increasing contact area. This may explain why with increased loading the MR decreases.

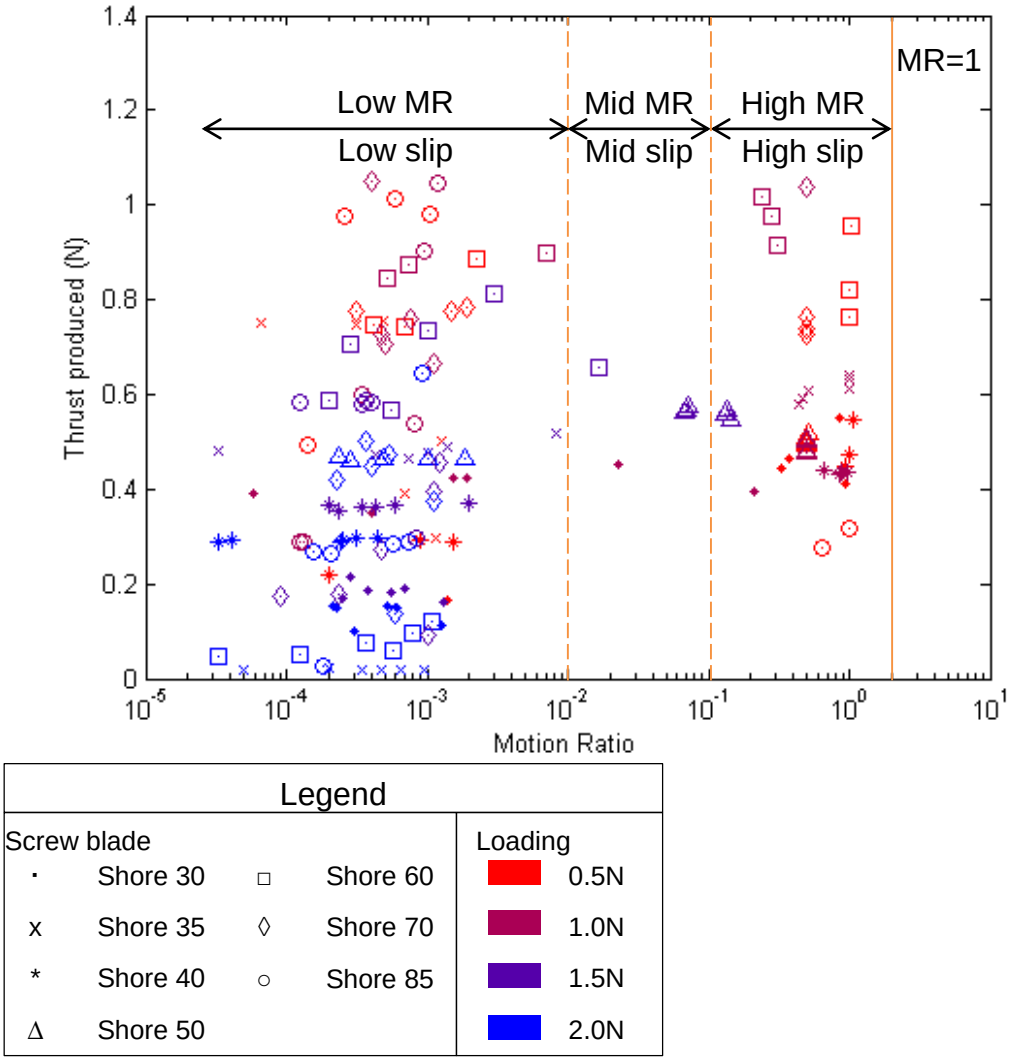

Figure 6.29 Motion ratio against thrust for all data sets. Marker shape shows screw blade compliance and colour shows loading condition, as detailed in the legend to the right of the plot.

There is no clear correlation between MR and thrust, however Figure 6.29 shows a correlation between loading and thrust. The highest thrust values are produced at a loading of 0.5N and 1.0N, with 2.0N producing the least thrust. There is also a correlation between screw blade compliance and thrust, the highest thrust values are produced from screws with a shore value of 60 or above.

To investigate these traits in more detail a single compliance was analysed. Figure 6.30 shows the results from a single blade compliant screw (shore 60) taken from the data set from Figure 6.29, which shows the relationship between loading and motion ratio and thrust production. A loading of 1.0N produces marginally greater thrust across the range of motion ratios than 0.5N loading, with the least thrust generated with a loading of 2.0N. A

correlation between loading and motion ratio can be seen, increased loading reduces the MR.

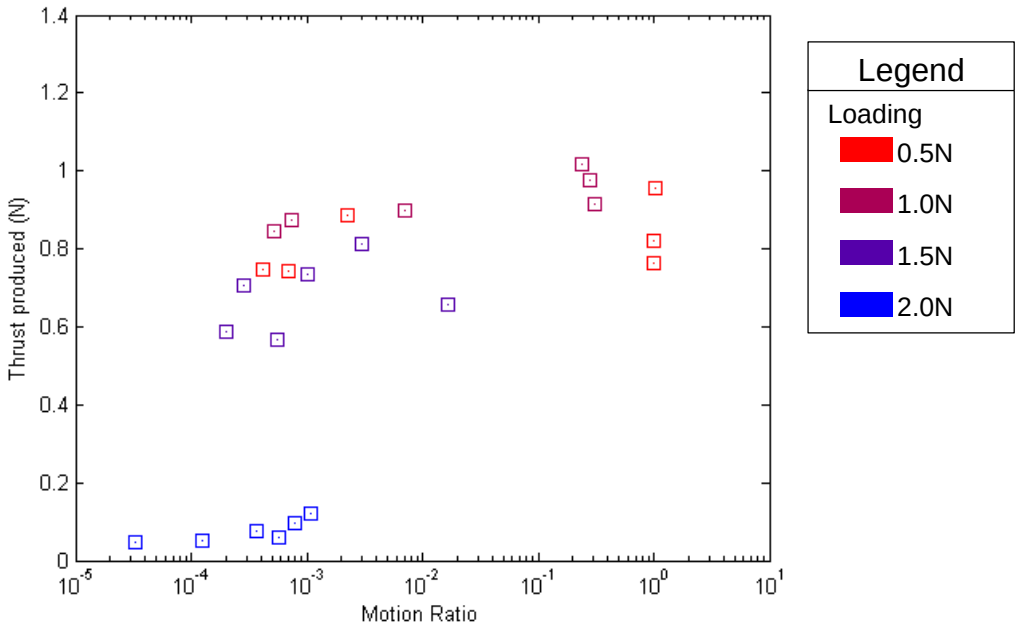

Figure 6.30 Motion ratio against thrust for experiments with screws of shore value 60. Marker colour shows loading condition, as detailed in the legend to the right of the plot.

While the demand angular velocity is an input to the system, the motion ratio is an output and thus will be affected by the inputs. In this respect to understand how the screws perform the effect of compliance and loading on motion ratio must also be explored.

6.4.4 Discussion

The effects of stick-slip, normal loading and screw blade compliance are discussed for their individual effects upon the thrust generated in terms of motion ratio classification.

6.4.4.1 Effects Of Stick-Slip

During the experimental testing, it was evident that the screws did not always rotate at a constant velocity. While in some cases the screws would rotate, in other cases they would remain almost stationary (stalled) throughout. In some stall cases, the screws would temporarily overcome the friction against the tissue and rotate; this would often result in a high peak velocity while the average velocity remained low. Viewing the data in terms of velocity versus thrust does not give any clear trend. When the screw is stationary against the tissue with a torque applied to the screw there will be transmission of forces. A stalled screw does not necessarily mean there is zero net thrust and so the thrust is not directly proportional to the screw

velocity. To ascertain if high average velocity (close to the desired velocity) results in a greater thrust generated than low average velocity, such as a stalled or partially stalled screw, the motion ratio metric is used.

The data collected throughout the experiments gives the instantaneous velocity of the screw at the sample time. Using this, the displacement may be obtained through integrating the velocity.

Classifying the results in terms of motion ratio provides a means to identify trends between stalled and non-stalled screws. Figure 6.29 shows a scatter plot of all the data points collected. Initially ignoring the loading and shore hardness of the screws and examining the spread of data, as shown in Figure 6.29, two vertical clusters can be seen. These clusters show a range of thrusts with a motion ratio of range 10^{-4} to 10^{-3} (low MR), and around 10^{0} (high MR). As predicted by the theoretical model a stalled screw does not result in zero thrust, which is shown by thrust of similar proportions being generated in the two clusters. There is a difference between the two clusters, there are no cases of zero thrust in cases where the screw has a high motion ratio. This means that a high motion ratio results in thrust however thrust is not wholly dependent on a high motion ratio.

6.4.4.2 Effects Of Loading

Introducing loading into the analysis, from Figure 6.29 it can be seen that there is distinct banding. The high motion ratio cluster is formed entirely of normal loading cases 0.5N or 1.0N. The greatest thrusts are produced by these same loading cases. The 1.5N loading cases produced between 0.6N and 0.1N of thrust with the 2.0N loading case producing below 0.5N of thrust. This separation shows that normal loading has an effect on the thrust production.

To assess the effect of normal loading upon thrust Figure 6.30 shows the data from a single compliance screw set (Shore 60) plotted on the same axes as Figure 6.29. A trend of decreasing motion ratio with increasing normal loading can be seen as well as decreasing thrust production with increasing loading. The normal loading would appear to have an effect on both the motion ratio and the thrust production. The two highest normal loading cases show a tighter cluster of data points compared to the lighter two loading cases; both these two cases (0.5N and 1.0N) have results from both the high and low MR range as indicated by the annotations in Figure 6.29.

6.4.4.3 Effects Of Compliance

Comparing the thrust produced for each of the different compliance screws, it can be seen that the highest thrust values are produced from screws with a shore value of 60 or above. Similar to previously discussed, the 1.5N and 2.0N normal loading cases produce less thrust than the lighter loading cases.

For the screws with Shore values 30, 35 and 40, the highest thrust production is generally for the lowest normal loading case and least for the largest loading case. While the largest loading case generally produces the least thrust in the other sets, the peak thrust comes from 1.0N normal loading (Shore 60, 70 and 85).

It can be seen that compliance of the screw has an effect on the thrust production; it is not known if the compliance of the screws has an effect on the motion. There is no visible trend or correlation between the compliance and MR shown in the data presented in Figure 6.29. To establish the reason for the banding trend seen in the motion ratio, the motion of the screws must be further analysed. As previously mentioned, the screws fit into three separate categories: slip, stick and stick-slip.

The first of these, slip, occurs when the screw is able to rotate, albeit with some resistance to motion. Throughout the sampled period, the screw moves at almost constant velocity matching that of the demand. This can be seen illustrated in Figure 6.26, which shows a data set that is representative of screws performing in the slip state. The data shown is for Shore 60, 0.5N normal loading. The stall time is calculated by the number of samples reporting 0 rad/s over the total number of samples. The mean velocity across the data of 4.9rad/s and has a motion ratio of 0.98.

The stick case is where a screw spends the majority of the testing period stationary. This is due to the resistance against rotation being too high or the resistance to the blades slipping being too great. In order for the screw to rotate, slip condition, the blades must rotate against the tissue surface. This results in the contact point between the screw and the tissue moving along the screw's axis of rotation. This has been discussed in detail earlier in this chapter, Figure 6.27 shows data from a set that is representative of the stick (data: Shore 85, Loading: 2.0N). The vast majority of sample time the screw is idle, 92.2%, resulting in a low mean velocity and motion ratio.

The combination of the two aforementioned cases, stick-slip, occurs when the screw is able to momentarily overcome the frictional forces and rotate.

This results in a motion ratio, which is in the range of 10^{-2} to 10^{-1}. Many of these cases saw the screw spending approximately equal time stalled and rotating, although not always rotating at the desired velocity. Figure 6.28 shows a data set which is representative of stick-slip cases (Data: Shore: 30, Loading: 0.5N). A spread of velocities between stalled and the desired velocity occurs due to the acceleration and deceleration the screw experiences as it moves between stick and slip states.

In Chapter 2 the minimum force required to perforate a colon was established through literature to be $14kN \cdot mm^{-2}$. The outer surface area of each screw shaft, ignoring the thread is $603.2mm^{-2}$. Assuming the screw without thread sinks to half its diameter into the tissue, the contact area is 301.6 mm^{-2}. For two screws, the combined surface area of contact is $603.2mm^{-2}$. For a pressure of $14kN \cdot mm^{-2}$, this would resolve as a force of 8.44N applied to the screws. This is much greater than the 2N applied throughout the testing. The exact surface area of contact between the tissue and screws is not known; this is because the contact dynamics are dependent on local variations in the tissue thickness and compliance, screw blade compliance and normal loading. This describes a worst case scenario and it is likely the forces applied by the screws will be lower than this and thus avoid loading the tissue traumatically.

6.4.4.4 Tissue Damage Sustained Through Parametric Sweep

The colon used through the parametric sweep experiments had a thick sub-mucosa tissue layer to it, as seen in Figure 6.24 and has a different appearance to the tissue used in earlier experimentation, as seen in Figure 6.22. After the parametric sweep experimentation had been carried out there were no signs of visible damage to the mucosa where the screws had actuated.

6.5 Summary of Contact Locomotion Analysis

It has been shown through the work detailed in this chapter that it is feasible to produce thrust from rotating screws against colon. The experimental data shows that the screws do provide a locomotion strategy capable of providing contact-based thrust against this highly deformable and changeable surface. A counter rotating screw pair is able to generate up to 1N of thrust when in contact with tissue. Should the full 4 screw device produce double this, i.e. 2N of thrust, then it should be able to progress along the colon with minimal restriction from the tether.

The compliance of the screw material does not yield a major effect upon the thrust generation, allowing for a compliance to be selected which best suits the environment. The normal loading applied to the screws does however yield a clear trend; when deployed the device will have the ability to alter the loading applied to the screws using the arm expansion mechanism as detailed in Chapter 4, allowing for local adjustments to be made to increase traction and thrust. The compliance of the screw does however have a visible effect on the integrity of the tissue, a reduction in the shore value results in reduced visible tissue damage.

Motor velocity does not play a large role in the thrust production as initially expected, loading and compliance are more significant factors. Motion ratio plays a limited role in thrust, which is as to be expected: while the screw has torque applied, it is still imposing a force upon the tissue. Normal loading does play a role, the highest thrusts are obtained from 0.5N and 1.0N loads. Friction against the screw core opposes rotation however, the threads need to be in contact with the tissue to produce thrust. This may explain why the higher normal loading cases produce less thrust: increased friction against the screw core will result in an increased resistance to motion.

Screw-tissue interaction forms into three categories: Slip (<25% stall), stick (>75% stall) and stick-slip (~50% stall). From Figure 6.29, the spread of data shows there is no trend between the motion ratio and the thrust produced. It may be useful to reduce screw slippage against tissue when deployed; as the screw slipping against the mucosa will be highly likely to cause trauma of some type, and such for minimising trauma understanding the factors, which increase the likelihood of slippage, will be important.

In Summary, the analysis of screw based locomotion shows:

- Screw based contact locomotion is feasible
- Screw blade compliance can be changed to reduce visible trauma
- Screw-tissue interaction can be summarised into three categories:
    - Slip (<25% stall)
    - Stick (>75% stall)
    - Stick-slip (~50% stall)
- The thrust generated is not reliant upon a single factor but several
- Screw angular velocity does not have a direct effect on thrust
- Normal loading applied by the screws on the tissue surface has an effect on thrust production

Chapter 7
Prototype System Analysis – Experimental Testing in Phantom and Ex-vivo Porcine Tissue

In Chapter 5 and Chapter 6, the screw locomotion system has been experimentally assessed in discrete modes of operation. This chapter covers the experimental assessment of a complete 2:1 scale prototype, to determine the system's ability to propel itself in a more realistic and complex, fluid filled environment. To facilitate this, two functional scale prototypes were built, as discussed in this chapter and Chapter 4, and tested in a series of environments.

7.1 Aims of Testing

A functional four-screw scale prototype device was assessed to determine the effectiveness of the locomotion system as a whole. During the fluid testing of the device, a single screw was tested in isolation. In using a complete four-screw system, the effects of counter rotating screws can be examined. This will provide insight into the practical maximum thrust the four-screw system can generate. The contact based testing carried out on the system involved a statically held pair of screws. In utilising an unrestrained scale prototype, the traction and thrust generated by the locomotion system will be ascertained in terms of being able to move the device. The locomotion system will be tested for its ability to traverse tissue sections as well as navigate through a complex environment similar to that of final application. This analysis was conducted to provide a detailed experimental simulation of the device in action, to further substantiate the contributions to amphibious locomotion for intra-luminal medical devices.

To assess the four-screw device, the following objectives were set.

- Assess the ability to provide thrust in a pure fluid condition
- Assess the ability to traverse on a flat tissue, in the following conditions
    - Non-flooded
    - Flooded
- Assess the ability to traverse a tissue lumen, in the following conditions
    - Non-flooded, collapsed
    - Non-flooded, open
    - Flooded, open

7.2 Production of a Scale Prototype

A 2:1 scale prototype was built with parts manufactured using an Additive Layer Manufacturing (ALM) machine and bought components, as discussed in Chapters 3 and 4. Following this, an open-loop control system was developed to allow the device to be controlled throughout the testing.

7.2.1 Construction

The assembled 2:1 scale functional prototype (referred to as the “four-screw device” hence forth) can be seen in Figure 7.1. It should be noted that two devices of identical geometry and motor-gearbox combinations were produced; only the colour of the rapid prototyped parts differs. Due to the porous nature of the plastic components from rapid prototyping, those, which were in contact with biological materials, were disposed of after use.

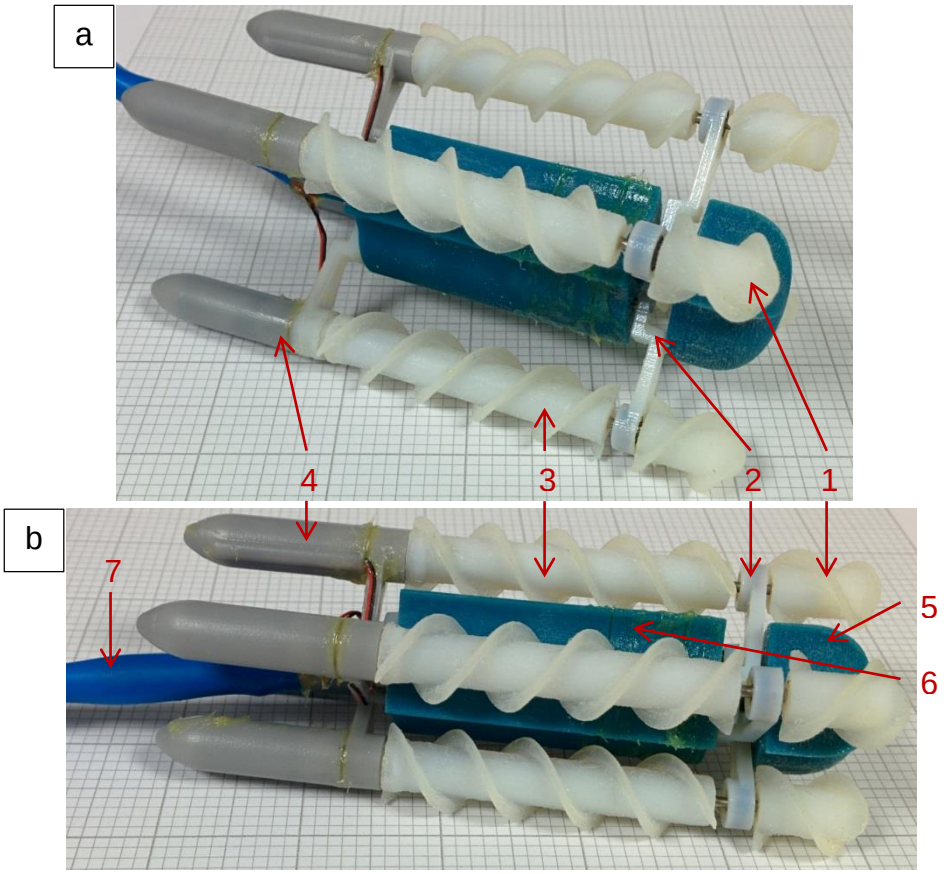

Figure 7.1 Assembled 2:1 scale prototype for testing, photographed on a 2mm grid. Device is shown in open state (a) and closed state (b) with the tether leaving the rear to the left. Annotations show: 1) Front-section screw; 2) Controllable arm section; 3) Mid-section screw; 4) Screw motor housing; 5) Front chassis section with space for camera module; 6) Central chassis section housing arm motor and gears; 7) Communications tether.

Several of the components, such as the gears and shafts, needed to be connected in order for the device to function. These were attached using an adhesive agent (Superglu, Loctite) which could be removed to allow for deconstruction and re-use of components. As previously stated, while the porous plastic parts were disposed of after use the metal components were recovered and sterilised for further use. The adhesive used could be dissolved using an acetone solution and cleaned using a laboratory grade disinfectant “TriGene”.

The motors were coated in a non-conducting grease (bearing grease, Castrol) to prevent moisture ingress and short-circuiting of electrical connections. Grease was applied to the openings of the motor housings and cable entry points to prevent ingress of moisture and seal the system. This can be seen in the photographs in Figure 7.1, by the yellow substance around the motor housings at the rear of the device. This allowed the device to operate in flooded conditions without the connections between rapid prototyped parts being watertight.

7.2.2 Control Hardware

To power and drive the four-screw prototype a tethered connection was chosen for convenience and simplicity. This allowed the motor control hardware to be located off-device with the tether directly linking the motors to the controlling hardware. The motor control hardware was situated away from the experimental area to prevent moisture contact. A two-meter multi-core tether was used, allowing the device to be operated and progress along a section of colon unhindered by tether length constraints. The tether length was selected to match that which would be used when the device is deployed. The motor controller hardware was the same as in previous chapters, which was connected to signal generation hardware (CompactRIO, National instruments). Figure 7.2 shows a diagrammatic map of the hardware and connections between hardware devices as used during the testing.

7.2.3 Control Software

The computer interface (LabVIEW, National Instruments) allows each of the motors to be controlled in an automated state or a fly-by-wire approach through a human interface device (HID). Automated motor control allows for specific voltages to be applied to the motors to generate step or ramp increase/decrease to motor voltage to provide repeatable control signals to the prototype. The HID allows analogue input control over device velocity

and direction: this is interpreted by the software to generate motor-specific signals to allow steering. A Microsoft Xbox 360 pad was chosen as it provides a range of analogue and digital inputs with readily available driver support. The Microsoft Xbox 360 pad includes built-in analogue-digital-converters (ADCs) removing the need for signal conditioning from the HID input.

Through using the analogue input on the HID, the user can alter the demand power output and direction. The control program interprets these into specific signals for each motor to match the desired output vector. The demand power is used as the mean of the motor power outputs and the demand direction used to generate the power ratio between the motors.

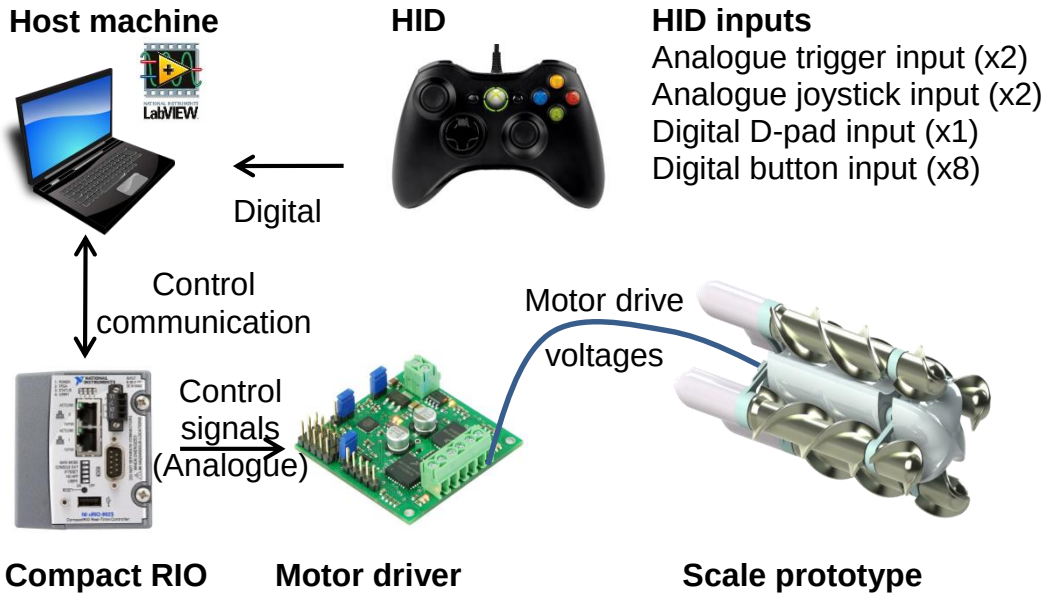

Figure 7.2 Prototype testing hardware configuration

For the device to turn left, the right hand side needs to increase output relative to the left. This can be done through increasing the right output, decreasing the left output or a variation of the two. A steering algorithm was developed, detailed below, which adjusts the output of both screws to achieve a difference in thrust resulting in a turning motion. The algorithm takes the desired velocity and steering angle as inputs and returns the drive signal for each screw.

To achieve a scaling factor for each screw drive signal, the developed steering algorithm utilises trigonometric relationships. Using a sine curve, motors opposite from each other will receive equal and opposite demand signals when multiplied by the sine of their position (equation 7.1). This approach was used to allow for change in position of the screws due to

expansion, as when the arms move from the closed position to the open position, the screws rotate about the body (Figure 7.3).

Figure 7.3 Orientation of screws about the chassis in closed (a) and open (b) arm positions

$$V_{left} = sine\left(\frac{3\pi}{2}\right) \cdot V_d,\ V_{right} = sine\left(\frac{\pi}{2}\right) \cdot V_d \qquad \textbf{7.1}$$

Table 7.1 Notation definition

V_d	Demand velocity
V_{left}	Velocity of left motor
V_{right}	Velocity of right motor

When a left command is issued, the left motor has a negative control voltage and the right motor has a positive control voltage, resulting in a zero turning radius. To control how much the system turns, the demand velocity needs to be supplied as a function of direction. This will allow forward locomotion while turning, as a zero turning radius may not always be required. By knowing the motor position relative to the chassis, and the horizontal component of the velocity, the steering of the system can be controlled through equation 7.2 (see Table 7.1 for definitions):

$$V_m = V_d - V_d \cdot \left(V_x \cdot sine(\theta)\right) \qquad \textbf{7.2}$$

At specific locations, the sine function will return a negative response, causing one motor to speed up while the other slows down.

To decouple top/bottom motors from left/right, a sine and cosine function are used. For example, for a motor at position $\theta = \pi/2$, ie to the right of the chassis, a horizontal component will result in a direct change in output, $\text{sine}\left(\frac{\pi}{2}\right) = 1$ whereas a vertical component will result in zero change in output, $cosine\left(\frac{\pi}{2}\right) = 0$. The control function using this approach can be seen in equation 7.3 (see Table 7.2 for definitions).

$$V_m = V_d - V_d \cdot \left(V_x \cdot sine(\theta) + V_y \cdot cosine(\theta)\right) \quad \textbf{7.3}$$

The function applicable to any number of motors spread equally about the chassis in any orientation about the device. Through altering the angle θ of each motor, the specific motor control voltage can be calculated. This approach does not require a motor to be in a set location, allowing adaption of the system as well as compensation for a non-responsive motor in the event a motor may fail during deployment.

Table 7.2 Notation definitions

V_m	Motor velocity
V_d	Demand velocity
V_x	X component of the demand velocity
V_y	Y component of the demand velocity
θ	Motor position in radians about the chassis centre.

In each of the tissue or phantom based assessments the automated control system was used to assess the straight line performance of the device in a repeatable method. This setup was configured such that it increased the voltage from 0v to 1.25v (25%) in 0.0005v (0.01%) steps each 100ms, giving an acceleration time of 2.5s. The analogue control was used to assess the steering ability as well as the motors at full voltage (5v). Current was not actively limited and dependant on the loading of each motor.

7.3 Methods of Assessment

Experimental testing was divided into three separate strands:

- Pure fluid locomotion
- Amphibious locomotion in phantom lumen
- Amphibious locomotion in ex-vivo porcine tissue

The pure fluid locomotion was carried out to allow assessment of a full four-screw system in comparison to earlier testing on a single screw in Chapter 5. The amphibious locomotion was carried out initially using a phantom lumen, before moving to an ex-vivo porcine colon sample. The phantom testing was carried out as this provided a repeatable means of testing the system in an environment free from bio-hazardous substances. Once the system had been tested in a repeatable means, the move to biological tissue was made

allowing a complete simulation of the device to be carried out experimentally.

The thrust generated for each of the fluid assessment experiments were collected using a load cell allowing for quantitative data to be analysed. The phantom and ex-vivo tissue assessments did not use sensors to log data, however a video camera was used to record each experiment: still frames for each of the experiments are displayed in this chapter.

7.3.1 Assessment Of The Device In Fluid

In Chapter 5 it was hypothesized that a four-screw system would produce up to 4 times the thrust of a single screw. To test this hypothesis and ascertain the peak thrust in fluid that the device can generate an assessment of the system was carried out. To acquire data throughout this assessment, the Fluid Propulsion Testing Rig (Chapter 5) was modified to include a 6-axis load cell (Nano 17, ATI). A 6-axis load cell was selected to allow investigation of the turning torques as well as straight line thrust to be measured. In using a load cell with X, Y and Z axes along with roll, pitch and yaw; perpendicular force vectors can be excluded allowing the thrust along the device length to be measured.

The 2:1 prototype was attached to the load cell via a modified nose section. The load cell was securely fastened to the metal struts in the rig. The cross beam was adjusted so the prototype was immersed in fluid with the supporting strut free from contact with the fluid tank and the load cell kept free of liquid contact. Figure 7.4a shows a diagram of the arrangement; Figure 7.4b shows a photograph of the assembled testing apparatus.

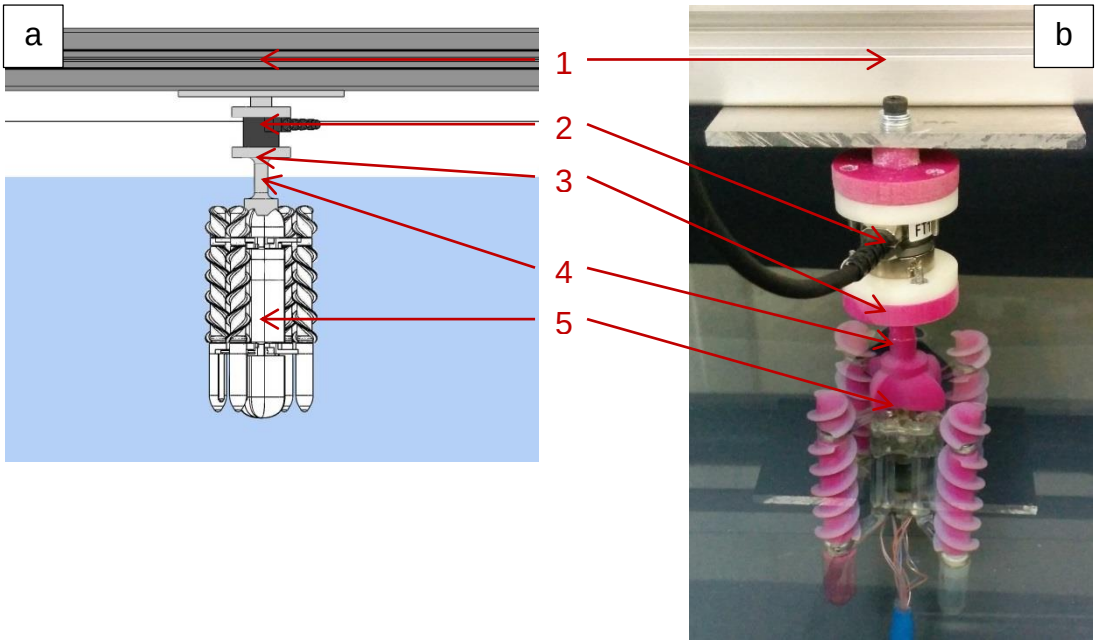

Figure 7.4 Prototype testing with the Fluid Propulsion Testing rig a) schematic of full prototype testing setup within the rig. b) photograph of assembled full prototype inside the rig. Annotations show 1: supporting cross beam in rig; 2: 6 axis load cell; 3: 4 screw prototype nose attachment piece; 4: fluid level; 5: 4 screw prototype.

Each motor was supplied with a constant voltage, as the motors do not include encoders no control over velocity was applied and the system ran in an open loop. The arms were positioned in the open or closed position for testing and remained stationary throughout. Using modified software from the Fluid Propulsion Testing rig to record the readings from the 6-axis load cell data was logged at 100Hz for 60s. Each of the unique motor voltage and arm position setups were repeated 3 times. An experimental setup matrix can be seen in Table 7.3.

The pitch of the screws was selected as a compromise between fluid and contact based locomotion. In fluid testing 40mm and 20mm pitch screws were used, however in contact conditions the 40mm pitch screws were unable to rotate and did not generate measurable thrust. The 20mm pitch screws were selected as they had a blade angle in the optimal range of 40° and 45° (88), and formed an integer number of rotations about the shaft. Smaller pitches are capable of generating greater torque, however from the calculations in Chapter 5 it can be seen that they will produce less thrust in fluid situations. Further optimisation into the blade angle/pitch may be carried out as future work to allow the system the largest thrust generation between contact and fluid states.

Table 7.3 Experimental variables for fluid testing of the complete prototype

Screw pitch	20mm
Arm position	Closed (90° coverage), Open (0° coverage)
Motor voltage	1.5v, 3v, 4.5v, 6v
Repeats	3 for each unique configuration

Two separate experiments were conducted using the fluid set up as described. The first experiment aimed to evaluate the systems straight line performance by supplying the same voltage to each screw. The second experiment aimed to evaluate the system's ability to produce turning torques, which would be used in manoeuvring the device, through supplying separate voltages to each screw.

After the data was collected, it was analysed. A second order Butterworth filter was applied with a cut off frequency of 1Hz. It is expected that noise will be introduced from the system though mains power (50Hz sine) and through oscillation of the screws due to minute off-centre mass being rotated, producing noise at a similar frequency to the motor angular velocity. As the system is held static and motors run continuously, any thrust generated should be a non-oscillatory response and any oscillatory responses will be an artefact of system noise. After the data was filtered, for each of the repeats with the same physical arrangements the recorded data sets were appended. The combined data set was used for the calculation of the mean thrust and the standard deviation.

7.3.2 Assessment Of The Device In A Phantom Lumen

Tissue phantoms provide a means to test on repeatable materials allowing greater control over the variables changed between experiments. A series of experiments were conducted on the four-screw system to test the locomotion system in contact-biased and fluid-biased situations. As the phantom tissue does not accurately resemble the surface properties of tissue it was used along-side tissue testing. Two different synthetic phantoms were used, each to test separate aspects of the locomotion system. A PVA based cyrogel "hydrogel" lumen was used to assess the contact based locomotion in a supported and unsupported lumen. A low density polyethylene (LDPE) lumen was used to create a flooded environment through which the prototype would swim. The LDPE lumen was transparent allowing full visuals of the device to be recorded as it progressed

along the lumen, the hydrogel lumen was translucent providing a partially obscured view.

Hydrogel is a PVA based phantom that was produced to resemble tissue in terms of its mechanical properties, and was produced by a member of the CoDIR team. Hydrogel is widely used to resemble soft biological tissue (101-103) in terms of bulk mechanical properties, however the global geometry and surface properties do not represent biological tissue. The surface is low friction with a film that is similar to the mucosa layer within a colon. The material is continuous in properties throughout and can be produced to the same properties each time. The advantage of this is that experiments can be carried out without changes in tissue sample introducing uncontrolled variables.

A length of LDPE lumen was used to form a phantom colon in terms of length due to availability. The production of a hydrogel lumen is a complex process and at time of testing a length greater than 200mm was not available. The use of the secondary lumen allowed a longer testing environment to be simulated.

Three experimental assessments were carried out using the hydrogel lumen, each designed to assess different aspects of the locomotive strengths of the four-screw system. For the first method the hydrogel lumen was attached to two solid pipe sections (40mm diameter, Figure 7.5 annotation 2) and suspended from a beam (Figure 7.5a). The purpose of this is to provide a fully unsupported lumen through which the device can be tested; any forces exerted on the lumen would not be restrained by the surrounding environment, allowing the lumen to stretch. This setup models a gas insufflated lumen without tissue surrounding the lumen preventing displacement. The device was inserted at an end such that the screws could obtain purchase on the lumen walls. Once inserted the device was driven with the HID.

A second setup featured the lumen placed on a bench without any support in terms of holding the lumen open and the device inserted (Figure 7.5b). The end of the lumen was held shut to simulate approaching a collapsed lumen, although it would not be possible to open the lumen, due to it being held shut; the device may be able to stretch the lumen to aid opening the passageway.

To assess the device in an open lumen, the hydrogel lumen was held open at the far end after the device had been inserted (Figure 7.5c). This allowed

the device to be tested in a way that resembles a traverse along a gas insufflated colon, such as an air pocket.

A summary of these experimental procedures is outlined in Table 7.4.

Table 7.4 Summary of phantom assessments

Assessment	Method	Objectives
Suspended hydrogel lumen	A section of hydrogel lumen suspended in air to remove support.	Assess the device in an air-filled lumen which does not have support to restrict stretching and deformation from the device under gravity and forces imposed by the device
Supported collapsed hydrogel lumen	A section of hydrogel lumen laid flat on a worktop and held closed.	Assess the ability of the device to progress through a section of lumen which is collapsed
Supported open hydrogel lumen	A section of hydrogel lumen laid flat on a worktop and help open	Assess the ability of the device to traverse an open and unblocked section of lumen
Fluid-insufflated LDPE lumen	A section of LDPE lumen was prepared and fluid insulated to resemble the inflation of a colon within a hydro-colonoscopy procedure	Assess the ability of the device to progress through a fluid filled and non-obstructed lumen, providing a best-case scenario for hydro-colonoscopy

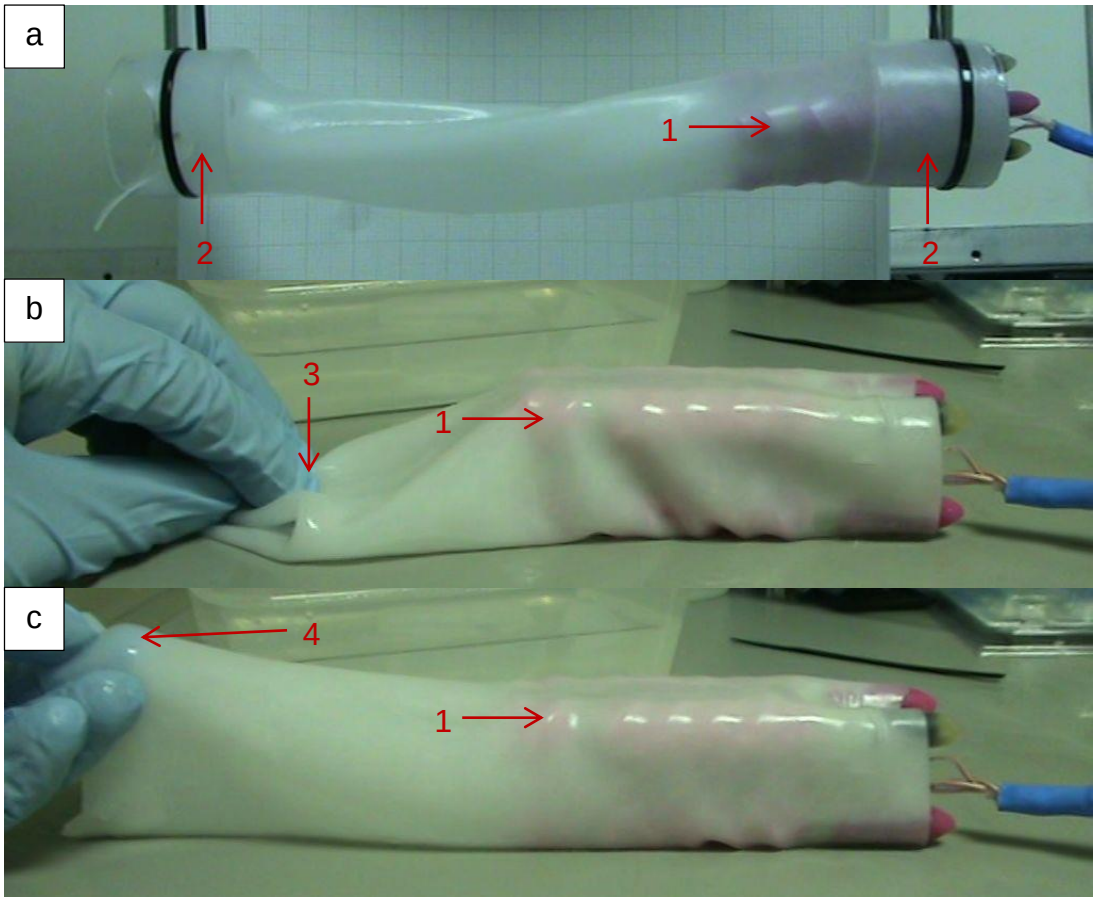

Figure 7.5 Contact-biased testing of the four-screw device using hydrogel phantom lumen a) unsupported lumen, b) supported closed lumen, c) supported open lumen. Annotations show 1) shows the device location as seen through the translucent lumen, 2) rigid end supports, 3) lumen held shut, 4) lumen held open.

The fluid-biased testing of the system was carried out using a length of LDPE lumen, which was sealed at one end, filled with deionised water. This was placed in a hard plastic container in a shape approximately resembling a colon (Figure 7.6). The corners were positioned such that they would remain partially open throughout. The open end was supported above the container such that a head of pressure kept the lumen insufflated. The device was inserted at the open end and tether supplied to allow the device to move. Using the HID, the device would be driven along the lumen.

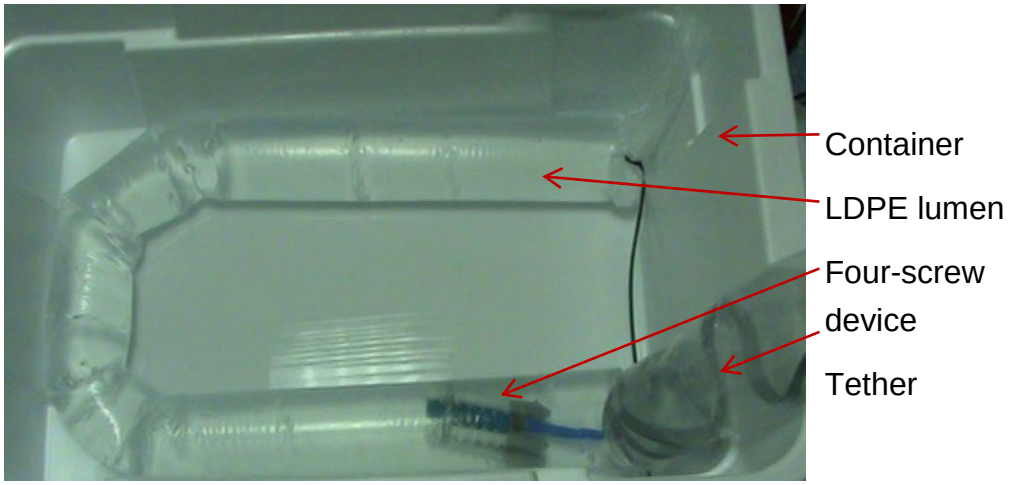

Figure 7.6 Fluid-biased testing of the four-screw device using a LDPE phantom lumen

7.3.3 Assessment Of The Device With Ex-vivo Porcine Colon Tissue

To produce quantifiable data on the movement of the device on tissue a series of experiments were designed to assess the locomotion system. A total of six different experimental procedures are carried out each assessing different environmental conditions the device may experience.

For each of the six ex-vivo tissue experiments carried out, porcine colon was used. The porcine colon was emptied of faeces through applying pressure along the length of the colon, mimicking natural peristalsis, and then flushed with warm water until the effluent flow ran clear. The colon sections were then used immediately for testing purposes and disposed of after use. The process of emptying the colon was designed to reduce mechanical actions that may alter the properties of the tissue, such as scraping with instruments.

For the experiments that featured flat tissue sections, automated velocity control was applied to the motors, as described earlier in this chapter. The experiments that involved a complete luminal section of colon saw the device controlled using the HID.

The following sections detail the ex-vivo experiments with a summary of the testing methods and objectives can be seen in Table 7.5

7.3.3.1 Ex-vivo Experimental Setup 1: Flat Non-Flooded Tissue Contact

A section of ex-vivo porcine tissue was cut longitudinally and placed within a plastic container (Figure 7.7). The prototype system was placed on the tissue sample at one end with the direction of travel facing along the sample length. This resembled a large section of the colon which is gas insufflated

where the device would remain in contact with a single surface, the surface it rests upon under gravity.

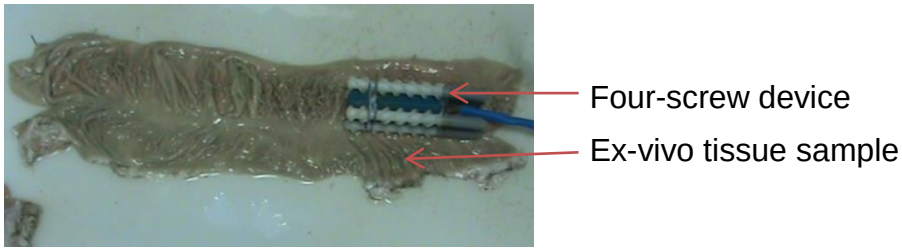

Figure 7.7 Four-screw device seen in contact with tissue sample in a non-flooded environment

7.3.3.2 Ex-vivo Experimental Setup 2: Flat Flooded Tissue Contact

A section of tissue was prepared in line with setup 2; this time the plastic container was filled with water to submerge the prototype system (Figure 7.8). The two screws not in contact with the tissue were disabled through the software control such that any locomotion developed would come from the screws interfacing with the tissue. This resembled a large section of the colon which is fluid insufflated where the device would remain in contact with a single surface.

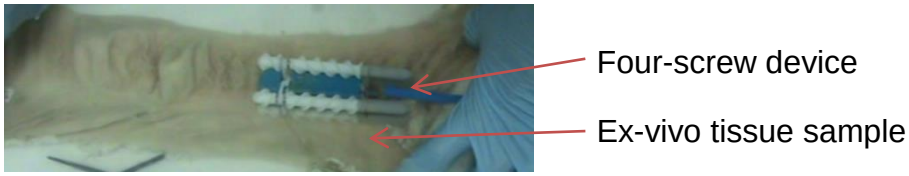

Figure 7.8 Four-screw device seen in contact with tissue sample in a flooded environment

7.3.3.3 Ex-vivo Experimental Setup 3: Unsupported Non-Flooded Colonic Lumen Contact

A section of intact colon lumen was prepared and placed within the container with the device inserted nose first into the lumen (Figure 7.9). This setup was designed to resemble a section of non-insufflated and non-fluid filled colon where the device would be in contact with the entire lumen, and there are no tissue structures outside the colon to maintain an open passageway.

Figure 7.9 Four-screw inserted into a non-supported colon length

7.3.3.4 Ex-vivo Experimental Setup 4: Supported Non-Flooded Colonic Lumen Contact.

A section of lumen was attached to two plastic pipe sections of 40mm diameter. These were suspended from a beam such that the length of lumen was supported between the plastic cylinders (Figure 7.10). The device was inserted into the lumen via one of the openings nose first. This experiment was designed to resemble a gas insufflated and non-fluid-filled section of the colon where there are tissue structures outside the colon to maintain rough position however, the colon is free to move (mobile colon).

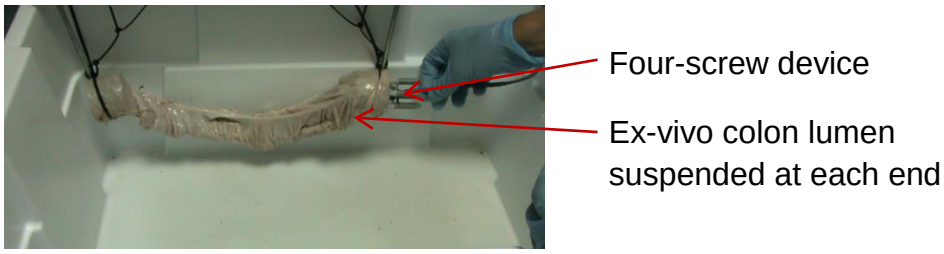

Figure 7.10 Four-screw device seen inserted into a length of ex-vivo colon, suspended between two rigid sections of pipe to allow the lumen to remain open. Gloved hand seen inserting the four-screw device into the lumen.

7.3.3.5 Ex-vivo Experimental Setup 5: Unsupported Flooded Colonic Lumen Contact

This set up resembles a similar environment to set up 4, however the lumen is fluid filled (Figure 7.11). The configuration from experimental setup 4 was submerged so the lumen was fluid filled and air removed, and the device deployed via an open end.

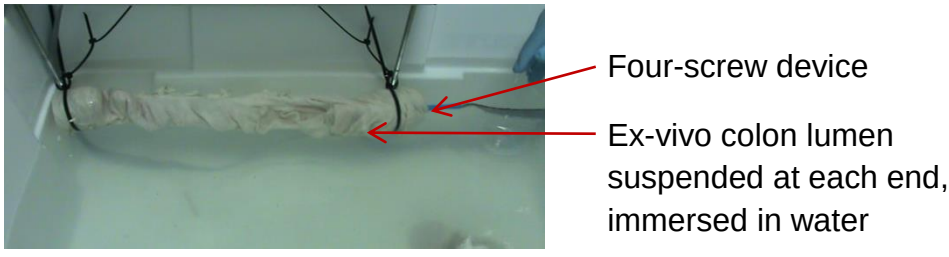

Figure 7.11 Length of ex-vivo colon suspended in a fluid tank, suspended between two rigid sections of pipe to allow the lumen to remain open. The four-screw device has been inserted to the right.

7.3.3.6 Ex-vivo Experimental Setup 6: Insufflated Complete Lumen

A section of lumen was prepared and sealed at one end. The other end was attached to a section of plastic pipe of 40mm diameter (Figure 7.12). A length of flexible plastic piping was attached to the other end of the rigid pipe. Water was poured into the open end of the flexible pipe such that the

colon was filled and air removed. The open end of the flexible pipe was secured in an upright position such that it provided a head of water to maintain the insufflation of the colonic lumen, simulating the inflation pressure of a hydro-colonoscopy procedure. The device was inserted into the colon lumen via the open end. This experimental setup is designed to resemble a complete hydro-colonoscopy environment.

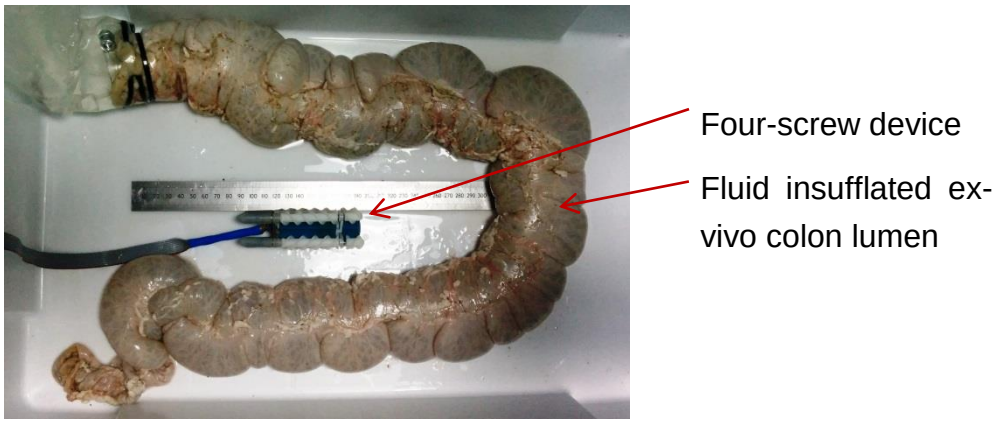

Figure 7.12 Four-screw device next to a fluid insufflated ex-vivo colon, 300mm rule shown for scale.

Table 7.5 Summary of ex-vivo porcine tissue tests

Assessment	Method	Objectives
1. Flat non-flooded tissue contact	A section of opened colon laid flat in a non-flooded container	To assess the ability of the screw locomotion method to provide sufficient traction to traverse a section of tissue in a non-flooded environment
2. Flat flooded tissue contact	A section of opened colon laid flat in a flooded container	To assess the ability of the screw locomotion method to provide sufficient traction to traverse a section of tissue in a flooded environment
3. Unsupported non-flooded lumen	A section of colon lumen suspended in air to resemble no support from connecting tissue	Assess the device in an air-filled colon which does not have support to restrict stretching and deformation from the device under gravity and forces imposed by the device
4. Supported non-flooded lumen	A section of colon lumen laid flat in a non-flooded container	Assess the device in a fluid-void collapsed colon which is supported to restrict stretching and deformation from the device
5. Unsupported flooded lumen	A section of colon lumen suspended in fluid to resemble no support from connecting tissue	Assess the device in a fluid-filled colon which does not have support to restrict stretching and deformation from the device under gravity and forces imposed by the device
6. Fluid-insufflated lumen	A section of colon lumen fluid insulated to resemble the inflation of a colon within a hydro-colonoscopy procedure	Assess the ability of the device to progress through a fluid filled colon lumen, providing a realistic scenario for hydro-colonoscopy

7.4 Results

The central motor was attached to the driving gear for the arm operation using an adhesive, Figure 7.13. The torque generated by the motor and the forces on the arms during expansion caused the adhesive bond to break. Future designs should include a keyway style interaction to overcome this. Testing throughout this chapter was carried out with the screws held in the closed position unless otherwise stated.

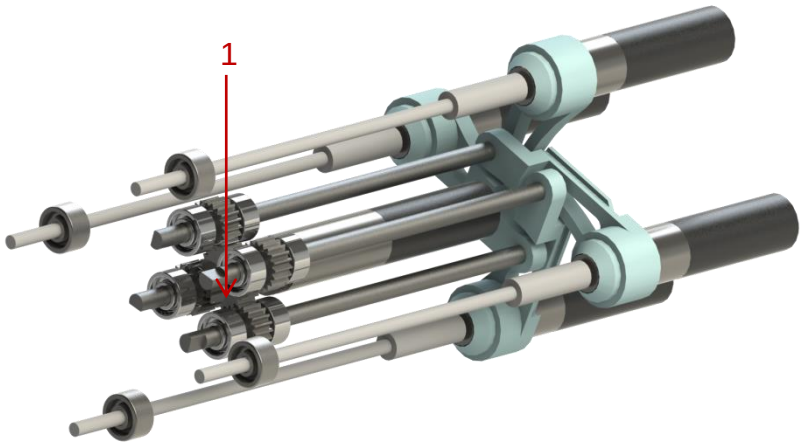

Figure 7.13 Computer model showing arrangement of gears and shafts within the developed system

7.4.1 Fluid Assessment Results

In the fluid assessment, the device was assessed for thrust production with all motors running and turning torque production with motor velocities varied between motors.

Figure 7.14 shows the results from the thrust generated by the four-screw system suspended in a tank of fluid. Across both the open and closed arm position data, the thrust is proportional to the motor supply voltage. Given the high standard deviation of the data, the open and closed states are not distinguishable. With an increase in the motor supply voltage there is an increase in signal noise, which is estimated to be caused by a higher motor rotation velocity resulting in greater vibrations.

Across the higher voltages, the signal noise is greater for the closed position compared to the open position. Due to slight manufacturing or assembly defects resulting in an off-centre rotation, the screw-body separation would vary throughout the rotation. This is estimated as a source of the higher noise in the closed position due to the altering fluid flow; as well as the noise across the whole system generated by rotational masses.

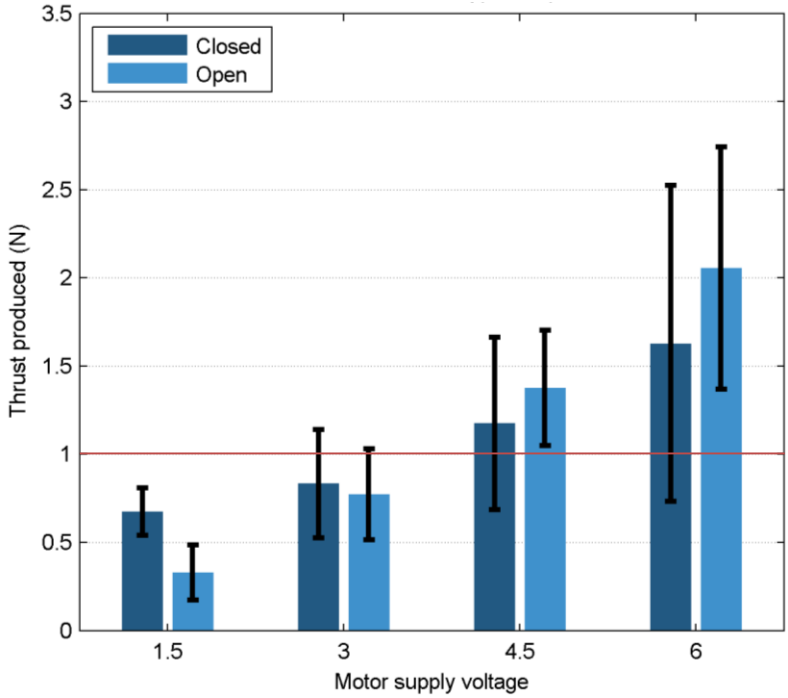

Figure 7.14 Thrust generated against motor voltage for the four-screw prototype in water. Error bars show standard deviation. Solid line at 1N shows the predicted thrust needed to traverse a colon.

This 6-axis load cell used in the experiment was used to acquire the thrust produced in different axes. Figure 7.15 shows the range of forces produced by a single screw when driven at full voltage. The single screw generates approximately 0.2N of thrust. Due to a single screw rotating, a net torque is also applied to the system.

A second set of data was collected for two counter rotating screws operated at full voltage, the results from which are shown in Figure 7.16. When a counter rotating pair of screws is actuated, the system produces approximately 0.5N of thrust. While the thrust output increases with the introduction of a screw, approximately doubling, the torque about the axis of thrust increases as well. This is unexpected as the counter rotating motions should reduce the torque. This increased torque in the Y-axis is intended to turn the device allowing fluid based navigation.

The pair of screws produce a greater torque about X-axis than originally expected; if the screws are of equal mass and velocity, their moments should cancel out. As the motors were controlled using open-loop control, i.e. no velocity feedback, it is not possible to fully determine the cause of this torque other than it is likely to be caused by a combination of the screw mass and the motor velocity.

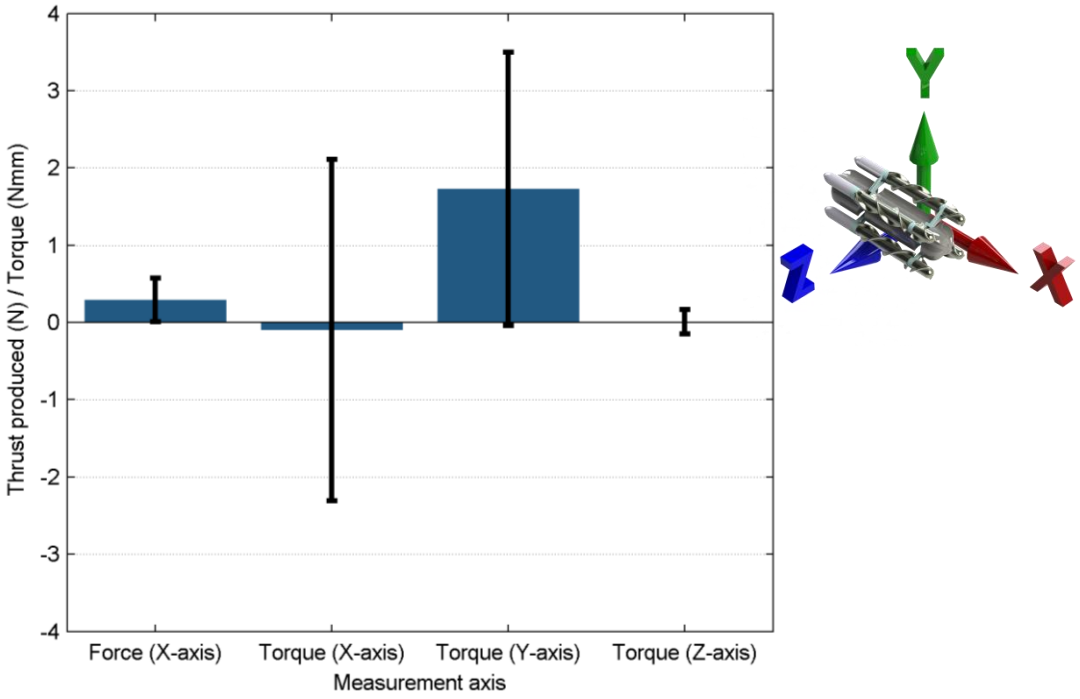

Figure 7.15 Output thrust and torque generated from a single screw of the 4-screw prototype actuated at full voltage. Bars shows mean value, bars show standard deviation. Insert to right shows a schematic of the four-screw system with axis arrows to aid visualisation.

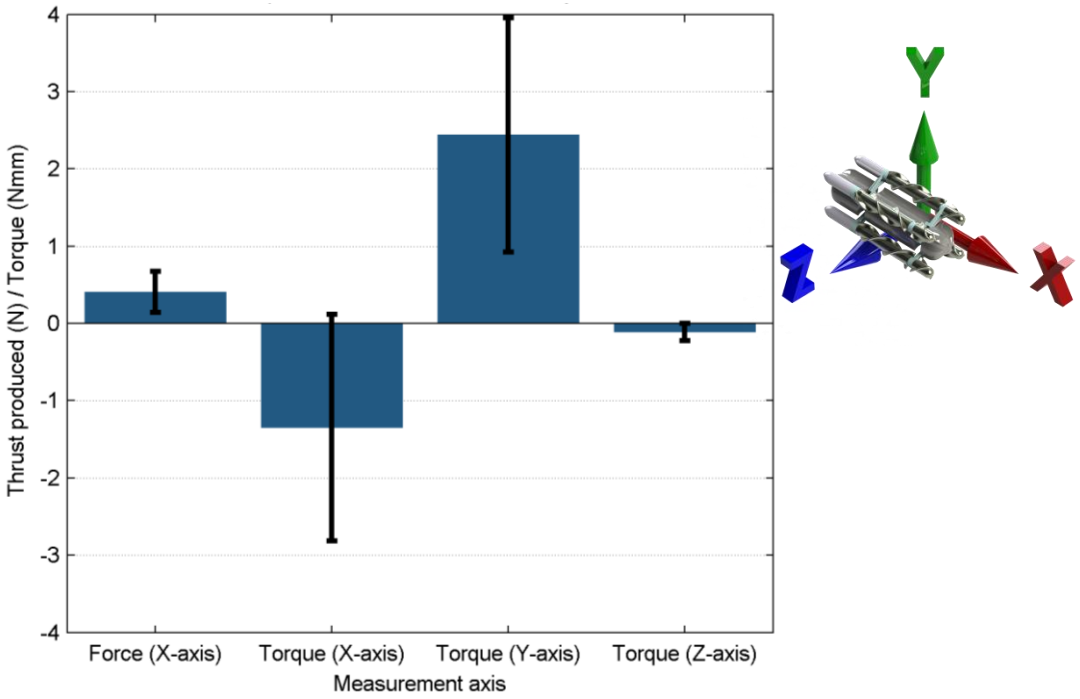

Figure 7.16 Output thrust and torque generated from a screw pair of the 4-screw prototype actuated at full voltage. Bars shows mean value, bars show standard deviation. Insert to right shows a schematic of the four-screw system with axis arrows to aid visualisation.

With a single screw producing approximately 0.2N of thrust (20mm pitch screw), this is greater than the thrusts recorded during the fluid assessment

(approximately 0.1N, Chapter 5). While the angular velocity of the screw is not known, and may be a reason why the thrust produced is greater; it may also be due to the conditions around the screw. The single screw experiment featured a bearing and bracket below the screw inline of the thrust, while the actual device does not.

When comparing a single screw on the prototype to a pair of counter rotating screws the thrust increases from approximately 0.2N to approximately 0.5N. This increase of over 2x is expected to be caused by the interaction of the flows from the counter rotating screws decreasing the laminar flow of the surround fluid. When utilising all four of the screws (Figure 7.14), the thrust increases to approximately 2N, a four-fold increase from two screws.

7.4.2 Phantom Assessment Results

When the device was inserted into the suspended hydrogel lumen, it was able to traverse to the midpoint of the lumen's length. Figure 7.17 shows frames taken sequentially at five-second intervals showing the traverse of the device through the suspended hydrogel lumen. When the four-screw device reached the midpoint of the lumen, the deflection caused by the mass of the device caused it to become stuck. The nose of the device angled into the luminal wall created an impassable situation, circled in Figure 7.17f. The base of the lumen has displaced by approximately 30mm at this point, from measurements taken from the grid behind the lumen: while the lumen diameter has remained close to constant. The low friction of the hydrogel lumen walls prevented the device from reversing and the screws spinning freely. This was observed across a number of repeats and not a product of poor steering.

In the section of closed hydrogel lumen the device was able to traverse up until the diameter of the lumen restricted the progress. Figure 7.18 shows frames taken sequentially at five second intervals showing the traverse of the device through the closed hydrogel lumen. When the device reached a point where it would only be able to progress if the lumen was stretched, it was unable to progress any further. The screws continued to rotate however was insufficient thrust generated to produce forward motion. The device was however able to reverse along the lumen from this position.

When the section of the hydrogel lumen was held open, the device was able to traverse the entire length of the lumen. Figure 7.19 shows frames taken sequentially at five second intervals showing the traverse of the device through the open hydrogel lumen. The device was able to traverse the

length in both forward and backward directions at the same rate. The length of lumen was approximately 200mm in length, with the device traversing approximately 60mm in 5 seconds as measured using the video frames.

When the device was inserted into the insufflated flexible LDPE lumen and piloted, it was able to traverse the straight sections with relative ease, Figure 7.20. Each frame was taken at 10-second intervals from the video of the experiment. As the device approached the corners, it became difficult to turn the device, owing to its large turning circle and relatively long body length. Due to the tether forming an S-bend on insertion, the device was hindered in terms of mobility on the initial straight section (Figure 7.20 annotation 2). The device was reversed and then run forward at full power to remove the tether bend, seen in Figure 7.20d to Figure 7.20g. As the device approached the second corner, seen top left (Figure 7.20 annotation 3), the folds in the plastic lumen covered the aperture making it impossible for the device to progress any further without external intervention (Figure 7.20I, annotation 3).

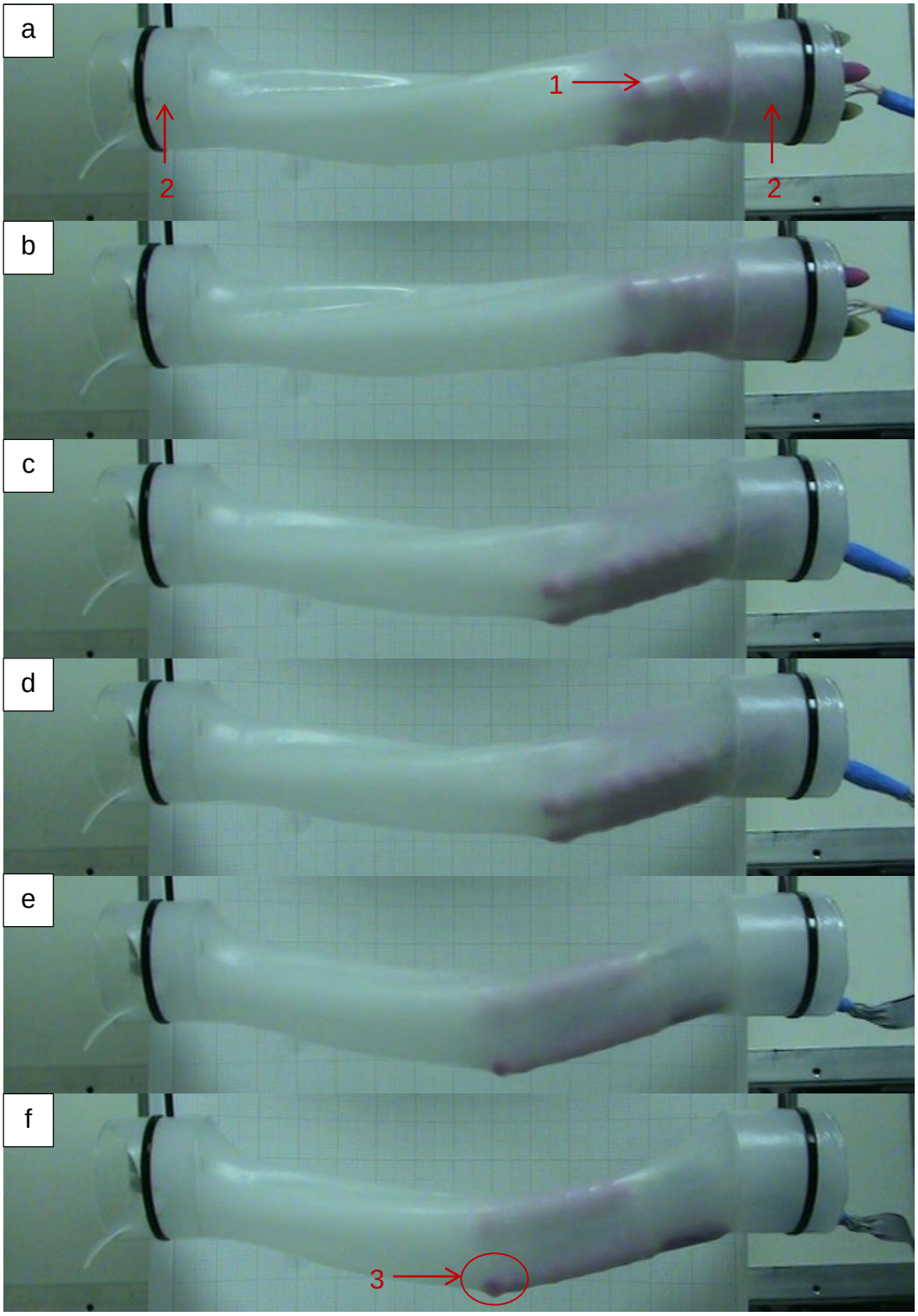

Figure 7.17 Frames taken from video showing the device traversing along the unsupported hydrogel lumen. First frame shows initial setup at 0s; each sequential frame taken at 5s intervals showing the device's progress. Grid shown in the background is 20mm spacing of darker lines. Annotations show 1) Four-screw device, 2) cylinder end supports 3) lumen stretching about the screw nose with the device unable to progress any further along the lumen.

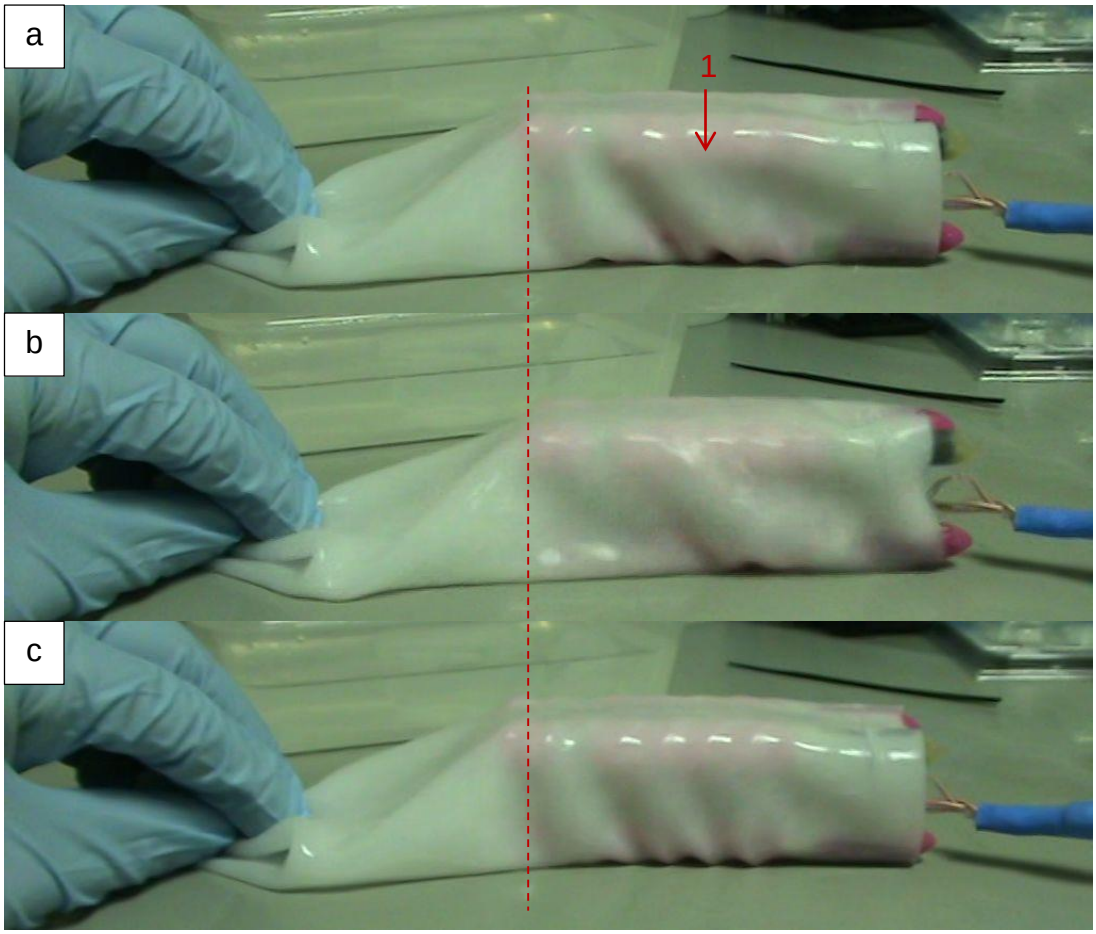

Figure 7.18 Frames taken from video showing the device in the hydrogel lumen on a desk with the far end held shut. First frame shows initial setup at 0s; each sequential frame taken at 5s intervals showing the device's progress. Annotation 1 shows the four-screw device seen through the translucent lumen, dashed line shown to aid visualisation of device progress.

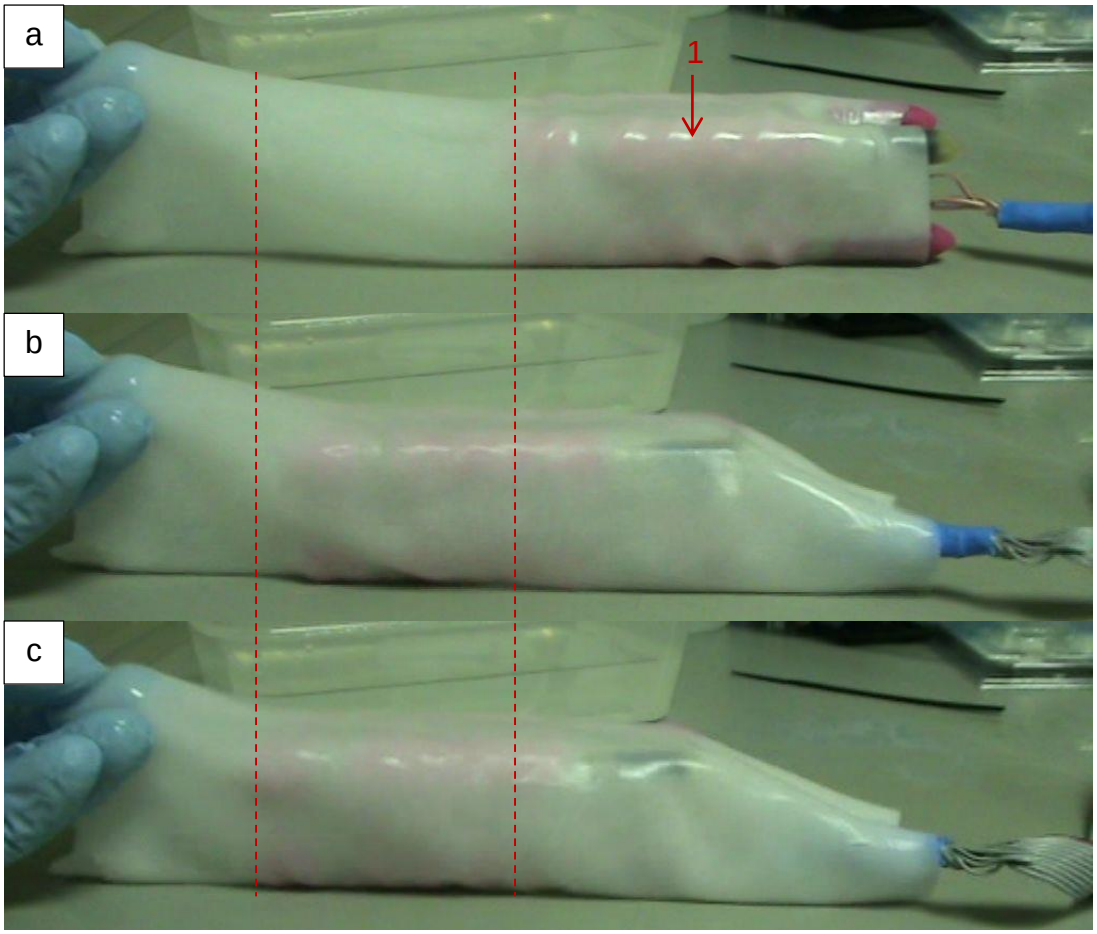

Figure 7.19 Frames taken from video showing the device in the hydrogel lumen on a desk with the far end held open. First frame shows initial setup at 0s; each sequential frame taken at 5s intervals showing the device's progress. Annotation 1 shows the four-screw device seen through the translucent lumen, dashed lines shown to aid visualisation of device progress.

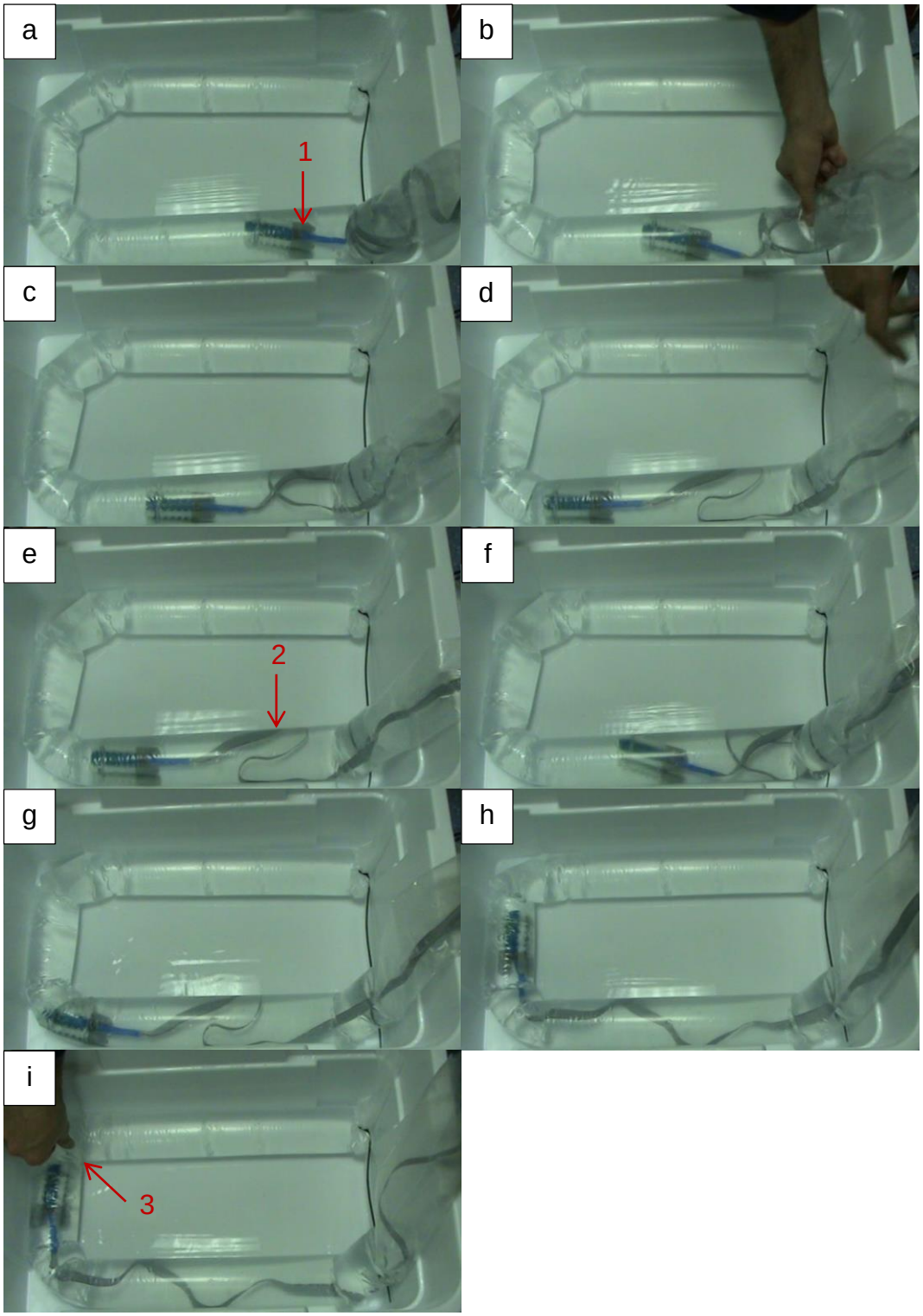

Figure 7.20 Frames taken from video showing the device in the flooded LDPE lumen. First frame shows initial setup at 0s; each sequential frame taken at 10s intervals showing the device's progress. Annotations show: 1) Four-screw device; 2) Tether "S" bend preventing progress; 3) flexure in lumen preventing further progress.

7.4.3 Ex-vivo Tissue Assessment

In the ex-vivo experimental setups 1 and 2 the device moved with ease in the environment, with the device beginning to move at 0.9v (18% power). At 1.25v (25% power) the device would move at considerable (50mm·s^{-1}) speed across the surface. Through using the HID the device could be steered across the surface however the turning circle was large. This posed difficultly in directing the device in the desired direction.

Experimental setup 1 was carried out to assess if the device was able to generate tractive forces using the screws alone against planar tissue in a non-flooded environment. The four-screw device was placed on a length of tissue and the screws in contact with the tissue actuated. The device traversed the tissue length, as seen in the frames of Figure 7.21, at a high rate of progression, taking 2 seconds to cover the length.

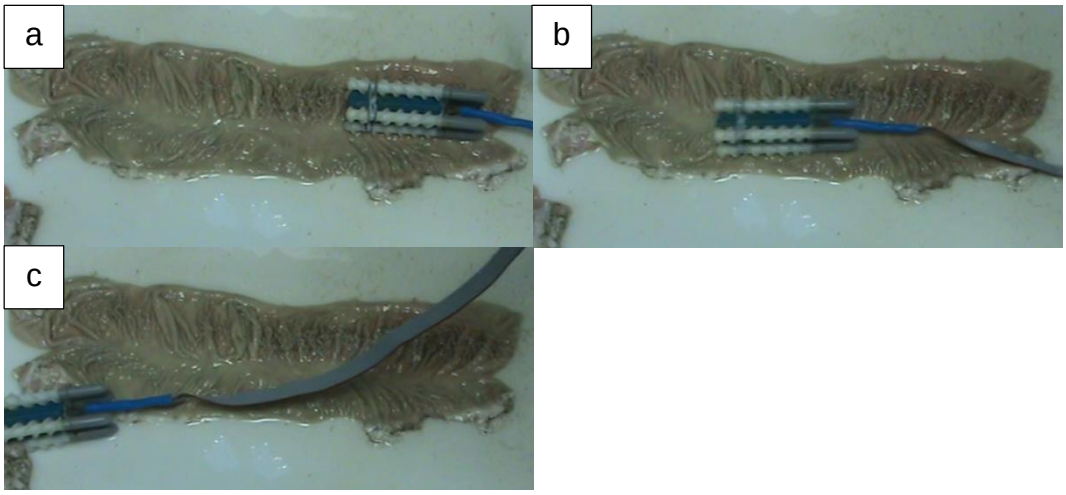

Figure 7.21 Frames taken from video showing the device against ex-vivo porcine tissue in a non-flooded environment. First frame shows initial setup at 0s; each sequential frame taken at 1s intervals showing the device's progress.

Experimental setup 2 involved testing the four-screw device in contact in a flooded condition. The device was able to traverse the length of tissue with considerable ease, although the rate of progression as determined thorough examination of the video frames is slower than in a non-flooded condition. Figure 7.22 shows still images taken from the video at 1s intervals showing the device traversing the tissue length. The tissue was held flat throughout to prevent it moving. The tether was left free and did not constrict movement of the device.

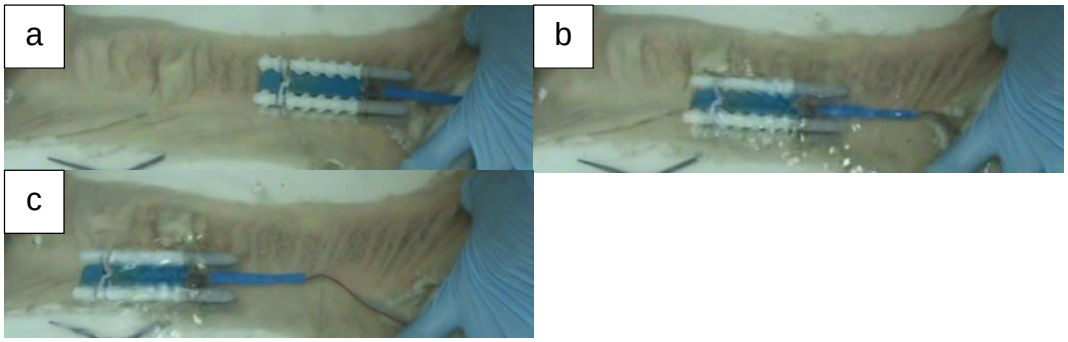

Figure 7.22 Frames taken from video showing the device against ex-vivo porcine tissue in a flooded environment. First frame shows initial setup at 0s; each sequential frame taken at 1s intervals showing the device's progress.

In the non-flooded colon lumen tests (ex-vivo experimental setups 3 and 4), the device was unable to progress along the lumen. Although the screws would spin, the traction generated was not enough to overcome the resistance to motion imposed by the lumen. Active control of the arms was not possible with the prototype, which may have affected the device's ability to move. This was caused by the torque required to actuate the arms breaking the adhesive bond used to join the gear and motor shaft. Similar to the phantom assessment, when a screw end became lodged against a haustration or fold in the lumen, the device is unable to progress further. The photographs of the lumens seen in Figure 7.23 show a high amount of haustrations, which protrude when the lumen is not insufflated. While active control of the device diameter was not available, this high degree of haustrations would likely pose a difficult challenge regardless. When the lumen was flooded, ex-vivo setup 5, the device was unable to progress any further than during the non-flooded experiments. The flooding did not open the lumen, nor did it minimise the obstructions caused by the haustrations. The three non-insufflated lumen experiments show that the device is not able to successfully operate in a non-inflated lumen. The inflation of the lumen is required to unblock the passageway and remove obstructions caused by haustrations.

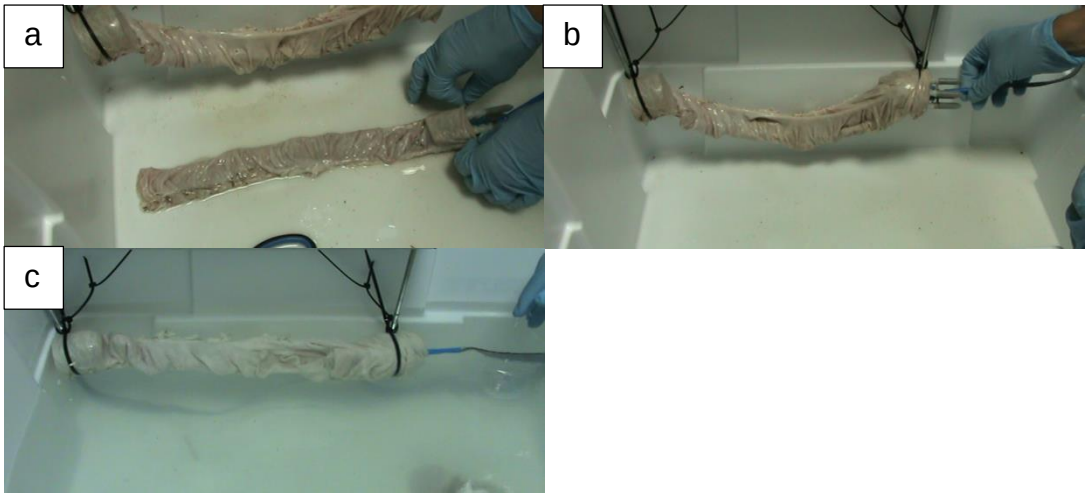

Figure 7.23 Still frames taken from video of the prototype testing. Showing a) unsupported non-flooded lumen; b) supported non-flooded lumen; c) supported flooded lumen.

Ex-vivo experimental setup 6 involved a fluid insufflated colon that provided a less challenging environment and closer to the hydro-colonoscopy application. With the haustrations inflated, the device was able to move to a small degree. In the straighter sections, the device was able to move along the colon; however, it would become stuck in the haustrations and unable to progress further. With external manipulation, it was able to progress to the first pseudo flexure.

Figure 7.24a shows a photograph of the device alongside the prepared colon ready for insertion. While the colon looks comparatively large compared to the device; the haustrations fold in almost the entire radius of the lumen creating a very narrow environment to operate in. Figure 7.24b shows a still frame taken from video shot of the testing with the device deployed in the colon. Due to the colon being opaque in nature, the progress of the device cannot be easily seen throughout the recorded video footage, and so still frames are not shown.

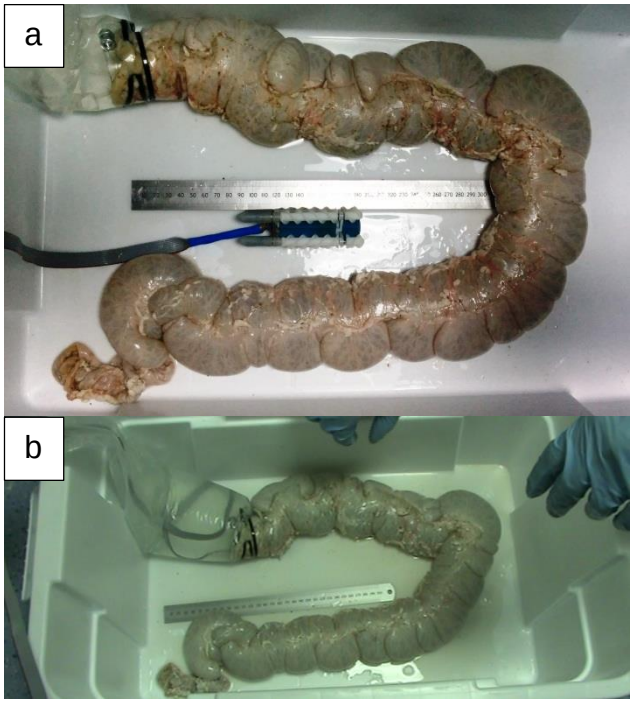

Figure 7.24 Photographs showing testing of the four-screw device in a fluid insufflated ex-vivo porcine colon. Showing a) photograph of the device alongside insufflated colon before deployment, 30cm rule is shown for scale; b) image taken from video during testing with the device inside the colon.

Figure 7.25 shows an annotated photograph of the insufflated lumen showing the extent of the haustrations. It can be seen that the space within the colon is very tortuous and difficult to navigate. The image also includes blue rectangles showing the approximate locations where the device became stuck and required external manual adjustments to progress along the lumen. At these locations, a vision system on the device would enable better control of the position and allow it to drive towards an opening. The locations are approximate based on physical examination of the lumen during the experiment; actual locations are unknown due to the opaque nature of the colon.

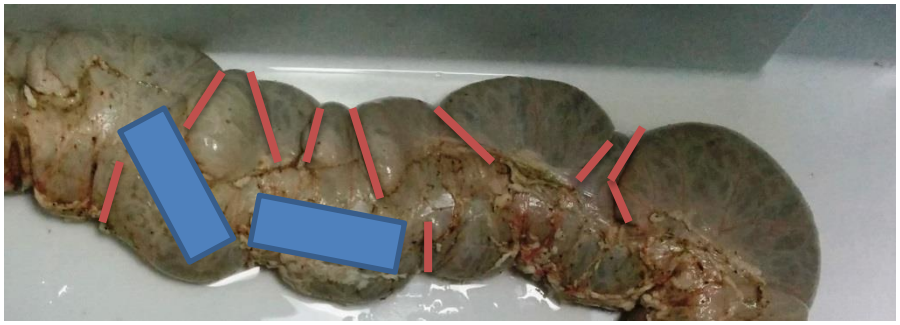

Figure 7.25 Image of an insufflated colon used during testing with red lines showing haustrations and blue rectangles showing approximate locations of the device where it became partially stuck. Image seen shows a cropped section of Figure 7.24a

7.5 Discussion

The aim of experimentally assessing the four-screw locomotion system as a scale prototype was to demonstrate the system's ability to traverse a lumen in realistic conditions. To assess the four-screw system in terms of the principle methods of locomotion and compare to previously carried out assessments, the assessment was carried out in three discrete sections, as detailed in the aims section of this chapter.

7.5.1 Thrust Generation In Fluid

The device, when tested in a fluid based environment was able to produce up to 2N of thrust with the arms in the open position and the motors at full voltage; and 1.5N with the arms in the closed position. In Chapter 5 it was predicted that the complete system would be able to produce up to 1N of thrust in a fluid situation, the thrust from a single screw (up to 0.3N, Chapter 5) would not multiply directly for a four-screw system due to increased losses in the fluid. From the results in this chapter, the four screws are able to produce greater than four times the thrust of a single screw.

The increase in thrust compared to the predicted thrust could simply be due to the screws rotating at a higher angular velocity. As the motors do not have any feedback to them, the exact velocity of each motor is not known. While the specifications for the motors state a maximum no-load velocity (discussed in Chapter 4), the loading due to the bearing resistance and resistance to motion from the fluid are unknowns and so the actual motor velocity is not predictable. Using the theoretical model in Chapter 5, the angular velocity required from each screw would be over 1000 $rad \cdot s^{-1}$, which exceeds the motor's output by a large factor. Thus, an increase in screw angular velocity is not the major contributing factor to the increased thrust.

A single screw, when rotated in fluid, imparts motion upon the fluid. This motion, is in line with the direction of motion of the screw, and so the fluid will rotate about the screw's axis of rotation in the direction the screw rotates. It was observed that after the single screw (Chapter 5) had been running for some time, the fluid would swirl about the tank in the same direction as the screw rotated. A counter rotating system imparts two contradictory motions on the fluid, which in a simplistic theoretical sense negate each other's effect; a more practical explanation is the flows mix in a turbulent way and yield no net direction on the overall fluid body. The prototype has two of these pairs. This causes a more chaotic or turbulent motion in which the fluid motion decays without any net motion, which may attribute to the increased thrust seen. A diagram illustrating these can be seen in Figure 7.26.

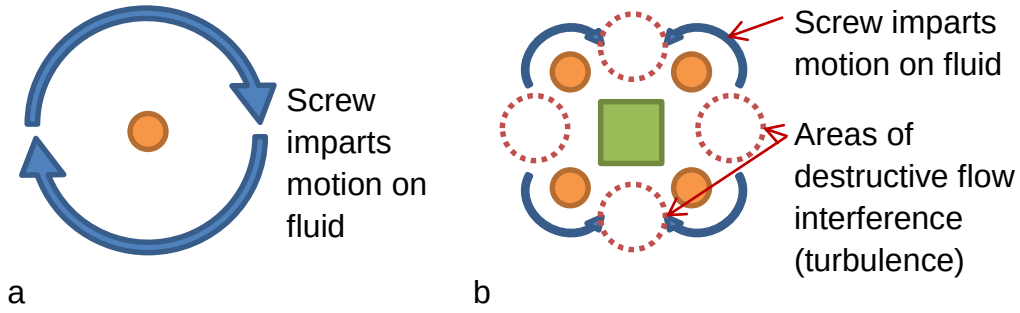

Figure 7.26 Illustrations showing fluid flow (blue arrow) about rotating screws (orange circles). Showing a) single screw when rotated causes a net flow in the fluid as indicated by the blue arrows encircling the screw. b): 4 counter rotating screws (orange circles) positioned about a chassis (green square) do not result in a net direction of fluid flow.

Turbulent flow consists of irregular fluctuations and is not arranged in smooth paths or layers such as laminar flow. While the flow close to the screws may follow a constant path, further away from the screws where these opposing flows meet will result in a turbulent interaction. Further modelling of the fluid flow would be necessary to gain a detailed understanding of this phenomena but is beyond the scope of this work. Observations of the fluid tank confirms the flow is not laminar during actuation of the four screws, there was a high degree of surface motion during actuation, which decayed within 10s of the screws halting. In a complex environment such as the colon where the walls are not regular or consistent, the flow may be turbulent about the device to a greater extent due to the interactions between the flow and the colonic walls. As previously discussed in Chapter 5, the thrust is a product of imparting motion upon the

fluid from the screws. If the fluid moves in unison with the screws then little motion will be imparted, and so little thrust produced, a turbulent flow however will allow greater thrust to be generated by the screws.

Similar to the results seen in Chapter 5, the system produces high thrust with the arms in an open state. This increase in thrust between the arm positions at higher motor velocities may be also a product of turbulent flow. The chassis of the device will block the propagation of fluid flow to a greater extent while the screws are closer. With the arms in the open position, the flows about the screws will have a larger area of interaction. It is speculated that this may explain the reason behind the trends seen.

7.5.2 Moving Through A Lumen

When the device was tested in terms of pure-contact locomotion in the hydrogel phantom lumen it was able to move providing the pathway was clear. In the unsupported lumen when the device stretched the lumen creating a localised recess, it became stuck and unable to progress further. Similarly in the hydrogel lumen when laid on the bench and held shut at the far end, the device was unable to push along the lumen once the diameter had restricted sufficiently enough not to fit the device without stretching the lumen. When the lumen was on the bench and held open, it was able to progress freely in both the forward and backward directions.

These traits were also observed in the ex-vivo experiments. When the ex-vivo colon was held open in an unsupported arrangement, similar to the hydrogel phantom lumen, the device was unable to progress due to the tip becoming stuck on a recess; however, for the ex-vivo lumen this was a natural haustration and not due to stretching the material. When the ex-vivo lumen was laid on a surface, the device was equally unable to progress. These cases are for a non-insufflated lumen, conditions that the device is unlikely to meet when deployed for hydro-colonoscopy. This highlights that the locomotion system is reliant upon the insufflation of the colon, something which conventional colonoscopes are reliant upon as well.

When the four-screw locomotion system was deployed in an insufflated lumen, in both hydrogel and tissue models, it was able to traverse providing the passageway was clear. In the transparent LDPE lumen, it was possible to steer past obstructions. When the device was deployed in the ex-vivo lumen, as biological tissue is opaque, navigation of the device was impractical without externally assessing the location of the device. With the

inclusion of video feed from the device, navigation would be easier; the final procedure would not be carried out without live video feed to aid navigation.

When in a fluid environment, the device is capable of producing thrust beyond the predicted minimum required. With the two discrete modes (arm locations open and closed) showing promise, the four-screw locomotion system has potential to traverse a colonic lumen. The major blocking issue over the current prototype traversing a colon is navigation; with no ability to see where the device is facing, steering is impractical. With the inclusion of visual feedback through a camera, traversing a colon is a strong possibility for the four-screw system.

7.6 Summary of Experimental Assessment of a Scale Prototype in Phantom and Ex-vivo Lumina

This chapter covered the experimental assessment of a four-screw device to build upon the testing carried out in previous chapters on the propulsion from a single screw in fluid (Chapter 5) and trust from a counter rotating pair in contact (Chapter 6). The assembled four-screw system was then tested in a fluid insufflated ex-vivo porcine colon to resemble the environment the device will be operated in.

7.6.1 Assessment Of The Device In Fluid Conditions

The assessment of the device in a pure fluid environment showed that the locomotion system is able to generate greater than predicted thrusts. The counter rotating screws were able to reduce the losses due to fluid motion when compared to a single screw. Experimentation on measuring the turning torques generated by driving a single pair show that the device is able to generate torque which should allow steering capabilities.

7.6.2 Assessment Of The Device In Contact Conditions

When assessed on a flat section of tissue the device was able to successfully traverse in both non-flooded and flooded conditions. The screw when in contact with the tissue was able to generate enough traction to propel the device along the sample length. The resistance from the fluid in the flooded environment did not visually hinder the progress of the device when relying solely upon tissue contact for locomotion.

During deployment in non-flooded phantom lumen, the device was able to progress providing the passageway was unobstructed; the screws were able to gain sufficient traction against the hydrogel surface to progress. When

deployed in a non-flooded ex-vivo porcine colon the device became stuck against haustrations and was not able to traverse.

In conclusion, the current device shows an ability to traverse using contact-based locomotion providing the pathway is clear. Similarly, the colonoscope suffers difficulty progressing through a colon with obstructions as noted in the literature (Chapter 2). This is not a failing of the device but down to the very tortuous environment.

7.6.3 Assessment Of The Device In Amphibious Conditions

When deployed in the fluid insufflated lumen, both phantom and ex-vivo porcine colon, the device was able to traverse through use of amphibious locomotion. The phantom lumen posed the lesser of the two challenges as the passageway was free from haustrations and there were no navigational complications. During the less tortuous sections of the ex-vivo porcine colon, the device was able to traverse, however due to navigational challenges it was not able to pass haustrations without external manipulation.

When operated in a fluid-filled non-collapsed lumen, the device was able to traverse at a greater rate than in a fluid-void non-collapsed lumen. It is predicted that this is due to the combined thrust from contact-based and fluid-based locomotion. The fluid medium plays a role in thrust production, which compliments the medical advantages from hydro-colonoscopy (as discussed in Chapter 2).

7.6.4 Assessment Of The Four-Screw Locomotion System

The system has been designed to reduce luminal wall contact throughout the procedure. As the system operates best in open sections of the colon and using a fluid based locomotion strategy, this aim can be met without degrading the propulsive system to avoid contact. When deployed the system will not use contact-based locomotion in isolation, the fluid surrounding the screws will play a role in thrust production. The experiments using insufflated lumen show the locomotion system is able to perform in hybrid conditions where thrust is generated through a mixture of contact and non-contact locomotion strategies. In conclusion, the four-screw system has demonstrated it meets the aims defined in Chapter 3.1 of producing an amphibious locomotion system.

Chapter 8
Discussions

This thesis has presented the development of a novel robot for colonic inspection during a hydro-colonoscopy procedure. Central to this is the development of an amphibious locomotion system for use in an intra-luminal environment where the lumen is a soft, wet and highly deformable biological tissue.

The previous chapters have presented the development and experimental testing of subsystems and the full robotic system in appropriate environments. For each testing phase, a situation-specific test rig has been required to be designed and built. This chapter considers the implications of this work as a whole and the contributions it brings to the field of medical robotics.

8.1 Feasibility of the Hydro-colonoscopy Robotic Concept

Understanding the process of colonic inspection, and the strengths and weaknesses of both traditional colonoscopy and hydro-colonoscopy, is crucial to the development of the robotic system. The feasibility of carrying out robotic hydro-colonoscopy is important upon the development of any robotic colonoscopy device. Technical and clinical restraints will have an impact on the feasibility for deploying a robotic system for hydro-colonoscopy. There are no current market available robotic hydro-colonoscopy devices, and development of such is still in the early stages.

For a robotic system or platform to operate within the colon and carry out a colonoscopy procedure, the device must be able to compensate for a wide range of environmental geometries and conditions. These include restricted or collapsed sections, tight flexures and colonic ailments requiring reduction of contact; for example, diverticula disease can pose a problem for a colonoscopist, as the passage through the colon can be very unclear.

The literature search on current “next generation” colonoscopy devices in Chapter 2 covered many different approaches and methods of providing locomotion. A summary of the devices covered can be seen in Table 8.1.

Table 8.1 Summary of “next generation” colonoscopy devices

Device	Locomotion method	Strengths	Weaknesses
PillCam, Given Imaging	Passive, peristaltic. Does not require insufflation.	Minimal to no trauma, can be easily swallowed	Unguided and un-steerable. Desired areas of the colon can receive limited or no imagery.
Magnetically guided colonoscope, Valdastri et al. (56)	External robotic manipulator drives soft-tethered colonoscope. Utilises gas insufflation.	External robotic arm does not have power and size limitations of internal devices	Requires large external manipulator
Crawling device, Quirini et al. (53)	Leg based crawling. Utilises gas insufflation	Opens lumen as it progresses	High risk of perforation from legs
4 propeller device, Tortora et al. (54)	Swimming, utilises fluid insufflation	Tether-less, self-contained and small	Limited battery life, can’t pass collapsed sections
2 module helical bodied device, Zhou et al. (75)	Counter rotating helically grooved body sections, utilises gas insufflation	Same diameter as existing colonoscopes	Unable to actively steer
Multi module, soft bodied device, Shikanai et al. (76)	Counter rotating helically grooved body sections, utilises gas insufflation	Able to expand to match colon diameter	Long body cannot pass tight bends or flexures

Table 8.1 cont…

Device	Locomotion method	Strengths	Weaknesses
Single screw, Kim and Kim (77)	Single rotating helically grooved body section, utilises gas insufflation	Simple drive mechanism	Reduced propulsive output, unable to steer, has a tendency to twist lumen
Bellow device, Phee et al. (80)	Inchworm, utilises gas insufflation	Uses pressure to adhere to surface, no gripping trauma	Colon stretches with device step netting zero movement
Passive inchworm, Kim and Kim (77)	Barbed inchworm, utilises gas insufflation	Passive gripping of mucosa through soft barbs.	Colon stretches with device netting zero movement. Unable to reverse

Robotically assisted colonoscopy has been attempted by several researchers though the development of robotic platforms, as detailed in Table 8.1. These include systems which are both externally actuated and self-actuated, with all of the device reviewed using a single mode of locomotion. The addition of a fluid body to robotic colonoscopy has been proposed and assessed by other researchers, notable Tortora et al. (54). Using the strengths of other systems as a basis for the development and understanding the weaknesses of other systems, the four-screw system developed through this thesis utilises both fluid-based and contact-based locomotion strategies.

It has been shown that a fluid fills the entire colon, allowing for an amphibious device to traverse the entire length. This reiterates the research of others (7, 24-26) that a fluid filled colon is opened to a greater extent without distortion of length compared to a gas-filled colon.

Through the work of other researchers and the experimentation carried out through Chapter 7 it can be seen that robotic hydro-colonoscopy is feasible, with several researchers developing such systems. A variety of locomotion systems have been used to varying degrees of success with work within this thesis expending upon these in producing an amphibious locomotion system.

8.2 Contributions Throughout the Research

The research undertaken throughout this thesis has led to several contributions to the wider research community. These are discussed through this chapter as follows:

- Variable geometry locomotion system
- Amphibious locomotion using Archimedes' screws
- Development of a theoretical model and experimental analysis of screws in fluid-based locomotion
- Development of a theoretical model and experimental analysis of screws in contact-based locomotion against colonic tissue
- Tissue trauma from screw interaction
- Development of testing environments for experimental assessment of the amphibious locomotion system

8.2.1 Variable Geometry Locomotion System

The developed locomotion system features the ability to adapt the device's diameter by positioning the screws around the chassis. This allows a small minimum diameter for passing the more constricted sections of the colon. In using an overlapping arm technique, the system is able to achieve a large range of diameters (40 to 60mm) as seen in Figure 8.1 and discussed in Chapters 3 and 4. Across the field of intra-luminal locomotion and related areas of robotic locomotion, there is no known device that is able of providing a similar range of diameter adaption. The only device which is known to offer a variable geometry is that developed by Shikanai et al. (76), which has the ability to inflate independent screw sections to change the diameter (Figure 8.2). The authors however do not note the expansion range, other than the diameter of the system is 30mm.

When a shaped balloon is inflated, such as on the device developed by Shikanai et al. (76), the features tend to become less distinct with increased inflation. The thread depth of a screw is important for generation of the thrust, both in contact and in fluid. Inflating a screw poses many problems in

designing the screw; the thread depth needs to be preserved throughout the inflation. Threads with a thicker cross section to the screw body membrane will require a greater force to stretch and thus inflate less; this will result in the thread depth effectively being reduced. The inflation of such screws will also require on-board pressure generation or a larger tether to deliver the pressure required. The approach utilised by the device in this thesis does not have these side effects while still exploiting the advantages of a variable geometry.

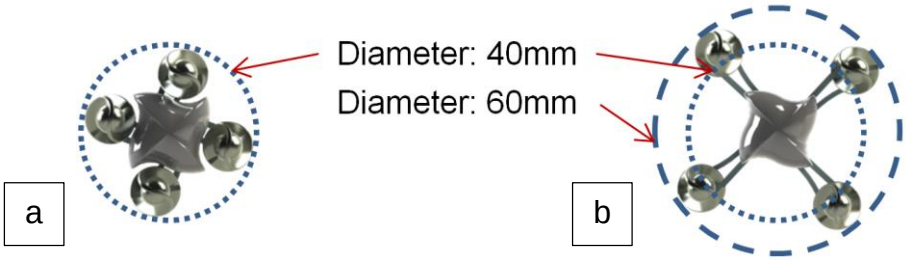

Figure 8.1 Diagram showing the variable geometry range of the developed four-screw device

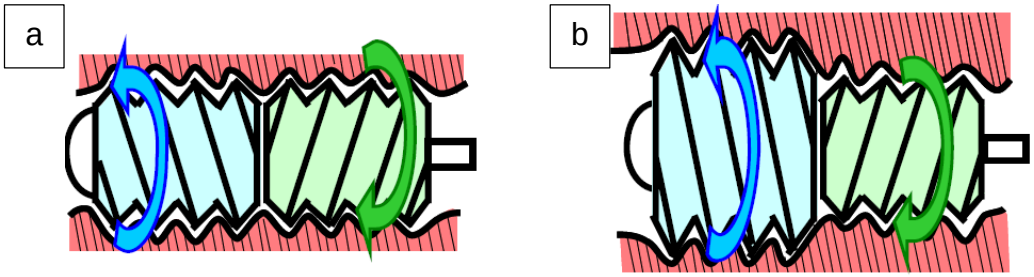

Figure 8.2 Diagram showing the variable geometry of the device developed by Shikanai et al. (76)

Using the variable geometry of the developed system, where the colon diameter permits, the device may move the arms to apply a bias towards a fluid or contact based locomotion strategy. Contact pressure between the screws and colon can alter the thrust capabilities and so for improved contact-based locomotion the contact pressure should be controlled. It can therefore be seen that through using variable geometry both the fluid and contact based locomotion modes can be optimised by adapting the position of the screws.

This key novelty does not feature on any known intra-luminal device and poses great potential in not only increasing thrust output but increasing the viability and success of robotics in intra-luminal applications.

8.2.2 Amphibious Locomotion using Archimedes' Screws

The use of a fully amphibious locomotion system and single drivetrain simplifies the mechanical complexity of the developed system. This decreases the overall size of the system allowing it to be readily produced at a functional scale.

To fully assess the amphibious performance of a system, it is important to understand the conditions in which it will operate. The modes of contact that an amphibious screw based systems will experience can be classified into the following states:

1. Hard contact: non-deformable or displaceable surface
2. Soft contact – deformable surface: e.g. tissue
3. Soft contact – displaceable surface: e.g. sand
4. No contact: pure fluid based locomotion

The condition states that the developed device will encounter are 2 and 4 as outlined above.

On deformable surfaces which do not displace (contact condition 2), for example biological tissue, screws are able to traverse as shown in detail in Chapters 6 and 7. The developed four-screw device was able to move across tissue samples in both dry and flooded states (Figure 8.3). When deployed in a lumen, the device was able to traverse a section of phantom tissue however, it would become stuck on the haustrations in an ex-vivo porcine colon sample (Figure 8.4).

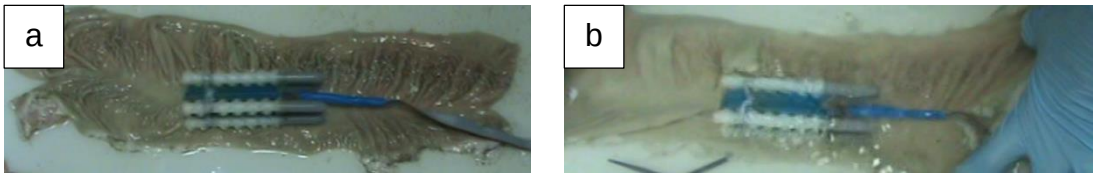

Figure 8.3 Four-screw device in contact with ex-vivo porcine colon in dry (a) and flooded (b) conditions

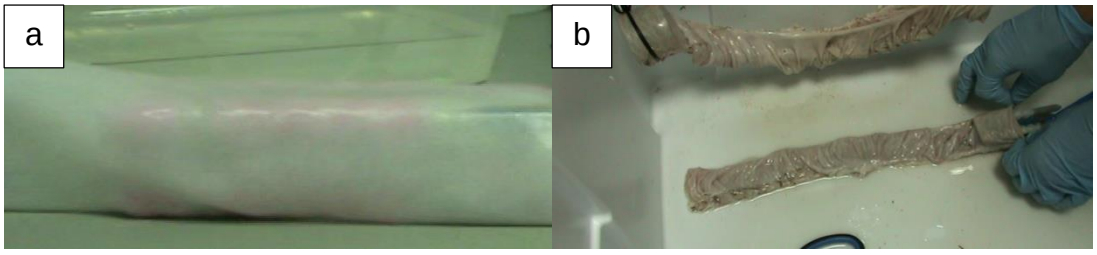

Figure 8.4 Experimental testing of the four-screw device in lumens. Photographed in a phantom lumen (left) and ex-vivo porcine colon (right). The phantom lumen shown is opaque in nature, which obscures the view however, the pink screws are visible through the lumen.

In the research by Shikanai et al. (76) the developed multi-module device was deployed in an ex-vivo and in-vitro porcine colon to test the locomotion system (Figure 8.5). As previously mentioned it was unable to pass tight flexures however, it was able to traverse straight sections of the colon. Both cases feature a non-fluid filled colon resembling contact condition 2.

Figure 8.5 Ex-vivo (left) and in-vitro (right) testing of the device developed by Shikanai et al. (76)

Where no contact is available or desired, the developed four-screw system can generate thrust using the screws in a fluid filled environment (contact condition 4). Chapters 5 and 7 experimentally assessed and discussed the developed system's ability to traverse a fluid filled lumen. Figure 8.6 shows the developed four-screw device swimming along a phantom lumen, which formed part of the prototype testing carried out in Chapter 7.

Figure 8.6 The developed four-screw device swimming in a fluid filled phantom lumen

As shown, screws can operate in all four of these situations (to limited success in some cases), whereas a wheeled or tracked vehicle cannot. A wheeled vehicle is susceptible to becoming stuck in displaceable terrain, example contact condition 3. Wheeled and tracked vehicles are unable to operate in open fluid (contact condition 4). Propeller driven vehicles are only able to operate in open fluid.

Testing of screws in this thesis was carried out on a soft, non-displaceable surface (colonic tissue) and in open fluid, which compliments the research by Shikanai et al. (76) and Nagaoka et al. (46) on the ability of a screw to generate thrust in a wide range of environmental conditions.

The arrangement of four screws in counter rotating pairs allows the system to be non-dependant on orientation to provide contact or surface based locomotion (Figure 8.7). With no preference in orientation, complications in control are minimised. The clinician does not need to compensate for the device rolling longitudinally, such as providing different inputs. The control system does not need to adjust screw rotation either; rolling onto a side will not result in the device moving or turning erratically.

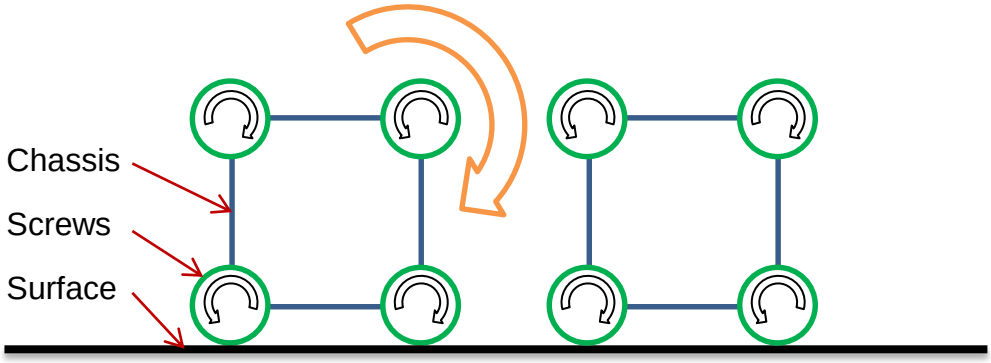

Figure 8.7 Non-preferential orientation of the developed four-screw device. As the device is rotated along its length (orange arrow), two counter rotating screws remain in contact with the surface.

Non-preferential orientation is a common theme within intra-luminal robotic devices. Many adopt a cylinder with rounded ends as a general shape, which allows ease of transition along the colon while not requiring a designated top (Figure 8.8). The system developed in this thesis includes a major advantage over those covered, it does not depend on a single medium for locomotion.

The reviewed locomotion methods that operate within a fluid filled colon rely solely upon the fluid medium. Differences in anatomy, or even natural processes such as flatulence may create air pockets in some patients. It is these air pockets, or fluid-void sections, which will prevent progression of the swimming based devices. The amphibious locomotion of the system designed within this is thesis is a novel design; it is able to overcome obstacles that hinder the progress of the other systems reviewed.

The reviewed contact based devices do not make use of the increased insufflation of using fluid over gas to open the colon, which may hinder progress due to the flexures remaining partially collapsed. The force required to traverse a collapsed section has been noted by several researchers as a major hurdle for medical devices and prevents further progress along the lumen.

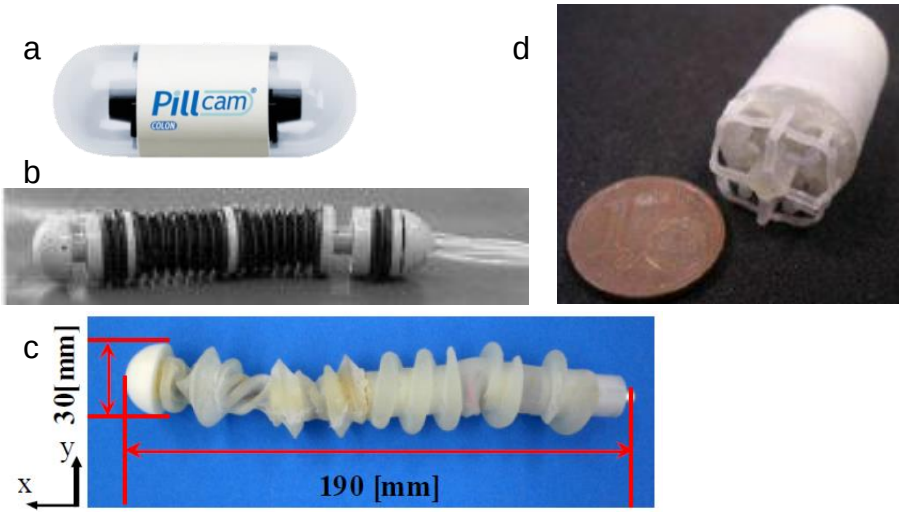

Figure 8.8 Colonoscopy robots without orientation bias. Devices shown a) PillCam, Given Imaging; b) Bellow inchworm device, Phee et al. (80); c) Concentric counter rotating section device, Shikanai et al. (76); d) Propeller based active capsule, Tortora et al. (54)

Through experimental testing of the developed system, it has been seen that the system performs best in fluid based situations. While it is able to traverse using contact-based locomotion, this is a slow rate of progress and will pose greater navigational challenges than swimming. Therefore, to allow for lower procedure times and reduced colon wall contact the swimming mode should be used where possible, with the contact mode being reserved for collapsed sections or those with fluid voids.

8.2.3 Development of a Theoretical Model and Experimental Analysis of Screws in Fluid-Based Locomotion

It was discussed in Chapter 5 that the thrust generated from a screw when rotated is explained by boundary layer theory. Extruder pumps and other industrial uses of screws operate the screw within an enclosed volume with often viscous fluids; their methods of moving the media along the shaft are substantially different to the application on the four-screw device. The research undertaken for this thesis explores new uses of screws that have not been fully realised.

The theoretical model built for a single screw in an open fluid (Chapter 5) predicted twice the thrust of the physical set up. The model assumes a linear gradient of fluid velocity from the base of the channel to the top, and does not consider the sides for simplicity; which will account for some of the differences in thrust produced. The model also assumes the surrounding fluid is completely stationary throughout operation, giving the largest change in fluid velocity. As observed, the screw imparts motion on the fluid not only

in the axial direction but also in the direction of rotation. This will reduce the velocity change in the fluid and consequently reduce the thrust. The exit velocity is relative to the environment, which may be a cause in the difference between theoretical and experimental thrusts.

The thrust from a multi-screw system was stipulated to be up to *N* times that of a single screw system (where *N* is the number of screws), such that a four-screw system would produce up to four times the thrust of a single screw. However, in Chapter 7 this was seen to not be the case. The four-screw device was able to produce approximately 8 times the thrust of a single screw. With this knowledge, the reasons why the single-screw model and single-screw experimental results do not match can be re-assessed. With a four-screw system comprising of two counter-rotating pairs, the net rotational motion imparted on the fluid should be zero. The conflicting rotational flows of fluid should destructively interfere causing a turbulent but relatively stationary body of fluid. Noting this, it would appear that the reason why the single screw experimental results were less than expected is because the step change between the fluid body and screw was not as expected: the movement in the body of fluid was decreasing the efficiency of the screw.

Screw propulsion has been shown as not only possible but also practical through the application of the scale four-screw device. Experimentally assessing the device in a fluid filled lumen showed it was capable of traversing using fluid-based thrust in combination with contact-based thrust.

8.2.4 Development of a Theoretical Model and Experimental Analysis of Screws in Contact-Based Locomotion

In the field of intra-luminal robotics there is a trade-off between the ability to generate thrust and reduction in trauma. The interaction between screws and a soft non-displaceable surface is not widely understood or researched. Research on intra-luminal devices, which utilise screw-based locomotion, have not included analysis on this interaction, with simplistic models assuming perfect traction being used. The research undertaken for this thesis improves upon this understanding and allows for greater advances to be made on screw-based locomotion systems in intra-luminal applications.

The pitch of the screws was selected as a compromise between fluid and contact based locomotion. In fluid testing 40mm and 20mm pitch screws were used, however in contact conditions the 40mm pitch screws were unable to rotate and did not generate measurable thrust. The 20mm pitch

screws were selected as they had a blade angle in the optimal range of 40° and 45° (88), and formed an integer number of rotations about the shaft. Smaller pitches are capable of generating greater torque, however from the calculations in Chapter 5 it can be seen that they will produce less thrust in fluid situations. Further optimisation into the blade angle/pitch may be carried out as future work to allow the system the largest thrust generation between contact and fluid states.

The interaction between a rotating screw and tissue can be divided into two components: sliding and rotating (Figure 8.9). These two contact states while easier to model in separation are dependent on each other and thus need to be analysed simultaneously. These require validation of the fiction coefficients in the parallel and normal direction to the thread (see chapter 6.1.1). As experimental testing helps validate a theoretical model, full testing of the system was carried out to ascertain the key factors. The data gathered from this allowed exploration into the contact dynamics between tissue and screws. Further work on a mathematical model was not undertaken, as the aim of this thesis is to produce a locomotion system, not model the contact dynamics of screws on tissue, although the findings are an interesting outcome.

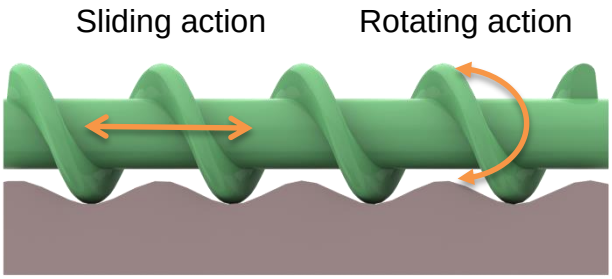

Interaction between a screw and tissue is formed by two discreet actions; both are required for normal operation.

Figure 8.9 Screw-tissue interaction actions. Orange arrows show movement of screw (green) against tissue.

Tissue has a non-linear response to loading and so assumptions cannot be made on a constant response. Understanding of the interactions between screws and tissue, and tissue response changes with time, leads to the understanding that repetitive actions applied to a section of tissue will cause a different response and increase in trauma.

As seen in the experimental data, when a torque is applied to a screw that is in contact with tissue, even without any rotation there is thrust generated by the system. A screw, when in contact with tissue can act in one of three states:

- Slip
- Stick
- stick-slip

The three states have been shown through experimental testing to be capable of thrust production.

The experimental data shows that the contact dynamics do not have a notable influence on thrust generation within the setup parameters used during testing. They are an output of the system and a result of different tissue samples behaving in different ways. The inputs to the system are normal loading and demand velocity. The demand velocity does not have a noticeable effect on the thrust, or discrete groups would be visible in terms of thrust produced. Normal loading on the other hand does appear to have a significant effect on the thrust production.

While motor demand, normal loading and tissue properties affect the interaction case and thrust, the interaction case can be useful in optimising thrust output. Measurements of thrust on the device when deployed may be difficult to calculate, however the screw-tissue interaction states are easier to infer.

There is no evidence found in the literature of exploration these contact dynamics, with other researchers who have used screws against tissue using simpler models for thrust generation. Shikanai et al. (76) calculated the horizontal component of thrust from a screw rotation to derive the thrust generated by a screw in contact and does not consider the contact dynamics between the screws and tissue.

While the device by Shikanai et al. (76) does have the ability to change the normal loading on the luminal walls, the authors do not consider the effects this has on the thrust produced by the system. The results discussed in Chapter 6 show that increasing the normal loading can improve the ability to produce thrust from screws to an extent, greater loading past this point reduces the thrust capabilities.

The research undertaken throughout this thesis has explored the contact dynamics between a rotating screw and tissue with the aim to better understand how thrust is generated and which input factors cause desirable changes on thrust. While changing the pitch of a screw has an obvious effect, normal loading of the system does not have a proportional correlation to thrust generation. Future work exploring this characteristic in more detail

will allow the variable geometry of the system to be exploited to increase the thrust production of a screw based locomotion system.

8.2.5 Tissue Trauma from Screw Interaction

During experimental testing of the device, the samples were visually assessed for signs of trauma compared to control samples. The experimentation with rigid screws revealed sections of obvious wear to the tissue, while the compliant screws did not. The trauma caused by the rigid screws was a result of the screw blades wearing against the tissue. From this observation, the slip case of screw-tissue interaction is estimated to be the largest source of tissue damage. Screw-tissue interaction should be actively managed as part of any control system to limit the screws from slipping.

Trauma from screw-tissue interaction will occur from repetitive actions. These will occur the greatest when the device is not moving relative to the tissue and the screws are rotating, such as the slip case. Trauma is likely to also occur through compression of the tissue by the expanding mechanism, the screws have a larger contact area compared to a wheel that spreads out the loading applied to the tissue when expanding; this will reduce the possible trauma. However, a limit on the maximum expansion force is needed.

Subjective analysis on tissue may be carried out using histological techniques to further quantify tissue damage. Histology focuses on looking at damage to cell structure as an indication of trauma. This approach may provide a more accurate indication of the cellular damage caused through screw-tissue interaction, however won't provide data on inflammation based responses which screw-tissue interaction may cause in living tissue. Further testing on screw-interaction coupled with histological analysis on the samples will provide a greater understanding of the damage sustained. The mechanisms for damage may be linked the fluid being removed from local sections of tissue though the movement of screw threads against the tissue surface. Histology will reveal if micro-tears are caused in tissue as a result of the screw-tissue interaction, these micro-tears will cause tenderness and inflammation to the tissue post-procedure, increasing the recovery times.

8.2.6 Development Of Testing Environments for Experimental Assessment of the Amphibious Locomotion System

Due to the new and relatively unexplored territory of a screw rotating against tissue there were no available rigs appropriate for conducting this research. This required the development of custom testing rigs and control software.

The use of phantom tissue was explored throughout the research to provide a non-bio-hazardous and repeatable medium for testing upon. Tissue, being a biological material, is naturally non-standard and each sample will vary. Using phantom tissue would reduce the spread in results for repeats allowing trends to be explored. However, the use of screws on tissue is dependent on several mechanical aspects of the tissue-screw interface, all of which cannot be modelled by phantom tissue.

While there are simulators for colonoscopy on the market, such as those offered by Buyamag (Figure 8.10), these are not often very realistic in terms of mechanical properties: they favour realistic geometry over material properties. The simulators include PVC based lumens with varying internal structures, which resemble haustrations, but unfortunately have different mechanical properties and surface properties to biological material. These simulators while useful for training the use of a colonoscope, do not model tissue accurately enough to acquire data on the performance of a system. The experimental testing of the device is dependent on the surface interaction and the mechanical properties of the tissue for thrust generation and trauma limitation; for these main reasons biological tissue was used over these simulators.

Tissue trauma is difficult to quantify. While there are underlying indicators for trauma, such as pain and inflammation, it can be very subjective. These identifiers are unavailable in phantom tissue and ex-vivo tissue; limiting the quantification of trauma to mechanical damage. For this damage to be observed, the medium used must wear in a similar fashion and rate to mucosa and colonic tissue in general. While ex-vivo tissue will not have the same inflammatory response, it will wear to the same degree as live tissue, allowing the identification of abrasive and other mechanical wear damage.

Figure 8.10 Market available colonoscopy trainer, abdomen unit shown left and views inside phantom colon shown right featuring haustrations. Anatomical model available from Buyamag Inc.

Two custom designed and built testing rigs were used through the experimental testing of the fluid and contact states in isolation. The contact specific rig, Traction and Contact Testing rig (Chapter 6), was developed specifically to allow the experimental testing of screws against biological tissue. Testing of the functional prototype was carried out using biological tissue as this resembles the final environment in terms of contact dynamics much greater than colonoscopy training aids.

8.3 Development of the Four-Screw Prototype System

The system as developed through this thesis has been designed for prototype. This uses high-cost production techniques such as “3D” printing which would not be used in a system that has been designed for manufacture. Where possible off-the-shelf components have been used, however the requirement for one-off bespoke components cannot be removed due to the nature of the application.

The current scaled design has a number of pragmatic design choices that could be optimised in future prototypes. The design choices were made in order to allow a proof of concept system to be produced and tested.

8.3.1 Prototype Scale

The system was produced at a scale of 2:1 due to the availability of components, giving it a diameter of 40 to 60mm. A traditional colonoscope has a diameter of 13-15mm, which allows it to stretch the colon to a lesser

extent. A robotic approach would need to have a similar diameter such that it was able to compete with the traditional colonoscope. At a scale of 1:1, the device would have a diameter of 20-30mm. The minimum outer diameter of 20mm includes the compliant screw blades, which when compressed will reduce the diameter, closing the gap between the diameter of a colonoscope and the device.

The actuators in a system are the dominating factor on the overall size of the vehicle or device (Chapter 3). For a miniature robot, the actuators make up a large majority of the device volume, while allowing for transmission of power plays a large role in the arrangement of the locomotion effectors and the actuators. At small scales, using direct drives simplifies the design by removing the need for bulky and efficiency reducing transmission systems. Motors of less than 6mm diameter are not widely available. A decision was made to use available components for production of a prototype rather than research into fabrication of small scale components such as motors. Through further work, it is practically and technically feasible to produce the design at a scale of 1:1.

8.3.2 Fabrication of the Prototype

Some components required could not be purchased in a pre-assembled state and were required to be fabricated. The use of “3D printing” allowed greater flexibility in the design of the fabricated components. Large scale production methods such as injection moulding can produce parts with a high degree of accuracy that rival the latest 3D printing technology in a vast range of materials. 3D printing however has the advantage of being able to rapidly adapt to new designs, and allows for quick successive iterations of a design to be produced and tested, without design and production of moulds and dies.

When selecting a fabrication method, the materials used also played a role. Materials must be non-water soluble and biocompatible. For any system that is to be deployed in a water-filled or water-based environment, the materials must be able to survive exposure. While the plastics used within ALM machines are not water soluble, they are often porous due to the layering process. The porous material will allow eventual fluid ingress resulting in possible short circuiting of electronic components, but will certainly be a source of contamination. The environment the device operates in is a biohazard by nature and so it is preferable that the inner components stay free from contamination, from this stand point non-porous materials are preferable.

8.3.3 Control Considerations

The current system does not have feedback from the screw or arm expansion motors. Without feedback, the current method of control is through an open-loop system: these require greater skill to operate, with an increased risk of trauma and the device becoming stuck. A closed-loop control system requires motor feedback, which could be achieved through addition of motor velocity sensors and arm position sensors.

Motor velocity sensors could be added through market available encoders, or through embedding magnets and Hall Effect sensors into the screws. In measuring the current draw from the motor, along with the feedback from the Hall Effect sensor, basic statistics from the screws could be ascertained.

Using ALM techniques, load sensing could be built into the arms of the device allowing the loading on each arm to be calculated. Research carried out by Pang et al. (104) on flexible load cells which are able of measuring a variety of loading conditions (pressure, sheer, torque) may be utilised in the construction of the device components. The components could be produced with veins or channels for insertion of soft load cells with the build being resumed after their application; producing components with embedded load sensing capabilities. This would allow the control system to function in several states. It is envisioned that the following three states would be employed by a control system.

To produce a device for initial testing feedback was overlooked for feasibility of construction and manufacture. These trade-offs meant that a closed-loop control system could not be used on the current generation although this does not man future generations will be without feedback allowing closed-loop control.

Chapter 9
Summary, Conclusions and Future Work

The aim of this thesis was to produce an amphibious locomotion system appropriate for traversing the human colon. To achieve this aim, a number of research objectives were set.

- Design a locomotion system that:
  - Is able to generate propulsive force in fluid and air filled sections or combinations of such
  - Minimises trauma to colonic tissue
  - Can accommodate the varying geometry of the colon
- Evaluate the locomotion system in:
  - Fluid locomotion state (fluid filled colon sections)
  - Contact locomotion state (air filled colon sections)
- Construct and evaluate a scale prototype of the full system using ex-vivo porcine colon

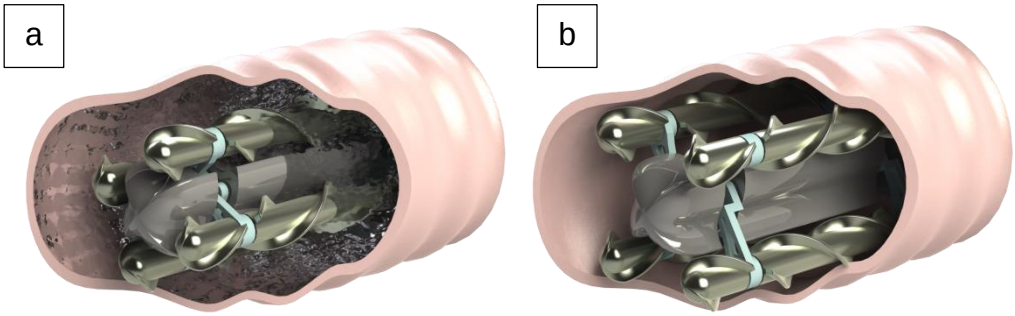

Figure 9.1 Computer model of the four-screw device, a) closed state in a fluid filled lumen; b) open state in a fluid-void colon

9.1 Locomotion System Design

The locomotion system developed in this work features four screws arranged equally spaced about a central chassis in two counter rotating pairs (Figure 9.1), as detailed in Chapters 3 and 4.

Through experimentation carried out in Chapter 6, it was shown that the normal loading between the screw and tissue plays a role in the generation of propulsive thrust. There is a critical contact loading force at which the peak thrust is produced with diminishing thrust for loading conditions either side of this. The variable geometry system allows for the normal loading of the screws against the tissue to be adjusted to operate within this critical loading condition.

It is estimated that trauma is most likely to occur when the screw threads slip longitudinally against the mucosa (Chapter 6). In controlling the normal loading applied to the screws and the screw angular velocity, the trauma caused by the threads slipping longitudinally can be actively limited. The use of compliant materials for the screw threads provides a passive trauma limiting system, with the screw blades buckling to minimise potential tissue damage. While trauma may still occur from excessive slippage such as an uncontrolled movement of the device, the combination of passive and active trauma minimising systems gives the designed locomotion system a possible means to reduce trauma when compared to traditional colonoscopy methods.

In using a common actuation effector for both fluid-based and contact-based locomotion, the system can operate in hybrid situations without mechanically switching between modes. This allows for increased dexterity and control in the high deformable and variable environment which is the colonic lumen.

9.2 Experimental Assessment of the Locomotion System

Custom testing apparatus was designed to assess the locomotion system in discrete modes of operation. The use of such apparatus allowed an incremental design process to be adopted allowing results from testing to feed directly into the development of each iteration of the locomotion system.

In this thesis, the mechanics for thrust generation from a rotating screw in fluid has been discussed with the development of a theoretical model (Chapter 5). This model was complimented through experimental testing of a screw and analysed for its relevancy, Chapter 5, and shown to produce meaningful thrust.

This thesis has covered research into the contact dynamics between rotating screws and biological tissue (Chapter 6), classifying the contact into three conditions: stick, slip and stick-slip. Thrust generated by a screw in contact with tissue is not a function of angular velocity as initially assumed, but a function of the normal loading (contact pressure). The screw blade material compliance has a weak proportional correlation against thrust, with an increase in Shore value resulting in an increased thrust. Future work will involve fine-tuning of the optimal normal loading for thrust generation and material compliance for maximum thrust and minimum trauma.

9.3 Experimental Assessment of a Functional Scale Prototype

A functional scale four-screw prototype was built and experimentally tested in both phantom lumen and ex-vivo porcine colon environments. The four-screw device demonstrated an ability to traverse through a fluid filled phantom lumen when the passageway was clear of blockages; the device was however unable to traverse a lumen where it was required to stretch or open the lumen. On straight, blockage-free sections of the lumen (phantom or biological), the device was able to generate sufficient thrust to traverse in an amphibious state.

When experimentally assessed in a collapsed ex-vivo porcine colon the four-screw prototype system was unable to neither open the lumen nor traverse along the length. The haustrations caused a significant obstruction, which prevented progress. In a fluid-insufflated ex-vivo porcine colon the device was able to traverse providing the lumen was unblocked. As the current prototype does not include a vision system and it is not possible to see through colonic tissue, navigation of the device was extremely challenging. Should the navigation issues be overlooked the device demonstrated an ability to traverse using amphibious locomotion in a fluid-insufflated lumen. Future work will see the inclusion of vision systems for navigation and inspection.

Experimental testing of the system in an amphibious state (Chapter 7) demonstrated the designed locomotion system's ability to produce propulsive thrust in an environment resembling the final application. Although testing in a collapsed lumen resulted in unsuccessful attempts to traverse in both fluid-filled and fluid-void lumen, reconstructions of fluid-filled colons from clinical trials carried out by the CoDIR team have shown that the colon does not contain collapsed sections when fluid-insufflated. This reduces the reliance on the ability to traverse a collapsed lumen. While the trials show complete distension, this cannot always be assumed and such improvements to the amphibious locomotion system will be carried out as part of future work.

9.4 Contributions of the Research

The researched carried out for this thesis has seen the development of a novel amphibious locomotion system, utilising Archimedes' screws and a variable geometry chassis.

The key contributions towards research in medical robotics and the wider field of exploratory robotic devices are as follows:

- Variable geometry locomotion system (Chapters 3 and 4)
- Amphibious locomotion using Archimedes' screws (Chapters 5-7)
- Development of a theoretical model and experimental analysis of screws in fluid-based locomotion (Chapter 5)
- Development of a theoretical model and experimental analysis of screws in contact-based locomotion against colonic tissue (Chapter 6)
- Tissue trauma from screw interaction (Chapter 6)
- Development of testing environments for experimental assessment of the amphibious locomotion system (Chapters 5-7)

9.5 Future work

Through experimental assessments carried out as part of this thesis a number of areas have been identified for further work, this section covers these in greater detail.

The selection of locomotion strategy bias will likely be a function of a higher-level control system, with possible selection from the clinician. Clinicians with a great deal of experience in performing similar procedures should be used to enhance the system, allowing such experience to aid the traversing of the colon. While the control system can make choices based on environmental data and pre-programmed decision-matrices, this should not prevent the clinician making overriding choices on the locomotion bias.

- Miniaturisation

The current scale prototype was designed based upon commercially available components. Further development on the design and inclusion of newer technology will allow the overall size of the device to be reduced.

- Screw Control

Each of the screws operate in contact with tissue, in fluid or a combination of both. The operational environment of one screw might not match that of the other screws on the device; and so the control of the screws must be independent for each screw. The use of velocity sensors and current sensing from the motors will allow the control system to determine programmatically if a screw is acting against tissue, in fluid or spinning freely in air, allowing the development of a more robust control system.

Further research into the contact dynamics between screws and tissue, and the actions that cause trauma will allow a control system to actively minimise trauma.

- Arm Control

The results from Chapter 6 show that contact force applied between the screws and the tissue affects the thrust output. The variable geometry of the system allows the contact force applied by the device to the colon to be controlled. This can be used advantageously to increase the thrust generated by the locomotion system.

As detailed in Chapter 3, the arm expansion is controlled via a single internal motor and gearbox allowing all arms to move synchronously. By exploiting new capabilities of rapid prototyping techniques, load-sensing capabilities can be built into the arms allowing the forces applied to be measured in situ.

- Device Control

The control of the system will need to be simple in terms of interaction between the piloting clinician and the device. The human machine interface (HMI) will be comprised of two main elements, a visual display unit (VDU) and a human interface device (HID). The VDU will allow viewing of the camera feed and alerts from the control system such as peak force and screw slip state. The HID will allow the piloting clinician to issue commands to the device for navigation and operation.

A PID control system could be used to calculate a device thrust vector from the current device position as relayed from an IMU and the desired position as provided by the clinician through the HID. From this thrust vector, the relative thrust from each of the screws can be calculated and relayed to the motor controllers. Through differentially driving the motors, translation and rotation of the device could be achieved. Through using the IMU data, the camera feed on screen and motor signals could be rotated so commands are relative to the view; for example up on the VDU and HID always translates to the device top in real world co-ordinates.

The use of semi-autonomous systems is likely to become commonplace in the next 10 years. With increasing public trust in autonomous systems, there may be greater scope for robotic procedures. There will however be a strong onus on who is responsible in cases of failure and mal-treatment; will the engineer be held responsible for the machine they created?

References

1. MEINHARD, C.T., GUIDO. LIGHTDALE, CHARLES. *Gastroenterological endoscopy.* 2nd ed. Thieme, 2010.
2. VADER, J.P., B. BURNAND, F. FROEHLICH, R.W. DUBOIS, M. BOCHUD and J.J. GONVERS. The European Panel on Appropriateness of Gastrointestinal Endoscopy (EPAGE): Project and methods. *Endoscopy*, 1999, **31**(8), pp.572-578.
3. WINAWER, S.J., A.G. ZAUBER, R.H. FLETCHER, J.S. STILLMAN, M.J. O'BRIEN, B. LEVIN, R.A. SMITH, D.A. LIEBERMAN, R.W. BURT, T.R. LEVIN, J.H. BOND, D. BROOKS, T. BYERS, N. HYMAN, L. KIRK, A. THORSON, C. SIMMANG, D. JOHNSON and D.K. REX. Guidelines for colonoscopy surveillance after polypectomy: A consensus update by the US Multi-Society Task Force on Colorectal Cancer and the American Cancer Society. *Gastroenterology*, 2006, **130**(6), pp.1872-1885.
4. NCI. *The Cancer Imaging Archive, sponsored by the Cancer Imaging Program, DCTD/NCI/NIH* [online]. 2011. [Accessed]. Available from: http://www.cancerimagingarchive.net.
5. STANDRING, S. *Gray's anatomy.* The anatomical basis of clinical practice. Churchill Livingstone, 2008.
6. GAVIN, D.R., R.M. VALORI, J.T. ANDERSON, M.T. DONNELLY, J.G. WILLIAMS and E.T. SWARBRICK. The national colonoscopy audit: a nationwide assessment of the quality and safety of colonoscopy in the UK. *Gut*, 2013, **62**(2), pp.242-249.
7. BROCCHI, E., P. TOMASSETTI, D. CAMPANA and R. CORINALDESI. Warm water and oil for the difficult colon. *Gastrointestinal Endoscopy*, 2009, **69**(2), pp.391-391.
8. GUYTON, A.C. and J.E. HALL. *Textbook of Medical Physiology.* Twelfth edition ed. Saunders Elsevier, 2011.
9. SAUNDERS, B.P.P., R. K. S. WILLIAMS, C. B. Intraoperative measurement of colonic anatomy and attachments with relevance to colonoscopy. *British Journal of Surgery*, 1995, **82**(11), pp.1491-1493.
10. SHIELS, W.E., D.R. KIRKS, G.L. KELLER, F.R. RYCKMAN, C.C. DAUGHERTY, B.L. SPECKER and D.W. SUMMA. Colonic Perforation By Air And Liquid Enemas - Comparison Study In Young-Pigs. *American Journal of Roentgenology*, 1993, **160**(5), pp.931-935.
11. SIEGEL, R., J.M. MA, Z.H. ZOU and A. JEMAL. Cancer Statistics, 2014. *Ca-a Cancer Journal for Clinicians*, 2014, **64**(1), pp.9-29.
12. FERLAY, J., H.R. SHIN, F. BRAY, D. FORMAN, C. MATHERS and D.M. PARKIN. Estimates of worldwide burden of cancer in 2008: GLOBOCAN 2008. *International Journal of Cancer*, 2010, **127**(12), pp.2893-2917.
13. BUPA. *Diverticular disease* [online]. [Accessed 29 January 2015]. Available from: http://www.bupa.co.uk/health-information/directory/d/diverticular-disease.
14. FORCE, U.S.P.S.T. Screening for colorectal cancer: U.S. Preventive Services Task Force recommendation statement. *Annals of Internal Medicine*, 2008, **149**(9), pp.627-37.

15. BLOTIERE, P.O., A. WEILL, P. RICORDEAU, F. ALLA and H. ALLEMAND. Perforations and haemorrhages after colonoscopy in 2010: A study based on comprehensive French health insurance data (SNIIRAM). *Clinics and Research in Hepatology and Gastroenterology*, 2014, **38**(1), pp.112-117.
16. WINAWER, S.J., A.G. ZAUBER, M.N. HO, M.J. OBRIEN, L.S. GOTTLIEB, S.S. STERNBERG, J.D. WAYE, M. SCHAPIRO, J.H. BOND, J.F. PANISH, F. ACKROYD, M. SHIKE, R.C. KURTZ, L. HORNSBYLEWIS, H. GERDES and E.T. STEWART. Prevention Of Colorectal-Cancer By Colonoscopic Polypectomy. *New England Journal of Medicine*, 1993, **329**(27), pp.1977-1981.
17. BOWLES, C.J.A., R. LEICESTER, C. ROMAYA, E. SWARBRICK, C.B. WILLIAMS and O. EPSTEIN. A prospective study of colonoscopy practice in the UK today: are we adequately prepared for national colorectal cancer screening tomorrow? *Gut*, 2004, **53**(2), pp.277-283.
18. WAYE, J.D. and E. BASHKOFF. Total colonoscopy - is it always possible. *Gastrointestinal Endoscopy*, 1991, **37**(2), pp.152-154.
19. NAVANEETHAN, U., G. KOCHHAR, H. PHULL, P.G.K. VENKATESH, F.H. REMZI, R.P. KIRAN and B. SHEN. Severe disease on endoscopy and steroid use increase the risk for bowel perforation during colonoscopy in inflammatory bowel disease patients. *Journal of Crohns & Colitis*, 2012, **6**(4), pp.470-475.
20. LEVIN, T.R., W. ZHAO, C. CONELL, L.C. SEEFF, D.L. MANNINEN, J.A. SHAPIRO and J. SCHULMAN. Complications of colonoscopy in an integrated health care delivery system. *Annals of Internal Medicine*, 2006, **145**(12), pp.880-886.
21. BELL, G.D., J. HANCOCK, J. PAINTER, R.S. ROWLAND, D. NYLANDER, S. DOGRAMADZI, C. ALLEN, J.S. BLADEN and W.S. ATKIN. Pain during flexible sigmoidoscopy and colonoscopy: When and why does it occur? *Gut*, 2000, **46**, pp.A30-A30.
22. CHENG, W.B., M.A.J. MOSER, S. KANAGARATNAM and W.J. ZHANG. Analysis of and mathematical model insight into loop formation in colonoscopy. *Proceedings of the Institution of Mechanical Engineers Part H-Journal of Engineering in Medicine*, 2012, **226**(H11), pp.858-867.
23. ---. Overview of upcoming advances in colonoscopy. *Digestive Endoscopy*, 2012, **24**(1), pp.1-6.
24. LEUNG, J.W., S.K. MANN, R. SIAO-SALERA, K. RANSIBRAHMANAKUL, B. LIM, H. CABRERA, W. CANETE, P. BARREDO, R. GUTIERREZ and F.W. LEUNG. A randomized, controlled comparison of warm water infusion in lieu of air insufflation versus air insufflation for aiding colonoscopy insertion in sedated patients undergoing colorectal cancer screening and surveillance. *Gastrointestinal Endoscopy*, 2009, **70**(3), pp.505-510.
25. CHURCH, J.M. Warm water irrigation for dealing with spasm during colonoscopy: simple, inexpensive, and effective. *Gastrointestinal Endoscopy*, 2002, **56**(5), pp.672-674.
26. LEUNG, J.V., S. MANN and F.V. LEUNG. Options for screening colonoscopy without sedation: a pilot study in United States veterans. *Alimentary Pharmacology & Therapeutics*, 2007, **26**(4), pp.627-631.

27. CHAN, A.O., L.N. LEE, A.C. CHAN, W.N. HO, Q.W. CHAN, S. LAU and J.W. CHAN. Predictive factors for colonoscopy complications. *Hong Kong medical journal = Xianggang yi xue za zhi / Hong Kong Academy of Medicine*, 2015, **21**(1), pp.23-9.
28. SFAKIOTAKIS, M., D.M. LANE and J.B.C. DAVIES. Review of fish swimming modes for aquatic locomotion. *Oceanic Engineering, IEEE Journal of*, 1999, **24**(2), pp.237-252.
29. MULLER, U.K., E.J. STAMHUIS and J.J. VIDELER. Hydrodynamics of unsteady fish swimming and the effects of body size: Comparing the flow fields of fish larvae and adults. *Journal of Experimental Biology*, 2000, **203**(2), pp.193-206.
30. XIAOBO, T., D. KIM, N. USHER, D. LABOY, J. JACKSON, A. KAPETANOVIC, J. RAPAI, B. SABADUS and Z. XIN. An Autonomous Robotic Fish for Mobile Sensing. *In: Intelligent Robots and Systems, 2006 IEEE/RSJ International Conference on*, 9-15 Oct. 2006, 2006, pp.5424-5429.
31. HUOSHENG, H., L. JINDONG, I. DUKES and G. FRANCIS. Design of 3D Swim Patterns for Autonomous Robotic Fish. *In: Intelligent Robots and Systems, 2006 IEEE/RSJ International Conference on*, 9-15 Oct. 2006, 2006, pp.2406-2411.
32. TERADA, Y. and I. YAMAMOTO. An animatronic system including lifelike robotic fish. *Proceedings of the IEEE*, 2004, **92**(11), pp.1814-1820.
33. HIROSE, S., M. MORI and IEEE. *Biologically inspired snake-like robots.* IEEE ROBIO 2004: Proceedings of the IEEE International Conference on Robotics and Biomimetics. New York: Ieee, 2004.
34. AYERS, J., N. RULKOV, D. BRADY, A. WESTPHAL and M. HUNT. Controlling a lamprey-based robot with an electronic nervous system. *Society for Neuroscience Abstract Viewer and Itinerary Planner*, 2008, **38**.
35. CRESPI, A., A. BADERTSCHER, A. GUIGNARD and A.J. IJSPEERT. Swimming and Crawling with an Amphibious Snake Robot. *In: Robotics and Automation, 2005. ICRA 2005. Proceedings of the 2005 IEEE International Conference on*, 18-22 April 2005, 2005, pp.3024-3028.
36. SHUMEI, Y., M. SHUGEN, L. BIN and W. YUECHAO. An amphibious snake-like robot: Design and motion experiments on ground and in water. *In: Information and Automation, 2009. ICIA '09. International Conference on*, 22-24 June 2009, 2009, pp.500-505.
37. YAMADA, H., S. HIROSE and IEEE. Study on the 3D shape of active cord mechanism. *In: 2006 Ieee International Conference on Robotics and Automation*. New York: Ieee, 2006, pp.2890-2895.
38. ROH, S.G. and H.R. CHOI. Differential-drive in-pipe robot for moving inside urban gas pipelines. *Ieee Transactions on Robotics*, 2005, **21**(1), pp.1-17.
39. ROMAN, H.T., B.A. PELLEGRINO and W.R. SIGRIST. Pipe crawling inspection robots - an overview. *Ieee Transactions on Energy Conversion*, 1993, **8**(3), pp.576-583.
40. RICHARDSON, R., S. WHITEHEAD, T. NG, Z. HAWASS, A. PICKERING, S. RHODES, R. GRIEVE, A. HILDRED, A. NAGENDRAN, J. LIU, W. MAYFIELD, M. TAYOUBI and R.

BREITNER. The "Djedi" Robot Exploration of the Southern Shaft of the Queen's Chamber in the Great Pyramid of Giza, Egypt. *Journal of Field Robotics*, 2013, **30**(3), pp.323-348.

41. CHOI, C., B. PARK and S. JUNG. The Design and Analysis of a Feeder Pipe Inspection Robot With an Automatic Pipe Tracking System. *Ieee-Asme Transactions on Mechatronics*, 2010, **15**(5), pp.736-745.
42. JIANCHENG, Y., T. YUANGUI, Z. XUEQIANG and L. CHONGJIE. Design of a wheel-propeller-leg integrated amphibious robot. *In: Control Automation Robotics & Vision (ICARCV), 2010 11th International Conference on*, 7-10 Dec. 2010, 2010, pp.1815-1819.
43. BROOKS, S. *Ice Challenger* [online]. 2001. [Accessed Last accessed 28 June 2013]. Available from: http://www.icechallenger.com/icechallenger/ [ONLINE].
44. LIANG, J., G. FERRI, C. LASCHI, B. MAZZOLAI and P. DARIO. Experimental results of a novel amphibian solution for aquatic robot. *In: Robotics and Automation (ICRA), 2010 IEEE International Conference on*, 3-7 May 2010, 2010, pp.2261-2266.
45. LIEDKE, J., L. WINKLER, H. WORN and IEEE. *An alternative locomotion unit for mobile modular self-reconfigurable robots based on archimedes screws.* 2013 9th International Symposium on Mechatronics and Its Applications. New York: Ieee, 2013.
46. NAGAOKA, K., M. OTSUKI, T. KUBOTA, S. TANAKA and IEEE. Terramechanics-based Propulsive Characteristics of Mobile Robot Driven by Archimedean Screw Mechanism on Soft Soil. *In: Ieee/Rsj 2010 International Conference on Intelligent Robots and Systems*. New York: Ieee, 2010.
47. KERR, R.A. PLANETARY SCIENCE Mars Rover Trapped in Sand, But What Can End a Mission? *Science*, 2009, **324**(5930), pp.998-998.
48. PATHE, B. *New American Swamp Vehicle - The Marsh Screw* [online]. 1964. [Accessed Last accessed 15 May 2015]. Available from: http://www.britishpathe.com/video/new-american-swamp-vehicle-the-marsh-screw-amphibi.
49. ORTIZ-OSHIRO, E., I. SÁNCHEZ-EGIDO, J. MORENO-SIERRA, C.F. PÉREZ, J.S. DÍAZ and J.Á. FERNÁNDEZ-REPRESA. Robotic assistance may reduce conversion to open in rectal carcinoma laparoscopic surgery: systematic review and meta-analysis. *International Journal of Medical Robotics and Computer Assisted Surgery*, 2012, **8**(3), pp.360-370.
50. JAYNE, D.G., P.R. CULMER, J. BARRIE, R. HEWSON and A. NEVILLE. Robotic platforms for general and colorectal surgery. *Colorectal Disease*, 2011, **13**, pp.78-82.
51. CIUTI, G., A. MENCIASSI and P. DARIO. Capsule endoscopy: from current achievements to open challenges. *IEEE reviews in biomedical engineering*, 2011, **4**, pp.59-72.
52. MENCIASSI, A. and P. DARIO. Miniaturized robotic devices for endoluminal diagnosis and surgery: A single-module and a multiple-module approach. *In: Engineering in Medicine and Biology Society, 2009. EMBC 2009. Annual International Conference of the IEEE*, 3-6 Sept. 2009, 2009, pp.6842-6845.

53. QUIRINI, M., A. MENCIASSI, S. SCAPELLATO, C. STEFANINI and P. DARIO. Design and fabrication of a motor legged capsule for the active exploration of the gastrointestinal tract. *Ieee-Asme Transactions on Mechatronics*, 2008, **13**(2), pp.169-179.
54. TORTORA, G., P. VALDASTRI, E. SUSILO, A. MENCIASSI, P. DARIO, F. RIEBER and M.O. SCHURR. Propeller-based wireless device for active capsular endoscopy in the gastric district. *Minimally Invasive Therapy & Allied Technologies*, 2009, **18**(5), pp.280-290.
55. MENCIASSI, A., P. VALDASTRI, K. HARADA and P. DARIO. *Single and Multiple Robotic Capsules for Endoluminal Diagnosis and Surgery.* Surgical Robotics: Systems Applications and Visions. Berlin: Springer-Verlag Berlin, 2011.
56. VALDASTRI, P., G. CIUTI, A. VERBENI, A. MENCIASSI, P. DARIO, A. AREZZO and M. MORINO. Magnetic air capsule robotic system: proof of concept of a novel approach for painless colonoscopy. *Surgical Endoscopy and Other Interventional Techniques*, 2012, **26**(5), pp.1238-1246.
57. NADERI, N., S. NAJARIAN, A. HOSSEINALI and H. KAREVAN. Modeling and dynamic analysis of the worm-like part of an innovative robot applicable in colonoscopy. *International Journal of Medical Robotics and Computer Assisted Surgery*, 2013, **9**(3), pp.371-378.
58. AREZZO, A., A. MENCIASSI, P. VALDASTRI, G. CIUTI, G. LUCARINI, M. SALERNO, C. DI NATALI, M. VERRA, P. DARIO and M. MORINO. Experimental assessment of a novel robotically-driven endoscopic capsule compared to traditional colonoscopy. *Digestive and Liver Disease*, 2013, **45**(8), pp.657-662.
59. HONDA, T., K.I. ARAI and K. ISHIYAMA. Micro swimming mechanisms propelled by external magnetic fields. *Ieee Transactions on Magnetics*, 1996, **32**(5), pp.5085-5087.
60. ISHIYAMA, K., K.I. ARAI, M. SENDOH, A. YAMAZAKI and IEEE. *Spiral-type micro-machine for medical applications.* Mhs 2000: Proceedings of the 2000 International Symposium on Micromechatronics and Human Science. New York: Ieee, 2000.
61. SUDO, S., S. SEGAWA and T. HONDA. Magnetic swimming mechanism in a viscous liquid. *Journal of Intelligent Material Systems and Structures*, 2006, **17**(8-9), pp.729-736.
62. GUO, S.X., Q.X. PAN and M.B. KHAMESEE. Development of a novel type of microrobot for biomedical application. *Microsystem Technologies-Micro-and Nanosystems-Information Storage and Processing Systems*, 2008, **14**(3), pp.307-314.
63. QINXUE, P., G. SHUXIANG and T. OKADA. Development of a wireless hybrid microrobot for biomedical applications. *In: Intelligent Robots and Systems (IROS), 2010 IEEE/RSJ International Conference on*, 18-22 Oct. 2010, 2010, pp.5768-5773.
64. PALAGI, S., V. PENSABENE, L. BECCAI, B. MAZZOLAI, A. MENCIASSI, P. DARIO and IEEE. Design and development of a soft magnetically-propelled swimming microrobot. *In: 2011 Ieee International Conference on Robotics and Automation*. New York: Ieee, 2011.
65. ABBOTT, J.J., O. ERGENEMAN, M.P. KUMMER, A.M. HIRT, B.J. NELSON and IEEE. Modeling magnetic torque and force for

controlled manipulation of soft-magnetic bodies. *In: 2007 Ieee/Asme International Conference on Advanced Intelligent Mechatronics, Vols 1-3*. New York: Ieee, 2007, pp.841-846.

66. BAI, C., J. SURONG, L. YAODONG and C. SUN. Modeling and Analyzing the Screw-In Propulsion Mechanism for a Bio-Inspired Micro-Robot. *In: Bioinformatics and Biomedical Engineering (iCBBE), 2010 4th International Conference on*, 18-20 June 2010, 2010, pp.1-5.
67. ANDRE, W., S. MARTEL and IEEE. Preliminary design of an autonomous microrobot propelled by magnetotactic bacteria. *In: 2007 Ieee/Asme International Conference on Advanced Intelligent Mechatronics, Vols 1-3*. New York: Ieee, 2007, pp.138-143.
68. PURCELL, E.M. LIFE AT LOW REYNOLDS-NUMBER. *American Journal of Physics*, 1977, **45**(1), pp.3-11.
69. LAUGA, E. and T.R. POWERS. The hydrodynamics of swimming microorganisms. *Reports on Progress in Physics*, 2009, **72**(9).
70. PURCELL, E.M. The efficiency of propulsion by a rotating flagellum. *Proceedings of the National Academy of Sciences of the United States of America*, 1997, **94**(21), pp.11307-11311.
71. ZHANG, L., J.J. ABBOTT, L.X. DONG, B.E. KRATOCHVIL, D. BELL and B.J. NELSON. Artificial bacterial flagella: Fabrication and magnetic control. *Applied Physics Letters*, 2009, **94**(6).
72. ABBOTT, J.J., K.E. PEYER, M.C. LAGOMARSINO, L. ZHANG, L.X. DONG, I.K. KALIAKATSOS and B.J. NELSON. How Should Microrobots Swim? *International Journal of Robotics Research*, 2009, **28**(11-12), pp.1434-1447.
73. YE, Z., S. REGNIER and M. SITTI. Rotating Magnetic Miniature Swimming Robots With Multiple Flexible Flagella. *Robotics, IEEE Transactions on*, 2013, **PP**(99), pp.1-11.
74. IKEUCHI, K., K. YOSHINAKA, S. HASHIMOTO, N. TOMITA and IEEE. *Locomotion of medical micro robot with spiral ribs using mucus.* Mhs '96 - Proceedings of the Seventh International Symposium on Micro Machine and Human Science: Toward Micro-Mechatronics in 21st Century. New York: I E E E, 1996.
75. ZHOU, Y.S., Y.X. QUAN, K. YOSHINAKA and K. IKEUCHI. A new medical microrobot for minimal invasive surgery. *Proceedings of the Institution of Mechanical Engineers Part H-Journal of Engineering in Medicine*, 2001, **215**(H2), pp.215-220.
76. SHIKANAI, M., N. MURAI, K. ITOH, H. ISHII, A.T. AKANISHI, K.T. ANOUE, S. IEIRI, K. KONISHI and M. HASIZUME. Development of a robotic endoscope that locomotes in the colon with flexible helical fins. *In: Engineering in Medicine and Biology Society, 2009. EMBC 2009. Annual International Conference of the IEEE*, 3-6 Sept. 2009, 2009, pp.5126-5129.
77. KIM, Y.T. and D.E. KIM. *A Novel Propelling Mechanism Based on Frictional Interaction for Endoscope Robot.* Advanced Tribology. Beijing: Tsinghua University Press, 2009.
78. RENTSCHLER, M.E., J. DUMPERT, S.R. PLATT, D. OLEYNIKOV, S.M. FARRITOR and K. IAGNEMMA. Mobile in vivo biopsy robot. *In: Robotics and Automation, 2006. ICRA 2006. Proceedings 2006 IEEE International Conference on*, 15-19 May 2006, 2006, pp.4155-4160.

79. LEE, J.S., B. KIM and Y.S. HONG. A flexible chain-based screw propeller for capsule endoscopes. *International Journal of Precision Engineering and Manufacturing*, 2009, **10**(4), pp.27-34.
80. PHEE, L., A. MENCIASSI, D. ACCOTO, C. STEFANINI and P. DARIO. Analysis of robotic locomotion devices for the gastrointestinal tract. *In:* R.A. JARVIS and A. ZELINSKY, eds. *Robotics Research*. Berlin: Springer-Verlag Berlin, 2003, pp.467-483.
81. POIGNET, P., A. CHEMORI, N. ZEMITI and L. CHAO. Some control-related issues in mini-robotics for endoluminal surgery. *In: Engineering in Medicine and Biology Society, 2009. EMBC 2009. Annual International Conference of the IEEE*, 3-6 Sept. 2009, 2009, pp.6850-6855.
82. JOSEPH, W., G. VERMEEREN, L. VERLOOCK, M.M. HEREDIA and L. MARTENS. Characterization of personal RF electromagnetic field exposure and actual absorption for the general public. *Health Physics*, 2008, **95**(3), pp.317-330.
83. MARTINEZ-BURDALO, M., A. MARTIN, A. SANCHIS and R. VILLAR. FDTD Assessment of Human Exposure to Electromagnetic Fields From WiFi and Bluetooth Devices in Some Operating Situations. *Bioelectromagnetics*, 2009, **30**(2), pp.142-151.
84. CHANSON, H. *Applied hydrodynamics: an introduction to ideal and real fluid flows.* Boca Raton, Florida: CRC Press, 2009.
85. DE SILVA, C.W. *Mechatronics: an integrated approach.* Boca Raton, Fla; London: CRC Press, 2005.
86. WILAMOWSKI, B.M. and J.D. IRWIN. *Control and mechatronics.* Boca Raton, Fla; London: CRC Press Inc, 2011.
87. CARLTON, J.S. *Marine Propellers and Propulsion.* Materials & Mechanical. Butterworth-Heinemann, 2007.
88. KARWA, R. *A Text Book of Machine Design.* Laxmi Publications Pvt Limited, 2002.
89. KRUTH, J.P., M.C. LEU and T. NAKAGAWA. Progress in Additive Manufacturing and Rapid Prototyping. *CIRP Annals - Manufacturing Technology*, 1998, **47**(2), pp.525-540.
90. MORELLE, R. *Working gun made with 3D printer* [online]. 2013. [Accessed 06 October]. Available from: http://www.bbc.co.uk/news/science-environment-22421185.
91. FOX, S. *Transatlantic: Samuel Cunard, Isambard Brunel, and the Great Atlantic Steamships.* HarperCollins, 2003.
92. BRINDLE, S. *Brunel: The Man who Built the World.* Weidenfeld & Nicolson, 2005.
93. UHLIG, D.V.S., M. S. Post Stall Propeller Behavior at Low Reynolds Numbers. *46th AIAA Aerospace Sciences Meeting and Exhibit*, 2008, (January 2008).
94. FLAXMAN, Y.S.L., A. V.; OSTROUKHOV, S. P.; USTINOV, M. P.; SHUSTOV, A. V.; KORNUSHENKO A. V.;. Experimental Investigations Of Propellers At Low Reynolds Numbers. *3rd US-European Competition and Workshop on Micro Air Vehicle Systems (MAV07) & European Micro Air Vehicle Conference and Flight Competition (EMAV2007)*, 2007, (September 2007).

95. BRANDT, J.B.S., M. S.;. Propeller Performance Data at Low Reynolds Numbers. *49th AIAA Aerospace Sciences Meeting*, 2011, (January 2011), pp.pp1-18.
96. STOKES, G.G. *On the Effect of the Internal Friction of Fluids on the Motion of Pendulums.* Pitt Press, 1851.
97. SCHLICHTING, H. *Boundary layer theory.* London: Pergamon Press, 1955.
98. GRAY, J. The mechanism of locomotion in snakes. *J Exp Biol*, 1946, **23**(2), pp.101-20.
99. SWINDLE, M.M., A. MAKIN, A.J. HERRON, F.J. CLUBB and K.S. FRAZIER. Swine as Models in Biomedical Research and Toxicology Testing. *Veterinary Pathology*, 2012, **49**(2), pp.344-356.
100. YAMADA, H. *Strength of biological materials.* Strength of Biological Materials. 1970.
101. AHEARNE, M., Y. YANG, A.J. EL HAJ, K.Y. THEN and K.K. LIU. Characterizing the viscoelastic properties of thin hydrogel-based constructs for tissue engineering applications. *Journal of the Royal Society Interface*, 2005, **2**(5), pp.455-463.
102. JIANG, S., S. LIU and W. FENG. PVA hydrogel properties for biomedical application. *Journal of the Mechanical Behavior of Biomedical Materials*, 2011, **4**(7), pp.1228-1233.
103. ZHU, J.M. and R.E. MARCHANT. Design properties of hydrogel tissue-engineering scaffolds. *Expert Review of Medical Devices*, 2011, **8**(5), pp.607-626.
104. PANG, C., G.-Y. LEE, T.-I. KIM, S.M. KIM, H.N. KIM, S.-H. AHN and K.-Y. SUH. A flexible and highly sensitive strain-gauge sensor using reversible interlocking of nanofibres. *Nat Mater*, 2012, **11**(9), pp.795-801.